

## Design of sintering-stable heterogeneous catalysts

Gallas-Hulin, Agata; Kegnæs, Søren; Riisager, Anders

*Publication date:*  
2017

*Document Version*  
Publisher's PDF, also known as Version of record

[Link back to DTU Orbit](#)

*Citation (APA):*  
Gallas-Hulin, A., Kegnæs, S., & Riisager, A. (2017). Design of sintering-stable heterogeneous catalysts. Kgs. Lyngby: DTU Chemistry.

## DTU Library

Technical Information Center of Denmark

---

### General rights

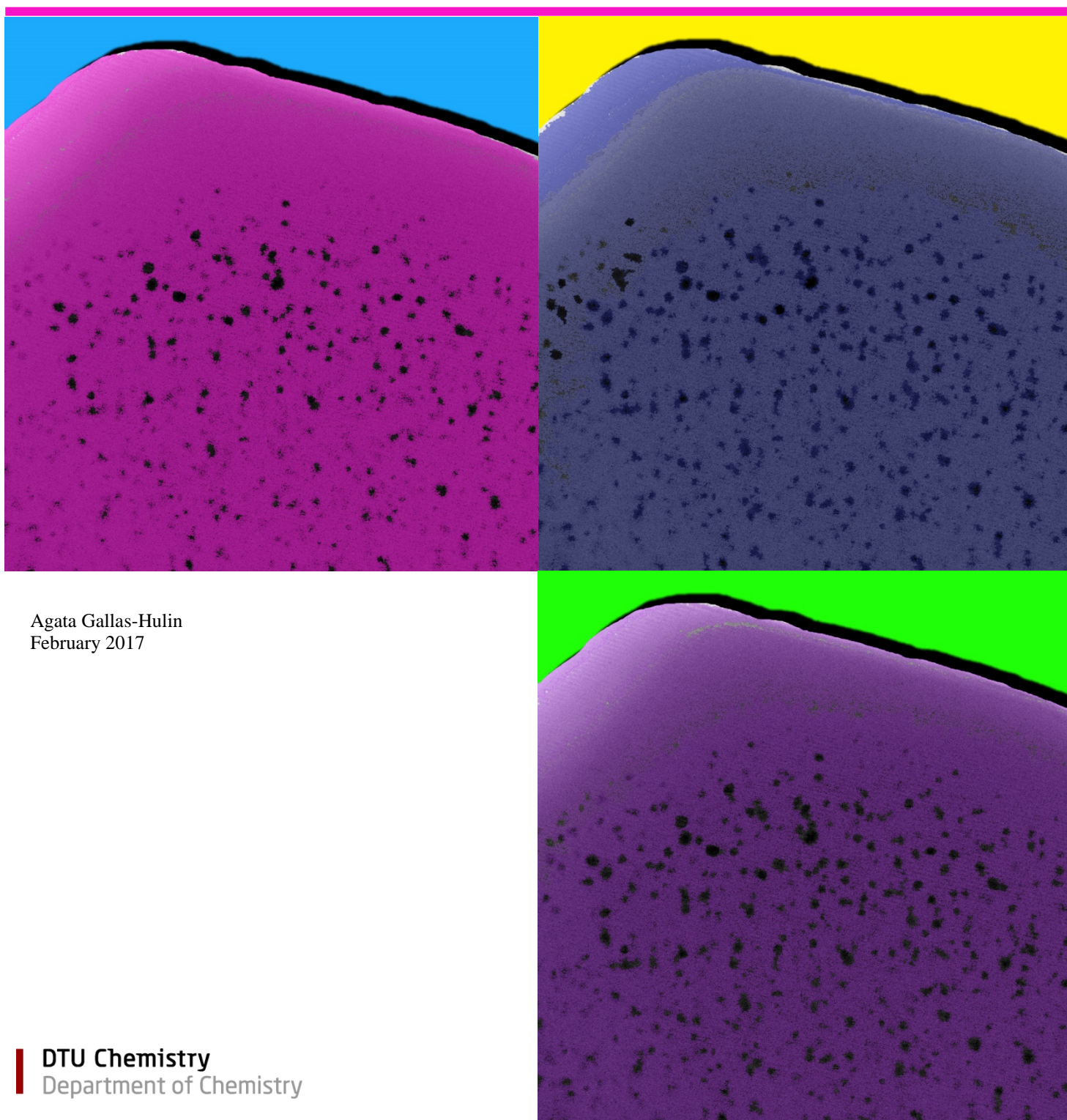
Copyright and moral rights for the publications made accessible in the public portal are retained by the authors and/or other copyright owners and it is a condition of accessing publications that users recognise and abide by the legal requirements associated with these rights.

- Users may download and print one copy of any publication from the public portal for the purpose of private study or research.
- You may not further distribute the material or use it for any profit-making activity or commercial gain
- You may freely distribute the URL identifying the publication in the public portal

If you believe that this document breaches copyright please contact us providing details, and we will remove access to the work immediately and investigate your claim.

# Design of sintering-stable heterogeneous catalysts

Department of Chemistry



Agata Gallas-Hulin  
February 2017



## Preface

This thesis was submitted as a partial requirement for obtaining a PhD degree from Technical University of Denmark. This thesis is based on work carried out at the Centre for Catalysis and Sustainable Chemistry (CSC) at Department of Chemistry, under supervision of Associate Professor Søren Kegnæs and Professor Anders Riisager from May 2013 to February 2017. The project was founded by Danish National Research Foundation and Technical University of Denmark.

At this point I would like to thank everybody who contributed in any way to the success of this project. Special acknowledgements go to Associate Professor Søren Kegnæs, the supervisor of my thesis, for his help and feedback throughout the project. I would like to express my deep gratification to all my colleagues from the CSC group and DTU Chemistry for a stimulating working atmosphere and discussion and support in the moments of doubt.

---

Agata Gallas-Hulin, February 2017



## Abstract

One of the major issues in the use of metal nanoparticles in heterogeneous catalysis is sintering. Sintering occurs at elevated temperatures because of increased mobility of nanoparticles, leading to their agglomeration and, as a consequence, to the deactivation of the catalyst. It is an emerging problem especially for the noble metals-based catalysis. These metals being expensive and scarce, it is worth developing catalyst systems which preserve their activity over time. Encapsulation of nanoparticles inside zeolites is one of the ways to prevent sintering. Entrapment of nanoparticles inside the crystalline framework of a zeolite creates a steric hindrance against agglomeration into larger clusters.

In the present study, experimental protocols for encapsulation of metal nanoparticles inside zeolites were developed. Two different methodologies were proposed to encapsulate gold, palladium and platinum nanoparticles inside silicalite-1 - the pressure assisted impregnation and reduction method (PAIR), and *in situ* incorporation method. PAIR is based on modified incipient wetness impregnation technique in which the impregnation of a zeolite with a solution of metal precursor and its reduction are performed under elevated pressure. *In situ* incorporation is a one-pot procedure based on simultaneous growth of a zeolite and entrapment of metal precursor in a form of ethylenediamine complex inside the forming crystalline network, leading to encapsulated metal nanoparticles after reduction in hydrogen.

The PAIR procedure was used to successfully synthesize gold nanoparticles, 2-3 nm in size inside silicalite-1 and ZSM-5. Silicalite-1 with 2 nm palladium nanoparticles uniformly distributed on the external surface of the crystal was synthesized as well using the PAIR method. The *in situ* incorporation method was used to produce single metal palladium and platinum nanoparticles, 2-3 nm in size, and bi-metallic palladium/platinum nanoparticles inside silicalite-1.

Materials were primarily characterized using XRD, nitrogen physisorption, TEM, and XRF techniques. STEM and XPS were also used in selected cases. Synthesized catalysts were able to decompose formic acid with ~ 85% selectivity towards hydrogen at temperatures around 100 °C. Palladium/silicalite-1 catalysts were shown to be very active in Suzuki cross-coupling reaction of bromobenzene and 4-methoxyphenylboronic acid in methanol at 70 °C reaching yields of ~ 85% after 45 min. Oxidation of allyl alcohol to its methyl esters at ambient conditions showed a very low activity of gold/silicalite-1 catalyst due to limited diffusion and possible adsorption of products inside the pores of zeolite.

It was shown that the PAIR method and *in situ* incorporation method are feasible and easy protocols for synthesis of metal nanoparticles encapsulated inside a zeolite matrix. Small size, stability towards sintering and high activity of nanoparticles obtained using the PAIR method and *in situ* incorporation method makes these two protocols promising for further research.



## Resumé

Et af de største problemer ved brug af metalnanopartikler i heterogen katalyse er sintring. Sintring sker ved høje temperaturer på grund af øget mobilitet af nanopartikler, hvilket leder til deres agglomering, og som konsekvens deraf til deaktivering af katalysatoren. Det er et stigende problem, specielt for ædelmetal baseret katalyse. For disse metaller, som er dyre og sjældne, er det værd at udvikle katalytiske systemer som sikrer en bevaret aktivitet med tiden. Indkapsling af nanopartikler indeni zeolitter er en af måderne at forhindre sintring. Ved at fange nanopartikler indeni det krystallinske skelet af en zeolit, danner en sterisk hindring mod agglomering til større klynger.

I dette studie blev eksperimentelle protokoller for indkapsling af metalnanopartikler indeni zeolitter udviklet. To forskellige metodikker blev foreslået til at indkapsle guld-, palladium- og platinnanopartikler indeni MFI zeolitter: den tryk-hjulpel imprægnering og reduktions metode (PAIR) og *in situ* inkorporeringsmetoden. PAIR er baseret på modificeret begyndende fugtigheds imprægnerings teknik hvor imprægneringen af zeolitten med en opløsning af metalsaltet og dennes reduktion er udført under forøget tryk og lavere temperaturer. *In situ* inkorporering er en et-trins procedure baseret på samtidig groning af zeolit og indespærring af metalsaltet i form af ethylendiamin kompleks indeni det groende krystallinske netværk, ledende til indkapslede metalnanopartikler efter reduktion i hydrogen.

PAIR proceduren blev brugt til vellykket at syntetisere guldnanopartikler, 2-3 nm i størrelse, indeni silicalite-1 og ZSM-5 og 2 nm palladium nanopartikler ensartet fordelt på den udvendige overflade af silicalite-1 krystaller. *In situ* inkorporeringsmetoden blev brugt til at producere enkeltmetal partikler af palladium og platin nanopartikler, 2-3 nm i størrelse, og bi-metallisk palladium/platin nanopartikler indeni silicalite-1.

Materialer var primært karakteriseret ved brug af XRD, nitrogen fysisorption, TEM og XRF teknikker. STEM og XPS blev også brugt i udvalgte tilfælde. De syntetiserede katalysatorer kunne nedbryde myresyre med ca. 85% selektivitet mod hydrogen ved temperaturer omkring 100 °C. Palladium/silicalite-1 katalysatorer blev vist at være meget aktive i Suzuki krydskoblings reaktioner af brombenzen og 4-methoxyphenylborsyre i metanol ved 70 °C med opnåede udbytter på ca. 85% efter 45 min. Oxidation af allylalkohol til dets methyl estre ved omgivende betingelser viste meget lav aktivitet af guld/silicalite-1 katalysatoren på grund af begrænset diffusion og mulig adsorption af produkter indeni zeolittens porer.

Det blev vist, at PAIR metoden og *in situ* inkorporeringsmetoden er gennemførlige og er lette protokoller for syntese af metalnanopartikler indkapslet indeni en zeolitmatrix. Små størrelse af nanopartikler og deres høje aktivitet i testede reaktioner gør disse to protokoller lovende for videre forskning.





# Table of Contents

Preface.....	i
Abstract.....	iii
Resumé.....	v
<b>1. Introduction.....</b>	<b>1</b>
<b>1.1 Background.....</b>	<b>1</b>
1.1.1 General considerations.....	1
1.1.2 Encapsulation of gold, palladium and platinum nanoparticles.....	3
<b>1.2 Scope of thesis.....</b>	<b>5</b>
1.2.1 Pressure assisted impregnation and reduction – PAIR.....	5
1.2.2 In situ incorporation method.....	6
<b>1.3 Thesis overview.....</b>	<b>7</b>
<b>2. Methods.....</b>	<b>9</b>
<b>2.1 Transmission electron microscopy (TEM).....</b>	<b>9</b>
<b>2.2 Scanning transmission electron microscopy (STEM).....</b>	<b>9</b>
<b>2.3 Nitrogen physisorption.....</b>	<b>10</b>
<b>2.4 X-ray diffraction (XRD).....</b>	<b>10</b>
<b>2.5 X-ray photoelectron spectroscopy (XPS).....</b>	<b>10</b>
<b>2.6 X-ray fluorescence (XRF).....</b>	<b>11</b>
<b>2.7 Temperature programmed reduction (TPR).....</b>	<b>11</b>
<b>2.8 Attenuated Total Reflection (ATR).....</b>	<b>11</b>
<b>3. Synthesis of materials.....</b>	<b>13</b>
<b>3.1 Zeolite preparation.....</b>	<b>13</b>
3.1.1 Materials.....	13
3.1.2 Synthesis of silicalite-1.....	13
3.1.3 Synthesis of LTA.....	13
3.1.4 Synthesis of ZSM-5.....	14
3.1.5 General procedure for ion exchange.....	14
<b>3.2 Synthesis of zeolite supported metal nanoparticles.....</b>	<b>14</b>
3.2.1 Materials.....	15
3.2.2 General procedure for the impregnation method.....	15
3.2.3 General procedure for the PAIR method.....	15
3.2.4 General procedure for the <i>in situ</i> incorporation method.....	16
<b>4. Pressure assisted impregnation and reduction – PAIR.....</b>	<b>19</b>
<b>4.1 PAIR method applied to gold in silicalite-1.....</b>	<b>20</b>
4.1.1 Synthesis conditions: $\text{HAuCl}_4 \cdot 3\text{H}_2\text{O}$ + 0.15 ml water.....	21
4.1.2 Synthesis conditions: $\text{HAuCl}_4 \cdot 3\text{H}_2\text{O}$ + 0.3 ml of different solvents.....	24
4.1.3 Synthesis conditions: $\text{AuCl}_3$ + 0.3 ml of different solvents.....	28
<b>4.2 PAIR method applied to gold in LTA and ZSM-5 zeolites.....</b>	<b>32</b>

4.2.1	Synthesis of gold nanoparticles in LTA.....	32
4.2.2	Synthesis of gold nanoparticles in ZSM-5 .....	34
<b>4.3</b>	<b>PAIR method applied to palladium and platinum in silicalite-1.....</b>	<b>36</b>
4.3.1	Synthesis of palladium nanoparticles in silicalite-1 .....	36
4.3.2	Synthesis of platinum nanoparticles in silicalite-1.....	39
<b>4.4</b>	<b>PAIR method applied to non-zeolitic support.....</b>	<b>39</b>
4.4.1	Synthesis of gold nanoparticles on mesoporous silica .....	39
<b>4.5</b>	<b>Study of the method.....</b>	<b>42</b>
4.5.1	Influence of the PAIR conditions on the morphology of the materials.....	42
4.5.2	Investigation on the reduction of gold species .....	44
4.5.3	Investigation on the artefacts arising from the solvents .....	46
<b>4.6</b>	<b>General discussion of the PAIR method.....</b>	<b>47</b>
4.6.1	Theoretical investigations .....	47
4.6.2	Comparison of the PAIR method and impregnation method .....	49
4.6.3	Influence of the solvent volume used for impregnation during the PAIR procedure.....	50
4.6.4	Influence of the choice of solvent used during the PAIR procedure.....	51
4.6.5	Influence of the choice of precursor used during the PAIR procedure .....	52
4.6.6	Influence of the choice of zeolite for the PAIR procedure.....	53
4.6.7	Application of PAIR for different metals.....	54
4.6.8	Application of PAIR to different kind of support .....	54
4.6.9	Consideration of the reduction under pressure during PAIR .....	54
<b>4.7</b>	<b>Final summary .....</b>	<b>55</b>
<b>5.</b>	<b><i>In situ</i> incorporation method .....</b>	<b>57</b>
5.1	Synthesis of palladium in silicalite-1 .....	57
5.2	Synthesis of platinum in silicalite-1.....	59
5.3	Synthesis of palladium and platinum in silicalite-1 in random incorporation.....	62
5.4	Synthesis of platinum and palladium in silicalite-1 in layered incorporation.....	65
5.5	Synthesis of gold in silicalite-1 .....	66
5.6	Conclusion .....	67
<b>6.</b>	<b>Decomposition of formic acid.....</b>	<b>69</b>
6.1	Background.....	69
6.2	Experimental.....	72
6.2.1	Materials .....	72
6.2.2	Catalyst characterization .....	72
6.2.3	General procedure.....	72
6.2.4	Calculations .....	73
6.3	Results and discussion.....	73
6.3.1	Diagnostic experimental testing of a catalyst.....	73
6.3.2	Performance of gold in silicalite-1 .....	75
6.3.3	Performance of gold in LTA and ZSM-5 zeolites.....	82
6.3.4	Performance of gold on amorphous mesoporous silica and titanium oxide.....	83
6.3.5	Performance of palladium in silicalite-1 .....	85
6.3.6	Performance of platinum in silicalite-1 .....	86
6.3.7	Performance of platinum and palladium in silicalite-1 .....	88

6.4	Conclusion.....	89
7.	Suzuki cross-coupling .....	91
7.1	Background.....	91
7.2	Experimental.....	95
7.2.1	Materials .....	95
7.2.2	Catalyst characterization.....	95
7.2.3	General procedure for the Suzuki cross-coupling reaction .....	95
7.3	Results and Discussion .....	96
8.	Oxidation of allyl alcohol.....	99
8.1	Background.....	99
8.2	Experimental.....	101
8.2.1	Materials .....	101
8.2.2	Catalyst characterization.....	102
8.2.3	Procedure of catalytic oxidation of allyl alcohol .....	102
8.3	Results and Discussion .....	102
8.3.1	Catalyst characterization.....	102
8.3.2	Catalytic activity .....	102
	Conclusion.....	109
	Appendix A .....	111
	Bibliography .....	117



# Chapter 1

## Introduction

This chapter provides the theoretical background of the project. Brief overview of the aspects of heterogeneous catalysis, nanoparticles in catalysis, chemistry of gold, sintering, zeolites and methods of preparation of heterogeneous catalysts are given in this section. Finally, the scope of the work is presented together with the organization of this thesis.

### 1.1 Background

#### 1.1.1 General considerations

Heterogeneous catalysis is one of the most important chemical processes in the industry, contributing to 90% of all chemical processes (Armor 2011). It is broadly used to convert raw materials into chemicals and fuels in a manner that is economical, efficient and with as low as possible environmental impact. The spectrum of applications of heterogeneous catalysis is very broad, ranging from food industry, pharmaceuticals, chemicals to petrochemicals and automobile industry.

Nowadays, many commercially important catalysts are high-surface-area solids with the active component being dispersed on their surface in the form of nanoparticles. Nanoparticles have higher surface-to-volume ratio compared to bulk materials, hence they exhibit higher activity due to larger area of active sites available for the reaction to occur. These nanoparticles are usually 1 – 50 nm in size (Bell 2003). In this size range the physical and chemical properties of nanoparticles are intermediate between those of single atoms or molecules and of bulk solids. The performance of such catalysts can be altered easily since the surface structure and electronic properties can change greatly with the size of nanoparticles (Schauermaun et al. 2013). It was shown by the example of CO oxidation over Au/TiO<sub>2</sub> catalyst that the size of gold nanoparticles played a crucial role and that only nanoparticles of size 2 – 3 nm were active in the reaction (Valden et al. 1998).

Gold nanoparticles attracted a lot of attention in the scientific community after the discovery of Haruta and Hutchings, who showed an extremely high activity of gold nanoparticles for the oxidation of CO (Haruta 2004). Before, gold was considered catalytically inert. After their discovery the research on gold nanoparticles for catalysis has been rapidly growing. Nowadays, gold catalysts are one of the most widely used in industry, applied for a wide range of selective oxidations and reductions, pollution control and fuel

cell applications (Haruta 2003). Commercial gold catalysts are prepared with very small gold nanoparticles,  $\leq 5$  nm in size on an appropriate metal oxide support. They become active at very low temperatures which is one of the most exciting aspects of catalysis by gold. Haruta reported activity of gold catalyst at temperatures as low as 200 K (Haruta et al. 1987). In general, precious metals, like gold, palladium and platinum are known for their high activity and selectivity in many catalyzed reactions.

Considering the catalysis by gold, sintering of gold nanoparticles is known as the most common obstacle in the processes catalyzed by this metal. The sintering of gold nanoparticles is facilitated by the presence of chloride ions, coming from the gold precursor, which remain in the catalyst after the synthesis. They were shown to noticeably promote agglomeration of gold nanoparticles (Haruta 2003); hence, the removal of chloride ions is necessary. Another parameter causing sintering of gold nanoparticles is elevated temperature at which most of heterogeneous gold catalysts operate, e.g. in automotive catalytic converter. At higher temperatures the mobility of nanoparticles increases what causes agglomeration into larger clusters (Hansen et al. 2013). As a result the activity of the catalyst decreases leading to complete deactivation over time. In order to limit sintering arising due to migration at elevated temperatures, entrapment of nanoparticles inside porous materials, crystalline or amorphous, has been proposed. The examples of such materials are zeolites or mesoporous silica. Especially, the use of zeolites as hosts for metal nanoparticles attracted a lot of attention in the scientific community.

Originally, zeolites were described as crystalline aluminosilicates of porous structure. Recently, the definition of zeolites has been extended to all the materials sharing the zeolite crystalline structure but with chemical composition considerably different from them, for example having phosphorous or only silica in their structures (Ramôa Ribeiro et al. 1995). Zeolites possess pores which are of molecular dimensions,  $< 8$  Å, which makes these materials molecular sieves. This very feature of zeolites is used in many of their applications, like hydrocarbon cracking (Weitkamp 2000), where selectivity towards the reactant size and shape is highly desirable. Another important feature is the versatility of zeolite structures available today. There is a huge number of zeolite structures that has been described in literature. The classification and approval of newly synthesized zeolites is done by the International Zeolite Association (IZA) which lists all zeolites structures known so far.

Zeolites are widely used in industry as adsorptive materials and for cracking, hydrocracking, isomerization and alkylation reactions (Weitkamp 2000). The spectrum of their applications has been extended recently for being hosts materials for nanoparticles. Entrapping metal nanoparticles inside the pores of zeolites provides a bifunctional catalyst with metal nanoparticles catalyzing the reaction and the porosity of the zeolite providing the shape-selectivity in the reaction. The shape-selective catalysis in zeolites includes the reactant shape selectivity, product shape selectivity and transition state shape selectivity. Additionally, the crystalline framework of zeolites provides a steric hindrance for nanoparticles against migration at elevated temperatures, providing stability towards sintering. This feature is desired for the reactions catalyzed by metal nanoparticles operating at high temperatures and has been applied for synthesis of sintering stable precious metal-nanoparticles.

Among many zeolites the MFI zeolites are one of the most widely used for industrial applications (Čejka et al. 2007). Silicalite-1 and ZSM-5 are examples of zeolites having MFI structure. Silicalite-1 is a purely silica material, while ZSM-5 is composed from both silica and alumina in a specific ratio. The presence of aluminum in the crystal framework affects a range of material properties, like the hydrophobic/hydrophilic surface properties, density of acid sites and their strength, and thermal and chemical stability. The MFI zeolites have well defined pore system with pore openings in the range of 0.45 – 0.6 nm

(McCusker et al. 2001). Another example of a zeolite containing silica and alumina is LTA zeolite with extremely small pore size of 0.3 – 0.45 nm (McCusker et al. 2001).

There have been many publications in the literature presenting the synthesis of heterogeneous catalysts with gold nanoparticles encapsulated inside the MFI zeolite matrix. Two different methodologies are described: bottom-up and top-down approaches. In the bottom-up approach the nanoparticles are synthesized and deposited on the silica precursor which is then used for the synthesis of the final zeolite. As a result, nanoparticles end up embedded inside the zeolite. The bottom-up synthesis was used by Højholt et al. (2011) who reported the encapsulation of small gold nanoparticles inside ZSM-5 by using 2-step process of gold-seeding of silica precursor followed by hydrothermal zeolite growth, yielding nanoparticles 3-10 nm in size located both inside and outside of zeolite crystals.

In the top-down approach, nanoparticles are “inserted” into the zeolite framework using impregnation or deposition-precipitation techniques. Mielby et al. (2014) reported gold catalyst prepared by incipient wetness impregnation method on recrystallized silicalite-1 containing mesopores. Nanoparticles of gold were 2-3 nm in size and they were exclusively incorporated inside the zeolite crystals.

The examples of methods for incorporation of nanoparticles inside the zeolite matrix described above are complicated, time consuming, involve many synthesis steps, and long waiting times. Other, more classical methods of preparation of supported nanoparticles, like incipient wetness impregnation or deposition-precipitation methods meet severe limitations when applied for MFI zeolites and gold. The possible reasons are connected with the porosity of the zeolite material limiting the diffusion of a precursor solution inside the pores, mixed hydrophobic/hydrophilic character of the surface and low isoelectric point of the  $\text{SiO}_2$  and  $\text{SiO}_2\text{-Al}_2\text{O}_3$  materials (Haruta 2003, Corma 2008). Hence, new, efficient and easy protocols for the synthesis of gold nanoparticles inside the MFI zeolites are looked for.

### **1.1.2 Encapsulation of gold, palladium and platinum nanoparticles**

The encapsulation of small gold nanoparticles inside the ZSM-5 zeolite was reported by Otto et al. (2016) who showed the formation of monodisperse Au clusters 2 nm in size within ZSM-5 crystals using the mercapto-modified one-pot hydrothermal synthesis of gold nanoparticles during the zeolite growth. Li et al. (2013) reported gold nanoparticles 7.7 nm in size encapsulated inside hollow crystals of silicalite-1. Laursen et al. (2010) showed the encapsulation of gold nanoparticles in silicalite-1 yielding nanoparticles with quite large size distribution both encapsulated and deposited on the surface of the zeolite crystals. Naknam et al. (2007) reported incipient wetness impregnation of LTA zeolite with precursors of Pt and Au yielding the respective metallic nanoparticles which were, on average, 71 nm in size. Otto et al. (2016) who reported the synthesis of monodisperse gold clusters (1-2 nm) inside the LTA framework using a one-pot ligand-assisted hydrothermal synthesis in which the chelated gold species are incorporated inside the framework during the growth of zeolite.

Several publications report the synthesis of small gold nanoparticles on amorphous mesoporous silica support. Wang et al. (2013) reported the one-pot synthesis of Au nanoparticles 4-7 nm in size trapped inside the amorphous silica network. Sakurai et al. (2013) used the modified alkaline impregnation method to synthesize silica supported gold catalyst with gold nanoparticles 4-5 nm in size. Siddiqi et al. (2015) used a precursor-improved incipient wetness impregnation to obtain gold supported on silica catalyst with nanoparticles of gold being 1.5-2 nm in size. Delannoy et al. (2006) developed a modified incipient wetness procedure with additional ammonia washing of the impregnated sample to yield gold supported on silica catalyst with gold nanoparticles of approximately 4 nm in size. Bore et al. (2005) reported impregnation of



SBA-15 and MCM-41 with gold precursor yielding catalysts with gold nanoparticles 6-4 nm in size well distributed inside the pores of a support. Selvakannan et al (2013) reported a novel tryptophan mediated method to obtain SBA-15 and MCM-41 with incorporated gold nanoparticles of 3.8 nm in size.

There is plenty of recent literature on the topic of palladium nanoparticles encapsulation in zeolitic shells or incorporation inside the zeolite matrix. Dai et al. (2015) synthesized hollow ZSM-5 nanosized crystals with bimetallic CuO-Pd and CuO-Pt nanoparticles. Wang<sup>2</sup> et al. (2016) reported the solvent-free crystallization method for palladium nanoparticles (~7 nm) encapsulated inside silicalite-1 for the selective conversion of biomass. Cui et al. (2016) presented a one-pot synthesis of Pd nanoparticles encapsulated inside the mesoporous silicalite-1 nanocrystals using a PVP stabilized palladium species. The Pd nanoparticles were ~ 3 nm in size and exhibited a great sintering stability. Similarly, Prieto et al. (2016) showed a one-pot synthesis of nanocrystalline titanium silicalite-1 with encapsulated bimetallic Pd-Au nanoparticles (~ 5 nm) as an excellent bifunctional catalyst for propylene epoxidation. Navlani-Garcia et al. (2016) reported a synthesis of Pd incorporated inside the ion-exchanged ZSM-5 and Y zeolite for the preferential CO oxidation reaction, showing great stability and increased sintering stability due to strong interactions of palladium with the support. Ding et al. (2016) reported the one-pot synthesis of Pd encapsulated ZIF-8, belonging to metal-organic framework materials. They showed the procedure for spatial distribution of palladium nanoparticles inside the ZIF-8 crystals with respect to addition time of PVP-stabilized Pd precursor. The same group in Jiang et al. (2016) reported a synthesis of Pd@ZIF-8 material showing a great dependence of the morphology of the material, size and distribution of Pd nanoparticles and catalytic activity on the synthetic parameters of ZIF-8 versus. PVP-Pd. A review published by Sadjadi et al. (2016) gives a broad overview of the research performed on encapsulation of palladium nanoparticles inside various materials used in organic synthesis.

The recent research on encapsulation of platinum nanoparticles in zeolites focuses on procedures involving a use of hollow zeolites and one-pot synthesis, similarly as already described for the case of palladium. Dai et al. (2015) reported a hollow zeolite encapsulated Ni-Pt (~ 4.5 nm) nanoparticles, for dry reforming of methane, showing an increased sintering stability and coke resistance. Li et al. (2014) presented the synthesis of hollow shells of silicalite-1 with Pt nanoparticles of about 10 nm in size being exclusively located inside the hollow crystals and showing sintering stability at elevated temperatures. Qian et al. (2013) showed the synthesis of Pt encapsulated core-shell composites with cage-like mesoporous silica shells and zeolite H-ZSM-5 cores. The catalyst was tested in oxidation of toluene showing great activity and durability in prolonged tests. Philippaerts et al. (2011) described a Pt/ZSM-5 catalyst for the selective hydrogenation of fatty acids prepared using  $\text{Pt}(\text{NH}_3)_2\text{Cl}_2$  as precursor for the wet incipient impregnation technique yielding Pt NPs  $1.7 \pm 0.8$  nm in size. Liu et al. (2016) reported the novel procedure for the generation of single Pt atoms and Pt clusters formed within purely siliceous MCM-22. The Pt species show exceptionally high thermal stability in air up to 540°C and high size-selectivity for the hydrogenation of alkanes. Gu et al. (2016) presented the synthesis of Pt/MFI obtained using a two-step approach with the preconstruction of mesopores in zeolite in which the metallic species were deposited, was followed by coverage with silicalite-1 synthesis gel and recrystallization. The Pt particles were sintering-stable in CO oxidation at 600 °C and exhibited a size-selective properties in hydrogenation reaction of nitro-aryls.

The synthesis of mixed Pd-Pt bimetallic catalysts was reported by Osman et al. (2016) and Zhou et al. (2016). The former reported the synthesis of Pd-Pt bimetallic nanoparticles incorporated in ZSM-5 crystals using the wet incipient impregnation method coupled with sonication for the low temperature total methane oxidation. The latter showed the method for synthesis of ZIF-8 doped with Pt and Pd nanoparticles (~ 4.5 nm) tested in hydrogen adsorption measurements as a potential hydrogen storage material.

## 1.2 Scope of thesis

The aim of this thesis was to develop protocols for the synthesis of sintering stable gold nanoparticles encapsulated inside the matrix of silicalite-1. The emphasis was to develop a method which is of low complexity, fast and yields gold nanoparticles small in size ( $\leq 5$  nm) encapsulated inside the pores of silicalite-1. In the course of this study two methods were designed: pressure assisted impregnation and reduction (PAIR) and *in situ* incorporation method. The description of these protocols is given below.

Decomposition of formic acid in vapor phase was chosen as a model reaction to test the catalytic activity of all materials prepared using PAIR and *in situ* incorporation methods. Suzuki cross-coupling reaction was chosen to test the activity of palladium/silicalite-1 catalysts prepared using PAIR and *in situ* incorporation. One catalyst of gold/silicalite-1 prepared using PAIR was tested for oxidation of allyl alcohol as well.

The activity of gold catalysts prepared using the PAIR method was evaluated based only on one reaction – formic acid decomposition in vapor phase. Choosing another reaction, for example in liquid phase, could give additional insight into the performance of gold catalysts prepared using PAIR. It was not done due to limited time frame of this project. The investigations of the PAIR method and *in situ* impregnation method were limited to laboratory settings; scalability has yet to be performed.

### 1.2.1 Pressure assisted impregnation and reduction – PAIR

PAIR was developed in this study to synthesize gold nanoparticles encapsulated inside the matrix of silicalite-1. This method is based on a modified incipient wetness impregnation procedure. The principle of PAIR is the impregnation and reduction under elevated pressure of the support material containing precursor solution. The PAIR method involves following general steps:

- Wet incipient impregnation of the support with precursor solution, followed by mixing and grinding in a mortar
- Impregnation of the material under the elevated pressure of nitrogen
- Fast reduction of the impregnated material under mildly elevated temperature and pressure of hydrogen

The overview of the PAIR procedure is shown in Figure 1.1 together with comparison to the impregnation procedure (IM) used in this study. The principle of the PAIR method is to force the migration of the precursor solution into the pores of the zeolite by applying external pressure of inert gas which will not cause any precipitation of gold species or undergo any reaction with either the precursor solution or the zeolite itself. The next step is the fast reduction under elevated pressure of hydrogen (20 min of heating ramp) to reach a mild reduction temperature of 150 °C in order to ensure the limited sintering possibility of metal nanoparticles forming in the pores of a zeolite. For comparison, in the impregnation procedure, the catalyst is reduced in the hydrogen flow (1 bar) at 350 °C for 2 h, as shown in Figure 1.1.

The PAIR procedure was primarily applied to yield silicalite-1 with incorporated gold nanoparticles. Two different gold precursors ( $\text{HAuCl}_4 \cdot 3\text{H}_2\text{O}$ ,  $\text{AuCl}_3$ ), four different solvents (water, methanol, acetonitrile, 1-butanol), and two different solvent volumes (0.3 ml, 0.15 ml) were used to study the synthesis conditions of the PAIR method. The scope of the method was extended further for gold in ZSM-5, LTA and amorphous mesoporous silica, and palladium and platinum in silicalite-1. The experimental results are shown in Chapter 4. Chapter 4 also contains theoretical investigations behind the PAIR procedure.

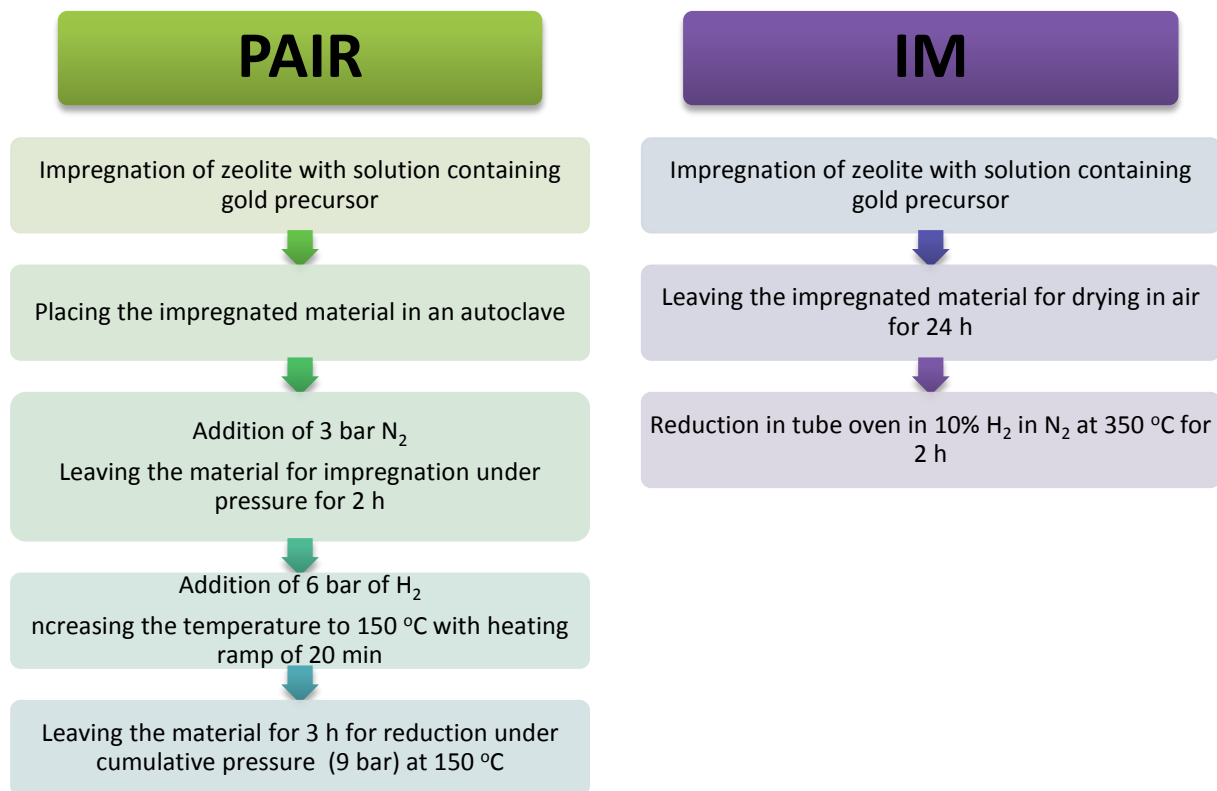


Figure 1.1 Schematic comparison of the PAIR and impregnation (IM) methodologies used in this study.

### 1.2.2 *In situ* incorporation method

The *in situ* incorporation is a one-pot method developed in order to encapsulate metal nanoparticles inside silicalite-1 channels during the growth of the zeolite crystals. It was based on the work published by Wang et al. (2016). In principle, the solution containing metal precursor in a form of ethylenediamine complex is added to the zeolite synthesis gel and subjected to hydrothermal synthesis conditions for 4 days. During the hydrothermal synthesis, simultaneous growth of the zeolite crystals and incorporation of the metal complex into the zeolite framework occurs. In this way nanoparticles will be formed inside the matrix of silicalite-1. After the crystallization is over, the product is separated, washed, calcined in air at 550 °C for 8 h and subjected to flow of 10% H<sub>2</sub> in N<sub>2</sub> at 350 °C for 2h for reduction of the metal complex to metal nanoparticles. The scheme of the *in situ* incorporation procedure is presented in Figure 1.2. The mechanism of this process has not been investigated yet; however, the present study comprises experiments which characterize the process to some extent.

The *in situ* incorporation method was applied to yield palladium, platinum, gold and bimetallic palladium-platinum nanoparticles incorporated into silicalite-1. The metals were introduced to the zeolite synthesis gel in a form of chloro-ethylenediamine complexes. The choice of ethylenediamine as ligand was adapted from the original work of Wang et al. (2016). The results from this study are given in Chapter 5.



**Figure 1.2.** Schematic representation of the *in situ* incorporation methodology used in this study for the synthesis of metal nanoparticles encapsulated inside silicalite-1.

### 1.3 Thesis overview

This thesis is composed of eight chapters and one appendix. Chapter 1 was presenting the background of the project and the scope of this thesis. Chapter 2 contains brief description of analytical methods used for characterization of materials synthesized in this study. Chapter 3 gives all experimental details about the synthesis of materials described in this study. Chapter 4 contains results from applying the PAIR method for encapsulation of gold nanoparticles inside silicalite-1. Chapter 5 presents the results from *in situ* incorporation of nanoparticles into silicalite-1. Chapter 6 covers the formic acid decomposition over catalysts synthesized using the PAIR method and *in situ* incorporation method. Chapter 7 contains results from Suzuki cross-coupling over palladium/silicalite-1 catalysts synthesized using PAIR and *in situ* incorporation method. Chapter 8 presents the investigation on allyl alcohol oxidation over gold catalyst prepared using the PAIR method and gold supported on titania. Finally, Chapter 9 provides the conclusion from the performed work. Appendix A lists my publications and disseminations.



## Chapter 2

### Methods

In this chapter, the analytical methods used for characterization of the prepared catalysts are described briefly. The purpose of the analyses and the equipment used in this study are provided as well.

#### 2.1 Transmission electron microscopy (TEM)

TEM is an analytical technique used to determine the morphology of the specimen. The principle of TEM is the same as of light microscope with the difference that TEM uses electrons instead of light. Since the wavelength of electrons is much smaller than of light the resolution achieved by TEM is much higher than for the light microscope, and in some cases can reveal detail on the atomic scale. In a TEM analysis the beam of electrons is generated in the electron gun chamber and travels along the microscope through a set of electromagnetic lenses to reach a very thin specimen. After passing through the specimen, the beam reaches the CCD camera where the signal can be transformed into the pixel image. Due to electron scattering occurring in the specimen, the crystal structure and analytical composition of the sample can be determined. For the latter such methods as Energy Dispersive X-ray Spectroscopy (EDXS) and Electron Energy Loss Spectroscopy (EELS) are used (Goodhew et al. 2001).

In the present study, TEM analysis was used to investigate the morphology of the prepared catalysts – size and shape of metal nanoparticles, crystallinity and possible damage of a zeolite support. From the images, the particle size distribution was calculated based on measurement of diameter of nanoparticles. FEI Tecnai T20 G2 microscope operating at 200 eV was used for the analysis. Specimens were prepared from powder samples on copper grids covered with holey carbon.

#### 2.2 Scanning transmission electron microscopy (STEM)

STEM is a type of TEM in which the electron beam is focused in a probe onto a specimen (Goodhew et al. 2001). This probe is scanned over the specimen in a raster and the transmitted signal is transformed into a pixel image. Scanning the probe in raster makes it possible to use STEM for analytical mapping of the sample. EDXS, EELS and High-Angle Annular Dark Field (HAADF) can be used for this purpose. HAADF is a particularly useful tool when it comes to analysis of specimen containing high atomic number elements. It produces images where the contrast is directly related to the atomic number/s of element/s present in the sample – the higher the atomic number of the element the brighter it appears in the image (reverse to TEM).

STEM was used in this study to view selected catalysts prepared using *in situ* incorporation method. HAADF detector was used to compose a dark-field image of the sample. EDXS analysis was applied for chemical mapping of the samples in order to determine a distribution of palladium and platinum nanoparticles inside the zeolite crystals. FEI Titan Analytical 80-300ST TEM operating at 100 eV or 300 eV was used for the analysis. Specimens were prepared from powder samples on holey carbon copper grids.

### 2.3 Nitrogen physisorption

Nitrogen physisorption is a powerful technique used for characterization of porous solids. Parameters like surface area, pore volume and pore size distribution are possible to determine using this technique. The principle of nitrogen physisorption is a controlled adsorption of gaseous nitrogen on the surface of a solid material. In a typical experiment a solid sample is outgassed at elevated temperatures in vacuum and/or flowing gas (usually helium) in order to remove any pre-adsorbed species coming from the atmosphere. Then the specimen is cooled down to cryogenic temperature under vacuum and gaseous nitrogen is admitted in controlled doses. After each dose, the pressure in the sample chamber is allowed to equilibrate and the amount of adsorbed gas is calculated. The amount of gas adsorbed at each pressure gives rise to adsorption isotherm, which defines the amount of nitrogen necessary to form a monolayer over the external surface and the pores of the solid specimen. From the shape of adsorption isotherm the surface area, pore size, pore volume, pore area and pore shape can be determined (Thommes 2010).

In the present study, nitrogen physisorption measurements were used to characterize the porosity of the synthesized zeolites and catalysts. Total pore volume, micropore volume, external surface area, and BET area were obtained from this analysis. All the measurements were carried out on ASAP 2020 Micromeritics at temperature of liquid nitrogen. Prior to analysis samples were outgassed in vacuum at 200 °C for 12 h. Total pore volume was calculated from the isotherm adsorption branch at  $p/p_0 = 0.95$ . Micropore volume and external surface area were calculated using the t-plot method. BET surface area was calculated using the BET method.

### 2.4 X-ray diffraction (XRD)

XRD is an analytical technique used to address all issues related to crystal structure of solids. Parameters like lattice constants and geometry, identification of unknown materials, defects, stresses, etc. are possible to detect and analyze using this technique (Cao 2004). In a typical experiment, a collimated beam of X-rays is incident on a specimen and is diffracted by the crystalline phases in the specimen. The intensity of scattering is measured as a function of diffraction angle, giving rise to a diffraction pattern. The obtained diffraction pattern is used to identify the crystalline phases in the sample. The analysis is based on peak positions which are compared to those from standard data.

In this study, the XRD technique was used to confirm the crystallinity of zeolite supports and the presence of metal nanoparticles in the samples. The measurements were performed on Huber G670 with  $\text{CuK}_{\alpha 1}$  radiation from a focusing quartz monochromator. The diffraction patterns were recorded for 10 min at room temperature at  $2\theta$  intervals of  $3^\circ - 100^\circ$ . The obtained diffraction patterns were analyzed based on comparison with JCPDS indexes.

### 2.5 X-ray photoelectron spectroscopy (XPS)

XPS is a technique used for analyzing the surface chemistry of a material. Information like elemental composition, empirical formula, chemical state or electronic state can be obtained from the XPS spectrum. During the analysis, a specimen is irradiated by X-ray beam under very small angle which causes the emission of photoelectrons from only down to 10 nm below the surface. The kinetic energy of these

photoelectrons is measured and the XPS spectrum is recorded by counting the emitted electrons over the range of kinetic energies. The appearing peaks refer to atoms which emit electrons of a particular characteristic energy. The energies of these peaks are the basis for identification of the specimen composition and quantification (Wagner et al. 1979).

In this study, the XPS technique was used for selected samples to check the deposition of metal nanoparticles on the external surface of zeolites and confirm their chemical composition. The analysis was performed on XPS-ThermoScientific apparatus operating with Al K $\alpha$  radiation under ultra-high vacuum ( $2 \cdot 10^{-10}$  mbar).

## **2.6 X-ray fluorescence (XRF)**

XRF is an analytical technique used to determine the chemical composition of a specimen. During the measurement, the sample is irradiated by an X-ray beam which causes emission of fluorescent X-rays with discrete energies characteristic of the elements present in the specimen. The recorded spectrum serves as a basis for qualitative and quantitative analysis of the sample (Beckhoff et al. 2006).

In the presented study, the XPS analysis was used to determine the wt% loading of palladium and platinum in catalysts prepared by the *in situ* incorporation method. The measurement was carried out on PANalytical Epsilon3-XL machine equipped with high resolution silicon drift detector (SDD) and X-ray tube excitation (Rh, Ag, Mo anode materials, 20 kV, 100  $\mu$ A). Catalysts were tested as powders. The metal loading in the samples was calculated from calibration lines.

## **2.7 Temperature programmed reduction (TPR)**

TPR technique is used to characterize solid materials in terms of number of reducible species present in the specimen and their reduction temperature. In a typical experiment, the sample is exposed to the flow of analysis gas which is typically hydrogen in argon or nitrogen, while the temperature of the sample is increased linearly with time. The uptake of hydrogen is monitored as a function of temperature of the specimen. The consumption of hydrogen occurs at every specific temperature at which the reduction of a specie takes place (Webb 2003).

In this study, the TPR measurements were used to determine the reduction temperature of different gold precursors dissolved in different solvents and to confirm the total reduction of gold species at the end of the PAIR procedure. The Micrometrics Autochem-II apparatus was used for the analysis. Samples were heated from 30 °C to 300 °C with a heating ramp of 10 °C/min in reducing gas mixture of 4% H<sub>2</sub> in Ar. Water formed during analysis was captured in a dry ice cold trap.

## **2.8 Attenuated Total Reflection (ATR)**

ATR is a sampling method used in infrared spectroscopy (IR) in which the sample is analyzed directly without any preparation procedures. In the typical experiment, the IR beam is directed with a certain angle onto a crystal with a high refractive index, e.g. diamond. The beam is reflected in the crystal in a way that it exceeds beyond the surface of the crystal into a specimen which is placed on the crystal. The beam interacts with the specimen and where the sample absorbs energy, the reflected beam is attenuated. Then, it returns to the crystal, exits on the opposite side and heads to a detector. The changes in the IR beam are recorded and based on this an IR spectrum is composed. Qualitative and quantitative analysis can be performed based on the obtained spectrum. The main advantage of this method is the minimal sample preparation - sample is simply placed on a crystal, and analysis of specimens in their natural states – no need of pressing a sample into pellet, heating or grinding (Stuart 2005).



In this study the ATR technique was used to investigate for the presence of residual solvents left after the synthesis in the selected catalysts prepared using PAIR. The Nicolet iS5 spectrometer with ATR-cell with diamond top plate was used for the analysis. Catalysts were tested as powders in air at room temperature.

## Chapter 3

### Synthesis of materials

This chapter provides details about the synthesis of materials used in this study. The synthesis of zeolites – silicalite-1, LTA and ZSM-5, used as support for metal nanoparticles are described. The three protocols of introduction of metal nanoparticles into the pores of zeolites are described, being the PAIR method, the *in situ* incorporation method and impregnation method, all described in Chapter 1. These methods were applied to synthesize gold, palladium and platinum nanoparticles encapsulated inside the matrix of zeolites.

### 3.1 Zeolite preparation

The experimental details for the synthesis of silicalite-1, LTA and ZSM-5 zeolites are presented in this section. Additionally, the procedure for ion exchange ( $\text{Na}^+ \rightarrow \text{H}^+$ ) applied to LTA and ZSM-5 is described.

#### 3.1.1 Materials

Materials used for the zeolite synthesis: tetraethylorthosilicate (TEOS, > 99.0% Sigma Aldrich), tetrapropylammonium hydroxide (TPAOH, 1 M aqueous solution, Sigma Aldrich), sodium aluminate anhydrous ( $\text{NaAlO}_2$ , solid, technical, Sigma Aldrich), sodium metasilicate pentahydrate ( $\text{Na}_2\text{SiO}_3 \cdot 5\text{H}_2\text{O}$ , solid, > 95% Aldrich), sodium hydroxide (NaOH, solid, > 98% Fluka), ammonium nitrate ( $\text{NH}_4\text{NO}_3$ , solid,  $\geq 99.5\%$ , Sigma Aldrich). All the materials were used as received without any further purification.

#### 3.1.2 Synthesis of silicalite-1

Tetraethyl orthosilicate (8.3 ml) was added dropwise to a tetrapropylammonium hydroxide solution (13.3 ml) under stirring in a Teflon beaker. The mixture was stirred for 1 hour and then heated in a Teflon-lined stainless steel autoclave at 180 °C for 24 h under autogenous pressure. The product was collected by filtration, thoroughly washed with water until pH 7, dried at room temperature and then calcined for 10 h at 550 °C with a heating ramp of 2 h.

#### 3.1.3 Synthesis of LTA

Sodium aluminate (3.6 g) and sodium metasilicate (7.8 g) were separately dissolved in 20 ml of 1% sodium hydroxide in PE bottles (100 ml) and left on a shaking table for 20 min until homogeneous solutions were formed. Then, the solution of sodium metasilicate was quickly poured into the solution of sodium

aluminate and shaken until homogeneity in the closed bottle. The mixture was then placed in an oven for 20 h at 95 °C. The product was collected by filtration, thoroughly washed with water until pH 9, and dried in air for 24 h.

### 3.1.4 Synthesis of ZSM-5

Tetraethyl orthosilicate (8.3 ml) was added dropwise to the tetrapropylammonium hydroxide solution (13.3 ml) containing 0.15 g of sodium aluminate under stirring in a Teflon beaker (Si/Al = 40). The mixture was stirred for 1 hour and then heated in a Teflon-lined stainless steel autoclave at 180 °C for 24 h under autogenous pressure. The product was collected by filtration, thoroughly washed with water until pH 7, dried at room temperature and then calcined for 10 h at 550 °C with a heating ramp of 2h.

### 3.1.5 General procedure for ion exchange

The 1.00 g of zeolite was suspended in 80 ml 1 M NH<sub>4</sub>NO<sub>3</sub>, heated to 80 °C and stirred for 2 hours. Then, solid was separated by centrifugation (5 min, 3900 rpm) and washed three times with water with centrifugation between each wash. The entire procedure was repeated 3 times. The final product was collected, dried in air for 24 h and calcined in air for 10 h at 550 °C with a heating ramp of 2h.

## 3.2 Synthesis of zeolite supported metal nanoparticles

The procedures of the impregnation method, the PAIR method and *in situ* incorporation method are all described in this section. The impregnation method was primarily used to synthesize reference materials for the assessment of the PAIR method. The PAIR method was primarily used for the synthesis of gold nanoparticles encapsulated inside the pores of silicalite-1. The study was extended for the synthesis of gold nanoparticles encapsulated inside LTA, ZSM-5, and amorphous mesoporous silica, and palladium and platinum nanoparticles encapsulated inside silicalite-1. For each metal, different precursors were tried. The precursors are listed in Table 3.1. Different solvents were used - water, methanol, acetonitrile and 1-butanol. Two different volumes of solvents were used – 0.3 ml and 0.15 ml, for the preparation of metal precursor solution used for impregnation of the support in the PAIR method and impregnation method. The *in situ* incorporation method was applied in three different cases to synthesize such materials:

- Mono metallic Au, Pd or Pt nanoparticles in silicalite-1;
- Bi-metallic PdPt nanoparticles in silicalite-1 where nanoparticles of palladium and platinum are incorporated randomly inside the zeolite crystals;
- Bi-metallic PtPd nanoparticles in silicalite-1 where nanoparticles of platinum and palladium are incorporated in separate layers inside zeolite crystals;

The synthesis protocols for all three kinds of materials listed above are described separately in the following sections. The overview of the samples prepared with the respective methods and the applied synthesis conditions are gathered in Table 3.1.

**Table 3.1. Overview of the synthesis conditions used for preparation of samples described in this study.**

Method	Support	Volume of solvent / 0.99 g support (ml)	Solvents used	Precursors used
<b>Impregnation</b>	Silicalite-1	0.15, 0.3	water, methanol, acetonitrile, 1-butanol	HAuCl <sub>4</sub> ·3H <sub>2</sub> O, AuCl <sub>3</sub>
	Silica	0.15	water	HAuCl <sub>4</sub> ·3H <sub>2</sub> O
<b>PAIR</b>	Silicalite-1	0.15, 0.3	water, methanol, acetonitrile, 1-butanol	HAuCl <sub>4</sub> ·3H <sub>2</sub> O, AuCl <sub>3</sub> , Pd(NO <sub>3</sub> ) <sub>2</sub> ·2H <sub>2</sub> O, PdCl <sub>2</sub> , HPtCl <sub>6</sub> ·6H <sub>2</sub> O, PtCl <sub>4</sub> , PtCl <sub>2</sub>
	LTA	0.2	water, acetonitrile	HAuCl <sub>4</sub> ·3H <sub>2</sub> O
	ZSM-5	0.3	water	HAuCl <sub>4</sub> ·3H <sub>2</sub> O
	Silica	0.15	water	HAuCl <sub>4</sub> ·3H <sub>2</sub> O
<b>In situ incorporation</b>	Silicalite-1	-	-	AuCl <sub>3</sub> , PtCl <sub>4</sub> , PtCl <sub>2</sub> , PdCl <sub>2</sub>

### 3.2.1 Materials

Chemicals used for the preparation of zeolite supported metal nanoparticles: chloroauric acid (III) trihydrate (HAuCl<sub>4</sub>·3H<sub>2</sub>O, 99.9%, Aldrich), gold (III) chloride (AuCl<sub>3</sub>, ≥ 99.99% Aldrich), palladium nitrate dihydrate (Pd(NO<sub>3</sub>)<sub>2</sub>·2H<sub>2</sub>O, ~ 40% Pd basis, Aldrich), palladium (II) chloride (PdCl<sub>2</sub>, 99% Aldrich), chloroplatinic acid (VI) hexahydrate (HPtCl<sub>6</sub>·6H<sub>2</sub>O, ≥ 37.5% Fluka), platinum (IV) chloride (PtCl<sub>4</sub>, ≥ 99.99% Aldrich), platinum (II) chloride (PtCl<sub>2</sub>, ≥ 99.9% Aldrich), ethylenediamine (NH<sub>2</sub>CH<sub>2</sub>CH<sub>2</sub>NH<sub>2</sub> ≥ 99% Sigma Aldrich), acetonitrile (ACN, ≥ 99.9% Riedel-de Haën), methanol (MeOH, ≥ 99.9% Riedel-de Haën), 1-butanol (≥ 99.7% Riedel-de Haën), silica (Saint-Gobain Norpro), 10% H<sub>2</sub> in N<sub>2</sub> (AGA). Zeolites silicalite-1, LTA, and ZSM-5 were used as synthesized (according to 3.1 Zeolite preparation).

### 3.2.2 General procedure for the impregnation method

The support material (0.99 g) was impregnated with solution containing metal precursor corresponding to 1 wt% loading, according to data given in Table 3.1 and Table 3.2. The material was dried at room temperature overnight and then reduced in 10% H<sub>2</sub> in N<sub>2</sub> at 350 °C for 2 h with a heating ramp of 5 °C/min. The samples obtained from this procedure were named M\_IM (M corresponding to a metal name).

### 3.2.3 General procedure for the PAIR method

The support material (0.99 g) was impregnated with solution containing metal precursor corresponding to 1 wt% loading, according to data presented in Table 3.1 and Table 3.2. The material was then placed in the Teflon-lined stainless steel autoclave under 3 bar N<sub>2</sub> for 2 h for pressure assisted impregnation. Then, 6 bar of H<sub>2</sub> was added and the material was reduced under cumulative 9 bar pressure at 150 °C for 3 h. The material was left in the autoclave overnight to ensure a full reduction of gold species. The samples obtained from this procedure were named M\_PAIR (M corresponding to a metal name).

**Table 3.2. Masses of metal precursors corresponding to 1 wt% loading per 0.99 g of support used in the synthesis of zeolite supported metal nanoparticles using the PAIR method and impregnation method.**

Precursor	Mass corresponding to 1 wt% of metal / 0.99 g support (g)
$\text{HAuCl}_4 \cdot 3\text{H}_2\text{O}$	0.020
$\text{AuCl}_3$	0.015
$\text{Pd}(\text{NO}_3)_2 \cdot 2\text{H}_2\text{O}$	0.025
$\text{PdCl}_2$	0.016
$\text{HPtCl}_6 \cdot 6\text{H}_2\text{O}$	0.021
$\text{PtCl}_4$	0.017
$\text{PtCl}_2$	0.014

### 3.2.4 General procedure for the *in situ* incorporation method

#### *Procedure for single metal nanoparticles incorporated in silicalite-1*

The zeolite mixture was prepared by, first, mixing in a Teflon beaker 9.2 ml of deionized water with 16.2 g of TPAOH, followed by stirring (500 rpm) for 10 min. Then, 8.32 g of TEOS was added and the mixture was left for 6 h under stirring. In the meantime, the solution of metal precursor was prepared by mixing 0.28 mmol of metal precursor, according to Table 3.3, with 3 ml of water and 0.3 ml of ethylenediamine. The resulted solution was added dropwise to the zeolite synthesis mixture and left under stirring for 30 min. Finally, the mixture was transferred to the Teflon-lined stainless steel autoclave (without a magnetic stirrer!) and left for 4 days at 170 °C under static conditions. The collected solid product was separated by centrifugation for 5 min at 12000 rpm, washed four times with 50% ethanol in water, and left overnight in the oven for drying at 80 °C. Next, the powder was calcined in air at 550 °C for 8 h, followed by reduction in 10%  $\text{H}_2$  in  $\text{N}_2$  at 350 °C for 2 h.

**Table 3.3. Details of synthesis of single metal nanoparticles encapsulated in silicalite-1 prepared by the *in situ* incorporation method.**

Precursor	Mass introduced (g)	Amount of metal (mmol)	Amount of water (ml)	Amount of ethylenediamine (ml)
$\text{AuCl}_3$	0.055	0.28	3	0.3
$\text{PdCl}_2$	0.050			
$\text{PtCl}_4$	0.094			
$\text{PtCl}_2$	0.074			

#### *Procedure for bi-metallic PdPt nanoparticles randomly incorporated in silicalite-1*

The zeolite mixture was prepared by first mixing in a Teflon beaker 9.2 ml of deionized water with 16.2 g of TPAOH, followed by stirring (500 rpm) for 10 min. Then, 8.32 g of TEOS was added and the mixture was left for 6 h under stirring. In the meantime, solutions of metal precursors of Pd and Pt were prepared by separately mixing 0.14 mmol of  $\text{PdCl}_2$  and  $\text{PtCl}_4$  with 1.5 ml of water and 0.15 ml of ethylenediamine, as given in Table 3.4. First, the solution containing Pd was added dropwise to the zeolite

synthesis mixture and left for 30 min under stirring. Next, the Pt solution was added dropwise to the synthesis mixture and again left under stirring for 30 min. Finally, the mixture was transferred to the Teflon-lined stainless steel autoclave (without a magnetic stirrer!) and left for 4 days at 170 °C under static conditions. The collected solid product was separated by centrifugation for 5 min at 12000 rpm, washed four times with 50% ethanol in water, and left overnight in the oven for drying at 80 °C. Next, the powder was calcined in air at 550 °C for 8 h, followed by reduction in 10% H<sub>2</sub> in N<sub>2</sub> at 350 °C for 2 h.

**Table 3.4. Details of synthesis of bi-metallic PdPt nanoparticles incorporated randomly into silicalite-1 prepared by the *in situ* incorporation method.**

Precursor	Mass introduced (g)	Amount of metal (mmol)	Amount of water (ml)	Amount of ethylenediamine (ml)
PdCl <sub>2</sub>	0.025	0.14	1.5	0.15
PtCl <sub>4</sub>	0.047			

#### ***Procedure for bi-metallic PtPd nanoparticles incorporated in layers inside silicalite-1***

The procedure for bi-metallic PtPd incorporation where Pt and Pd nanoparticles are incorporated in separate layers inside silicalite-1 crystals was used to synthesize two kinds of materials with different metal loading and different times of crystallization applied after adding the first metal to a zeolite synthesis mixture. The first material was prepared with 0.11 mmol of metal precursor and left for 6 h for first crystallization. The second material was prepared with 0.07 mmol of metal precursor and left for 4 h for the first crystallization. Details of experimental procedure are given in Table 3.5 and described below.

**Table 3.5. Details of synthesis of bi-metallic PtPd nanoparticles incorporated in layers inside silicalite-1 prepared by the *in situ* incorporation method.**

Material	Amount of metal (mmol)	Amount of precursor (g)	Time of 1 <sup>st</sup> crystallization	Amount of water (ml)	Amount of ethylenediamine (ml)
PtPd/S-1_1	0.11	0.038	6 h	1.2	0.12
PtPd/S-1_2	0.07	0.024	4 h	0.75	0.075

The zeolite mixture was prepared by first mixing in a Teflon beaker 9.2 ml of deionized water with 16.2 g of TPAOH, followed by stirring (500 rpm) for 10 min. Then, 8.32 g of TEOS was added and the mixture was left for 6 h under stirring. In the meantime, the solution of metal precursor of Pt was prepared by mixing 0.11 mmol or 0.07 mmol of PtCl<sub>4</sub> with 1.2 ml of water and 0.12 ml of ethylenediamine or 0.75 ml water and 0.075 ml ethylenediamine. The solution of Pt was added dropwise to the zeolite synthesis mixture and left for 30 min under stirring. Next, the mixture was transferred to the Teflon-lined stainless steel autoclave (without a magnetic stirrer!) and placed in the oven at 170 °C under static conditions for 6 h or 4 h. After this time, the autoclave was cooled down in water to room temperature, opened, and the synthesis mixture was subjected to stirring for 5 min. In the meantime, the solution containing Pd was prepared by adding 0.11 mmol or 0.07 mmol of PdCl<sub>2</sub> to 1.2 ml of water and 0.12 ml of ethylenediamine or 0.75 ml water and 0.075 ml ethylenediamine. The Pd solution was added dropwise to the synthesis mixture and left under stirring for 30 min. Finally, the autoclave was closed again (without a magnetic stirrer!) and placed in

the oven at 170 °C for 4 days. After that, the collected solid product was separated by centrifugation for 5 min at 12000 rpm, washed four times with 50% ethanol in water, and left overnight for drying at 80 °C in the oven. Next, the powder was calcined in air at 550 °C for 8 h, followed by reduction in 10% H<sub>2</sub> in N<sub>2</sub> at 350 °C for 2 h.

## Chapter 4

### Pressure assisted impregnation and reduction – PAIR

In this chapter, the results from applying the PAIR method to produce gold incorporated silicalite-1 materials according to protocol described in Chapter 3 are presented. The scope of the PAIR method was investigated with respect to different precursors ( $\text{HAuCl}_4 \cdot 3\text{H}_2\text{O}$ ,  $\text{AuCl}_3$ ), volume of solvent (0.15 ml, 0.3 ml), the kind of solvent (water, methanol, acetonitrile, 1-butanol), type of zeolite (ZSM-5, LTA), and metal (palladium, platinum) used in the synthesis. The success criteria were the size of nanoparticles in the final product and their distribution inside or outside the support material. The materials synthesized using the PAIR method on silicalite-1 were compared with the materials prepared using the impregnation method for the same set of conditions.

All prepared catalysts were analyzed by nitrogen physisorption, XRD, TEM, and XPS, if relevant. The size of nanoparticles was estimated based on the TEM images. In each case 200 nanoparticles were measured. Based on these the average particle size and the particle size distribution were calculated. The mean value and standard deviation were calculated from the particle size distribution using the Gaussian distribution as approximation. Generally, the mean value is used in the discussion of results and the average value is brought to discussion when relevant. The mean particle size refers to the  $x$  value of a peak of Gaussian distribution of the particle size. It reflects the size of particles that are most abundant in the sample, neglecting the sizes at each end of the distribution. The average particle size takes into account all measured particles regardless of their size normalizing them with respect to the number of particles. In case the particles in a sample are mostly very small (2-3 nm) with a fraction of particles that are much larger (> 10 nm) then the mean number calculated from this distribution will underestimate the presence of large particles, while the average number will overestimate them. If both numbers are similar it means that the sizes of particles do not vary much. However, if the two numbers are much different from each other, it is an indication that both large and small nanoparticles are abundant in the sample.

In order to describe the sample with the most accuracy, both numbers should be taken into account since they carry complementary information. However, it has to be kept in mind that measurements of nanoparticles from TEM images carry large error arising from limited resolution possible to achieve during the analysis and an error connected with the precision of human eye in estimating the border of the nanoparticle during the measurement on a computer screen. These results should be treated as approximate, and interpreted together with results from other analytical techniques.



The sintering stability of gold nanoparticles encapsulated inside silicalite-1 was investigated for selected catalysts by exposing the sample either to additional reduction in 10% H<sub>2</sub> in N<sub>2</sub> at 350 °C for 2 h or to calcination in air at 400 °C for 2 h. The aim was to facilitate the migration of gold nanoparticles and possible agglomeration into larger nanoparticles occurring at elevated temperatures (Hansen et al. 2013). This served as a basis to relate the sintering stability with entrapment of nanoparticles inside the crystal framework of silicalite-1.

The following sections describe the results from the parametric study performed on the PAIR method in the order:

- PAIR method applied to gold in silicalite-1
  - HAuCl<sub>4</sub> + 0.15 ml water
  - HAuCl<sub>4</sub> + 0.3 ml solvent (water, methanol, acetonitrile)
  - AuCl<sub>3</sub> + 0.3 ml solvent (water, methanol, acetonitrile, 1-butanol)
- PAIR method applied to gold in LTA and ZSM-5
- PAIR method applied to palladium and platinum in silicalite-1
- PAIR method applied to non-zeolitic support
  - Amorphous mesoporous silica
- Study of conditions of the PAIR method

At the end of the chapter, the general discussion of applying the PAIR method for synthesis of zeolite encapsulated metal nanoparticles is performed individually in 5.6 *General discussion* for each set of parameters: volume of a solvent, choice of a solvent, choice of a precursor and choice of a zeolite. A theoretical consideration of the PAIR method is terms of diffusion of liquids in porous materials, wettability of solvents and their contact angles on different surfaces, capillary forces and size of solvated ions is attempted. Finally, the overall evaluation of the PAIR method and a conclusion are provided.

#### 4.1 PAIR method applied to gold in silicalite-1

Two kinds of precursors were investigated – HAuCl<sub>4</sub>·3H<sub>2</sub>O and AuCl<sub>3</sub>. The choice was based on the acidity of their solutions. The pH of the aqueous impregnation solution prepared with HAuCl<sub>4</sub>·3H<sub>2</sub>O was approximately zero (measured with lakmus pH paper) while for solution of AuCl<sub>3</sub> it was approximately 2.

For the volume of solvent, two values were chosen – 0.15 ml and 0.3 ml. The former being close to the pore volume determined for synthesized silicalite-1 from the nitrogen physisorption analysis (~ 0.176 cm<sup>3</sup>/g), to ensure the full adsorption of the liquid by the support material. The latter was chosen to produce a precursor solution with lower concentration of gold salt.

The solvents used in the study were chosen based on their protic/aprotic polar/apolar character. The idea behind was to select solvents that can easily dissolve a gold salt but also interact well and easily diffuse into a hydrophobic material which is silicalite-1. The synthesis of gold nanoparticle encapsulated silicalite-1 by the PAIR method was performed with the use of water, acetonitrile, methanol and 1-butanol as solvents. Water, methanol and 1-butanol are polar protic solvents while acetonitrile is a polar aprotic solvent. The protic properties of these solvents decrease in the order: water > methanol > 1-butanol > acetonitrile (Clayden et al. 2001).

#### 4.1.1 Synthesis conditions: $\text{HAuCl}_4 \cdot 3\text{H}_2\text{O}$ + 0.15 ml water

In this set of experiments, the PAIR method was compared with the impregnation method (see Chapter 3, section 3.2.2 *General procedure for impregnation method* and 3.2.3 *General procedure for the PAIR method* for synthesis details) for introducing the metal nanoparticles into/onto the support (nanoparticles can end up either on the external surface or inside the pores of the zeolite). The experiments were performed with  $\text{HAuCl}_4 \cdot 3\text{H}_2\text{O}$  as gold precursor dissolved in 0.15 ml of water and used for impregnation of 0.99 g of silicalite-1. Additionally, the as prepared catalysts were subjected to calcination (denoted as 'C' in the catalyst name) in air at 400 °C for 2 h in order to analyze the sintering stability of gold nanoparticles. The overview of the prepared catalysts is shown in Table 4.1. The characterization of the synthesized catalysts was performed by nitrogen physisorption, XRD and TEM techniques. The results are presented in Table 4.2, Figure 4.1 and Figure 4.2.

**Table 4.1.** The overview of gold in silicalite-1 catalysts prepared by the PAIR method and impregnation method using 0.15 ml of water as solvent and  $\text{HAuCl}_4 \cdot 3\text{H}_2\text{O}$  as a precursor, both subjected to additional calcination in air at 400 °C for 2 h.

Catalyst name	Treatment
Au/S-1_PAIR	PAIR
Au/S-1_PAIR_C	PAIR+ calcination in air at 400 °C for 2 h
Au/S-1_IM	Impregnation
Au/S-1_IM_C	Impregnation + calcination in air at 400 °C for 2 h

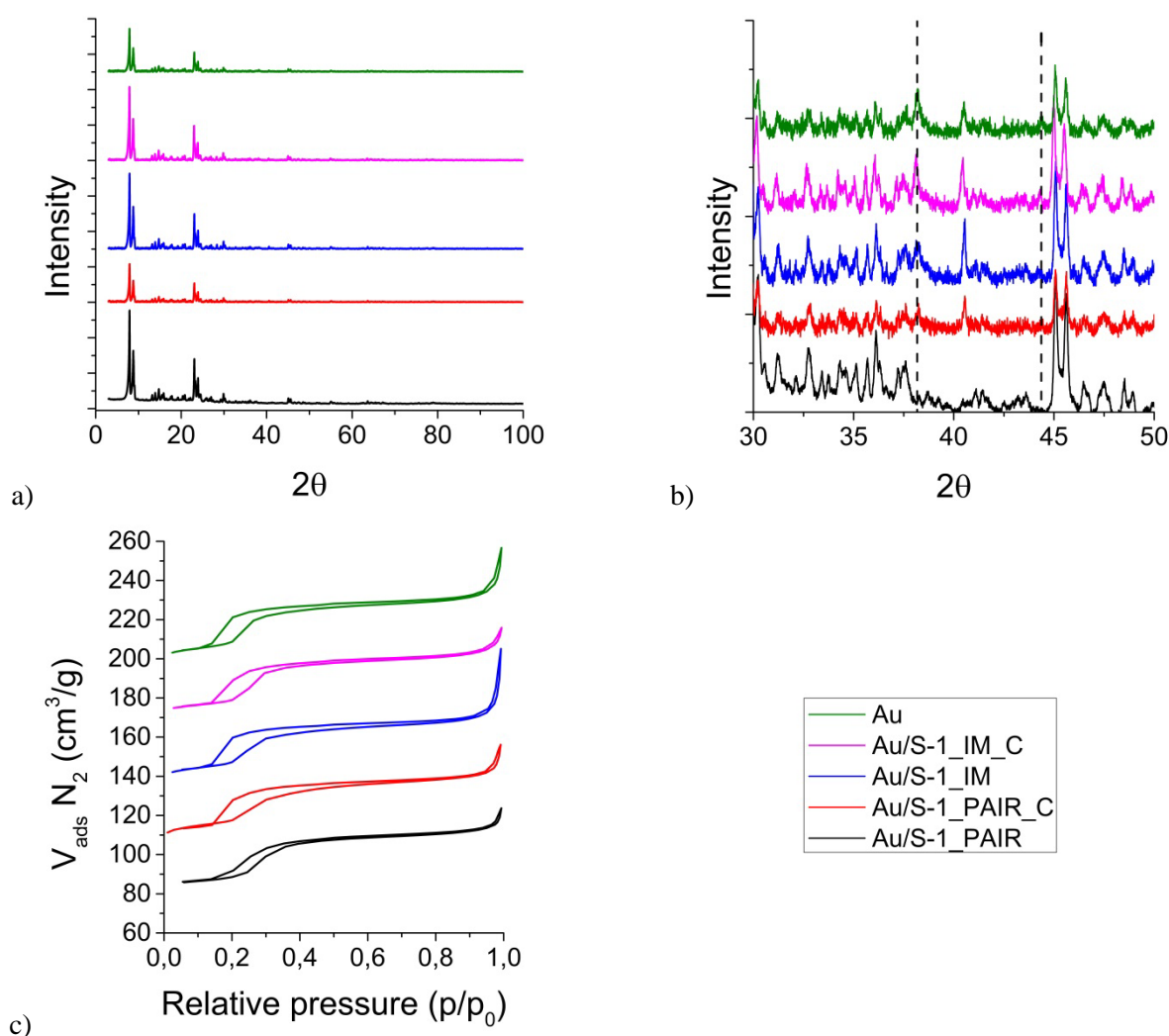
The XRD diffractograms of the synthesized catalysts are shown in Figure 4.1a. The crystalline phase was characterized as silicalite-1 by comparison with the JCPDS 040-19-6968 standard data. In the zoomed-in diffractogram showed in Figure 4.1b, the characteristic gold reflexes at  $2\theta = 38.17$  and  $2\theta = 44.37$  (JCPDS 010-71-4616) are visible for all the investigated catalysts, confirming the presence of gold in all samples.

The results from the nitrogen physisorption performed for all four catalysts are shown in Table 4.2. The values of the total pore volume did not change much between the parent material and the gold catalysts. However, the micropore volume decreased significantly what could indicate the blockage of the access to the micropores by the nanoparticles incorporated inside the zeolite channels. Similar phenomenon was observed by Cai et al. (2013) for gold nanoparticles encapsulated inside zeolite Y. The observed increase in the external surface area could indicate the presence of nanoparticles on the outer surface of the zeolite. For the Au/S-1\_IM and Au/S-1\_IM\_C the degrees of decrease in micropore volume and increase in the external surface area are larger than for the PAIR catalysts. The explanation could be that there were more surface nanoparticles in the samples prepared with impregnation method than with PAIR and they block the access to the inner pores of the zeolite (Jiang et al. 2009). The isotherms of the investigated materials obtained from the analysis are shown in Figure 4.1c. They all resemble the I type characteristic for the microporous material with the hysteresis loop typical for nitrogen adsorption in silicalite-1 (Thommes 2010).

**Table 4.2. Results from nitrogen physisorption analysis and particle size distribution for the catalysts prepared using the PAIR method and impregnation method with 0.15 ml of water as a solvent and chloroauric acid as a precursor, both subjected to additional calcination in air at 400 °C for 2 h.**

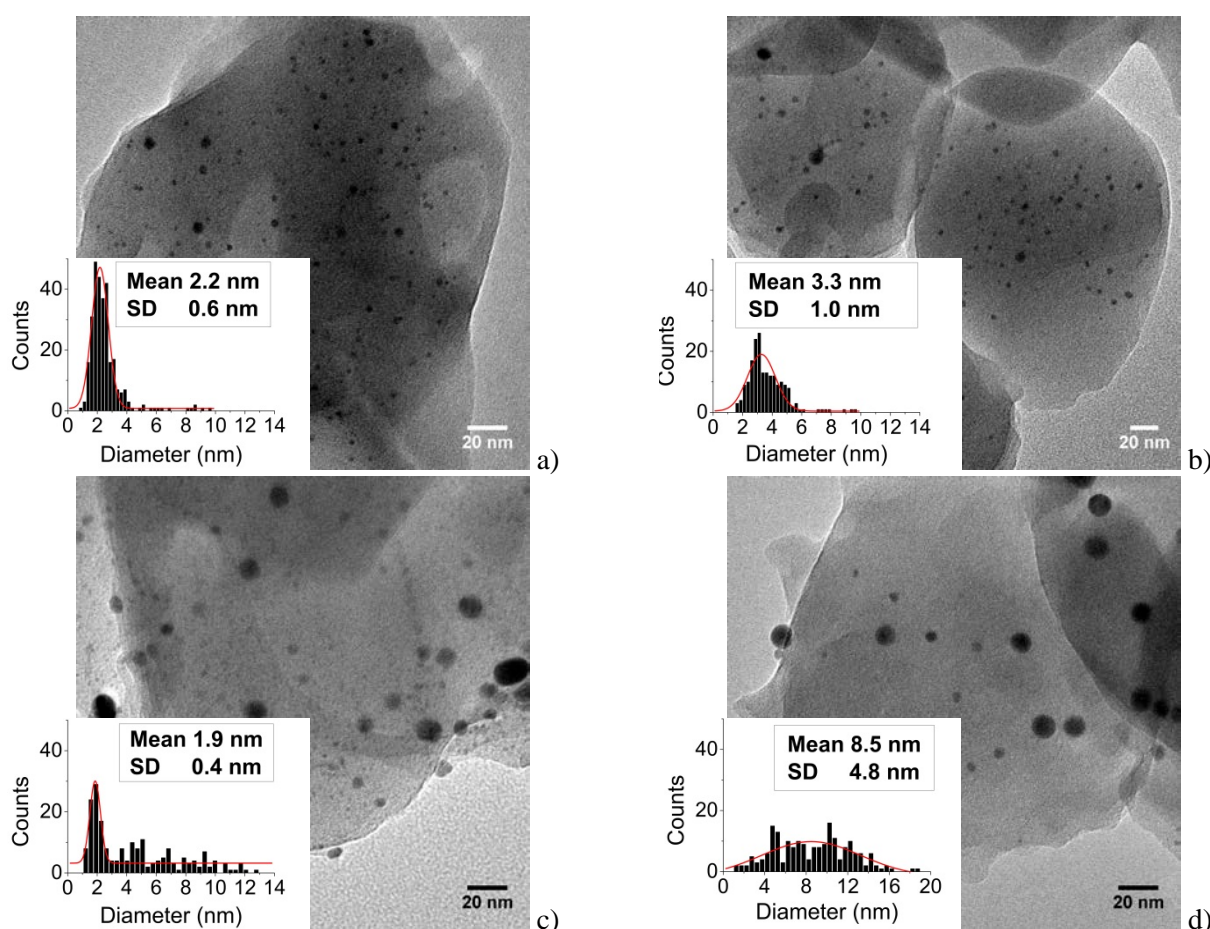
Catalyst name	Total pore volume (cm <sup>3</sup> /g)	Micropore volume (cm <sup>3</sup> /g)	External surface area (m <sup>2</sup> /g)	Total surface area BET (m <sup>2</sup> /g)	Mean <sup>1</sup> particle size (nm)	Average <sup>1</sup> particle size (nm)
S-1	0.176	0.111	60	296	-	-
Au/S-1_PAIR	0.173	0.094	100	293	2.2 ± 0.6	2.7 ± 2.2
Au/S-1_PAIR_C	0.174	0.090	107	292	3.3 ± 0.9	4.0 ± 2.5
Au/S-1_IM	0.178	0.072	162	297	1.9 ± 0.4	4.0 ± 2.5
Au/S-1_IM_C	0.177	0.071	160	297	8.4 ± 4.8	8.6 ± 3.6

<sup>1</sup> Value determined from the measurement of 200 particles from TEM images.



**Figure 4.1. a) XRD diffractograms, b) zoomed-in XRD diffractograms, c) nitrogen adsorption isotherms (offset of 50) of catalysts prepared using the PAIR method and impregnation method with 0.15 ml of water as a solvent and chloroauric acid as a precursor, both subjected to additional calcination in air at 400 °C for 2 h.**

The representative TEM images of the prepared catalysts are shown in Figure 4.2. In all samples, small gold nanoparticles are visible in the centers of the zeolite crystals, probably in the pores of silicalite-1. Large nanoparticles are visible as well, probably deposited on the external surface of zeolite crystals as they are far too large to fit into the pores of silicalite-1. The sizes of nanoparticles calculated for the respective catalysts are given in Table 4.2. For the samples prepared with the PAIR method, the mean particle size of gold in Au/S-1\_PAIR is  $2.2 \pm 0.6$  nm while for the calcined sample Au/S-1\_PAIR\_C it is  $3.3 \pm 0.9$  nm. This slight increase in the diameter of gold nanoparticles could be attributed to sintering facilitated by the additional calcination. The size of particles estimated for the Au/S-1\_IM and Au/S-1\_IM\_C samples is  $1.9 \pm 0.4$  nm and  $8.4 \pm 4.8$  nm, respectively. Comparing with the Au/S-1\_PAIR catalyst, the smaller size of gold nanoparticles obtained for Au/S-1\_IM is surprising. However, looking at the average particle size for Au/S-1\_IM, which is  $4.0 \pm 2.5$  nm, it can be concluded that even though there is a large number of rather small gold nanoparticles (the mean value of  $1.9 \pm 0.4$  nm), there is a significant number of large particles present in the sample that cannot be neglected. It is well depicted in the representative TEM image of Au/S-1\_IM, where both large and small nanoparticles can be spotted, as shown in Figure 4.2c. The additional calcination of this catalyst caused an increase in the particle size to  $8.4 \pm 4.8$  nm indicating severe sintering of gold nanoparticles, as presented in Figure 4.2d.



**Figure 4.2.** Representative TEM images and particle size distributions calculated for catalysts prepared using the PAIR method and impregnation method with 0.15 ml of water as a solvent and chloroauric acid as a precursor, and both subjected to additional calcination in air at 400 °C for 2 h: a) Au/S-1\_PAIR, b) Au/S-1\_PAIR\_C, c) Au/S-1\_IM, d) Au/S-1\_IM\_C.

Summarizing, the catalysts obtained using the PAIR method showed nanoparticles of gold with more narrow size distribution which were more stable towards sintering than when synthesized using the impregnation method. These results indicate the better performance of the PAIR method over the impregnation method for the applied set of synthesis conditions.

#### 4.1.2 Synthesis conditions: $\text{HAuCl}_4 \cdot 3\text{H}_2\text{O}$ + 0.3 ml of different solvents

The scope of the PAIR method was extended to study different solvents and different solvent volume used for the impregnation of silicalite-1 (see Chapter 3, section 3.2.3 *General procedure for the PAIR method* for synthesis details). Materials were prepared with water, methanol and acetonitrile as solvents. 0.3 ml of solvent per 0.99 g support was used for the impregnation.  $\text{HAuCl}_4 \cdot 3\text{H}_2\text{O}$  was used as gold precursor. Additionally, catalysts were subjected to calcination (denoted as ‘C’ in the sample name) in air for 2 h at 400 °C, in order to investigate the sintering stability of nanoparticles. The catalysts before calcination are referred to as ‘fresh catalysts’, while the catalysts after calcination as ‘calcined catalysts’. The overview of the prepared catalysts is given in Table 4.3. The results from the catalysts characterization by nitrogen physisorption, XRD and TEM are showed in Table 4.4, Figure 4.4 and Figure 4.3.

**Table 4.3. Overview of gold catalysts prepared with silicalite-1 using 0.3 ml of different solvents and chloroauric acid as a precursor using PAIR method alone and with additional calcination in air at 400 °C for 2 h.**

Catalyst name <sup>1</sup>	Solvent	Treatment
Au/S-1_3_H <sub>2</sub> O	Water	PAIR
Au/S-1_3_H <sub>2</sub> O_C		PAIR+ calcination in air at 400 °C for 2 h
Au/S-1_3_MeOH	Methanol	PAIR
Au/S-1_3_MeOH_C		PAIR+ calcination in air at 400 °C for 2 h
Au/S-1_3_ACN	Acetonitrile	PAIR
Au/S-1_3_ACN_C		PAIR+ calcination in air at 400 °C for 2 h

<sup>1</sup> 3 refers to a volume of solvent used in the synthesis i.e. 0.3 ml.

The XRD diffractograms of all investigated catalysts are shown in Figure 4.3a. The identification of the crystalline phase as silicalite-1 was performed based on comparison with the JCPDS 040-19-6968 standard data. In the zoomed-in diffractogram, showed in Figure 4.3b, the characteristic reflexes of gold at  $2\theta = 38.17$  and  $2\theta = 44.37$  (JCPDS 010-71-4616) are visible for all the catalysts. For samples prepared with water, Au/S-1\_3\_H<sub>2</sub>O and Au/S-1\_3\_H<sub>2</sub>O\_C, both reflexes of gold at  $2\theta = 38.17$  and  $2\theta = 44.37$  can be distinguished, and have the highest relative intensity from all the investigated catalysts. It could indicate the presence of higher amount of larger gold nanoparticles in samples prepared with methanol and acetonitrile. For materials prepared with methanol and acetonitrile only a weak peak at  $2\theta = 38.17$  is visible. The relative intensity of this peak is lower than for materials prepared with water and does not change with the additional calcination. It could indicate the presence of smaller gold nanoparticles which have higher sintering stability than in material prepared with water.

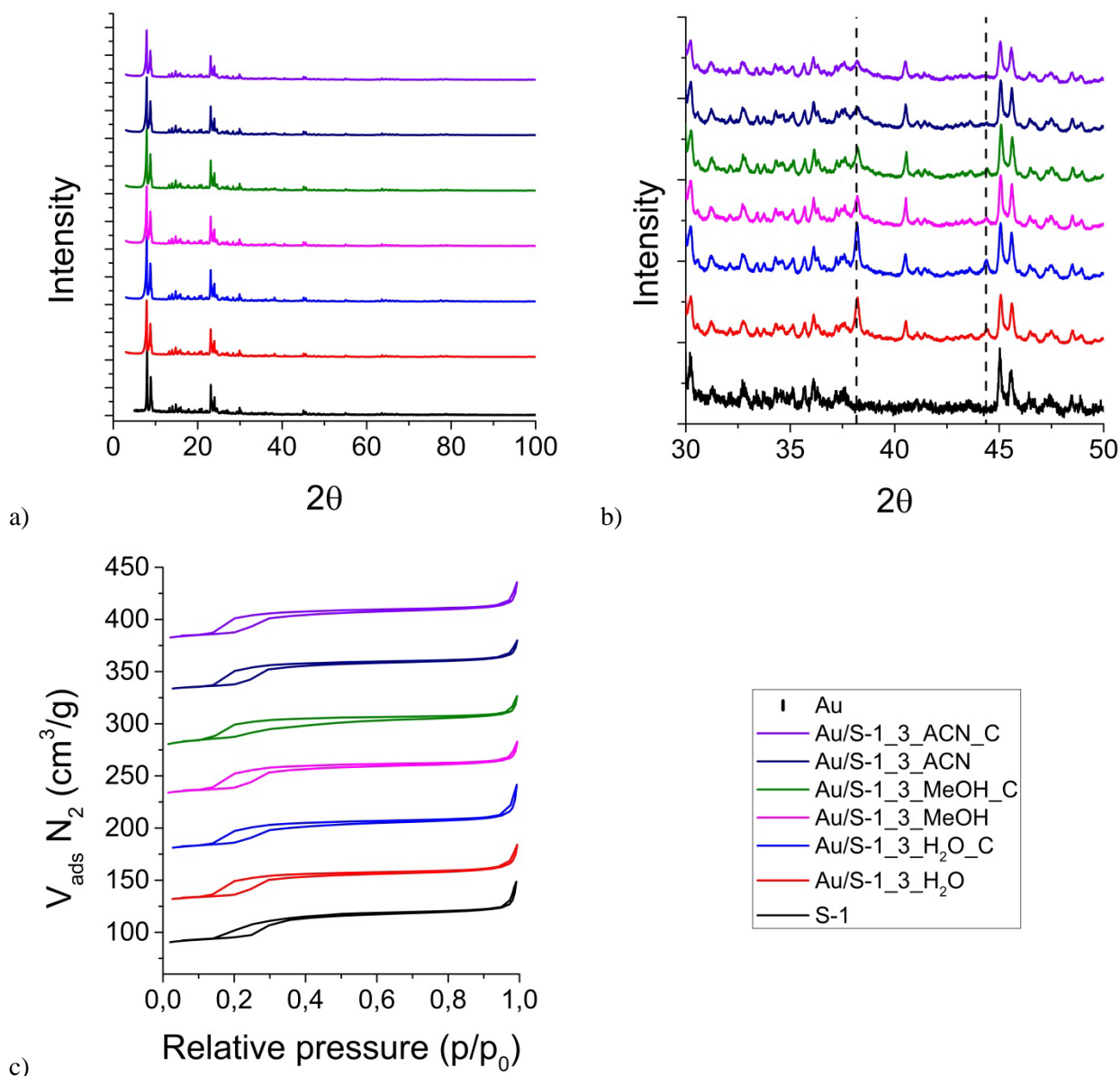
Results from nitrogen physisorption analysis are gathered in Table 4.4. The values of total pore volume decreased for all the catalyst compared to the parent material what might indicate the presence of nanoparticles in the pores of the zeolite (Cai et al. 2013). However, it did not change with additional calcination for any of the catalysts. The micropore volume increased with additional calcination while external surface area decreased. It could be explained by the migration of smaller particles from the inside of

the crystals to the surface due to enhanced mobility at high temperature or sintering of surface nanoparticles. The total BET area did not change for samples with and without calcination what could mean that no additional porosity or damage was created during calcination. The increase in external surface area between parent material and fresh catalysts could point towards the presence of nanoparticles on the outer surface of the crystals. The isotherms of the investigated catalysts obtained from the analysis are shown in Figure 4.3c. All isotherms are of type I characteristic for microporous material with the characteristic loop typical for MFI type of structure for the nitrogen adsorption (Thommes 2010).

**Table 4.4. Results from nitrogen physisorption analysis and particle size distribution obtained for catalysts prepared with 0.3 ml of solvent (water, methanol, acetonitrile) and chloroauric acid as precursor using the PAIR method alone and with additional calcination in air at 400 °C for 2 h.**

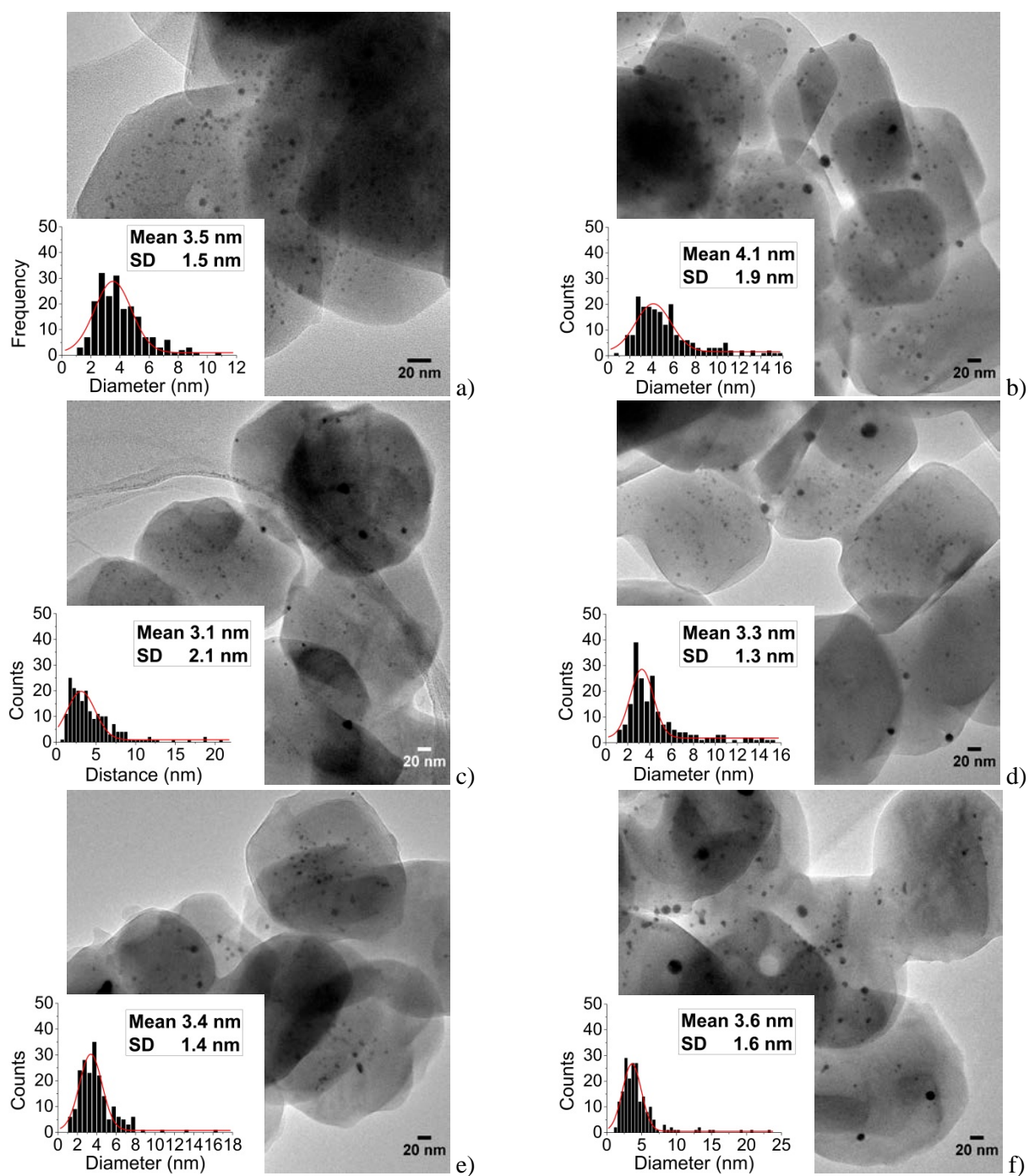
Catalyst name	Total pore volume (cm <sup>3</sup> /g)	Micropore volume (cm <sup>3</sup> /g)	External surface area (m <sup>2</sup> /g)	Total surface area BET (m <sup>2</sup> /g)	Mean <sup>1</sup> particle size (nm)	Average <sup>1</sup> particle size (nm)
S-1	0.192	0.096	126	318	-	-
Au/S-1_3_H <sub>2</sub> O	0.175	0.069	159	288	3.5 ± 1.5	4.0 ± 1.6
Au/S-1_3_H <sub>2</sub> O_C	0.173	0.095	92	287	4.1 ± 1.9	5.3 ± 2.9
Au/S-1_3_MeOH	0.178	0.072	161	296	3.1 ± 2.1	4.5 ± 3.3
Au/S-1_3_MeOH_C	0.169	0.096	93	293	3.3 ± 1.3	4.5 ± 2.7
Au/S-1_3_ACN	0.176	0.072	157	293	3.4 ± 1.4	3.9 ± 1.9
Au/S-1_3_ACN_C	0.176	0.095	97	293	3.6 ± 1.6	4.5 ± 3.1

<sup>1</sup> Value calculated from measurement of 200 nanoparticles from TEM images.



**Figure 4.3.** a) XRD diffractograms, b) zoomed-in XRD diffractograms, c) nitrogen adsorption isotherms (offset of 50) of catalysts prepared with 0.3 ml of different solvents (water, methanol, acetonitrile) and chloroauric acid as a precursor using the PAIR method alone and with additional calcination in air at 400 °C for 2 h.

The representative TEM images and particle size distributions of the prepared catalysts are shown in Figure 4.4. For all catalysts, small, well distributed nanoparticles, located inside the crystals of silicalite-1 are visible. Larger nanoparticles (>10 nm) probably deposited on the external surface of individual zeolite crystals are visible as well. The mean size of gold nanoparticles for all fresh catalysts was fairly similar -  $3.5 \pm 1.5$  nm for water,  $3.1 \pm 2.1$  nm for methanol, and  $3.4 \pm 1.4$  nm for acetonitrile. The mean size of nanoparticles after calcination increased slightly for Au/S-1\_3\_H<sub>2</sub>O\_C ( $4.1 \pm 1.9$  nm) while it remained in the same range for Au/S-1\_3\_MeOH\_C ( $3.1 \pm 1.3$  nm) and Au/S-1\_3\_ACN\_C ( $3.6 \pm 1.6$  nm). It could indicate a certain degree of sintering stability achieved by entrapment of gold nanoparticles inside the pores of silicalite-1.



**Figure 4.4.** TEM images and particle size distribution calculated for catalysts prepared with 0.3 ml of different solvents (water, methanol, acetonitrile) and chloroauric acid as a precursor using the PAIR method alone and with additional calcination in air at 400 °C for 2 h: a) Au/S-1\_3\_H<sub>2</sub>O, b) Au/S-1\_3\_H<sub>2</sub>O\_C, c) Au/S-1\_3\_MeOH, d) Au/S-1\_3\_MeOH\_C, e) Au/S-1\_3\_ACN, f) Au/S-1\_3\_ACN\_C.

In summary, materials synthesized using the PAIR method with methanol and acetonitrile showed smaller gold nanoparticles than when water was used for the synthesis. The particle size distribution was also more narrow for the organic solvents and the size. The gold nanoparticles showed also higher sintering stability when synthesized using organic solvents.



### 4.1.3 Synthesis conditions: AuCl<sub>3</sub> + 0.3 ml of different solvents

In this study, the materials were prepared using the PAIR method with the variation of solvents and different precursor of gold. Gold chloride – AuCl<sub>3</sub> was used as a precursor and dissolved in 0.3 ml of selected solvents: water, methanol, acetonitrile, and 1-butanol. Each of the prepared materials was subjected to additional reduction (denoted as ‘R’ in the catalyst name) in 10% H<sub>2</sub> in N<sub>2</sub> at 350 °C for 2 h in order to investigate the sintering stability of gold nanoparticles. The PAIR catalysts were compared with the catalysts prepared with the impregnation method (see Chapter 3, section 3.2.2 *General procedure for impregnation method* and 3.2.3 *General procedure for the PAIR method* for synthesis details). Table 4.5 shows the overview of the prepared catalysts. All samples were analyzed using nitrogen physisorption, XRD and TEM techniques. Data collected from these analysis is shown in Table 4.6, Figure 4.6, and Figure 4.5.

**Table 4.5. Overview of gold catalysts prepared with silicalite-1, 0.3 ml of different solvents (water, methanol, acetonitrile, 1-butanol) and AuCl<sub>3</sub> as precursor using impregnation method, the PAIR method alone and the PAIR method with additional reduction at 350 °C in 10% H<sub>2</sub> in N<sub>2</sub> for 2h.**

Catalyst name	Solvent	Treatment
Au/S-1_H <sub>2</sub> O_IM_AuCl <sub>3</sub>		Impregnation
Au/S-1_H <sub>2</sub> O_PAIR_AuCl <sub>3</sub>	Water	PAIR
Au/S-1_H <sub>2</sub> O_PAIR_R_AuCl <sub>3</sub>		PAIR + reduction at 350°C in 10% H <sub>2</sub> in N <sub>2</sub> for 2 h
Au/S-1_MeOH_IM_AuCl <sub>3</sub>		Impregnation
Au/S-1_MeOH_PAIR_AuCl <sub>3</sub>	Methanol	PAIR
Au/S-1_MeOH_PAIR_R_AuCl <sub>3</sub>		PAIR + reduction at 350°C in 10% H <sub>2</sub> in N <sub>2</sub> for 2 h
Au/S-1_ACN_IM_AuCl <sub>3</sub>		Impregnation
Au/S-1_ACN_PAIR_AuCl <sub>3</sub>	Acetonitrile	PAIR
Au/S-1_ACN_PAIR_R_AuCl <sub>3</sub>		PAIR + reduction at 350°C in 10% H <sub>2</sub> in N <sub>2</sub> for 2 h
Au/S-1_But_IM_AuCl <sub>3</sub>		Impregnation
Au/S-1_But_PAIR_AuCl <sub>3</sub>	1-Butanol	PAIR
Au/S-1_But_PAIR_R_AuCl <sub>3</sub>		PAIR + reduction at 350°C in 10% H <sub>2</sub> in N <sub>2</sub> for 2 h

The XRD diffractograms of the investigated catalysts are presented in Figure 4.5a. The crystallinity associated with the support material was identified as silicalite-1 based on comparison with the JCPDS 040-19-6968 standard data. The zoomed-in diffratogram in Figure 4.5b, shows peaks at  $2\theta = 38.17$  and  $2\theta = 44.37$  (JCPDS 010-71-4616), what confirms the presence of gold in the samples.

The results from nitrogen physisorption analysis are presented in Table 4.6. For the materials prepared with water and methanol the value of micropore volume visibly decreased, while the external surface area increased compared to the parent material. The reason for it might be the presence of nanoparticles on the outer surface of the crystals (Cai et al. 2013). For the materials prepared with acetonitrile and 1-butanol the values of micropore volume practically did not change. However, the change in the external surface area observed for these materials could point towards a damage done to the silicalite-1 structure (lower external surface area) or deposition of nanoparticles on the external surface (higher external surface area). The isotherms of the investigated samples obtained from nitrogen physisorption analysis are

shown in Figure 4.5c. The isotherms are of type I characteristic for microporous material with the hysteresis loop typical for adsorption of nitrogen in silicalite-1 (Thommes 2010).

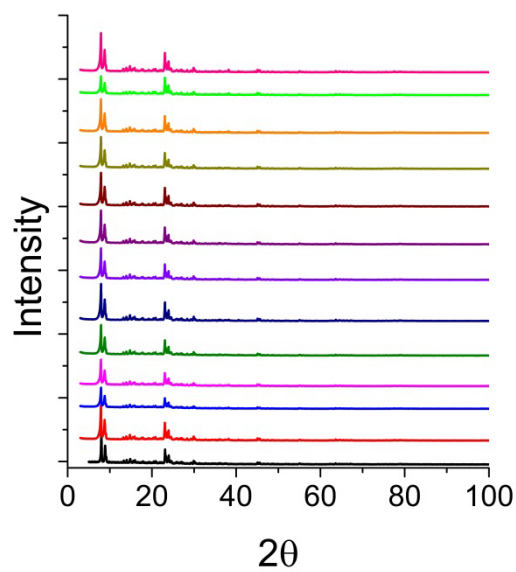
**Table 4.6. Results from nitrogen physisorption analysis and particle size distribution obtained for catalysts prepared with 0.3 ml of different solvents (water, methanol, acetonitrile, 1-butanol) and gold chloride as a precursor using impregnation method, the PAIR method and the PAIR method followed by additional reduction at 350 °C in 10% H<sub>2</sub> in N<sub>2</sub> for 2 h.**

Catalyst name	Total pore volume (cm <sup>3</sup> /g)	Micropore volume (cm <sup>3</sup> /g)	External surface area (m <sup>2</sup> /g)	Total surface area BET (m <sup>2</sup> /g)	Mean particle size <sup>1</sup> (nm)	Average particle size <sup>1</sup> (nm)
S-1	0.171	0.102	81	293	-	-
Au/S-1_H <sub>2</sub> O_IM_AuCl <sub>3</sub>	0.165	0.089	90	271	3.1 ± 1.2	4.4 ± 2.7
Au/S-1_H <sub>2</sub> O_PAIR_AuCl <sub>3</sub>	0.160	0.086	85	263	2.4 ± 1.4	3.7 ± 3.0
Au/S-1_H <sub>2</sub> O_PAIR_R_AuCl <sub>3</sub>	0.172	0.094	89	283	3.3 ± 1.7	4.5 ± 2.8
Au/S-1_MeOH_IM_AuCl <sub>3</sub>	0.176	0.093	104	297	3.4 ± 2.2	3.9 ± 2.1
Au/S-1_MeOH_PAIR_AuCl <sub>3</sub>	0.182	0.086	132	304	2.2 ± 1.0	2.6 ± 1.5
Au/S-1_MeOH_PAIR_R_AuCl <sub>3</sub>	0.179	0.081	138	296	2.7 ± 1.0	2.9 ± 0.9
Au/S-1_ACN_IM_AuCl <sub>3</sub>	0.176	0.102	83	300	2.2 ± 1.0	2.5 ± 1.3
Au/S-1_ACN_PAIR_AuCl <sub>3</sub>	0.166	0.106	67	293	2.0 ± 0.9	2.2 ± 0.9
Au/S-1_ACN_PAIR_R_AuCl <sub>3</sub>	0.174	0.098	94	299	1.6 ± 0.7	1.9 ± 1.1
Au/S-1_But_IM_AuCl <sub>3</sub>	0.174	0.093	104	296	2.0 ± 1.0	3.3 ± 2.7
Au/S-1_But_PAIR_AuCl <sub>3</sub>	0.159	0.104	62	284	1.6 ± 0.5	1.7 ± 0.7
Au/S-1_But_PAIR_R_AuCl <sub>3</sub>	0.180	0.102	94	305	1.6 ± 1.8	1.9 ± 1.1

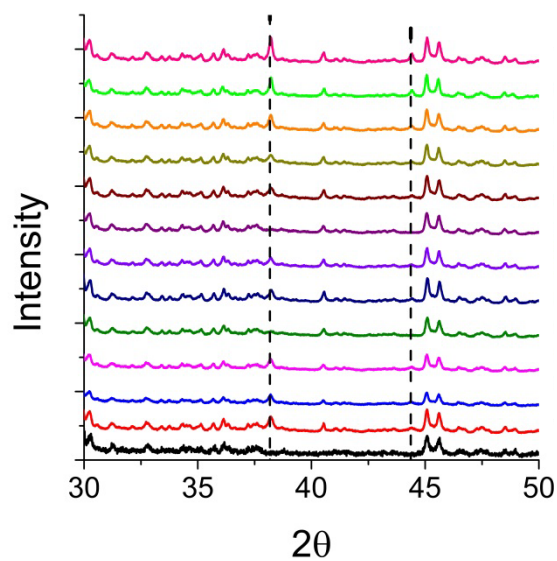
<sup>1</sup> Value calculated from measurement of 200 nanoparticles from TEM images.

The representative TEM images of the investigated catalysts are shown in Figure 4.6. In samples prepared with methanol, acetonitrile and 1-butanol, small gold nanoparticles well distributed inside zeolite crystals can be visible. For samples prepared with water only few nanoparticles can be spotted on the surface of the support. The sizes of gold nanoparticles calculated for the investigated catalysts are gathered in Table 4.6. The smallest values of the mean particle size were obtained for catalysts prepared with acetonitrile and 1-butanol, irrespectively of the preparation method and additional reduction. Comparing the mean values and average values of particles sizes, the largest difference occurs for the catalysts prepared with water irrespectively of the preparation method used. This indicates that the samples contain not only small gold nanoparticles 2-3 nm in size but also a fair number of larger aggregates. For the remaining catalysts, a difference in mean and average sizes of nanoparticles can be observed as well, but a difference is much smaller than for water catalyst.

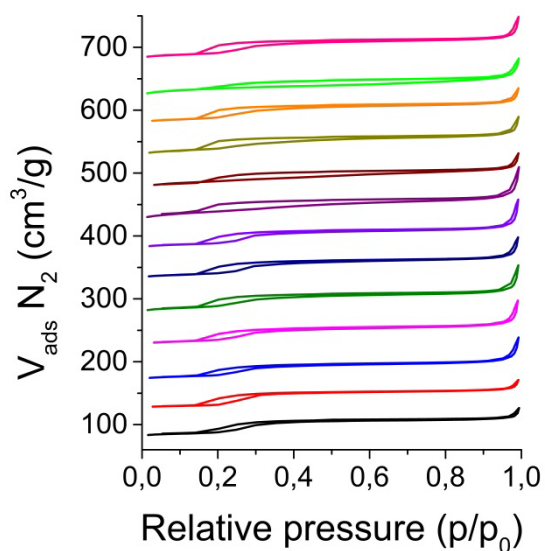
In summary, the organic solvents used during the synthesis with AuCl<sub>3</sub> as a precursor resulted in nanoparticles which were much smaller and with more narrow size distribution than when water was used in the PAIR method. All the organic solvents resulted in nanoparticles in a very similar size range; however, they were the smallest for acetonitrile and 1-butanol. Similar was observed when the impregnation method was used for the synthesis.



a)



b)



c)

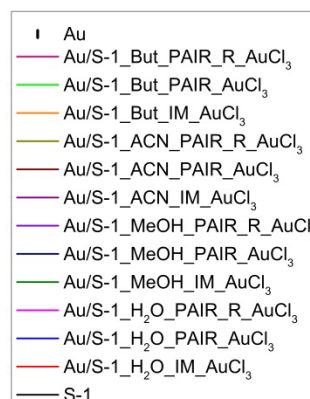
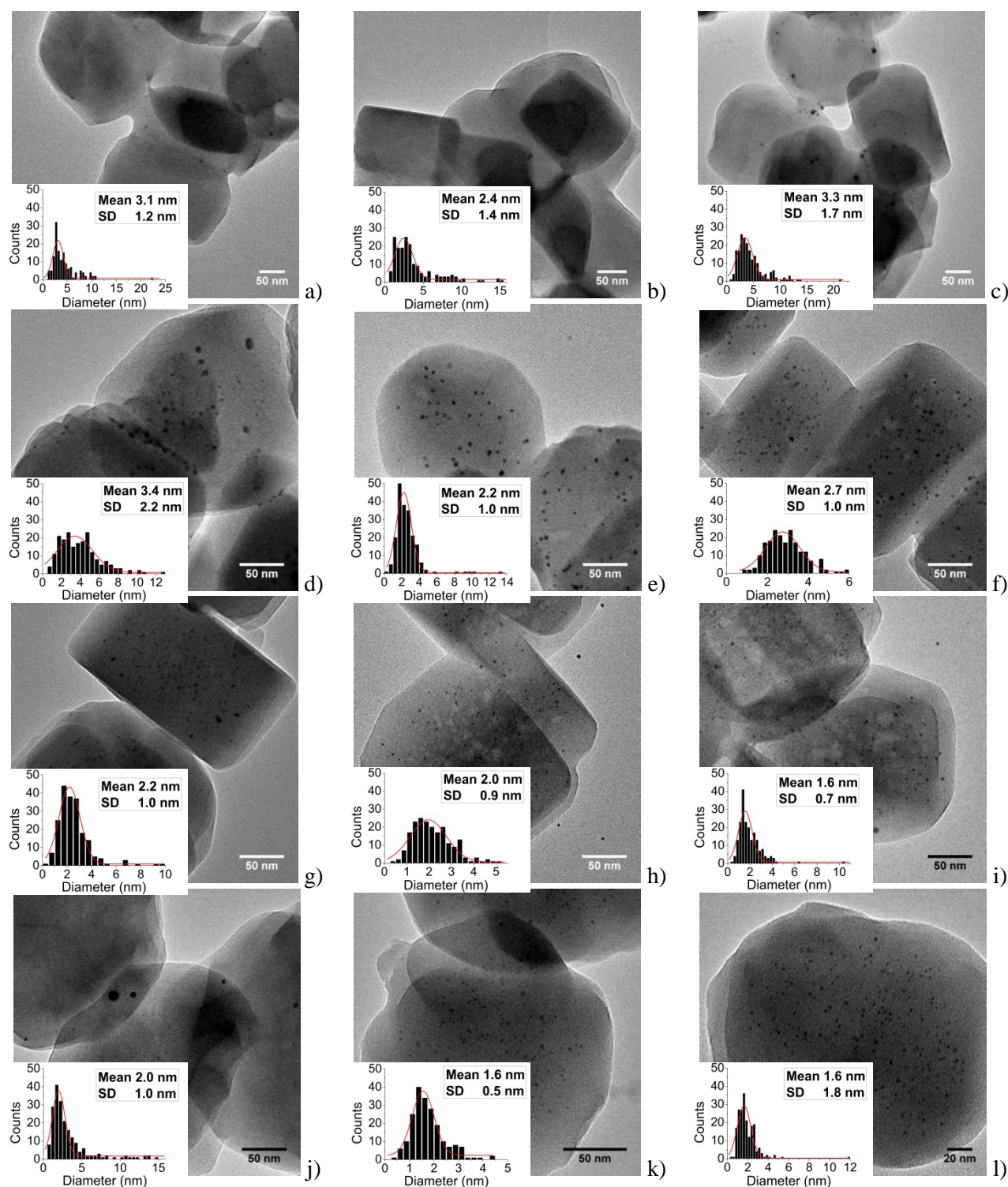


Figure 4.5. a) XRD diffractograms b) zoomed-in XRD diffractograms c) nitrogen physisorption isotherms (offset of 50) obtained for catalysts prepared with 0.3 ml of different solvents (water, methanol, acetonitrile, 1-butanol) and AuCl<sub>3</sub> as a precursor using simple impregnation method, the PAIR method and the PAIR method followed by additional reduction at 350 °C in 10% H<sub>2</sub> in N<sub>2</sub> for 2 h.



**Figure 4.6. Representative TEM images and particle size distribution calculated for catalysts prepared with 0.3 ml of different solvents (water, methanol, acetonitrile, 1-butanol) and gold chloride as precursor using impregnation method, the PAIR method alone and the PAIR method followed by additional reduction at 350 °C in 10% H<sub>2</sub> in N<sub>2</sub> for 2 h: a) Au/S-1\_H<sub>2</sub>O\_IM\_AuCl<sub>3</sub>, b) Au/S-1\_H<sub>2</sub>O\_PAIR\_AuCl<sub>3</sub>, c) Au/S-1\_H<sub>2</sub>O\_PAIR\_R\_AuCl<sub>3</sub>, d) Au/S-1\_MeOH\_IM\_AuCl<sub>3</sub>, e) Au/S-1\_MeOH\_PAIR\_AuCl<sub>3</sub>, f) Au/S-1\_MeOH\_PAIR\_R\_AuCl<sub>3</sub>, g) Au/S-1\_ACN\_IM\_AuCl<sub>3</sub>, h) Au/S-1\_ACN\_PAIR\_AuCl<sub>3</sub>, i) Au/S-1\_ACN\_PAIR\_R\_AuCl<sub>3</sub>, j) Au/S-1\_But\_IM\_AuCl<sub>3</sub>, k) Au/S-1\_But\_PAIR\_AuCl<sub>3</sub>, l) Au/S-1\_But\_PAIR\_R\_AuCl<sub>3</sub>.**

It was shown that the PAIR method can be successfully applied to synthesize gold nanoparticles encapsulated inside the pores of silicalite-1 with the use of different synthesis parameters – precursor, solvent,

volume of impregnation solution. It was shown that the size of gold nanoparticles and their stability towards sintering depends on the specific selection of these parameters. The detailed discussion of the results presented so far is performed at the end of this chapter, in 4.6 *General discussion*, where the theoretical considerations of the PAIR method are developed as well.

## 4.2 PAIR method applied to gold in LTA and ZSM-5 zeolites

The method was studied by applying the PAIR conditions to two different zeolites. LTA was chosen as a zeolite with very small pore size – 0.3 – 0.45 nm (McCusker et al. 2001). Zeolite ZSM-5 was chosen as aluminosilicate equivalent of silicalite-1, both having the same MFI structure.

### 4.2.1 Synthesis of gold nanoparticles in LTA

The synthesis of gold in LTA material using the PAIR method was performed according to procedure described in Chapter 3 (section 3.2.3 *General procedure for the PAIR method*) for the modified sets of conditions presented in Table 4.7. Samples Au/Na-LTA and Au/H-LTA were prepared from Na-form and H-form LTA, respectively. Two samples – Au/Na-LTA\_3/4 and Au/Na-LTA\_6/2 were prepared with variation in the pressure of nitrogen and its dwell time during the PAIR procedure without changing the parameters for hydrogen (6 bar, dwell of 3 h). Sample Au/Na-LTA\_ACN was prepared with acetonitrile as solvent. Figure 4.7 and Figure 4.8 show the results from XRD and TEM analysis for the investigated catalysts.

**Table 4.7. Overview of gold catalysts prepared with LTA as support by the PAIR method using different solvents and different experimental conditions during the synthesis.**

Catalyst name	Solvent	PAIR conditions variation <sup>1</sup>	
		N <sub>2</sub> pressure (bar)	N <sub>2</sub> dwell time (h)
Au/Na-LTA	Water	3	2
Au/H-LTA	Water	3	2
Au/Na-LTA_ACN	Acetonitrile	3	2
Au/Na-LTA_3/4	Water	3	4
Au/Na-LTA_6/2	Water	6	2

<sup>1</sup> p<sub>H<sub>2</sub></sub> = 6 bar, dwell<sub>H<sub>2</sub></sub> = 3h

The XRD diffractograms of the investigated catalysts are presented in Figure 4.7b. The crystal structure was characterized as LTA zeolite based on the comparison with JCPDS 010-73-2340 standard data, except for Au/H-LTA sample which showed no crystallinity. In zoomed-in diffractogram showed in Figure 4.7c, the characteristic reflexes of gold at  $2\theta = 38.17$  and  $2\theta = 44.37$  (JCPDS 010-71-4616) can be visible for all investigated catalysts, what confirms the presence of gold in the samples.

The nitrogen physisorption analysis was performed for the investigated catalysts; however it did not succeed. The possible explanation might be that gaseous nitrogen cannot penetrate pores of size  $\leq 0.45$  nm (Ferey 2007). Hence, it would not be able to get adsorbed in the pores of LTA which have pore size of 0.30-0.45 nm (McCusker et al, 2001).

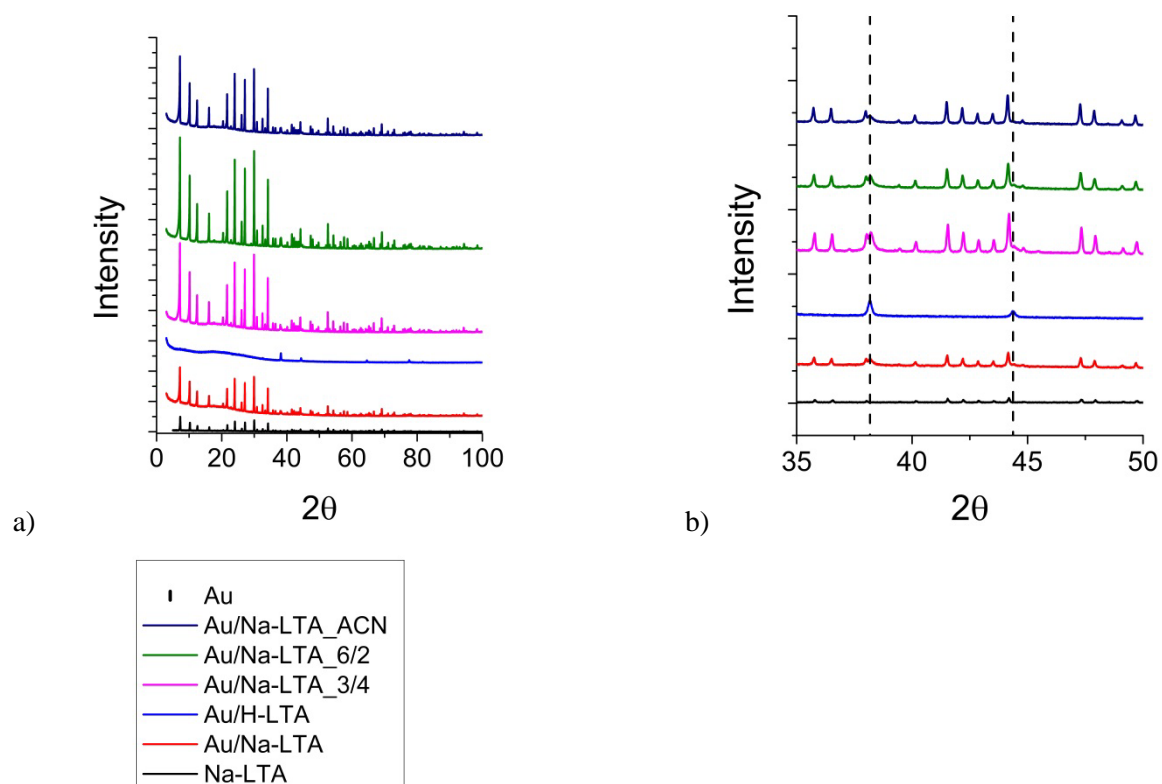


Figure 4.7. a) XRD diffractograms, b) zoomed-in XRD diffractograms of gold catalysts prepared with LTA using PAIR method applied to different solvents and different experimental conditions during the synthesis.

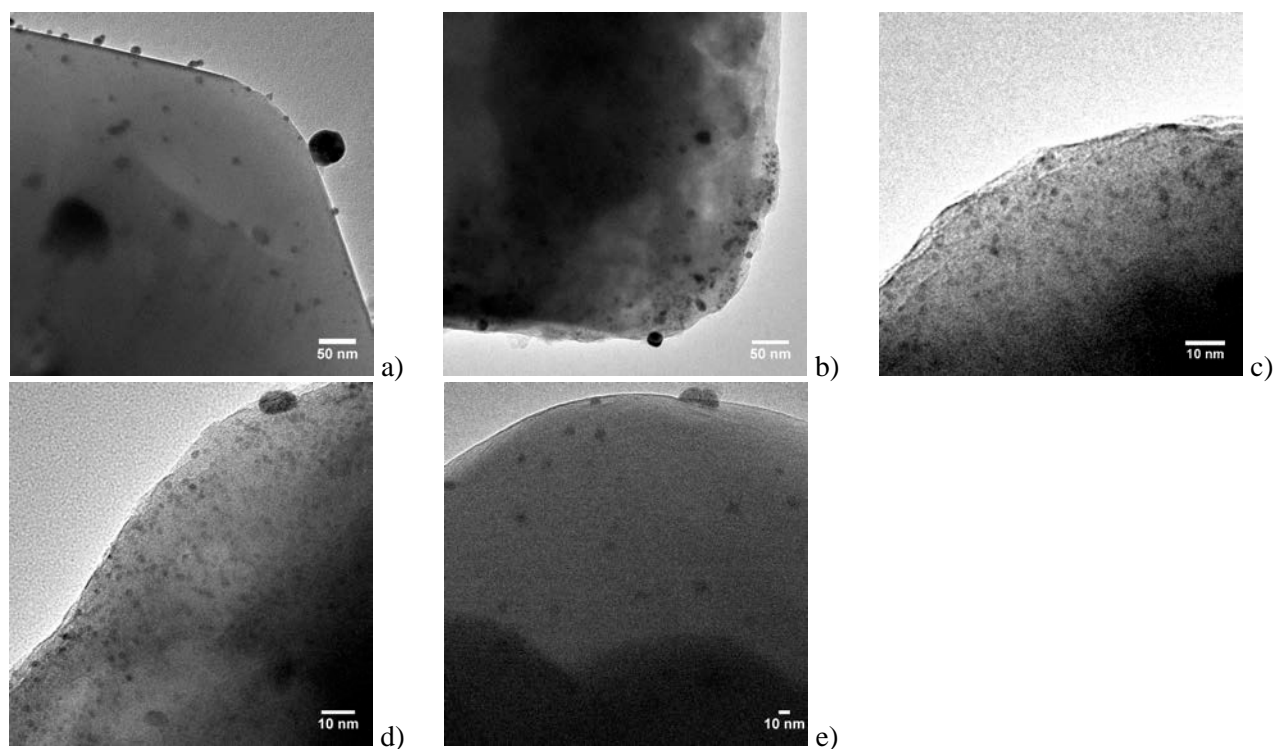


Figure 4.8. Representative TEM images of gold catalysts prepared with LTA as support by the PAIR method using different solvents (water, acetonitrile) and different experimental conditions during the synthesis: a) Au/Na-LTA, b) Au/H-LTA, c) Au/Na-LTA\_ACN, d) Au/Na-LTA\_3/4, e) Au/Na-LTA\_6/2.

Figure 4.8 depicts the representative TEM images of the investigated catalysts. The images confirm the presence of large gold nanoparticles in all samples which are 10 – 50 nm in size and located mostly on the external surface of zeolite crystals. However, Au/Na-LTA\_3/4 and Au/Na-LTA\_6/2 show additionally nanoparticles of gold 1 – 2 nm in size located inside the zeolite crystals close to the external surface. It might indicate that higher pressure or longer dwell time of nitrogen during the impregnation step in the PAIR procedure might have a significant influence on the penetration of the solution with gold precursor into the zeolite framework.

#### 4.2.2 Synthesis of gold nanoparticles in ZSM-5

The PAIR procedure was applied to synthesize gold nanoparticles incorporated inside the pores of ZSM-5 zeolite (see Chapter 3, section 3.2.3 *General procedure for the PAIR method for the synthesis details*). The Au/ZSM-5 material was characterized using nitrogen physisorption, XRD and TEM. Nitrogen physisorption analysis and XRD of the pure support material were performed for Na-ZSM (before ion-exchange). Results from characterization of Au/ZSM-5 are presented in Table 4.8, Figure 4.9 and Figure 4.10.

The XRD diffractograms of the investigated materials are presented in Figure 4.9a. Both materials were characterized as having MFI structure by comparison with the JCPDS 040-19-6968 standard data. It is clearly visible that ion exchange did not cause any damage to the crystalline structure of ZSM-5. In the zoomed-in diffractogram presented in Figure 4.9b, characteristic reflexes of gold at  $2\theta = 38.17$  and  $2\theta = 44.37$  (JCPDS 010-71-4616) are visible for Au/H-ZSM-5, confirming the presence of gold in the sample.

The results from nitrogen physisorption analysis are presented in Table 4.8. The increase in the total pore volume and decrease in the micropore volume can be observed for Au/H-ZSM-5 compared to Na-ZSM-5. The increase in the total pore volume could be explained by the removal of  $\text{Na}^+$  ions in the ion-exchange process and replacing them with  $\text{H}^+$  ions, which are much smaller in size (Silva et al. 2012). The decrease in the micropore volume could indicate presence of nanoparticles inside the pores of ZSM-5 (Cai et al. 2013). The isotherms obtained for Au/H-ZSM-5 and the parent material from the nitrogen physisorption analysis are shown in Figure 4.9c. The isotherms are of type I typical for the porous material with microporosity. The hysteresis loop is characteristic for the MFI structure in nitrogen physisorption analysis.

**Table 4.8. Results from nitrogen physisorption analysis and particle size distribution for gold catalysts prepared with ZSM-5 as support using the PAIR method.**

Sample	Total pore volume $\text{cm}^3/\text{g}$	Micropore volume $\text{cm}^3/\text{g}$	External surface area $\text{m}^2/\text{g}$	Total surface area BET $\text{m}^2/\text{g}$	Mean particle size <sup>1</sup> (nm)	Average particle size <sup>1</sup> (nm)
Na-ZSM-5	0.174	0.101	94	305	-	-
Au/H-ZSM-5	0.199	0.092	160	355	$1.9 \pm 0.8$	$2.1 \pm 0.7$

<sup>1</sup> Determined from the measurement of 200 nanoparticles from TEM images.

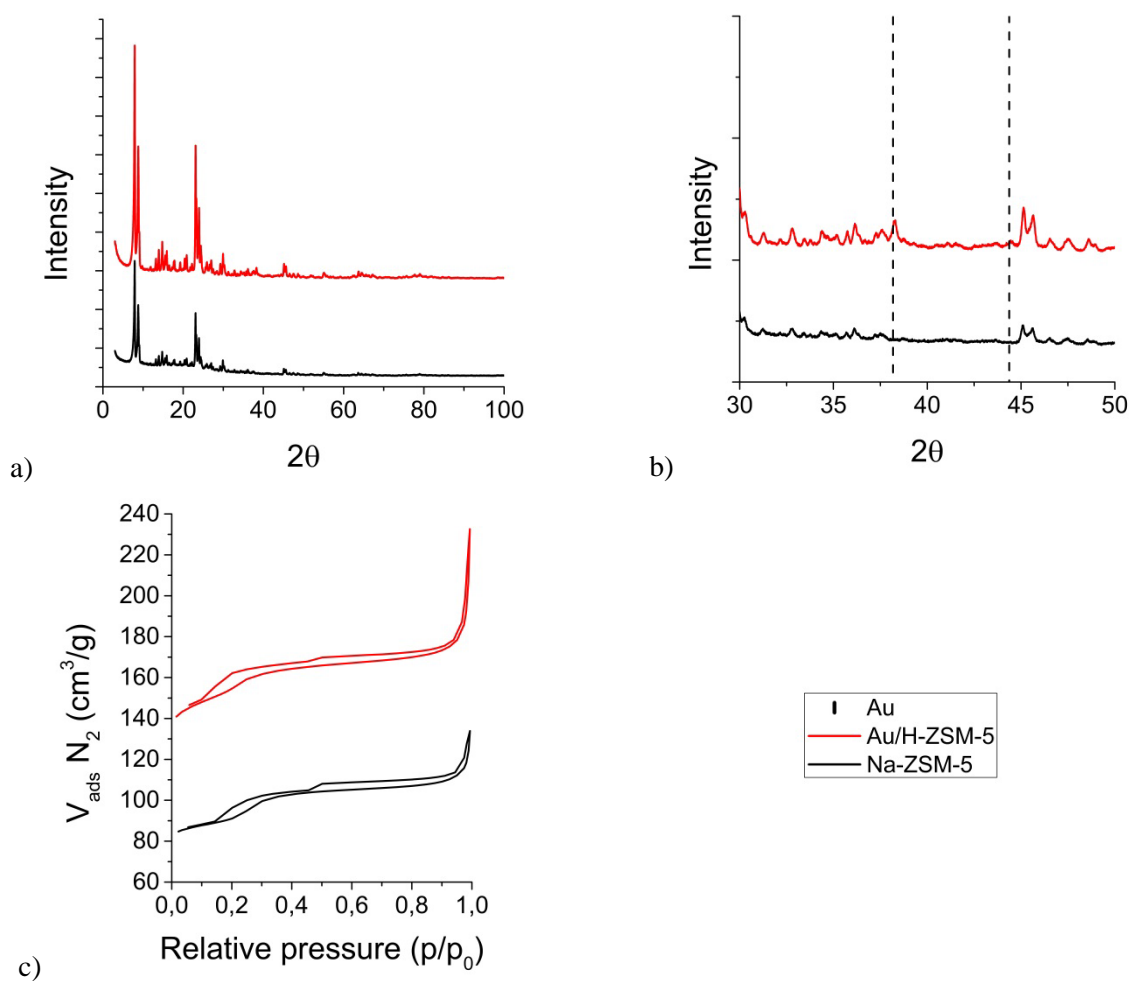


Figure 4.9. a) XRD diffractograms, b) zoomed-in XRD diffractograms, c) nitrogen adsorption isotherms (offset of 50) of gold catalyst prepared with ZSM-5 as support using the PAIR method.

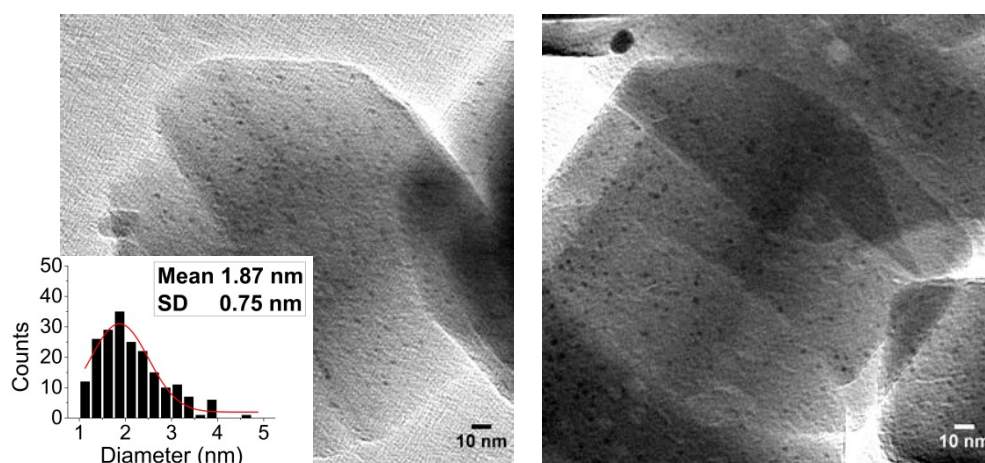


Figure 4.10. Representative TEM images and particle size distribution calculated for gold catalyst prepared with ZSM-5 using the PAIR method.



The representative TEM images of the Au/H-ZSM-5 catalyst are shown in Figure 4.10. Small gold nanoparticles  $1.9 \pm 0.8$  nm in size are visible, located in the center of the zeolite crystals. Large gold nanoparticles  $>10$  nm are present as well, located probably on the outer surface of the crystals.

It was shown that the PAIR method can be successfully applied to synthesize gold nanoparticles encapsulated inside the pores of ZSM-5 zeolite. The gold nanoparticles were small in size, encapsulated and uniformly distributed inside zeolite crystals. However, the use of LTA zeolite for the synthesis of gold catalyst using the PAIR method was non satisfactory. This was probably due to too small pores of LTA zeolite limiting the diffusion of gold species into the pores. The discussion of the results obtained for ZSM-5 and LTA, comparison with the published literature and comparison with gold/silicalite-1 materials prepared by the PAIR method are provided in 4.6 *General discussion* at the end of this chapter.

### 4.3 PAIR method applied to palladium and platinum in silicalite-1

#### 4.3.1 Synthesis of palladium nanoparticles in silicalite-1

The PAIR method was applied to obtain the palladium incorporated silicalite-1 (see Chapter 3, section 3.2.3 *General procedure for the PAIR method* for the synthesis details). The experiments were performed using various palladium precursors; however, only palladium nitrate gave a positive result. Hence, only results obtained for  $\text{Pd}(\text{NO}_3)_2 \cdot 2\text{H}_2\text{O}$  as Pd precursor are shown. The samples were prepared with three different solvents: water, methanol, acetonitrile. Data obtained from the analysis of the investigated catalysts using nitrogen physisorption, XRD, and TEM techniques are shown in Table 4.9, Figure 4.11 and Figure 4.12.

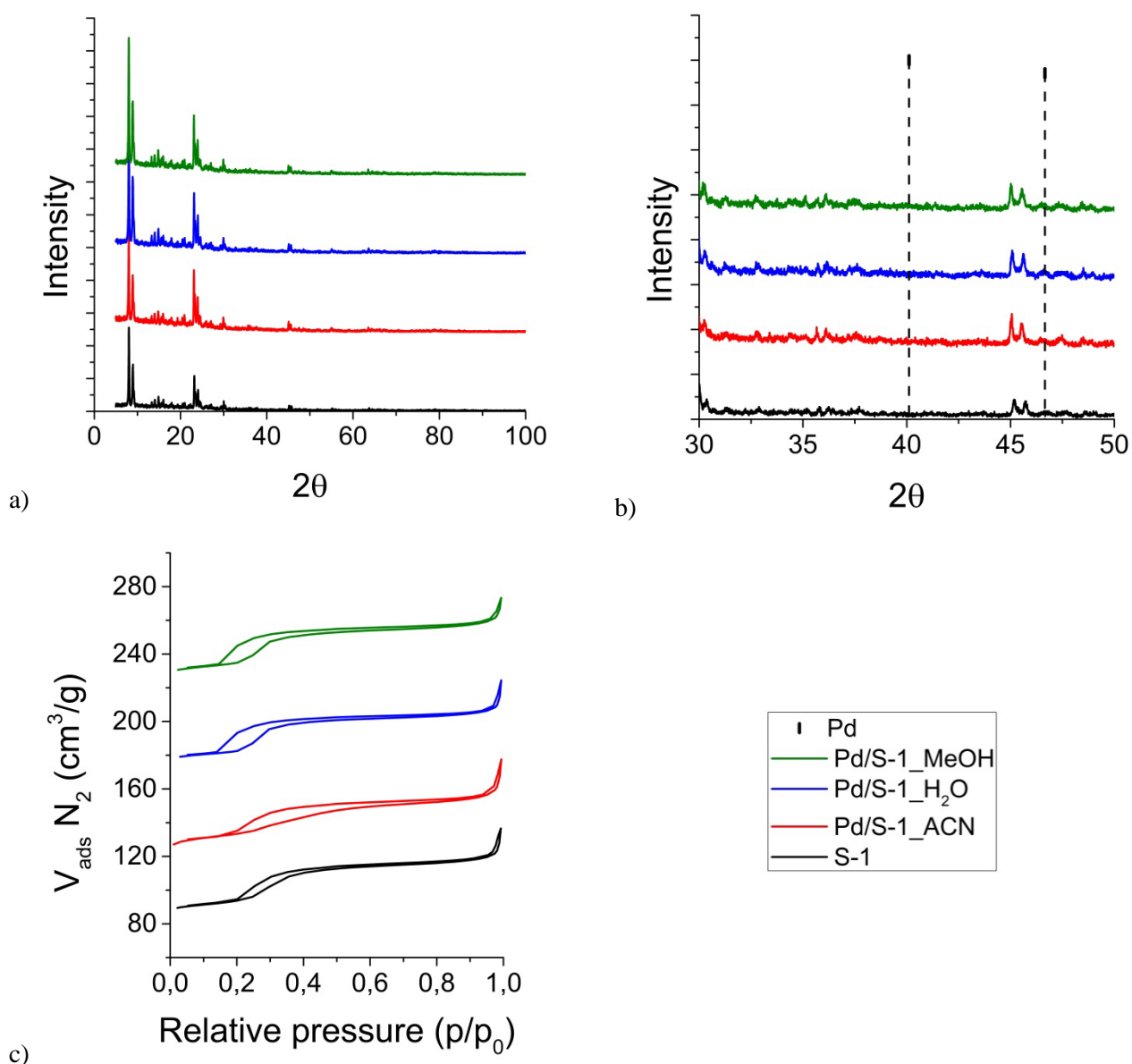
The XRD diffractograms of the investigated catalysts are presented in Figure 4.11a. The crystalline pattern was identified as MFI structure of silicalite-1 by comparison with the JCPDS 040-19-6968 standard data. The zoomed-in diffractogram in Figure 4.11b, depicts the diffraction pattern where the most intense characteristic reflexes of palladium at  $2\theta = 46.66$  and  $2\theta = 40.11$  are expected (JCPDS 000-05-0681). In the diffractograms of the investigated materials no peak associated to palladium is visible. The peak at  $2\theta = 40.11$  is present also in the pure silicalite-1 support; hence it is not associated with metallic palladium. Lack of palladium reflexes in XRD pattern might be explained by the low scattering ability of palladium, compared to gold, what means that more than 1wt% of palladium might be necessary to produce signal that is strong enough to be detected in XRD analysis.

Results from nitrogen physisorption analysis are gathered in Table 4.9. The value of the total pore volume decreased for all the prepared catalysts compared to the parent material. This could indicate the presence of nanoparticles in the samples (Cai et al. 2013). For Au/S-1\_H<sub>2</sub>O, the large decrease in micropore volume and simultaneous increase in the external surface area were observed. It could indicate either presence of nanoparticle inside the pores or deposition of nanoparticles on the external surface and blocking the access to the inner porosity of the crystals (Jiang et al. 2009). For Au/S-1\_ACN and Au/S-1\_MeOH samples, the decrease in external surface area was observed what could be associated with damage of the zeolites structure done during the PAIR synthesis. The isotherms obtained from the nitrogen physisorption analysis for the investigated catalysts are shown in Figure 4.11c. The presented isotherms are of type I and depict the characteristic hysteresis loop typical for the silicalite-1 zeolite (Thommes 2010).

**Table 4.9. Results from nitrogen physisorption and particle size distribution for palladium catalyst prepared with silicalite-1 and different solvents (acetonitrile, water, methanol) using the PAIR method.**

Catalyst name	Total pore volume (cm <sup>3</sup> /g)	Micropore volume (cm <sup>3</sup> /g)	External surface area (m <sup>2</sup> /g)	Total surface area BET (m <sup>2</sup> /g)	Mean particle size <sup>1</sup> (nm)	Average particle size <sup>1</sup> (nm)
S-1	0.185	0.104	99	313	-	-
Pd/S-1_ACN	0.165	0.103	61	279	2.2 ± 0.8	3.6 ± 2.3
Pd/S-1_H <sub>2</sub> O	0.164	0.070	143	275	4.3 ± 2.6	5.8 ± 3.7
Pd/S-1_MeOH	0.169	0.096	83	283	3.0 ± 1.7	4.9 ± 3.7

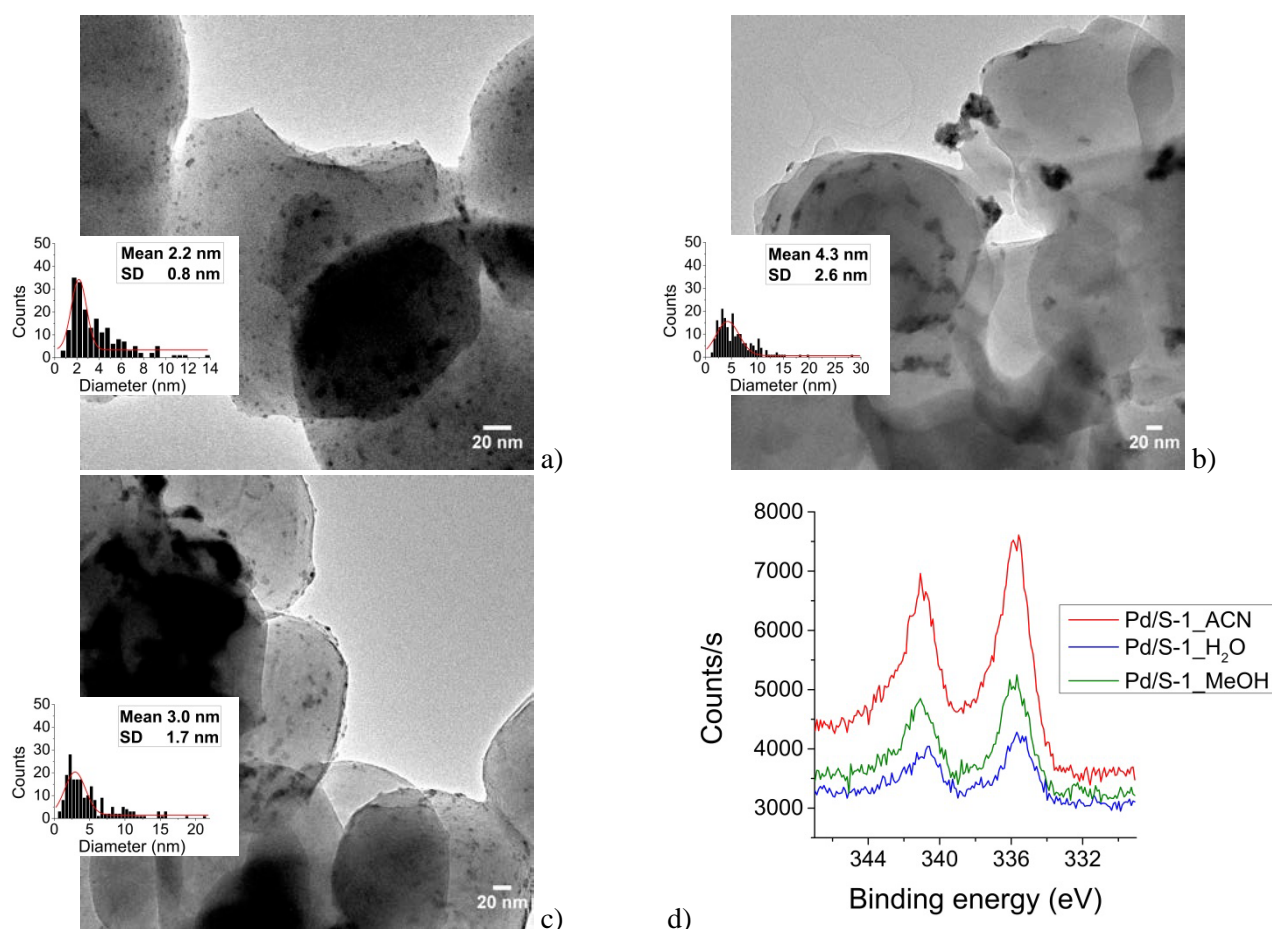
<sup>1</sup> Value determined from particle size distribution based on 200 particles measured from TEM images.



**Figure 4.11. a) XRD diffractograms, b) zoomed-in XRD diffractograms, c) nitrogen physisorption isotherms (offset of 50) of palladium catalysts prepared with different solvents (acetonitrile, water, methanol) using the PAIR method.**

Figure 4.12 presents the representative TEM images of the prepared catalysts. Images of Pd/S-1\_ACN and Pd/S-1\_MeOH show palladium particles that are well distributed on the surface of the zeolite crystals. There is no clear indication that Pd nanoparticles could be located inside the zeolite framework. The size of palladium particles was  $2.2 \pm 0.8$  nm for Pd/S-1\_ACN,  $4.3 \pm 2.6$  nm for Pd/S-1\_H<sub>2</sub>O, and  $3.0 \pm 1.7$  nm for Pd/S-1\_MeOH, as shown in Table 4.9. The nanoparticles in methanol and acetonitrile samples were more uniform in size and distribution over the support than for water sample. For water sample a lot of large aggregates of palladium 10 – 50 nm in size are visible on the external surface of silicalite-1. The presence of these large aggregates is well depicted in the value of average particle size of Pd/S-1\_H<sub>2</sub>O which is much higher than the mean particle size compared to Pd/S-1\_MeOH and Pd/S-1\_ACN samples, as shown in Table 4.9.

The size of nanoparticles for all three synthesized catalysts could be correlated with the amount of surface Pd detected in the XPS analysis, which is a surface-sensitive technique. Figure 4.12d shows the results from the XPS analysis performed for the investigated catalysts. The height of the signal associated with Pd decreases for the catalysts in order: Pd/S-1\_ACN > Pd/S-1\_MeOH > Pd/S-1\_H<sub>2</sub>O. The smaller the size of the particles the higher their surface area; hence, it could be speculated that Pd/S-1\_ACN having the particles which are the smallest in size would give the largest signal in XPS measurement, as observed.



**Figure 4.12.** TEM images and particle size distribution calculated for palladium catalysts prepared with different solvents using the PAIR method: a) Pd/S-1\_ACN, b) Pd/S-1\_H<sub>2</sub>O, c) Pd/S-1\_MeOH, d) XPS spectrum with palladium 3d scan.

It was shown that the PAIR method can be successfully applied to yield palladium nanoparticles supported on silicalite-1. With acetonitrile as solvent, palladium nanoparticles were small in size and uniformly deposited on the external surface of silicalite-1.

#### 4.3.2 Synthesis of platinum nanoparticles in silicalite-1

Application of PAIR method to incorporate platinum nanoparticles into zeolites was tested in the series of experiments involving variation in solvent (water, methanol, acetonitrile), zeolite type (S-1, ZSM-5, LTA) and platinum precursor ( $\text{H}_2\text{PtCl}_6 \cdot 6\text{H}_2\text{O}$ ,  $\text{PtCl}_4$ ) according to procedure described in Chapter 3 (section 3.2.3. *General procedure for the PAIR method*). None of the performed experiments yielded small Pt nanoparticles (< 100 nm) incorporated into zeolite matrix or deposited uniformly on its surface. The reason for it might be connected with different electronic structure of platinum compared to palladium and gold; hence different interaction of platinum species with solvents and support. More experimental work is necessary to study the PAIR method for the implementation in the synthesis of platinum in silicalite-1.

### 4.4 PAIR method applied to non-zeolitic support

#### 4.4.1 Synthesis of gold nanoparticles on mesoporous silica

The PAIR method was applied to amorphous mesoporous silica to yield gold catalysts on a non-zeolitic support. The PAIR procedure applied to mesoporous silica was compared with the impregnation method. Additionally, catalysts obtained in both ways were subjected to calcination in air at 400 °C for 2 h in order to investigate the sintering stability of gold nanoparticles. Table 4.10 gives the overview of the prepared materials. The analysis of the investigated catalysts was performed using nitrogen physisorption, XRD and TEM techniques, and presented in Table 4.11, Figure 4.14 and Figure 4.13.

**Table 4.10. Overview of the gold catalysts prepared with amorphous mesoporous silica as support using the PAIR method, simple impregnation method, and both followed by additional calcination in air at 400 °C for 2 h.**

Catalyst name	Treatment
Au/SiO <sub>2</sub> _PAIR	PAIR
Au/SiO <sub>2</sub> _PAIR_C	PAIR+ calcination in air at 400 °C for 2 h
Au/SiO <sub>2</sub> _IM	Impregnation
Au/SiO <sub>2</sub> _IM_C	Impregnation + calcination in air at 400 °C for 2 h

The XRD diffractograms of the investigated catalysts are shown in Figure 4.13a. No crystallinity connected to the support material was detected, as expected. Strong reflexes of gold are visible at  $2\theta = 38.17$  and  $2\theta = 44.37$  (JCPDS 010-71-4616) for all investigated catalysts indicating the presence of large gold nanoparticles.

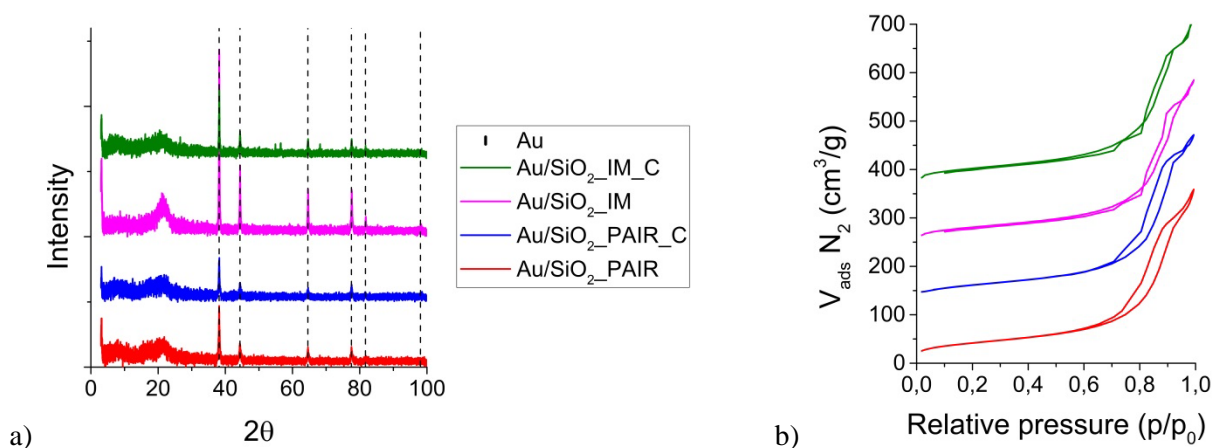
The results from nitrogen physisorption analysis of the investigated catalysts are shown in Table 4.11. A small decrease in the total pore volume occurred for all gold catalysts after impregnation compared to the pure silica support. It could be attributed to the presence of nanoparticles on the surface of the support blocking the access to inner pores (Cai et al. 2013). The remaining values of micropore volume, external surface area and BET surface area do not change much between the catalysts and the parent material. The

isotherms obtained from the nitrogen physisorption analysis are presented in Figure 4.13b. All of them are of IV type which is characteristic for mesoporous material (Thommes 2010).

**Table 4.11. Results from nitrogen physisorption and particle size distribution for gold catalysts prepared on amorphous mesoporous silica support with the PAIR method, simple impregnation method and both followed by additional calcination in air at 400 °C for 2 h.**

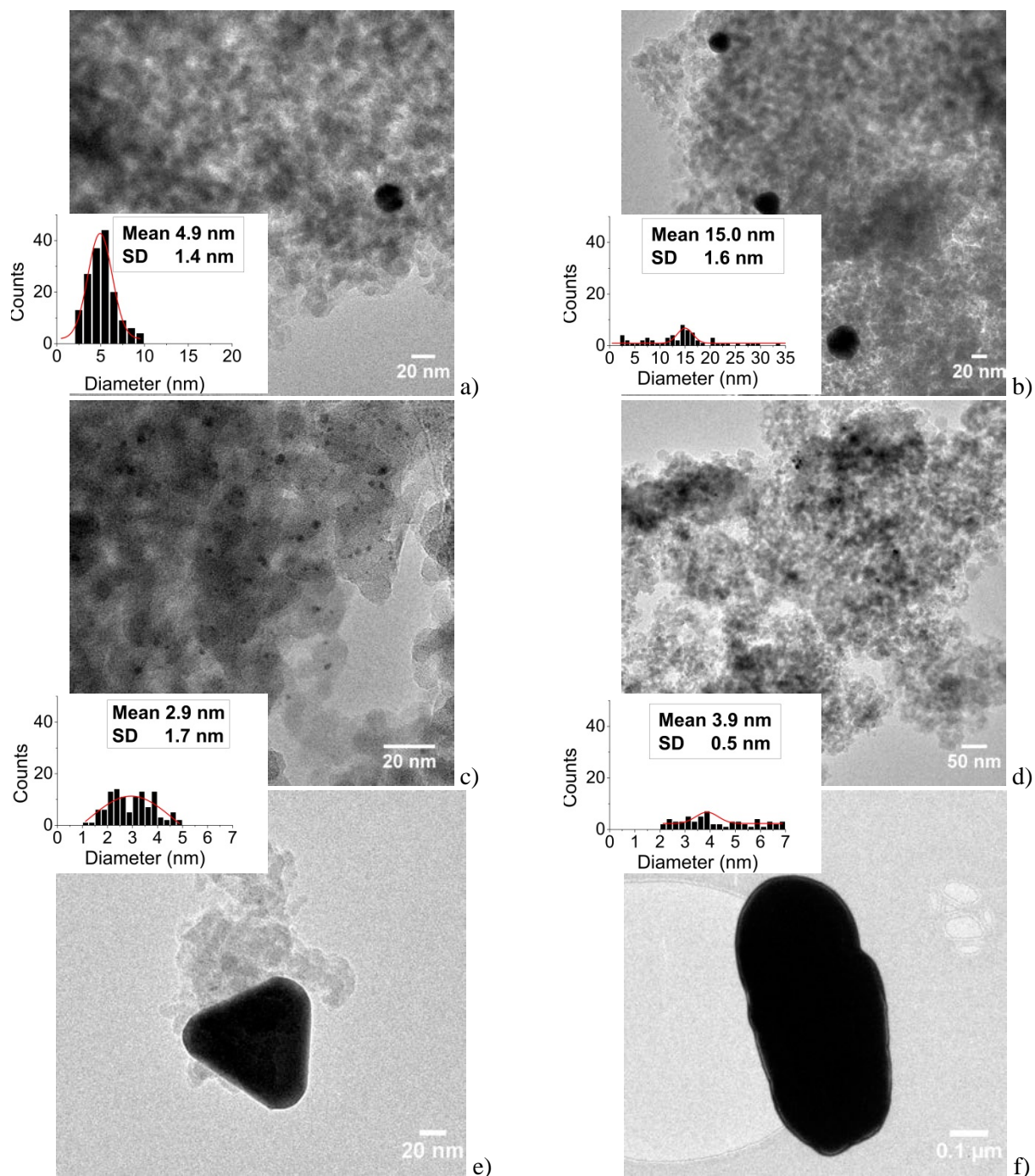
Catalyst name	Total pore volume (cm <sup>3</sup> /g)	External surface area (m <sup>2</sup> /g)	Total surface area BET (m <sup>2</sup> /g)	Mean <sup>1</sup> particle size (nm)	Average <sup>1</sup> particle size (nm)
SiO <sub>2</sub>	0.494	136	149	-	-
Au/SiO <sub>2</sub> _PAIR	0.476	141	151	4.9 ± 1.4	7.1 ± 5.3
Au/SiO <sub>2</sub> _PAIR_C	0.483	138	151	15.0 ± 1.6	16.7 ± 18.6
Au/SiO <sub>2</sub> _IM	0.472	136	148	2.9 ± 1.7	3.1 ± 1.0
Au/SiO <sub>2</sub> _IM_C	0.467	143	154	3.9 ± 0.5	4.6 ± 1.9

<sup>1</sup> Values determined from the measurements of 200 nanoparticles from TEM images.



**Figure 4.13. a) XRD diffractograms, b) nitrogen physisorption isotherms (offset of 120) of gold catalysts prepared on silica support using the PAIR method, simple impregnation method and both followed by additional calcination in air at 400 °C for 2 h.**

Figure 4.14 depicts the representative TEM images of the prepared gold catalysts. All samples show large nanoparticles of gold scattered around the support. Surprisingly, the particles obtained from the impregnation method have the average size of 3.1±1.0 nm which is smaller than the ones from the PAIR method, ~ 5nm (Table 4.11). Additionally, the respective samples subjected to calcination show much larger nanoparticles for the Au/SiO<sub>2</sub>\_PAIR\_C catalyst with broader size distribution than for Au/SiO<sub>2</sub>\_IM\_C. On the other hand, in both samples Au/SiO<sub>2</sub>\_IM and Au/SiO<sub>2</sub>\_IM\_C, very large nanoparticles of gold >100 nm were found.



**Figure 4.14. TEM images and particle size distribution calculated for gold catalysts prepared with amorphous mesoporous silica support using the PAIR method, simple impregnation method and both followed by additional calcination: a) Au/SiO<sub>2</sub>\_PAIR, b) Au/SiO<sub>2</sub>\_PAIR\_C, c) Au/SiO<sub>2</sub>\_IM, d) Au/SiO<sub>2</sub>\_IM\_C.**

It was shown that the synthesis of gold nanoparticles supported on amorphous mesoporous silica using the PAIR method yields the material with poor distribution of gold over the support and broad distribution of sizes of gold nanoparticles. It is suggested that more experimental work should be performed in order to improve the performance of this method on amorphous mesoporous silica support.

## 4.5 Study of the method

In this section, the study of the PAIR procedure is described. The analysis contains three sets of experiments:

- the variation of the physical conditions applied during the PAIR procedure (pressure and dwell time of hydrogen or nitrogen, heating ramp) and their influence on the morphology of the final materials determined by TEM
- reduction temperature of the gold species involved in the process – TPR analysis
- artefacts and residual solvent remaining in the final material after synthesis – ATR analysis

Details of each of the experiments are described below. Discussion and conclusion from the results are provided as well.

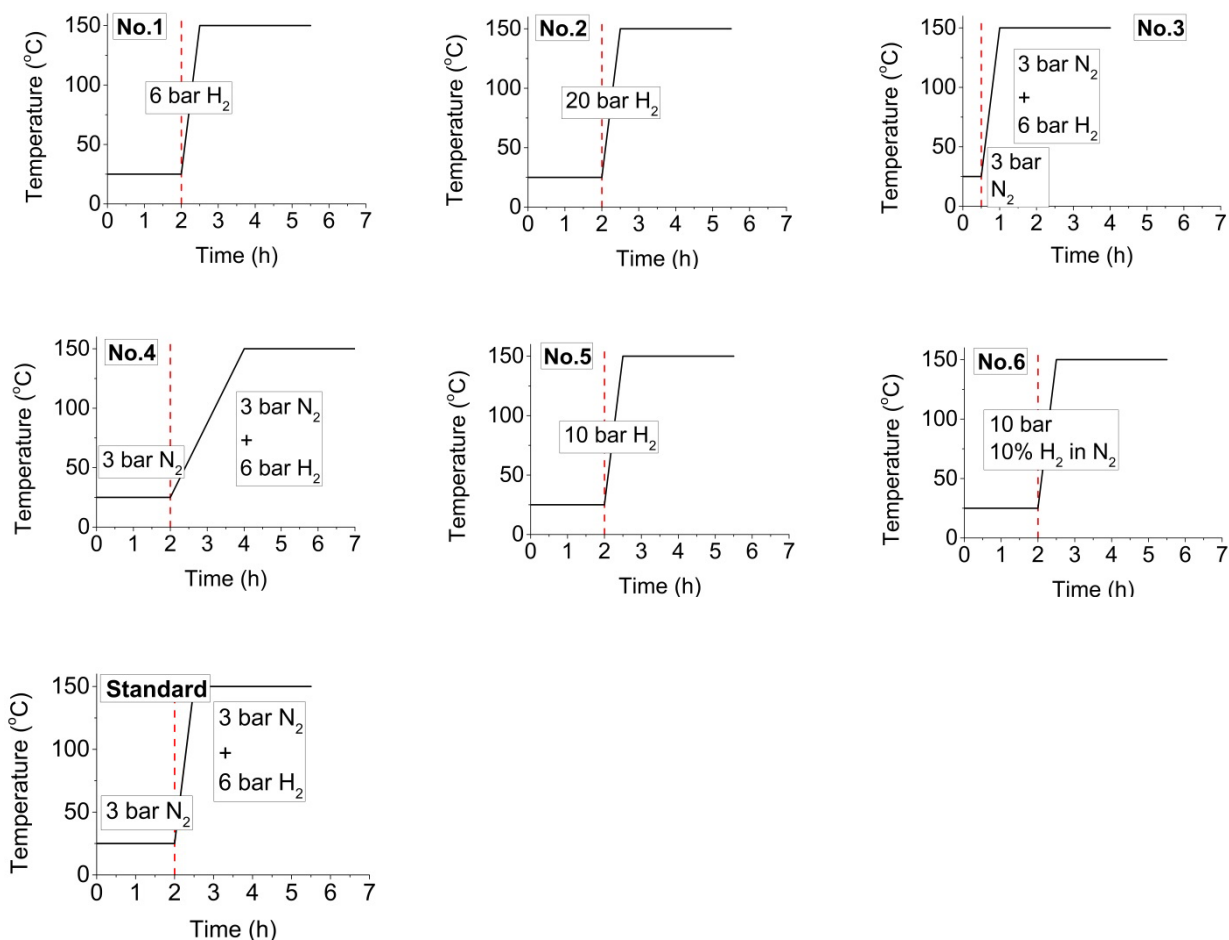
### 4.5.1 Influence of the PAIR conditions on the morphology of the materials

In this section the influence of the physical conditions applied during the PAIR method is analyzed with respect to morphology of the final material. The assessment is based on the TEM analysis of the obtained materials – size of gold nanoparticles and their location – external surface or pores of zeolite. The overview of the performed experiments is gathered in Table 4.12 and depicted in Figure 4.15.

The influence of nitrogen pressure and its dwell time, hydrogen pressure and its dwell time were investigated for two sets of catalyst preparation formulas: with  $\text{HAuCl}_4 \cdot 3\text{H}_2\text{O}$  + 0.3 ml water, and  $\text{AuCl}_3$  + 0.3 ml methanol, used for impregnation of silicalite-1. The temperature of the PAIR process remained unchanged, in order to limit the sintering possibility of gold nanoparticles during the reduction step. The entry referred as ‘‘Standard’’ gives the experimental conditions used to produce materials described in the previous sections of this chapter. For entries 1, 2, 5, 6 the experiment was performed with 2 h impregnation under 6 bar of hydrogen followed by reduction at the same pressure for another 3 h. No nitrogen was used in these experiments, except for entry 6 for which 10%  $\text{H}_2$  in  $\text{N}_2$  was used. Material from entry 3 was prepared with shorter nitrogen dwell time – only 0.5 h compared to 2 h in the standard experiment. Material from entry 4 was prepared with longer heating ramp – 2 h compared to 0.5 h used in the standard experiment. The graphical representation of the modified sets of conditions is shown in Figure 4.15.

**Table 4.12. Overview of the gold catalysts prepared with modified set of conditions applied to the PAIR method.**

No.	Precursor	Solvent 0.3 ml	$\text{N}_2$ pressure	$\text{N}_2$ dwell time	$\text{H}_2$ pressure	$\text{H}_2$ dwell time	Temperature	Heating ramp
1	$\text{HAuCl}_4 \cdot 3\text{H}_2\text{O}$	$\text{H}_2\text{O}$	-	-	6 bar	2 h + 3 h	150 °C	0.5 h
2	$\text{HAuCl}_4 \cdot 3\text{H}_2\text{O}$	$\text{H}_2\text{O}$	-	-	20 bar	2 h + 3 h	150 °C	0.5 h
3	$\text{HAuCl}_4 \cdot 3\text{H}_2\text{O}$	$\text{H}_2\text{O}$	3 bar	0.5 h	6 bar	3 h	150 °C	0.5 h
4	$\text{AuCl}_3$	MeOH	3 bar	2h	6 bar	3 h	150 °C	2 h
5	$\text{AuCl}_3$	MeOH	-	-	10 bar	2 h + 3 h	150 °C	0.5 h
6	$\text{AuCl}_3$	MeOH	10 bar 10% $\text{H}_2$ in $\text{N}_2$			2 h + 3 h	150 °C	0.5 h
<b>Standard</b>	-	-	<b>3 bar</b>	<b>2 h</b>	<b>6 bar</b>	<b>3 h</b>	<b>150 °C</b>	<b>0.5 h</b>

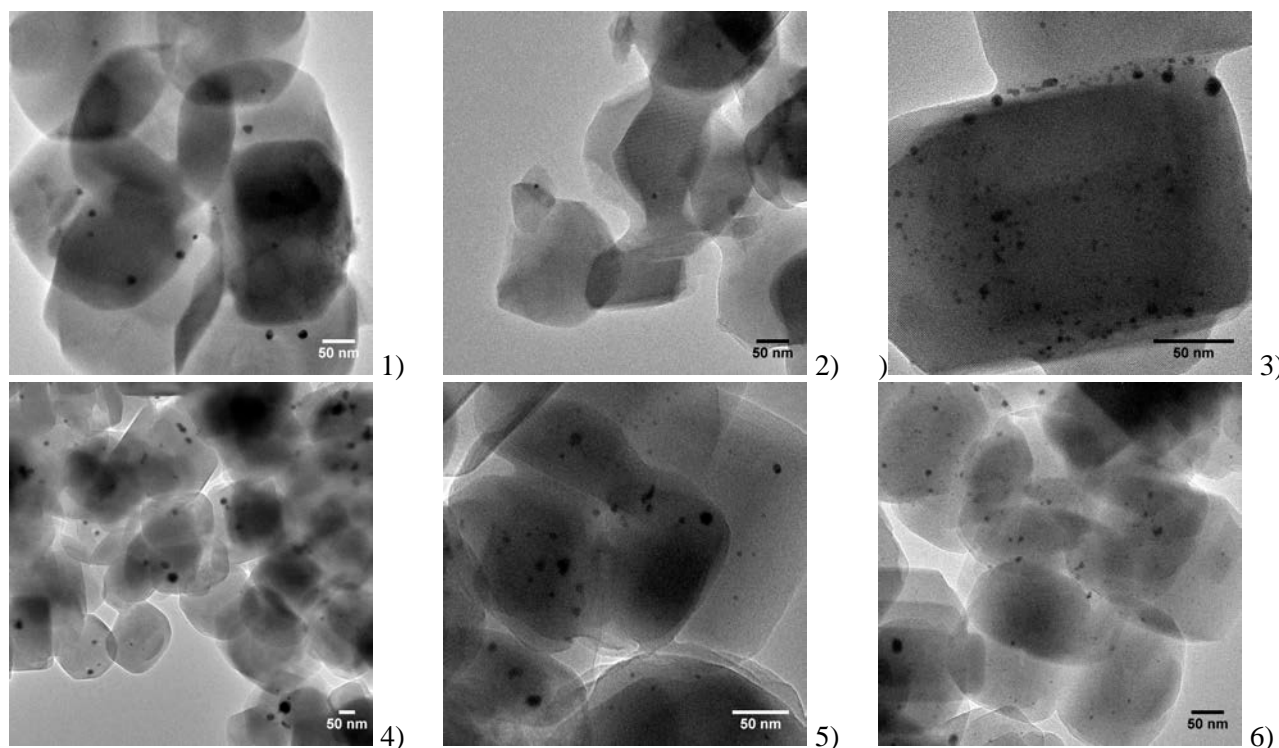


**Figure 4.15.** Graphical representation of the modified sets of conditions applied to the PAIR method to synthesize gold in silicalite-1 catalysts.

The representative images from TEM analysis are shown in Figure 4.16. The clear difference between the catalysts reported in previous sections, and the ones presented in Figure 4.16 can be visible. In general, nanoparticles of gold are larger in size and their distribution over the support is poor. For materials synthesized with the use of hydrogen alone (entry 1, 2, 5) the nanoparticles of gold were very difficult to spot in the sample and they were large in size, as shown in Figure 4.16. Shorter impregnation step under nitrogen, used in the synthesis of material in entry 3, resulted in a very limited incorporation of nanoparticles inside the support – nanoparticles were located on the external surface of the zeolite crystals or close to it. The use of 10% H<sub>2</sub> in N<sub>2</sub> during the whole PAIR procedure did not yield satisfactory results as well (entry 6) – nanoparticles were large and difficult to find in the sample. The prolonged heating ramp (entry 4) resulted in only large nanoparticles deposited on the surface of zeolite crystals.

Based on the presented results, composition and pressure of gases used during the PAIR procedure, longer times of impregnation under nitrogen and shorter heating ramp occurred to have an influence on the degree of encapsulation and nanoparticle size. The use of hydrogen or 10% H<sub>2</sub> in N<sub>2</sub> at high pressures for the impregnation step occurred to be ineffective for the procedure. All in all, the modification of the standard conditions used during the PAIR procedure was not necessary. The choice of conditions in the ‘‘standard’’ PAIR procedure yielded superior materials in terms of gold nanoparticle size and encapsulation degree, compared to any of the modified procedures presented in Table 4.12.





**Figure 4.16.** TEM images recorded for the gold catalysts prepared with the modified sets of conditions during the PAIR method. Numbers refer to the sample numbers in Table 5.13.

#### 4.5.2 Investigation on the reduction of gold species

In order to study the reduction temperature of different gold salts used in the study TPR experiments were performed. Figure 4.17 presents the results from the TPR analysis performed for the selected materials. Sample  $\text{HAuCl}_4 \cdot 3\text{H}_2\text{O}/\text{H}_2\text{O\_RED}$  refers to material synthesized using the PAIR method and therefore already reduced. Samples  $\text{HAuCl}_4 \cdot 3\text{H}_2\text{O}/\text{H}_2\text{O}$ ,  $\text{HAuCl}_4 \cdot 3\text{H}_2\text{O}/\text{MeOH}$ ,  $\text{HAuCl}_4 \cdot 3\text{H}_2\text{O}/\text{ACN}$ , and  $\text{AuCl}_3/\text{ACN}$  are unreduced samples prepared using impregnation method. All investigated catalysts were prepared with gold loading of 1wt% and 0.3 ml of solvent. The pure silicalite-1 sample was analyzed as a reference material.

The plots from TPR study of hydrogen consumption per g of sample versus temperature are shown in Figure 4.17. Comparing the plots recorded for the individual samples, it is visible that the choice of solvent does not influence the reduction temperature of gold. All three samples prepared with  $\text{HAuCl}_4 \cdot 3\text{H}_2\text{O}$  and different solvents (water, methanol, acetonitrile) got reduced at 210 °C. This is in good agreement with data reported by Baatz et al. (2008), Wiberg et al. (2001), and Merga et al. (2010). For the sample prepared with  $\text{AuCl}_3$  the reduction temperature was 160°C, as shown in Figure 4.17. The difference in reduction temperature between samples prepared with  $\text{HAuCl}_4 \cdot 3\text{H}_2\text{O}$  and  $\text{AuCl}_3$  might be connected with the different chemical structure of precursors used.  $\text{AuCl}_3$  when dissolved in water forms  $[\text{AuCl}_3(\text{OH})]^-$  ions, while  $\text{HAuCl}_4 \cdot 3\text{H}_2\text{O}$  dissolved in water forms  $\text{AuCl}_4^-$  ions (Corma et al. 2008). As described by Puddephat (1978) the redox potential of gold complex strongly depends on the complexation ligands – the lower the potential of a gold complex, the more difficult it undergoes the reduction, and the more stable the complex is. In  $[\text{AuCl}_3(\text{OH})]^-$ , chlorine is substituted by the hydroxy group what causes the increase in the redox potential of

the complex (and lower complex stability (Usher et al. 2009)). This results in lower temperature of reduction of Au(III) to metallic gold, as observed in the performed study for the AuCl<sub>3</sub> sample.

Baatz et al. (2008) and Ivanova et al. (2004) reported the existence of different gold (III) complexes according to pH values and chlorine concentration in the solution. Baatz et al. (2008) showed the dependence of the temperature of reduction recorded in TPR measurement on the pH of the precursor solution where the samples with low pH were much harder to reduce (higher temperature required) than those of higher pH. Higher reduction temperature was attributed to higher chlorine content in the complex with lower pH. For the samples investigated in this study, the pH of H<sub>2</sub>AuCl<sub>4</sub>·3H<sub>2</sub>O and AuCl<sub>3</sub> solutions measured during the synthesis procedure using the universal lakmus paper was determined as pH = 0 – 1 and pH = 3, respectively. Again, as observed in the performed TPR experiment, the sample impregnated with solution with lower pH and higher Cl<sup>-</sup> content prepared from H<sub>2</sub>AuCl<sub>4</sub>·3H<sub>2</sub>O precursor was much harder to reduce than the sample prepared from AuCl<sub>3</sub> having higher pH and containing lower concentration of chlorine.

Another explanation of the very low temperature of reduction of sample prepared with AuCl<sub>3</sub> might be that AuCl<sub>3</sub> is known to decompose upon heating at temperatures above 160 °C to form AuCl and finally Au<sup>0</sup> (Greenwood et al., 2001). All in all, the lower temperature required for reduction of AuCl<sub>3</sub> might make this precursor a better candidate for the synthesis of supported gold nanoparticles. Lower reduction temperature could limit the possible sintering of nanoparticles occurring during the reduction procedure.

The difference in amount of consumed hydrogen that can be observed between respective samples can be connected with the different times of drying of the catalysts. All the samples were prepared at the same time; however some of them had to ‘wait’ longer for the analysts. During that time smaller or higher amount of the sample could undergo reduction in air, leaving less unreduced gold species to give signal in the experiment.

The sample H<sub>2</sub>AuCl<sub>4</sub>·3H<sub>2</sub>O/H<sub>2</sub>O\_RED showed no hydrogen consumption indicating the complete reduction of gold species after the PAIR method. The successful reduction of metal nanoparticles using hydrogen at high pressures and mild temperature was also reported by Li et al. (2014) for gold-containing nanoparticles and Uznanski et al. (2010) for silver nanoparticles.

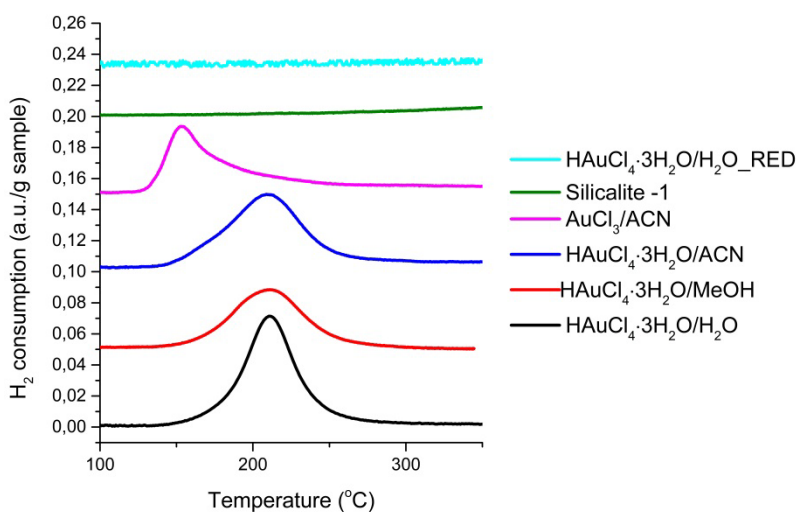


Figure 4.17. Results from TRP analysis (offset of 0.5) performed for the chosen catalysts prepared using the PAIR method.

### 4.5.3 Investigation on the artefacts arising from the solvents

ATR analysis was performed on selected catalysts, each prepared with different solvent: water, methanol, acetonitrile, 1-butanol, in order to investigate the possible residuals or artifacts coming from these solvents in the catalysts after the synthesis. All the catalysts were prepared by the PAIR method with  $\text{HAuCl}_4 \cdot 3\text{H}_2\text{O}$  dissolved in 0.3 ml of solvent. The ATR corrected spectrum recorded for the investigated samples is shown in Figure 4.18. The area of the spectrum shaded in grey refers to the region in spectrum where artifacts coming from the diamond crystal occur.

Comparing the signals obtained for different samples, the signal from the sample prepared with 1-butanol (purple line) shows features that are not visible for the remaining samples. The very weak vibrations located at  $\nu = 2962, 2875, 1728, 1466 \text{ cm}^{-1}$  are visible. The vibrations were characterized based on comparison with data recorded for n-butanol obtained from the National Institute of Standards and Technology (NIST), and are detailed in Table 4.13. All the vibrations were identified as coming from the alkyl groups of 1-butanol and none of the vibrations associated with the hydroxyl group (C-O stretch at  $\sim 1000 \text{ cm}^{-1}$  and O-H stretch at  $\sim 3200 \text{ cm}^{-1}$ ) could be visible in the spectrum. The vibrations probably originate from decomposition products of 1-butanol, deposited in the pores of the zeolite, which was not removed during the reduction step in the PAIR method. The presence of these leftovers might influence the activity of the catalyst; hence a special care was given to interpretation of the results from dehydrogenation of formic acid performed over this catalyst.

Table 4.13. Selected IR characteristic bands of 1-butanol present in the ATR spectrum recorded for the gold catalyst prepared with 1-butanol as solvent.

Wavelength ( $\text{cm}^{-1}$ )	Vibration mode
2962	$\text{sp}^3$ C-H stretching
2875	$\text{sp}^3$ C-H stretching
1728	$\text{CH}_2$ bend
1466	$\text{CH}_3$ bend

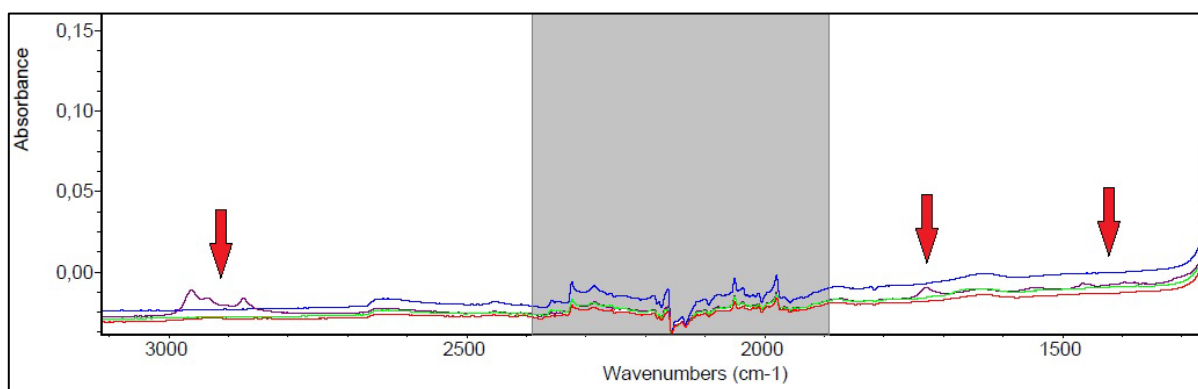


Figure 4.18. ATR spectra recorded for gold catalysts prepared with different solvents: water (green line), methanol (red line), acetonitrile (blue line) and 1-butanol (purple line) using the PAIR method. Red arrows indicate the characteristic bands of 1-butanol (purple line). The grey area refers to the part of the spectrum where artifacts from the diamond crystal occur.

## 4.6 General discussion of the PAIR method

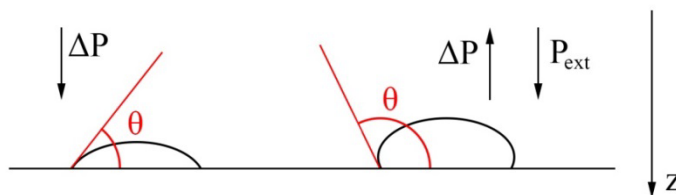
In this section, all the results presented so far are discussed. The influence of various parameters studied within the scope of the PAIR method (choice of solvent, precursor, and solvent volume, kind of zeolite, support, and metal) is discussed and compared to published results, when possible. Additionally, an analysis of the PAIR method is proposed from a theoretical point of view with respect to diffusion of liquids in porous materials, wettability of solvents and their contact angles on different supports and capillary forces.

### 4.6.1 Theoretical investigations

According to the nature of the interaction between a liquid and the surface of the porous material it is laid on, the potential penetration of this liquid into the porous system depends on two different forces – capillary pressure and the externally applied pressure. Capillary pressure is governed by Washburn's Equation 1.

$$\Delta P = \frac{4\gamma\cos\theta}{D} \quad (\text{Equation 1})$$

Where:  $\Delta P = P_L - P_G$  is the pressure difference across the meniscus between the liquid and the gas phase;  $\gamma$  is the surface tension of the liquid;  $\theta$  is the contact angle between the solid surface and the liquid;  $D$  is the diameter of the pore.



**Figure 4.19. Difference between wetting (left) and non-wetting (right) liquids with respect to contact angles  $\theta$  and pressures required for penetration of capillary pore.**

In the case of a wetting liquid,  $\theta < 90^\circ$  therefore  $\cos\theta$  in Equation 1 has a positive value, what means that  $\Delta P$  is oriented along the  $z$ -axis as shown in Figure 4.19 and the liquid can penetrate the pore by capillary action alone. In the case of a non-wetting liquid,  $\theta > 90^\circ$  therefore  $\cos\theta$  is negative so  $\Delta P$  is oriented against the  $z$ -axis and the liquid is expelled from the pore. To ensure that the non-wetting liquid penetrates the pore, an external pressure (oriented along the  $z$ -axis on Figure 4.19) must be applied to balance the negative capillary pressure. The minimum external pressure can be defined as Equation 2.

$$P_{ext} = -\Delta P \quad (\text{Equation 2})$$

What gives Equation 3:

$$P_{ex} = -\frac{4\gamma\cos\theta}{D} \quad (\text{Equation 3})$$

Equation 3 will be used to evaluate the PAIR method in terms of: external pressure applied during the synthesis and its dependence on the choice of solvent.

The values of contact angles for the four solvents used in this study (water, methanol, acetonitrile, 1-butanol) were obtained from the literature and they refer to the contact angles determined on the surface of hydrophobic silica. Here, silicalite-1 is assumed as a pure silica material with hydrophobic pores and channels (Trzpit et al. 2008, Eroshenko et al. 2001); however, it must be clarified that the hydrophobic/hydrophilic properties of silicalite-1 highly depend on the reagents used for the synthesis. The values of contact angles found for the four solvents in question are given in Table 4.14. The contact angle of all the organic solvents – methanol, acetonitrile and 1-butanol are very small compared to water, and they are all below  $90^\circ$ . Thus, according to equation (1) the capillary pressure would be enough to introduce their solutions into the pores of silicalite-1. In case of water, for which the contact angle is larger than  $90^\circ$ , the capillary pressure would have a negative sign and act in the opposite direction, preventing the liquid from entering the pores. Thus, in case of water, the external pressure would be required to push the solution inside the pores.

The minimum external pressure required to force water into the pores of hydrophobic silica was calculated using Equation 3 for two values of contact angle -  $\theta = 110^\circ$  and  $\theta = 102^\circ$ , and surface tension of water at  $25^\circ\text{C}$   $\gamma = 0.0727$  dynes/cm (Yaw et al. 2008). The values of required external pressure with respect to pore size are given in Table 4.15. For pores in the range of the ones found in silicalite-1 (0.45-0.6) (Table 4.16), the pressures needed to push water inside are extremely high, above 1000 bar, while the physically achievable values (6-20 bar) are obtained for pores in the range 5-10 nm. According to presented pressure calculations, it would be very difficult to force water solution into such small pores, meaning that only the larger pores or voids could be accessed. It could also mean that the micropores of silicalite-1 might never be accessed by the aqueous solution meaning that nanoparticles may theoretically be impossible to find in those pores.

However, zeolites, including silicalite-1, can have varying hydrophobic/hydrophilic properties arising from defects and damage on the surface and inside the pores introduced during the zeolite synthesis (Jesionowski et al. 2003). The more damage and defects present in the crystalline structure of the zeolite, the more hydrophilic sites are introduced into the structure which can act as preferential adsorption sites for water molecules (Huang et al. 2006). As a result the contact angle between water and silicalite-1 would be lower than assumed in the above calculations. Under these conditions, pressures of ranges achievable in the laboratory could be sufficient to embed nanoparticles in the pores of silicalite-1. This could explain a successful impregnation of silicalite-1 with aqueous gold precursor solution using pressures in the range 3-9 bar in the PAIR procedure.

**Table 4.14. Values of contact angles reported for the solvents used in the study of the PAIR method.**

Solvent	Contact angle	Reference
Water	110	Giovambattista et al. 2007
	102	Jayaraman et al. 2005
Acetonitrile	< 10	Hornig et al.2010
Methanol	< 55	Mirji et al. 2006
	10	Jayaraman et al. 2005
	20	Li et al. 2010
1-Butanol	< 5	Li <sup>2</sup> et al. 2014

**Table 4.15. Calculations of minimum external pressure required with respect to pore size diameter for water and hydrophobic silica for two values of water/silica contact angle.**

Pore diameter D (nm)	Minimum external pressure P <sub>ext</sub> (bar)	
	$\theta = 110^\circ$	$\theta = 102^\circ$
0.2	4973	3023
0.3	3315	2015
0.4	2486	1512
0.5	1989	1209
1	995	605
2	497	302
5	20	12
10	10	6

**Table 4.16. Pore size reported for zeolites used in the study of the PAIR method.**

Zeolite	Most representative pore size (nm) <sup>1</sup>
MFI (S-1, ZSM-5)	0.45 – 0.6
LTA	0.3 – 0.45

<sup>1</sup> McCusker et al. 2001

#### 4.6.2 Comparison of the PAIR method and impregnation method

The effect of the PAIR method in terms of size of nanoparticles and their stability towards sintering was investigated based on experiments performed for samples:

- Au/S-1\_PAIR described in 4.1.1 *Synthesis conditions: HAuCl<sub>4</sub> · 3H<sub>2</sub>O + 0.15 ml solvent*
- Au/S-1\_IM described in 4.1.1 *Synthesis conditions: HAuCl<sub>4</sub> · 3H<sub>2</sub>O + 0.15 ml solvent*

The mean sizes of gold nanoparticles found in the fresh and calcined samples (400 °C in air for 2 h) prepared using the PAIR method and impregnation method are shown in Table 4.17. For the samples prepared with PAIR the size of nanoparticles in the fresh catalyst was 2.2 ± 0.6 nm which increased to 3.3 ±

0.9 nm after calcination. For the material prepared with impregnation method the size of gold nanoparticles before calcination was  $1.9 \pm 0.4$  nm, and after  $4.0 \pm 2.5$  nm. The size of gold nanoparticles in sample prepared by impregnation before calcination was smaller; however, the increase in size of nanoparticles after calcination was much larger than for sample prepared with PAIR. The increase in the particle size after calcination could be associated with sintering of nanoparticles deposited on the external surface of zeolite crystal. If so, it could mean that there were more surface nanoparticles in the sample prepared with impregnation method than in the one prepared with PAIR.

Additionally, comparing the mean and average numbers for size of gold nanoparticles for the PAIR sample and impregnation sample, it is visible that the difference in values is much larger for the impregnation samples -  $1.9 \pm 0.4$  nm versus  $4.0 \pm 2.5$ , than for PAIR samples -  $2.2 \pm 0.6$  nm versus  $2.7 \pm 2.2$  nm. It could indicate that there were larger nanoparticles deposited on the external surface of silicalite-1 crystals in sample prepared with impregnation method. It is in good agreement with the increase in size of nanoparticles in this sample after calcination. The presented results could indicate that the PAIR procedure facilitates the formation of nanoparticles inside the pores of zeolite which exhibit increased sintering stability compared to the impregnation method.

**Table 4.17. Mean and average sizes of gold nanoparticles obtained for fresh and calcined materials prepared using PAIR and impregnation methods.**

Method used	Mean size (nm)		Average size (nm)	
	Fresh	Calcined <sup>1</sup>	Fresh	Calcined <sup>1</sup>
<b>PAIR</b>	$2.2 \pm 0.6$	$3.3 \pm 0.9$	$2.7 \pm 2.2$	$4.0 \pm 2.5$
<b>Impregnation</b>	$1.9 \pm 0.4$	$4.0 \pm 2.5$	$4.0 \pm 2.5$	$8.6 \pm 3.6$

<sup>1</sup>Calcined at 400 °C in ir for 2 h.

#### 4.6.3 Influence of the solvent volume used for impregnation during the PAIR procedure

The influence of the volume of solvent used in the synthesis on the size and sintering stability of gold nanoparticles in silicalite-1 is investigated based on results obtained for two samples prepared using the PAIR method:

- Au/S-1\_PAIR described in 4.1.1 *Synthesis conditions:  $\text{HAuCl}_4 \cdot 3\text{H}_2\text{O} + 0.15$  ml solvent*
- Au/S-1\_3\_H<sub>2</sub>O described in 4.1.2 *Synthesis conditions:  $\text{HAuCl}_4 \cdot 3\text{H}_2\text{O} + 0.15$  ml of different solvents*

Both samples were prepared with  $\text{HAuCl}_4 \cdot 3\text{H}_2\text{O}$  as a precursor and dissolved in either 0.15 ml or 0.3 ml of water. The mean sizes of nanoparticles are given in Table 4.18. Comparing the mean particle size for these two catalysts, a clear difference between  $2.2 \pm 0.6$  nm for Au/S-1\_PAIR and  $3.5 \pm 1.5$  nm for Au/S-1\_3\_H<sub>2</sub>O is visible. The volume of 0.15 ml is very close to the total pore volume of the silicalite-1 used for impregnation ( $0.176 \text{ cm}^3/\text{g}$ ); hence, less of the solution is prone to remain adsorbed on the external surface of zeolite crystals. It is believed that nanoparticles that are formed inside the zeolite framework are smaller than the ones on the surface since they meet the steric limitation of the crystal framework which limits their growth possibility and mobility for agglomeration and sintering (Hashimoto et al. 2008). However, when a significant volume of a precursor solution remains on the external surface, as it is in case of 0.3 ml-prepared samples, a distinctive amount of nanoparticles might be formed on the outer surface where they can grow and migrate easily. Since the amount of gold is the same in both cases, for 0.15 ml-catalyst the fraction of

gold that is left out on the surface is smaller than for 0.3 ml-catalyst. It means that more nanoparticles could be incorporated inside the zeolite channels and be of smaller size. It is directly associated with the quality of the catalyst as the catalytic activity of gold in nanometric scale highly depends on the size of nanoparticles (Haruta 2004). Hence, for the synthesis of zeolite with small gold nanoparticles incorporated inside the pores by the PAIR method, it might be advantageous to use a volume of solvent which is equal to or slightly lower than the total pore volume of a zeolite.

**Table 4.18. Mean particle sizes for samples prepared using PAIR with different volumes of water used for synthesis.**

Sample	Solvent volume (ml)	Mean size (nm)
Au/S-1_PAIR	0.15	2.2 ± 0.6
Au/S-1_3_H <sub>2</sub> O	0.3	3.5 ± 1.5

#### 4.6.4 Influence of the choice of solvent used during the PAIR procedure

The evaluation of the influence of the choice of solvent on the size and encapsulation of gold nanoparticles inside the silicalite-1 framework achieved using the PAIR procedure is performed in this section. The results from two sets of experiments serve as basis for this assessment:

- 4.1.2 Synthesis conditions:  $\text{HAuCl}_4 \cdot 3\text{H}_2\text{O} + 0.3 \text{ ml of different solvents}$
- 4.1.3 Synthesis conditions:  $\text{AuCl}_3 + 0.3 \text{ ml of different solvents}$

Four different solvents: water, methanol, acetonitrile, 1-butanol, were used to encapsulate gold nanoparticles from two different precursors:  $\text{HAuCl}_4 \cdot 3\text{H}_2\text{O}$ ,  $\text{AuCl}_3$ , inside the pores of silicalite-1. Mean sizes of gold nanoparticles from these samples are given in Table 4.19.

Solvents like 1-butanol, acetonitrile and methanol, by having alkyl groups in their structure are known to interact better with highly hydrophobic pores and channels in the zeolite (Trzpit et al. 2008, Eroshenko et al. 2001). Comparing the values of contact angles found for the solvents in question, shown in Table 4.14, the organic solvents have much lower contact angles on silica than water. It means that the organic solvents would wet the surface of silica better than water. In case of pure-silica zeolite, like silicalite-1, it can be directly associated with better distribution of solution over the support, including the inner pores of the zeolite. Following this thinking, it might be that the catalyst with the smallest nanoparticles and lowest fraction of nanoparticles deposited on the surface would be obtained with an organic solvent.

For  $\text{HAuCl}_4 \cdot 3\text{H}_2\text{O}$  precursor, the mean sizes of gold nanoparticles obtained from different solvents applied during the PAIR procedure were fairly similar:  $3.5 \pm 1.5 \text{ nm}$  for water,  $3.1 \pm 2.1 \text{ nm}$  for methanol, and  $3.4 \pm 1.4 \text{ nm}$  for acetonitrile, as shown in Table 4.19. However, the smallest nanoparticles were obtained for methanol. After calcination the mean size increased slightly for the water sample -  $4.1 \pm 1.9 \text{ nm}$ , and remained in the same range for methanol -  $3.1 \pm 1.3 \text{ nm}$ , and acetonitrile -  $3.6 \pm 1.6 \text{ nm}$ , samples. The increase in the particle size after calcination could be associated with sintering of nanoparticles deposited on the external surface of zeolite crystal. If so, it could mean that there were more surface nanoparticles in the sample prepared with water than with methanol or acetonitrile. This would support the hypothesis that solvents with smaller contact angles would diffuse better into the pores of silicalite-1 during the PAIR procedure, facilitating the formation of small nanoparticles inside the pores.



For  $\text{AuCl}_3$  precursor the mean sizes of gold nanoparticles obtained using organic solvents were smaller than for water, as shown in Table 4.19. The smallest nanoparticles were found in sample prepared with 1-butanol -  $1.6 \pm 0.5$  nm. The size of nanoparticles did not increase much after calcination for samples prepared with organic solvents. For the water sample the increase in particle size occurred from  $2.4 \pm 1.4$  nm to  $3.7 \pm 3.0$  nm. It is the biggest increase in the nanoparticle size recorded after calcination among samples prepared with  $\text{AuCl}_3$  as a precursor. For methanol the increase was from  $2.2 \pm 1.0$  nm to  $2.6 \pm 1.5$  nm and for acetonitrile from  $2.0 \pm 0.9$  nm to  $2.2 \pm 0.9$  nm. Similarly as for  $\text{HAuCl}_4 \cdot 3\text{H}_2\text{O}$  precursor, the smaller size of gold nanoparticles and their relative stability towards sintering in samples prepared with organic solvents could be connected with better wettability of silicalite-1 by these solvents. Hence, penetration of a solution and distribution of gold nanoparticles would be better in these samples.

**Table 4.19.** Mean sizes of gold nanoparticles obtained from two different precursors using the PAIR procedure applied to four different solvents.

Solvent	$\text{HAuCl}_4 \cdot 3\text{H}_2\text{O}$		$\text{AuCl}_3$	
	Fresh	Calcined <sup>1</sup>	Fresh	Calcined <sup>1</sup>
<b>Water</b>	$3.5 \pm 1.5$	$4.1 \pm 1.9$	$2.4 \pm 1.4^*$	$3.7 \pm 3.0$
<b>Methanol</b>	$3.1 \pm 2.1$	$3.1 \pm 1.3$	$2.2 \pm 1.0$	$2.6 \pm 1.5$
<b>Acetonitrile</b>	$3.4 \pm 1.4$	$3.6 \pm 1.6$	$2.0 \pm 0.9$	$2.2 \pm 0.9$
<b>1-butanol</b>	-	-	$1.6 \pm 0.5$	$1.7 \pm 0.7$

<sup>1</sup> Calcined in air at 400 °C for 2 h; \*not many nanoparticles were found; located on the external surface of silicalite-1

Summarizing, the presented results show that the choice of solvent for the synthesis of gold nanoparticles inside the pores of silicalite-1 might have a big influence on the size and sintering stability of nanoparticles. In general, organic solvents facilitated the formation of smaller nanoparticles encapsulated inside zeolite framework which were more stable towards sintering. However, it must be emphasized that the process of formation of nanoparticles is a very complex phenomena. As shown by Engelbrekt et al. (2013), the formation of nanoparticles of gold in solution is a very complicated process highly dependent on the environment in which the synthesis is performed. In the present study case the complexity of the process is enhanced by the presence of the zeolite matrix and possible variation in hydrophobic/hydrophilic character between pores and surface, their properties and interactions with solvents and solvated ions.

#### 4.6.5 Influence of the choice of precursor used during the PAIR procedure

The influence of the choice of precursor on the size and sintering stability of gold nanoparticles in silicalite-1 prepared using the PAIR method is investigated based on samples synthesized from two sets of experiments:

- 4.1.2 Synthesis conditions:  $\text{HAuCl}_4 \cdot 3\text{H}_2\text{O} + 0.3$  ml of different solvents
- 4.1.3 Synthesis conditions:  $\text{AuCl}_3 + 0.3$  ml of different solvents

The experiments performed for the two precursors in water show remarkably different results -  $\text{HAuCl}_4 \cdot 3\text{H}_2\text{O}$  used for catalyst Au/S-1\_3H<sub>2</sub>O gave gold nanoparticles of size  $3.5 \pm 1.5$  nm, as shown in Table 4.19, which were well distributed and encapsulated inside the silicalite-1 framework (Figure 4.4), while the gold nanoparticles prepared with  $\text{AuCl}_3$  precursor in catalyst Au/S-1\_H<sub>2</sub>O\_PAIR\_ AuCl<sub>3</sub> were  $2.4 \pm 1.4$  nm in size located mostly on the surface and difficult to spot in TEM analysis, indicating a very poor distribution around the support (Figure 4.6b). The difference in results obtained for the two precursors, more

acidic  $\text{HAuCl}_4 \cdot 3\text{H}_2\text{O}$  and less acidic  $\text{AuCl}_3$ , dissolved in water might be connected with the pH of the respective solutions and the isoelectric point of silicalite-1. Since silicalite-1 is a pure silica zeolite, the isoelectric point of silicalite-1 is 2 (Valtchev 2002). This means that at  $\text{pH} = 2$  the net charge on the surface of silicalite-1 is zero. The pH of  $\text{HAuCl}_4 \cdot 3\text{H}_2\text{O}$  solution used for impregnation is 1 and gold is in the form of  $(\text{AuCl}_4)^-$  ion (Corma et al. 2008). The pH of the  $\text{AuCl}_3$  solution is 3 and gold is in the form of  $(\text{AuCl}_3\text{OH})^-$  ion (Corma et al. 2008). At  $\text{pH} = 1$ , a surface of silicalite-1 would have positive charge and could strongly absorb anions such as  $(\text{AuCl}_4)^-$  through coulombic interactions. At  $\text{pH} = 3$ , a surface of silicalite-1 would be negatively charged; hence the repulsion forces would prevent the adsorption of  $(\text{AuCl}_3\text{OH})^-$  on its surface and formation of nanoparticles.

For the samples prepared by the PAIR method with  $\text{HAuCl}_4 \cdot 3\text{H}_2\text{O}$  and  $\text{AuCl}_3$  in methanol and acetonitrile, the particles in samples prepared with  $\text{AuCl}_3$  in organic solvents were smaller than in samples prepared with  $\text{HAuCl}_4 \cdot 3\text{H}_2\text{O}$  (Table 4.19). The reason for such difference in particle size obtained for these two precursors might be associated with their acidic character and solubility in organic solvents.  $\text{HAuCl}_4 \cdot 3\text{H}_2\text{O}$  is considered as strong acid while  $\text{AuCl}_3$  as mildly acidic (Puddephat, 1978). Hence, the stabilization of these ions in organic solvents, the solvation layer and interaction with the support would be different. These features could influence the size of gold nanoparticles formed in respective samples and explain the observed differences. As was already mentioned, the formation of nanoparticles is a very complex process strongly influenced by the environment of the ions during the synthesis (Engelbrekt et al. 2013).

#### **4.6.6 Influence of the choice of zeolite for the PAIR procedure**

##### **4.6.6.1 ZSM-5**

The use of ZSM-5 as a host material yielded a catalyst with gold nanoparticles incorporated inside the zeolite framework which were much smaller in size (mean size  $1.9 \pm 0.8$  nm) than for silicalite-1 (average size  $3.5 \pm 1.5$  nm) prepared with the same conditions (samples Au/H-ZSM-5 described in section 4.2.2 *Synthesis of gold in ZSM-5* and Au/S-1\_3\_H<sub>2</sub>O described in section 4.1.2 *Synthesis conditions:  $\text{HAuCl}_4 \cdot 3\text{H}_2\text{O} + 0.3$  ml of different solvents*). Similar difference was observed by Zhang et al. (2012) who reported Au/ZSM-5 and Au/S-1 catalysts with gold nanoparticles of average size 9.1 nm and 13.2 nm, respectively, prepared by deposition-precipitation method. As reported by Okumura et al. (2012), the acidic sites in ZSM-5 promote high dispersion and formation of smaller metal nanoparticles. Additionally, ZSM-5 having more hydrophilic character than silicalite-1 (Nakamoto et al. 1982) would have a lower contact angle with water than silicalite-1. This means that wettability of the surface of ZSM-5 would be better; hence better diffusion and dispersion of aqueous impregnation solution than in case of silicalite-1. This could explain a difference in the particle size of gold for those two zeolites obtained using the PAIR method. The presented results show that the scope of the PAIR method was successfully extended to synthesize small gold nanoparticles inside the pores of ZSM-5 zeolite.

##### **4.6.6.2 LTA**

The application of the PAIR method for the zeolite with very narrow pores – LTA is evaluated. The PAIR method used with the modified set of conditions, where either the pressure or the dwell time of nitrogen were increased, resulted in gold nanoparticles located both on the surface and incorporated inside the zeolite framework. Presumably, the small pore size in LTA occurred to be a limiting factor for the impregnation restricting the diffusion of the solvent into the pores. Zhang et al. (2012) reported catalyst

Au/LTA prepared using deposition precipitation method for which gold nanoparticles of 8 nm in size were located almost exclusively on the surface of the crystals. The diffusion limitation caused by small pores of LTA was overtaken by Otto et al. (2016) who reported the synthesis of monodisperse gold clusters (1-2 nm) inside the LTA framework using a one-pot procedure in which gold species were incorporated inside the framework during the growth of the zeolite.

The results presented above might indicate that the PAIR method is not the proper procedure for encapsulation of nanoparticles inside the pores of LTA zeolite. The superior results obtained from the one-pot protocols might discard the use of impregnation-based methods for the synthesis of LTA encapsulated with metal nanoparticles due to too high diffusion limitation caused by a small pore size of LTA.

#### **4.6.7 Application of PAIR for different metals**

The analysis of other metals, like platinum and palladium gave results other than expected. Platinum did not yield any catalyst where the particles were small enough to be spotted in TEM. On the other hand, the samples prepared with palladium resulted in catalyst where particles were solely located on the surface of the zeolites. The best result in terms of size and distribution of nanoparticles was obtained for palladium precursor dissolved in acetonitrile, yielding Pd nanoparticles  $2.2 \pm 0.8$  nm in size. The difference in performance of the PAIR method for these two metals compared with gold could be associated with the difference in electronic structure, charge of the ions used as precursors, or interaction with solvents and support. These experiments showed that the PAIR method could be used to produce materials with small metal nanoparticles evenly distributed on the external surface of a support, as was shown for palladium/silicalite-1.

#### **4.6.8 Application of PAIR to different kind of support**

The PAIR method applied to amorphous mesoporous silica as support resulted in nanoparticles with a mean particle size of  $4.9 \pm 1.4$  nm which were very prone to sintering –  $15.0 \pm 1.6$  nm after additional calcination. Particles were solely located on the surface of the support. Sakurai et al. (2013) and Siddiqi et al. (2015) also reported impregnation procedures using amorphous mesoporous silica as support which yielded gold nanoparticles supported on the external surface of silica. The successful encapsulation of gold nanoparticles inside the pores of amorphous mesoporous silica was performed by Wang et al. (2013) in the one-pot synthesis.

These results show that the PAIR method might not be a right procedure to synthesize gold nanoparticles incorporated inside the pores of amorphous mesoporous silica, and that, similarly as for LTA zeolite, the superiority of results obtained from one-pot methods might discard the impregnation-based procedures for metal encapsulation purposes in this kind of support.

#### **4.6.9 Consideration of the reduction under pressure during PAIR**

All the discussion provided so far was solely based on the impregnation step during the PAIR procedure. However, the reduction of the materials under increased pressure, which is a part of the PAIR procedure, was not considered. The elevated pressure during reduction of gold species entrapped inside the zeolite matrix could have a large influence on the size and dispersion of nanoparticles and ratio between encapsulated and surface nanoparticles.

## 4.7 Final summary

The PAIR method was successfully applied in a range of experiments to yield gold-incorporated silicalite-1. The method occurred to be more efficient in terms of sintering stability and size distribution of gold nanoparticles than the impregnation technique when water was used as a solvent. The versatility of the method was shown for different gold precursors and solvents used in the synthesis. The acidic precursor  $\text{HAuCl}_4 \cdot 3\text{H}_2\text{O}$  gave much better result than  $\text{AuCl}_3$  when dissolved in water. However, the use  $\text{AuCl}_3$  in organic solvents gave much better result than  $\text{HAuCl}_4 \cdot 3\text{H}_2\text{O}$ , even without the use of PAIR. Additionally, the application of the PAIR method was successfully shown for synthesis of palladium/silicalite-1 and gold/ZSM-5 materials.

In summary, the PAIR method was shown as a facile and easy way to obtain gold-incorporated silicalite-1 material. It is an efficient yet simple procedure facilitating the use of aqueous solution of gold precursor, competing directly with the impregnation method, able to produce catalysts with very small nanoparticles that are successfully incorporated inside the zeolite framework and exhibit increased stability towards sintering. The strong point of the PAIR method is the compromise between the simplicity and quality of the final material with respect to metal particle size and sintering stability, as was shown by the examples above. The low degree of complexity of the PAIR method could make it a good candidate for industrial application to yield gold-incorporated zeolites obtained from the aqueous precursor solutions, what makes it an environmentally friendly protocol. On the other hand, the use of elevated pressure during the synthesis might occur to be a drawback of the process in terms of costs, safety and technological requirements. The study of the PAIR method showed that by tuning the parameters of the synthesis it is possible to obtain materials with desired morphology and performance. Hence, there is a great potential for successfully applying the PAIR method to incorporate the particles of other metals inside other zeolite frameworks.



## Chapter 5

### ***In situ* incorporation method**

In this chapter, the results from applying the *in situ* incorporation method, described in Chapter 1 and Chapter 3, to synthesize metal nanoparticle incorporated silicalite-1 are presented. The *in situ* incorporation procedure was successfully applied to yield silicalite-1 with incorporated palladium, platinum and mixed bi-metallic PtPd nanoparticles. The synthesized materials were characterized using nitrogen physisorption, XRD, TEM, XPS and XRF techniques, and STEM if relevant.

The results are organized in sections with respect to the choice of metal used in the synthesis:

- Synthesis of palladium in silicalite-1
- Synthesis of platinum in silicalite-1
- Synthesis of bi-metallic palladium-platinum in silicalite-1
- Synthesis of gold in silicalite-1

The discussion of the results is done individually for each set of results in their respective sections. The general discussion about all the results from this chapter is provided at the end of the chapter together with a conclusion.

### **5.1 Synthesis of palladium in silicalite-1**

The synthesis of palladium nanoparticles incorporated inside the matrix of zeolite crystals was performed using the *in situ* incorporation method, according to procedure described in Chapter 3 (3.2.4 *General procedure for the in situ incorporation method*). The synthesized material was characterized using nitrogen physisorption, XRD, TEM, XPS and XRF techniques. Data from these analyses are shown in Table 5.1 and Figure 5.1.

Figure 5.1a presents diffractogram of Pd/S-1 catalyst obtained from XRD analysis. The recorded pattern was characterized as MFI structure silicalite-1 based on comparison with JCPDS 040-19-6968. In Figure 5.1b the zoomed-in diffractogram is presented where the most intense Pd peaks are to be expected. However, no characteristic reflexes of palladium are visible. The reason for it might be related to the very small size of palladium nanoparticles and low loading of palladium in the sample, which do not give strong

enough signal to be visible in XRD analysis. The small peak at  $2\theta = 46.66$  comes from silicalite-1, as was already explained in Chapter 4.

Table 5.1 gathers data collected from the nitrogen physisorption analysis. The values of total pore volume, micropore volume, external surface area and BET surface area are given for Pd/S-1 material. The total pore volume is much lower than the value recorded for the PAIR catalysts and pure silicalite-1 (Table 4.2, Table 4.4, Table 4.6) synthesized in this study and described in Chapter 4. The reason for this might be related to the presence of large number of small nanoparticles inside the crystals which are filling up the pores of the zeolite (Cai et al. 2013). Figure 5.1c shows the isotherm recorded for Pd/S-1 catalyst. The shape of the isotherm resembles the I type of isotherm characteristic for material with microporosity. The characteristic hysteresis loop in the isotherm is typical for the silicalite-1 zeolite in nitrogen physisorption analysis (Thommes 2010).

**Table 5.1. Results from nitrogen physisorption analysis and particle size distribution for palladium nanoparticles encapsulated in silicalite-1 prepared using the *in situ* incorporation method.**

Catalyst name	Total pore volume (cm <sup>3</sup> /g)	Micropore volume (cm <sup>3</sup> /g)	External surface area (m <sup>2</sup> /g)	Total surface area BET (m <sup>2</sup> /g)	Mean <sup>1</sup> particle size (nm)	Average <sup>1</sup> particle size (nm)	Metal loading <sup>2</sup> (wt%)
Pd/S-1	0.213	0.094	154	344	2.9 ± 1.7	3.3 ± 1.7	1.6

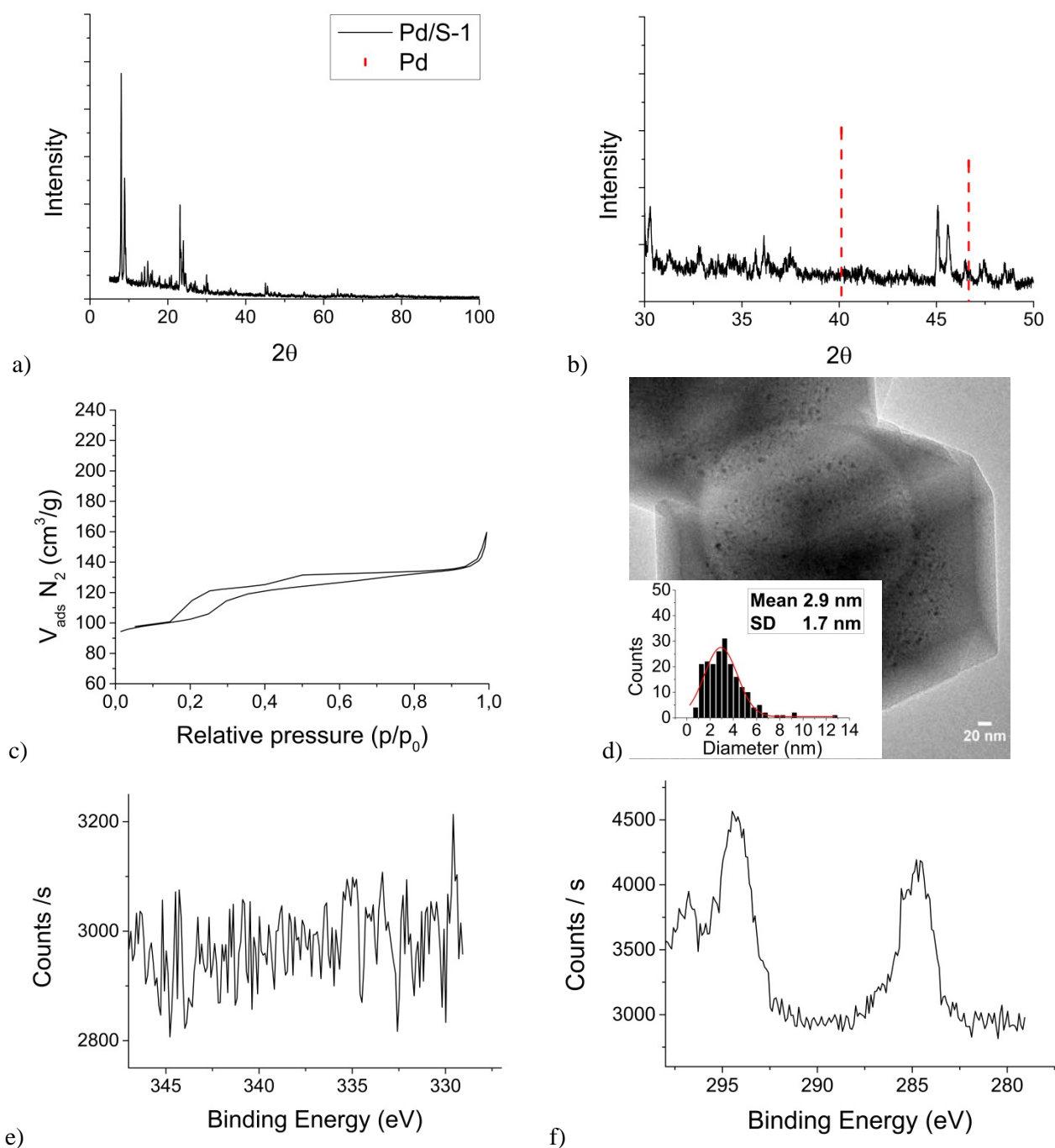
<sup>1</sup> Value based on 200 nanoparticles measured from TEM images; <sup>2</sup> determined from XRF.

In Figure 5.1d a representative TEM image of Pd/S-1 is shown. A lot of small nanoparticles of palladium are visible in the matrix of silicalite-1 crystal. The mean size of these nanoparticles was calculated to be 2.9 ± 1.7 nm based on measurement of 200 nanoparticles from TEM images. Such small size of palladium nanoparticles could explain lack of characteristic reflexes of palladium in XRD diffractogram measured for this sample.

XPS data recorded for the catalyst in question is presented in Figure 5.1e,f. No peak associated with Pd can be observed, as shown in Figure 5.1e, meaning that there were no Pd nanoparticles located on the surface or within approximately 10 nm from the surface of zeolite crystals. A very distinct carbon signal is observed in Figure 5.1f, indicating the presence of residual carbon species. The carbon signal may come from the leftovers of polymerized amine that were not removed during calcination.

The metal loading determined from XRF analysis for Pd/S-1 was 1.6 wt% as shown in Table 5.1. A similar material reported by Wang et al. (2016) had the Pd loading of 0.64 wt% and the mean particles size of 1.8 nm. In the present study, 1.5 times more Pd was introduced in the synthesis compared to the procedure reported by Wang et al. (2016). It yielded not only larger nanoparticles of Pd but also resulted in higher loading of metal in the zeolite matrix, as was expected.

It was shown that the *in situ* incorporation method is a feasible way to obtain well dispersed small palladium nanoparticles incorporated inside silicalite-1. The synthesis can be easily adjusted to prepare materials with different loading and size of palladium nanoparticles, what makes this method a versatile and simple procedure for a catalyst study.



**Figure 5.1.** a) XRD diffractogram, b) zoomed-in XRD diffractogram, c) nitrogen physisorption isotherm, d) representative TEM image and particle size distribution; e) XPS spectrum of the range corresponding to: e) palladium 3d signal, f) carbon 1s signal for Pd/S-1 catalyst prepared with *in situ* incorporation method.

## 5.2 Synthesis of platinum in silicalite-1

The *in situ* incorporation of platinum nanoparticles in silicalite-1 was performed according to procedure described in Chapter 3 (3.2.4 *General procedure for the in situ incorporation method*) with two platinum precursors: PdCl<sub>4</sub> and PdCl<sub>2</sub>, yielding catalysts labelled Pt/S-1\_Pt(IV) and Pt/S-1\_Pt(II),



respectively. The data obtained from catalysts characterization using nitrogen physisorption, XRD, TEM, XRF and XPS techniques are shown in Table 5.2, Figure 5.2 and Figure 5.3.

XRD data shown in Figure 5.2a depicts the diffractograms recorded for the investigated catalysts. The diffraction pattern was characterized as silicalite-1, for both samples based on comparison with JCPDS 040-19-6968 standard data. Figure 5.2b presents both diffractograms with the zoomed-in range where the characteristic reflexes of platinum occur. The peak of platinum at  $2\theta = 39.76$ , which is the most intense peak, indicates the presence of platinum nanoparticles in both catalysts. Platinum, as a high atomic number element has a high ability to scatter X-rays; thus, even very small nanoparticles of platinum could give enough scattering to produce visible peaks in XRD analysis.

Results from nitrogen physisorption analysis for Pt/S-1\_Pt(IV) and Pt/S-1\_Pt(II) catalysts are presented in Table 5.2. Similarly as for Pd/S-1, the value of total pore volume is lower compared to pure silicalite-1 sample (Chapter 4, Table 4.2, Table 4.4, Table 4.6) what could indicate the presence of nanoparticles inside the pores of silicalite-1 (Cai et al. 2013). In Figure 5.2c the isotherms of these catalysts are shown, and they both resemble the type I isotherm characteristic for the microporous material (Thommes 2010).

**Table 5.2. Results from nitrogen physisorption and particle size distribution for platinum encapsulated silicalite-1 catalysts prepared with different Pt precursors using the *in situ* incorporation method.**

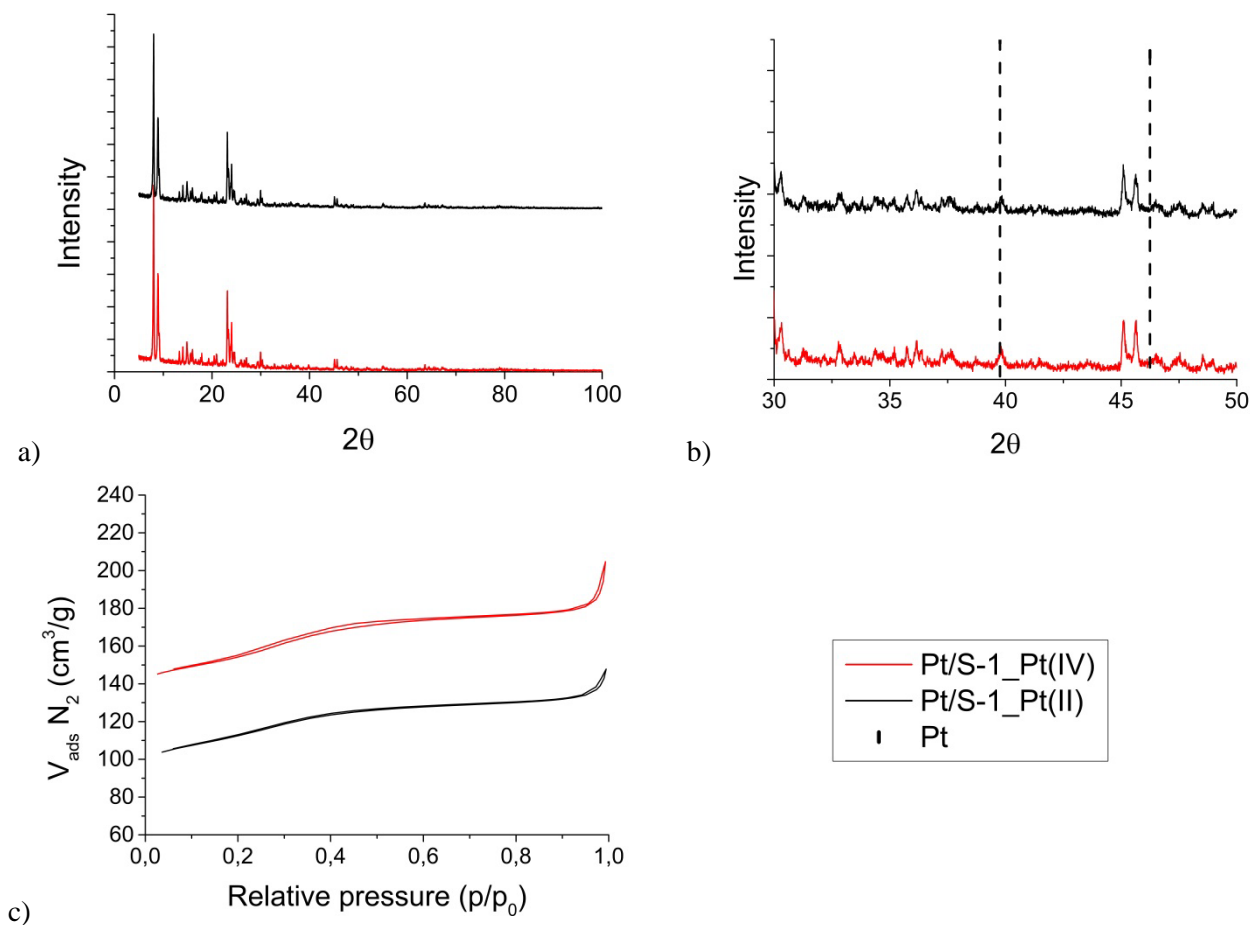
Catalyst name	Total pore volume (cm <sup>3</sup> /g)	Micropore volume (cm <sup>3</sup> /g)	External surface area (m <sup>2</sup> /g)	Total surface area BET (m <sup>2</sup> /g)	Mean <sup>1</sup> particle size (nm)	Average <sup>1</sup> particle size (nm)	Metal loading <sup>2</sup> (wt%)
Pt/S-1_Pt(IV)	0.203	0.109	121	352	2.2 ± 1.0	2.5 ± 1.1	1.1
Pt/S-1_Pt(II)	0.208	0.122	119	379	2.7 ± 1.0	3.2 ± 1.4	1.4

<sup>1</sup> Value based on 200 nanoparticles measured from TEM images; <sup>2</sup> determined from XRF.

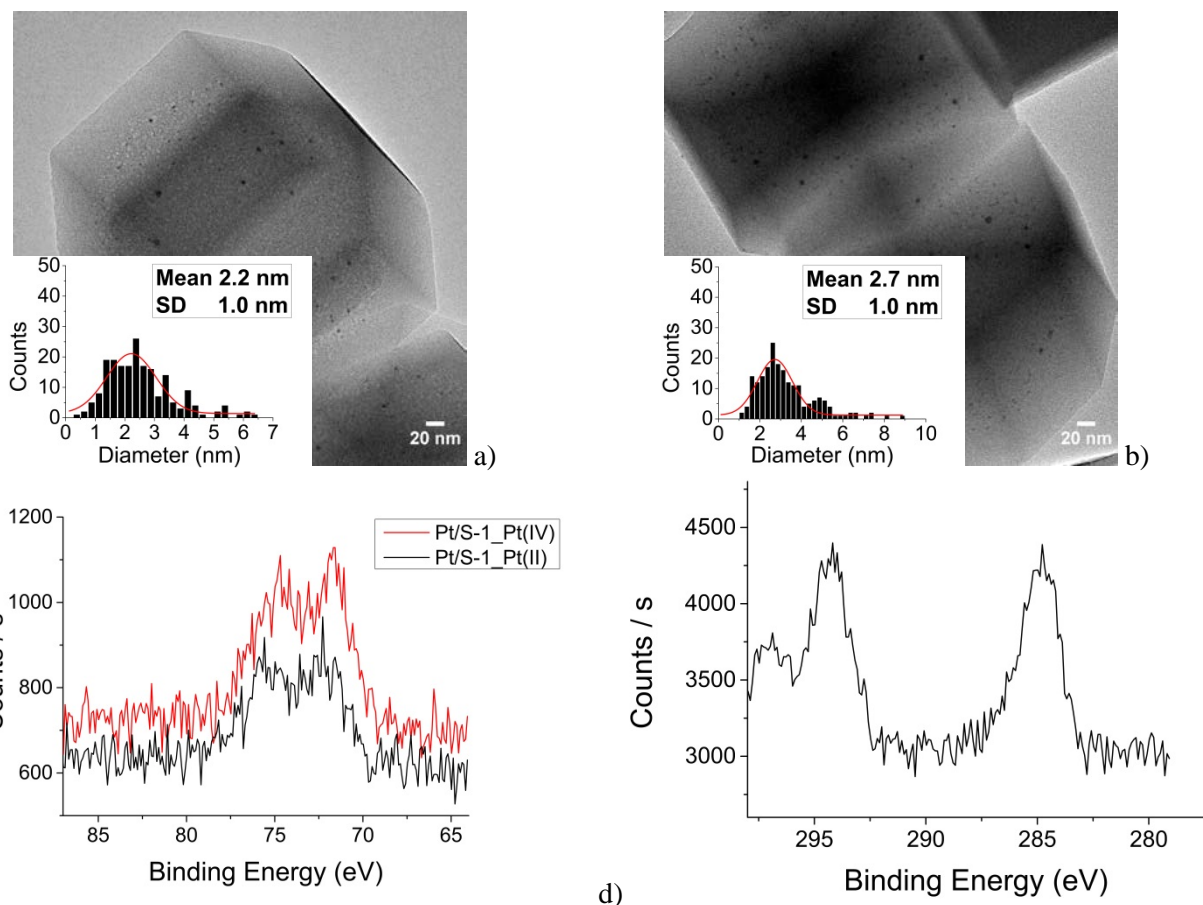
The TEM images of Pt/S-1\_Pt(IV) and Pt/S-1\_Pt(II) catalysts are shown in Figure 5.3a,b. Only small nanoparticles of platinum are visible in the matrix of silicalite-1 crystal. The size of the particles was estimated as  $2.2 \pm 1.0$  nm for Pt/S-1\_Pt(IV) and  $2.7 \pm 1.00$  nm for Pt/S-1\_Pt(II) (Table 5.2) based on measurement of 200 nanoparticles from TEM images.

Figure 5.3c presents XPS spectrum recorded for the two catalysts in the region where platinum signal is expected. Clearly, peaks of platinum were visible between 70-80 eV. This signal might be related to platinum nanoparticles located within 10 nm from the surface of the zeolite crystals, since none were spotted on the external surface in TEM analysis (Figure 5.3a,b). Similarly as for Pd/S-1, both catalysts contain residual carbon species that were not removed by calcination, as shown from XPS results in Figure 5.3d.

The platinum loading on the prepared catalysts, determined by XRF, is shown in Table 5.2. Platinum loading in Pt/S-1\_Pt(IV) and Pt/S-1\_Pt(II) samples was 1.1 wt% and 1.4 wt%, respectively. It could be extrapolated that the incorporation of platinum depends on the complex it forms with ethylenediamine – [Pt(en)<sub>2</sub>]Cl<sub>2</sub> or [Pt(en)<sub>3</sub>]Cl<sub>4</sub>. [Pt(en)<sub>2</sub>]Cl<sub>2</sub> is smaller, sterically less demanding, and more accessible due to vacant coordination spots around the metal center, than [Pt(en)<sub>3</sub>]Cl<sub>4</sub>. These characteristics could play an important role in the increased rate of incorporation of [Pt(en)<sub>2</sub>]Cl<sub>2</sub> rather than [Pt(en)<sub>3</sub>]Cl<sub>4</sub>. This could explain the higher loading of Pt on Pt/S-1\_Pt(II).



**Figure 5.2.** a) XRD diffractograms, b) zoomed-in XRD diffractograms, c) nitrogen adsorption isotherms (offset of 50) of platinum encapsulated silicalite-1 catalysts prepared with Pt(II) and Pt(IV) precursors using the *in situ* incorporation method.



**Figure 5.3.** Representative TEM images and particle size distribution of: a) Pt/S-1\_Pt(IV), b) Pt/S-1\_Pt(II); XPS spectrum with the range corresponding to: c) platinum 4f signal, d) carbon 1s signal for Pt/S-1\_Pt(IV) and Pt/S-1\_Pt(II) catalysts prepared using the *in situ* incorporation method.

In the present section it was shown that *in situ* incorporation method is a feasible method to synthesize platinum nanoparticles encapsulated inside the silicalite-1 crystals. It was presented that by using two different platinum precursors, materials with small well dispersed nanoparticles incorporated inside silicalite-1 can be obtained without any additional changes in the synthesis procedure.

### 5.3 Synthesis of palladium and platinum in silicalite-1 in random incorporation

The palladium-platinum bi-metallic silicalite-1 catalyst was synthesized according to procedure described in Chapter 3 (3.2.4 *General procedure for the in situ incorporation method*), with the purpose to randomly incorporate nanoparticles of palladium and platinum in the zeolite without creating an alloy. Data gathered in the characterization of the material by XRD, BET, STEM (operating at 100 eV) and XRF are shown in Table 5.3 and Figure 5.4.

XRD pattern recorded for the catalyst, shown in Figure 5.4a, depicts the crystallinity of the sample associated with the silicalite-1 phase, as determined from comparison with JCPDS 040-19-6968 standard data. In Figure 5.4b the zoomed-in diffractogram is shown. Two peaks are visible at  $2\theta = 46.66$  and  $2\theta = 39.96$ . The second peak at  $2\theta = 46.66$  was already ascribed to silicalite-1 (Chapter 4); however, the first one lies in between peak of platinum  $2\theta = 39.76$  and palladium  $2\theta = 40.11$ . The shift in peak position to smaller or larger diffraction angles in multi-metallic crystalline samples is usually attributed to increased or reduced

crystal lattice due to alloying of metals present in the sample (Wang<sup>3</sup> et al. 2014). Assuming that peak at  $2\theta = 39.96$  comes from platinum, as the higher scattering metal, the slight shift of its position to higher  $2\theta$  values could indicate the alloying of palladium with platinum to form an alloy structure. Similar behavior was observed by Zhang et al. (2013) for AgPd nanoparticles. The shift in the observed results for PdPt/S-1 sample is very small, of about 0.20, and the peak does not have a high intensity; hence more experiments are necessary to confirm the presence of PtPd alloy.

Table 5.3 presents the results from the nitrogen physisorption performed for PdPt/S-1 catalyst. The total pore volume is again very low, similar to Pd/S-1, Pt/S-1\_Pt(IV) and Pt/S-1\_Pt(II), what could indicate the presence of nanoparticles in the pores of silicalite-1 (Cai et al. 2013). The isotherm for PdPt/S-1, shown in Figure 5.4c, is the I type isotherm characteristic for the microporous material (Thommes 2010).

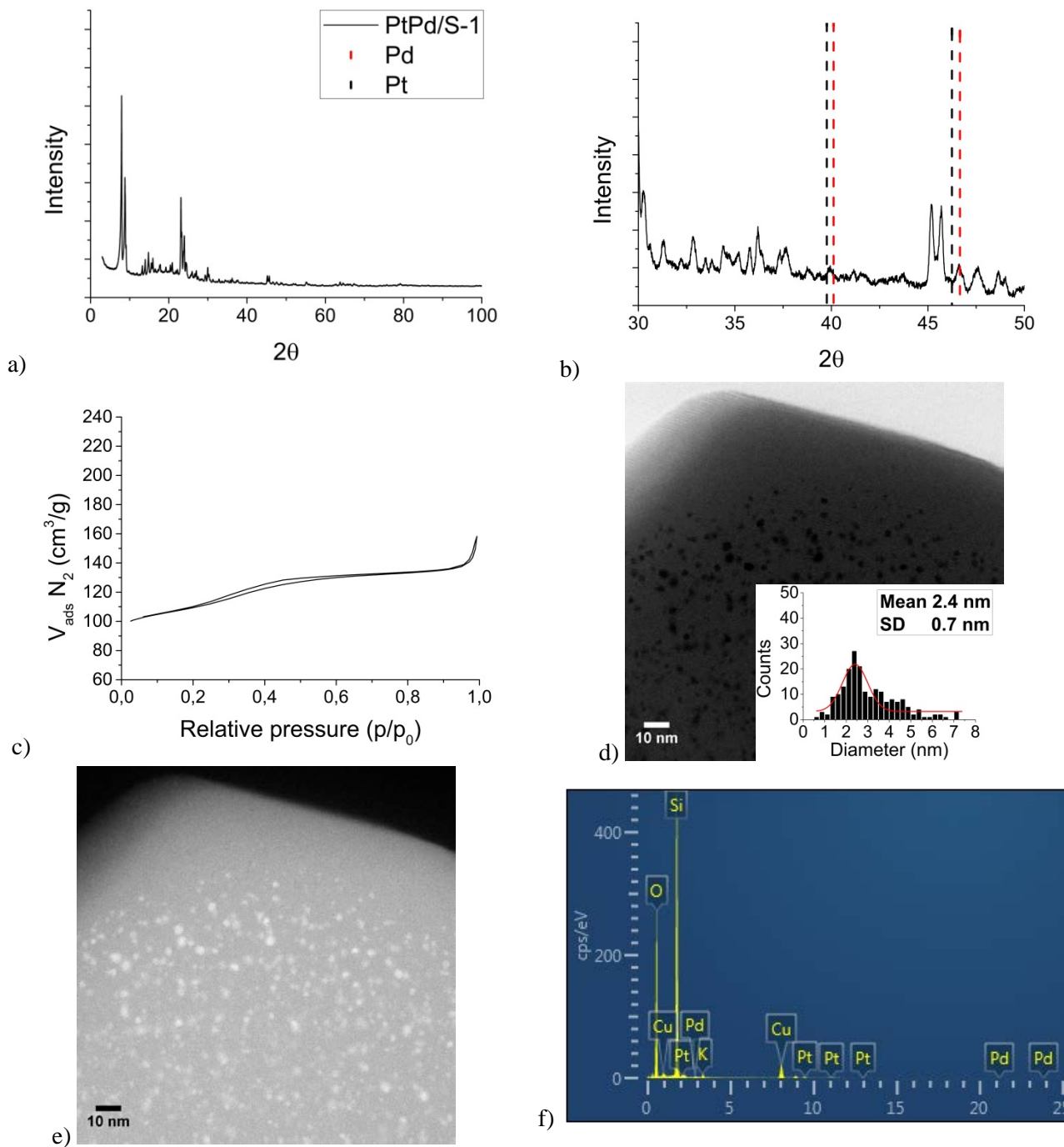
**Table 5.3. Results from nitrogen physisorption and particle size distribution for palladium-platinum randomly encapsulated inside silicalite-1 prepared using the *in situ* incorporation method.**

Catalyst name	Total pore volume (cm <sup>3</sup> /g)	Micropore volume (cm <sup>3</sup> /g)	External surface area (m <sup>2</sup> /g)	Total surface area BET (m <sup>2</sup> /g)	Particle <sup>1</sup> size (nm)	Average <sup>1</sup> particle size (nm)	Pd/Pt metal loading <sup>2</sup> (wt%)
<b>PdPt/S-1</b>	0.213	0.122	108	369	2.4 ± 0.7	3.0 ± 1.3	0.8/0.9

<sup>1</sup> Value based on 200 nanoparticles measured from STEM images; <sup>2</sup> determined from XRF.

The loadings of the metals, determined in XRF analysis are shown in Table 5.3. The loading of Pd was calculated as 0.8 wt% while platinum as 0.9 wt%.

STEM images of the PdPt/S-1 catalyst are shown in Figure 5.4d,e. Figure 5.4d depicts the bright filed (BF) image and Figure 5.4e its dark filed (DF) equivalent. On both STEM images small metal nanoparticles are visible in the matrix of silicalite-1; however, platinum and palladium nanoparticles can not be distinguished based on the intensity of scattering. The elemental mapping in STEM could not be performed due to too low loading of metals in the sample and too low intensity of the scattering they were able to produce. The size of nanoparticles, irrespectively of their kind, was calculated from particle size distribution as 2.4 ± 0.7 nm. Qualitative XEDS analysis performed on the sample during TEM analysis confirmed the presence of both Pd and Pt in the sample, as shown in Figure 5.4f.



**Figure 5.4.** a) Nitrogen physisorption isotherm, b) XRD diffractogram, c) zoomed-in XRD diffractogram, d) BF image from STEM and particle size distribution, e) DF image, f) XEDS spectrum of palladium-platinum randomly encapsulated in silicalite-1 using the *in situ* incorporation method.

It was presented that by using the *in situ* incorporation method, a material with bi-metallic nanoparticles of palladium and platinum can be synthesized. The method was shown to be an easy and feasible protocol employing a one-pot procedure in which palladium and platinum nanoparticles are simultaneously incorporated inside the matrix of silicalite-1 from a one synthesis mixture. The nanoparticles were small, well dispersed and exclusively located inside the zeolite channels.

## 5.4 Synthesis of platinum and palladium in silicalite-1 in layered incorporation

The palladium-platinum bi-metallic silicalite-1 catalyst was synthesized according to procedure described in Chapter 3 (3.2.4 *General procedure for the in situ incorporation method*), with the purpose to incorporate nanoparticles of palladium and platinum in separate layers inside the crystals of silicalite-1. Two samples were prepared, each with different amount of metal precursor and time of crystallization, according to Table 5.4. Data gathered in the characterization of the sample by XRF and STEM (operating at 300 eV) is shown in Table 5.4 and Figure 5.5.

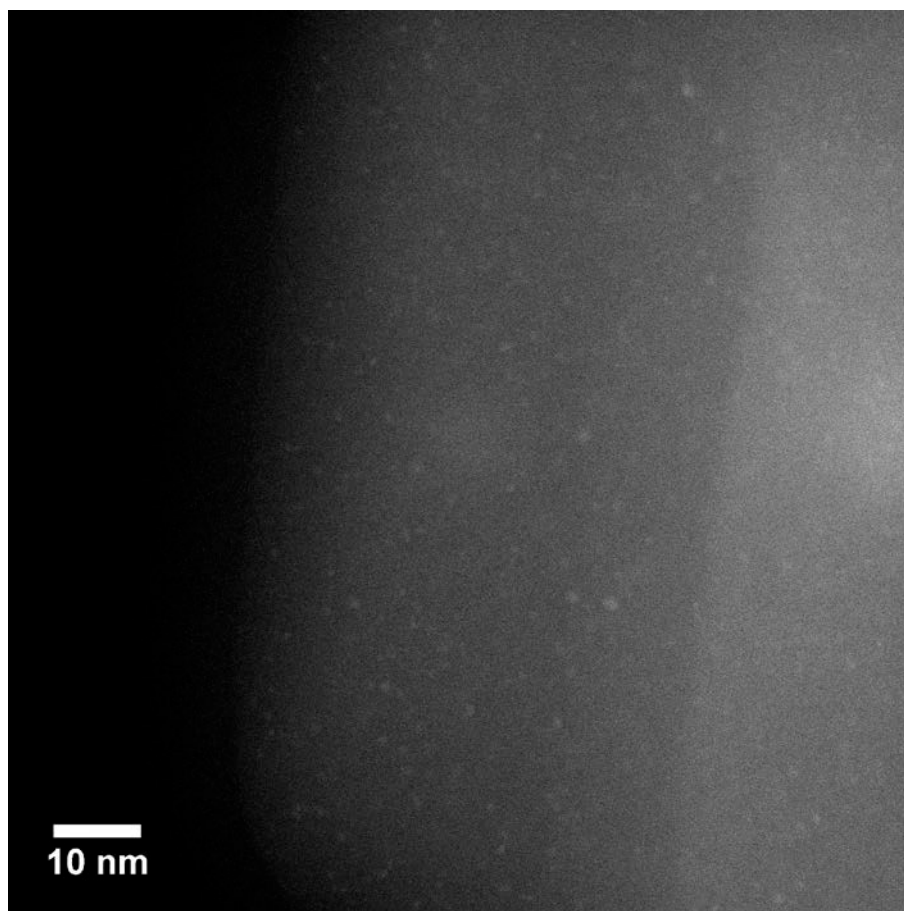
**Table 5.4. Overview of the conditions used for the preparation of platinum-palladium nanoparticles incorporated in layers in silicalite-1 and metal loading of palladium and platinum in the final materials prepared with *in situ* incorporation method.**

Catalyst name	Amount introduced <sup>1</sup>	Time of 2 <sup>nd</sup> incorporation	Metal loading of Pd/Pt (wt%) <sup>2</sup>
PtPd/S-1_1	40%	6h	0.3/0.6
Pt/Pd/S-1_2	25%	4h	0.2/0.3

<sup>1</sup>Compared to single metal synthesis; <sup>2</sup>determined from XRF analysis.

The XRF analysis performed on both samples revealed the metal loading of Pd/Pt equal to 0.3/0.6 wt% and 0.2/0.3 wt% for the respective catalysts, as shown in Table 5.4. The loading of Pt is higher than Pd for both catalysts. It was expected since Pt was introduced first before Pd; thus it spent more time in the synthesis mixture.

Figure 5.5 depicts the STEM image of PtPd/S-1\_1 showing a large number of small metal nanoparticles below 1 nm in size in the matrix of silicalite-1. In none of prepared catalysts the particles were incorporated in layers – the distribution of particles inside the silicalite-1 crystals was uniform, similarly as in the sample prepared with randomly incorporated PdPt nanoparticles, described in the previous section. Pt and Pd particles could not be distinguished between each other based on the intensity of scattering in STEM mode. The XEDS mapping performed on the samples did not give any insight into the location of Pt and Pd nanoparticles due to too low signal intensity coming from nanoparticles. The particles in PtPd/S-1\_2 were smaller than in PtPd/S-1\_1, and they could only be spotted on the high-resolution screen; hence their image is not shown in this thesis.



**Figure 5.5.** STEM DF image of platinum-palladium encapsulated silicalite-1 PtPd/S-1\_1 prepared using the *in situ* incorporation method.

The use of *in situ* incorporation method to produce the layered bi-metallic silicalite-1 material did not give the expected result. The particles were not incorporated in layers; instead they were uniformly distributed inside the zeolite crystals. On the other hand, it was shown that extremely small nanoparticles of platinum and palladium can be obtained using this method by varying the amount of metal precursor introduced in the synthesis.

It was shown that the *in situ* incorporation method can be successfully applied to synthesize bimetallic palladium-platinum nanoparticles in silicalite-1 where nanoparticles are randomly incorporated resulting in the mixed metal material. The nanoparticles were small in size and uniformly distributed inside the zeolite crystals. However, the same synthesis used to produce silicalite-1 with Pd and Pt nanoparticles incorporated in layers did not meet the objective and requires to be kept under development.

## **5.5 Synthesis of gold in silicalite-1**

The synthesis of gold in silicalite-1 using *in situ* incorporation method was performed as well, according to procedure described in Chapter 3 (3.2.4 *General procedure for the in situ incorporation method*). However, no nanoparticles of gold could be visible in the final sample in the TEM analysis. A possible reason could be connected with the gold complex formed with ethylenediamine. Even though the geometry of the complex – square planar (Marcon et al. 2003), is very similar to Pt(II) and Pd(II), the charge

and electronic structure are much different. These could have a large influence on the behavior of the complex in the synthesis mixture and the success of the final product. Therefore, the use of *in situ* incorporation method with gold requires more experimental work to produce gold nanoparticles incorporated in silicalite-1.

## 5.6 Conclusion

The *in situ* method for incorporation of metal nanoparticles in the silicalite-1 matrix using ethylenediamine as a complexation agent was successfully applied to yield materials with Pd, Pt and PdPt nanoparticles incorporated in silicalite-1. Based on the TEM images recorded for all the catalysts, the method yields nanoparticles that are 2 – 3 nm in size, and are incorporated inside the zeolite crystals. The size of nanoparticles in the final product shows dependence on the initial concentration of the metal precursor as shown by the example of synthesis using Pd and Pt/Pd nanoparticles. The composition and structure of the complex formed by the metal precursor with ethylenediamine seems to influence the incorporation process, as was illustrated by the examples of Pt (II) and Pt (IV) precursors used for the synthesis.

The *in situ* incorporation method performed in the present study provides a feasible and fairly non-complicated procedure for one-pot synthesis of silicalite-1 encapsulated metallic particles. Additionally, it is the first approach yielding mono-Pt and bi-metallic PdPt silicalite-1 materials using one-pot synthesis technique. However, this method is a time consuming protocol and involves complicated reactions kinetics. Moreover, the application of this method to other metals than palladium and platinum is not straightforward and requires additional development. On the other hand, a good balance between the quality of the produced materials (nanoparticle size, metal loading) and the simplicity of the experimental procedure could make this method a good candidate for the industrial application for the synthesis of metal incorporated zeolites. As a future perspective, the insight into the mechanism of incorporation and species involved in the process could help developing protocols for incorporation of other metals, especially transition metals, into other kinds of zeolite framework using this method.





## Chapter 6

### Decomposition of formic acid

Decomposition of formic acid was chosen as a test reaction in order to evaluate the activity of the catalysts prepared in the course of this study - catalysts prepared using the PAIR method, and *in situ* incorporation method, all described in details in Chapter 4 and Chapter 5. The gold in silicalite-1 catalysts prepared using the PAIR method were synthesized using different gold precursors, solvents and solvent volume. The evaluation of their activity was done based on comparison with reference materials synthesized using the same synthesis parameters by the impregnation method. Additionally, the activity of gold catalysts prepared on different zeolites – LTA, ZSM-5, titanium oxide and amorphous mesoporous silica was checked. The activity of palladium in silicalite-1 catalysts synthesized by the PAIR method and *in situ* incorporation method was evaluated. Platinum and palladium-platinum bi-metallic catalysts prepared by the *in situ* incorporation method were analyzed as well. The evaluation of the activity of the investigated catalysts was performed based on temperature of 50% conversion - the lower the temperature of 50% conversion the higher the activity of the catalyst.

Diagnostic experimental testing was carried out in order to check for the presence or absence of transport limitations occurring during formic acid decomposition over Au/S-1\_PAIR catalyst. Three reactions were designed to verify whether extraparticle or intraparticle concentration gradients and temperature gradients occur during the reaction. Additionally, the reaction was tested with no catalyst and with pure silicalite-1 in order to confirm the catalytic activity coming from gold nanoparticles for dehydrogenation of formic acid.

The content of this chapter includes the background about the formic acid decomposition based on recent literature, experimental section where the experimental procedures are explained, results and discussion section where all results are presented in separate sections and discussed, and a conclusion from the performed work.

### 6.1 Background

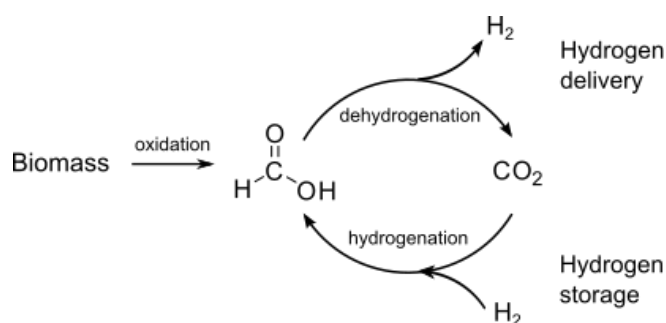
Nowadays, with the constantly growing population and the increasing standards of life, the consumption of energy is increasing dramatically. The growing energy demand is, still, covered by the exploration of fossil fuels. However, they deplete in alarming rates and negatively contribute to environmental and socio-economic changes. Thus, sustainable energy sources and technology connected with increasing their efficiency and availability are the main challenges of this century. Solar and wind

energy are the main renewable energy sources and their application and technology are experiencing a steadily growing development. In terms of energy storage and distribution, hydrogen is attracting an increasing attention as an efficient and emission-free energy source for fuel cell technology providing a great potential for mobile applications (Grasemann et al. 2012). Hydrogen is considered as one of the most efficient, cleanest and lightest fuels. The only product of burning hydrogen is water. It has three times higher energy content by weight and four times lower energy content by volume than gasoline, and burns faster than gasoline (Niaz et al. 2015).

Traditionally, large scale hydrogen is produced in the steam reforming of methane or the water-gas shift reaction which contribute to > 90% of the overall hydrogen production. Both of these processes have high energy consumption, require special purification techniques to remove impurities of CO and, most of all, need fossil fuels as feed what contributes to their irreversible consumption and emissions of greenhouse gases. Another way to produce hydrogen is the electrolysis of water, which is the most efficient way of water splitting without the direct CO<sub>2</sub> emission. However, it contributes to only about 3% of total hydrogen production (Enthaler et al. 2010).

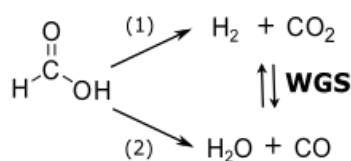
The use of hydrogen suffers from the practicality and safety issues connected with its storage and transportation in large quantities. Traditionally, hydrogen is stored either in gaseous or liquid form in specially designed containers. Both of these solutions have major drawbacks, like requirement of high-pressure apparatus or the high-energy liquefaction, contributing to the overall safety concerns connected with the application of hydrogen. Other ways of hydrogen storage include chemisorption or physisorption in selection of storage materials, like metal hydrides, carbon nanotubes, metal-organic frameworks, zeolites, ammonia, boranes, borates, etc. However, their use suffers from lack of reversibility, requirement of high temperature for hydrogen release or no reasonable storage capacity at room temperature suitable for large scale applications (Enthaler et al. 2010).

Recently, the use of carbon dioxide as a storage material for hydrogen has been investigated. The process is based on the reduction of carbon dioxide with hydrogen to form methanol or formic acid. It is a feasible way to capture and store CO<sub>2</sub> present in excess in the atmosphere and transform it into chemicals as potential hydrogen sources. The utilisation of CO<sub>2</sub> in formation of formic acid is preferred over the synthesis of methanol. In the synthesis of formic acid there are no by-products formed, while the formation of methanol involves a loss of one equivalent of hydrogen because water is formed. Thus, a formic acid-hydrogen CO<sub>2</sub> neutral cycle can be envisioned in which CO<sub>2</sub> acts as a hydrogen carrier that can be released and recaptured regardless of the place of use with the only requirement of readily available hydrogen (Figure 6.1).



**Figure 6.1. A possible carbon neutral cycle for the production, storage and delivery of renewable hydrogen based on catalytic formic acid decomposition.**

Formic acid is the simplest carboxylic acid. It occurs naturally in the venom of ants and bees. Formic acid is a major by-product from the biomass processing; it is non-toxic and has a high gravimetric (4.3 wt%) and volumetric energy density (53 g/L) at room temperature (Niaz et al. 2015). Decomposition of formic acid can follow two pathways: dehydrogenation (1) and dehydration (2) (Figure 6.2). The two reactions are connected by the water-gas shift (WGS) equilibrium. The first reaction is slightly exothermic while the second slightly endothermic; thus the selectivity for hydrogen is increased at lower temperatures (Bulushev et al. 2010). Formation of hydrogen is promoted in more basic conditions; hence the acidity of the support for a heterogeneously catalysed reaction and the pH of the reaction mixture for a homogeneous process influence the selectivity of the reaction. Decomposition of formic acid does not proceed spontaneously and a suitable catalyst is necessary for the reaction to proceed along the desired pathway (dehydrogenation or dehydration). Design of the catalyst is of crucial importance and both homogeneous and heterogeneous catalysts have been developed.



**Figure 6.2. Possible pathways of catalytic decomposition of formic acid: 1) dehydrogenation, and 2) dehydration, connected together by the water-gas shift (WGS) reaction equilibrium.**

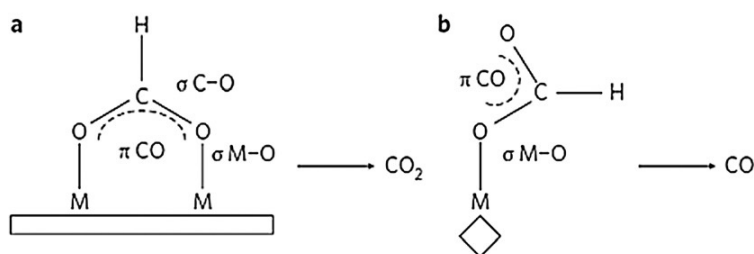
Recent developments in homogeneous catalysts for the decomposition of formic acid usually involve complexes based on Ru with different kind of ligands operating at ambient or close to ambient conditions. Loges et al. (2008) and Boddien et al. (2008) reported ruthenium homogeneous catalysts achieving superior activities and selectivities towards formic acid decomposition in liquid phase reaction at 40 °C and 25 °C, respectively. Morris et al. (2009) showed ruthenium complexes operating at 120 °C reaching extraordinary TOF numbers of 17000 – 18000 h<sup>-1</sup>. Considering the use of catalysts based on non-noble metals, Boddien et al. (2011) presented an iron/phosphine based catalyst for the selective liberation of hydrogen from formic acid reaching 95% conversion at 40 °C.

Design of heterogeneous catalysts for formic acid decomposition revolves around supported precious metal nanoparticles, especially palladium, gold and platinum. Alloys of PdAu or PdAg supported on carbon have been reported to achieve excellent conversions and selectivities towards hydrogen production from formic acid at moderate temperatures (~100°C) (Huang et al. 2010, Zhou et al. 2008, Tedsree et al. 2011, Zhang et al. 2013). Recently, Wang<sup>3</sup> et al. (2013, 2014) reported the synthesis of trimetallic heterogeneous catalyst, CoAuPd/C and NiAuPd/C for 100% selective dehydrogenation of formic acid in aqueous solution in room temperature. Employing first-row transition metals, which are cheaper and more available than noble metals, provides an economically interesting alternative to systems solely based on noble metals.

The above mentioned homogenous and heterogeneous catalysts for formic acid decomposition are just few examples reported over the past decade. Reviews by Enthaler et al. (2010), Grasemann et al. (2012), Sánchez et al. (2016) and Liao et al. (2015) provide a comprehensive overview of the advances in decomposition of formic acid in heterogeneous and homogeneous systems.

The mechanism of the formic acid decomposition over heterogeneous catalyst was studied by Kim et al. (1990) and Hoshi et al. (2007) who proposed the involvement of different kinds of active sites for the formation of CO<sub>2</sub> or CO. In this proposed mechanism, shown in Figure 6.3, the adsorption of formate specie

as a bidentate on the flat metal surface leads to the formation of CO<sub>2</sub> (a), while the adsorption as monodentate facilitates the formation of CO (b). Yoo et al. (2014) in the theoretical study of formic acid decomposition over various metal surfaces confirmed the dependence of formation of either CO<sub>2</sub> or CO on the way formic acid adsorbs on the active site of the catalyst.



**Figure 6.3. Proposed mechanism of CO<sub>2</sub> and CO formation during formic acid decomposition by the adsorption of formate species on different kind of active sites: a) bidentate, b) monodentate, as proposed by Kim et al. (1990) and Hoshi et al. (2007).**

Therefore, in this study, the PAIR method and *in situ* incorporation method were employed to synthesize effective catalysts for decomposition of formic acid in gas phase. The prepared catalysts contained single and bi-metallic gold, palladium or platinum nanoparticles encapsulated inside the framework of silicalite-1. The study was extended for gold nanoparticles in LTA and ZSM-5 zeolites, titanium oxide and amorphous mesoporous silica.

## 6.2 Experimental

### 6.2.1 Materials

All the chemicals used in the study were obtained from commercial suppliers and used as received without further purification: formic acid (HCOOH,  $\geq 96\%$ , Sigma Aldrich), argon gas (Ar, AGA).

### 6.2.2 Catalyst characterization

All investigated catalysts were characterized using TEM, XRD, and nitrogen physisorption. STEM, XPS and XRF were also used but only for selected materials. All details about the catalyst characterization are given in Chapter 4 and Chapter 5.

### 6.2.3 General procedure

The vapor-phase decomposition of formic acid was performed at atmospheric pressure in a 3 mm quartz fixed-bed reactor. Formic acid was introduced to the reactor by bubbling 40 ml/min of Ar through pure liquid formic acid at 20 °C, which resulted in gas composition of around 7% formic acid in Ar. The reaction gas was passed through the reactor, which contained 50 mg of fractionated catalyst (180–355  $\mu\text{m}$ ) held in place by two pieces of quartz wool. The product gas was analyzed by an online non-dispersive infrared detector to quantify CO and CO<sub>2</sub>. All catalysts were tested under the same reaction conditions by heating the reactor from 20 – 200 °C by 2 °C/min.

## 6.2.4 Calculations

The formation of hydrogen from decomposition of formic acid was based on the formation of CO<sub>2</sub> and CO. The conversion of formic acid was calculated as the ratio of the sum of CO and CO<sub>2</sub> concentrations to the initial concentration of formic acid in the gas stream. The initial concentration of the formic acid was obtained from the sum of CO and CO<sub>2</sub> signals at the plateau of the reaction where the full conversion of the reactant was assumed. The selectivity towards CO<sub>2</sub> was calculated from the ratio of CO<sub>2</sub> concentration in the gas stream to the sum of CO and CO<sub>2</sub> concentrations. The selectivity towards CO<sub>2</sub> corresponds to the selectivity towards H<sub>2</sub> as shown in Figure 6.2. The yield of H<sub>2</sub> formation was calculated from multiplying CO<sub>2</sub> selectivity by conversion of formic acid.

## 6.3 Results and discussion

The results from decomposition of formic acid over various catalysts prepared in this study are described in the following order:

- Diagnostic experimental testing for gold in silicalite-1
- Performance of gold in silicalite-1 prepared with:
  - PAIR, IM: HAuCl<sub>4</sub> + 0.15 ml water
  - PAIR: HAuCl<sub>4</sub> + 0.3 ml of different solvents (water, methanol, acetonitrile)
  - PAIR, IM: AuCl<sub>3</sub> + 0.3 ml of different solvents (water, methanol, acetonitrile, 1-butanol)
- Performance of gold in LTA and ZSM-5 prepared with PAIR
- Performance of gold on amorphous mesoporous silica prepared with PAIR and on titanium oxide
- Performance of palladium in silicalite-1 prepared with:
  - PAIR with different solvents (water, methanol, acetonitrile)
  - *In situ* incorporation method
- Performance of platinum in silicalite-1 prepared with:
  - *In situ* incorporation method with different precursors
  - Mixed palladium/platinum nanoparticles

Each section provides a short discussion of the results described in it and comparison with other relevant results from other sections. The chapter is closed up by the conclusion from the performed study.

### 6.3.1 Diagnostic experimental testing of a catalyst

The activity of gold catalyst prepared using the PAIR method was studied with respect to possible transport limitations occurring in the catalyst bed during the reaction. The formic acid decomposition over Au/S-1\_PAIR catalyst (described in Chapter 4, section 4.1.1 *Synthesis conditions: HAuCl<sub>4</sub>·3H<sub>2</sub>O + 0.15 ml*) was carried out for three different sets of conditions to check for the extraparticle and intraparticle concentration gradients and temperature gradients. The changes in CO<sub>2</sub> evolution during test reactions were monitored, and based on these the standard conditions used for the reaction were evaluated. The standard conditions refer to:

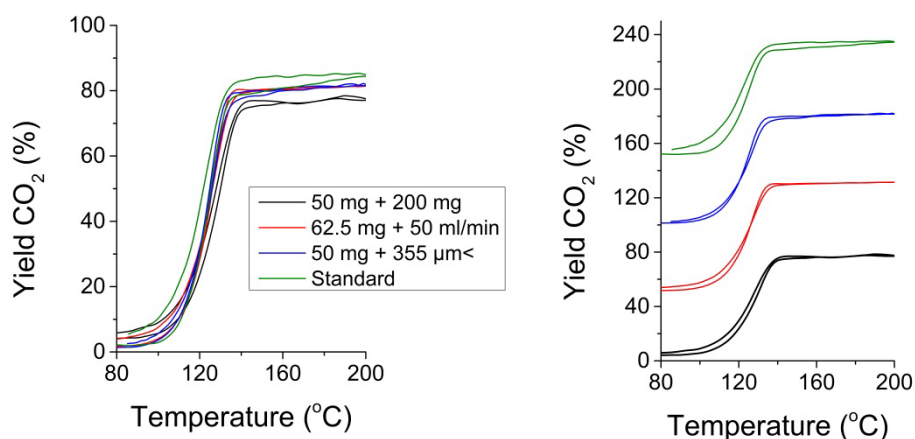
- amount of catalyst: 50 mg
- flow rate: 40 ml/min

- catalyst grain fraction: 180 – 355  $\mu\text{m}$

The possible extraparticle concentration gradients arising from the mixing flow around the catalyst particles were evaluated. The flow-rate and the amount of catalyst were simultaneously changed while keeping the space-time (defined as amount of catalyst/flow rate of reactant) constant. The amount of catalyst was increased from 50 mg to 62.5 mg and the flow rate of reactant from 40 ml/min to 50 ml/min. The yield of  $\text{CO}_2$  from this reaction is shown as a red line in Figure 6.4.

The intraparticle concentration gradients caused by the possible limited diffusion of reactants from the bulk of the fluid through the pores to the active sites were checked as well. In order to verify whether the rate of the reaction is particle size dependent the fraction of the catalyst grain was increased from 180–355  $\mu\text{m}$  to  $> 355\mu\text{m}$ . The yield of  $\text{CO}_2$  in this reaction is shown as a blue line in Figure 6.4.

The temperature gradients caused by inefficient heat removal or supply were evaluated as well. The catalyst bed was diluted with 200 mg of silica in order to increase the heat conduction in the bed. The yield of  $\text{CO}_2$  from this reaction is depicted as a black line in Figure 6.4.



**Figure 6.4.** Results from diagnostic tests performed on Au/S-1\_PAIR catalyst in order to study the transport limitations in the reactor during formic acid decomposition. An offset of 50 was added to each plot in the right-panel figure.

Comparing the results from all three diagnostic tests and from the standard experiment, depicted in Figure 6.4, the highest yield of  $\text{CO}_2$  was obtained for the standard experiment (green line), while the lowest for the experiment with the catalyst bed diluted with silica (black line). However, the yields from all performed experiments lay within the same range between 75 – 85%. A difference in 50% conversion temperature between the heat-up and cool-down reaction, shown in the right panel of Figure 6.4, does not exceed 10  $^{\circ}\text{C}$  for all performed tests.

These results indicate that the yield observed from the standard experiment might be up to 10% higher than the one obtained at conditions at which the transport limitations are minimized. Similarly, the 50% conversion temperature obtained from the standard test might carry up to 10  $^{\circ}\text{C}$  of experimental error due to transport limitations. Hence, the results presented in the following sections should be interpreted with these figures in mind.

Additionally, formic acid decomposition at standard test conditions was performed with no catalyst and with pure silicalite-1. The yields of  $\text{CO}_2$  from these reactions are shown in Figure 6.5. The yields recorded from these tests are very low  $< 5\%$ . Keeping in mind the results from diagnostic tests it is assumed

that the observed activity lies within the experimental error and that no conversion of formic acid occurred. This confirms that the reaction is catalyzed by metal nanoparticles.

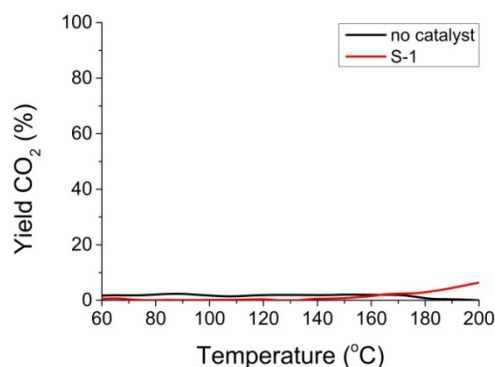


Figure 6.5. Yield of formic acid decomposition from tests carried out without a catalyst and with pure silicalite-1.

### 6.3.2 Performance of gold in silicalite-1

In this section, the activity of gold in silicalite-1 catalysts prepared using the PAIR method for the gas-phase decomposition of formic acid is described. The study includes catalysts of gold in silicalite-1 synthesized using different gold precursors, different solvents and different solvent volume. The characteristic of these materials was already provided in Chapter 4.

#### 6.3.2.1 $\text{HAuCl}_4 \cdot 3\text{H}_2\text{O} + 0.15 \text{ ml water}$

Decomposition of formic acid was performed over gold in silicalite-1 catalysts prepared by the PAIR method and impregnation method using  $\text{HAuCl}_4 \cdot 3\text{H}_2\text{O}$  as gold precursor and 0.15 ml of water as solvent (see Chapter 4, section 4.1.1 *Synthesis conditions:  $\text{HAuCl}_4 \cdot 3\text{H}_2\text{O} + 0.15 \text{ ml water}$* ). In order to evaluate the sintering stability of gold nanoparticles, the prepared fresh catalysts: Au/S-1\_PAIR and Au/S-1\_IM, were additionally calcined in air at 400 °C for 2 h and tested in the same reaction conditions. Results from the performed experiments are shown in Figure 6.6 and Table 6.1.

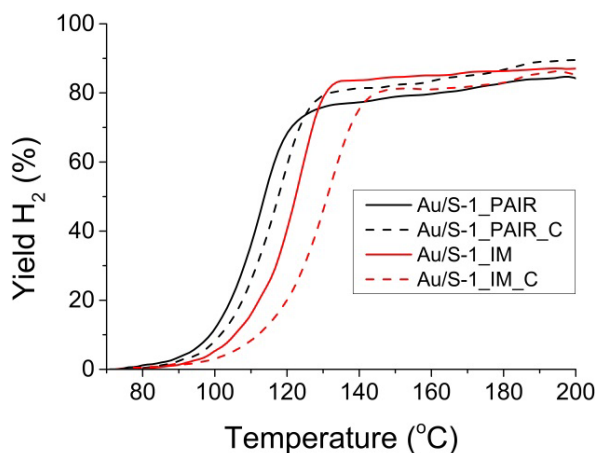


Figure 6.6. Yield of hydrogen formation in formic acid decomposition over fresh and calcined (in air at 400 °C for 2 h) catalysts prepared using the PAIR method and impregnation method using  $\text{HAuCl}_4 \cdot 3\text{H}_2\text{O}$  as gold precursor dissolved in 0.15 ml of water.



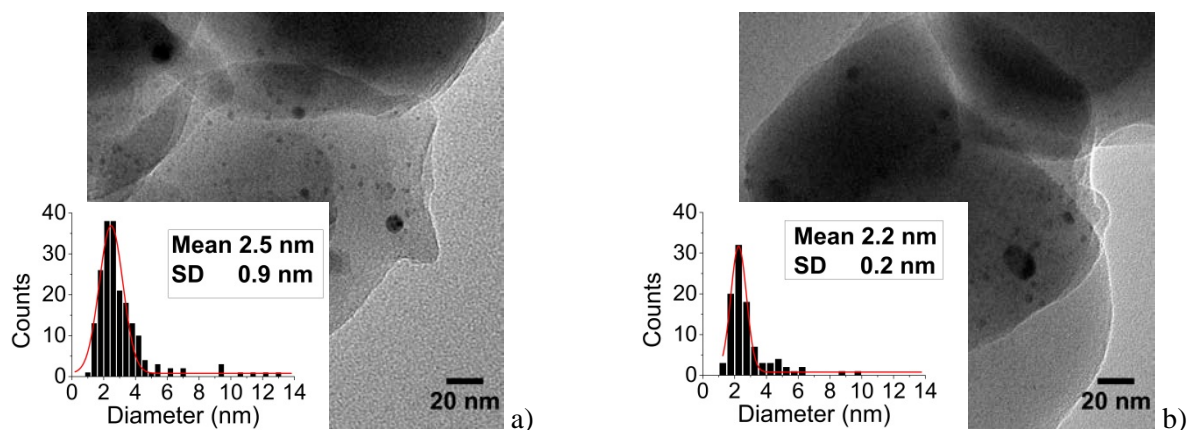
**Table 6.1. Data obtained from formic acid decomposition over gold catalysts prepared using  $\text{HAuCl}_4 \cdot 3\text{H}_2\text{O}$  as gold precursor dissolved in 0.15 ml of water by the PAIR method and impregnation method, both subjected to additional calcination in air at 400 °C for 2 h.**

Catalyst name	Selectivity $\text{H}_2$ (%)	Temperature of 50% conversion (°C)	Mean <sup>1</sup> particle size (nm)	Average <sup>1</sup> particle size (nm)
Au/S-1_PAIR	84	113	$2.2 \pm 0.6$	$2.7 \pm 2.2$
Au/S-1_PAIR_C	89	118	$3.3 \pm 0.9$	$4.0 \pm 2.5$
Au/S-1_IM	87	122	$1.9 \pm 0.4$	$4.0 \pm 2.5$
Au/S-1_IM_C	85	131	$8.4 \pm 4.8$	$8.6 \pm 3.6$

<sup>1</sup> Value determined from the measurement of 200 particles from TEM images.

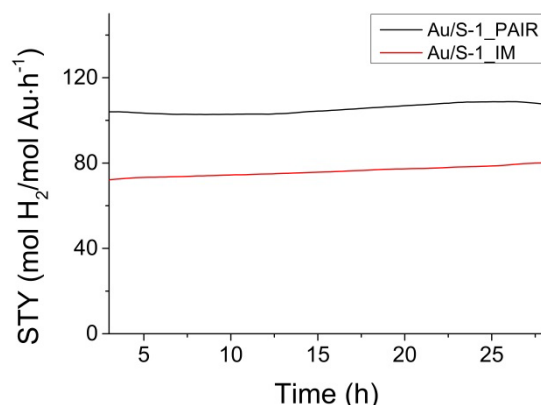
In Figure 6.6 the yield of hydrogen formation versus temperature of the reaction is shown for all four investigated catalysts. The sharp increase in the reaction rate is observed at temperatures between 80 °C and 120 °C followed by a plateau. The Au/S-1\_PAIR catalyst exhibited the highest catalytic activity for formic acid decomposition and reached 50% conversion at 113 °C. Even when calcined at 400 °C in air, the catalyst remained very active and reached 50% conversion at 118 °C. Au/S-1\_IM catalyst, prepared by impregnation method, reached 50% conversion at 122 °C. However, after its calcination the performance dropped to 131 °C, see Table 6.1. The lower activity was probably caused by the increase in the size of gold nanoparticles due to sintering at elevated temperatures. Indeed, the size of gold nanoparticles increased from 1.9 nm for the fresh catalyst Au/S-1\_IM to 8.4 nm for the calcined catalyst Au/S-1\_IM\_C. Similar behavior was observed by Laursen et al. (2010) who reported a decreased activity of the catalyst caused by sintering of gold nanoparticles at elevated temperatures. Selectivity towards  $\text{H}_2$  and  $\text{CO}_2$  for the investigated catalysts ranged between 84 – 89% above 100 °C. The yield of CO remained within the constant range for all catalysts, being between 10% and 15% at the end of reaction.

The morphologies of the spent Au/S-1\_PAIR and Au/S-1\_IM catalysts were investigated using TEM. The representative TEM images and particle size distributions of the spent Au/S-1\_PAIR and Au/S-1\_IM catalysts are shown in Figure 6.7. For both samples, the mean size of gold nanoparticles increased compared to the fresh samples. For the PAIR catalysts the nanoparticle size increased from  $2.2 \pm 0.6$  nm to  $2.5 \pm 0.9$  nm. For the catalyst prepared using impregnation method the size increased from  $1.9 \pm 0.4$  nm to  $2.2 \pm 0.2$  nm. The increase in particle size is very small what could indicate a sintering stability of gold nanoparticles achieved by encapsulation in a zeolite framework.



**Figure 6.7. Representative TEM images and particle size distribution of spent catalysts: a) Au/S-1\_PAIR, b) Au/S-1\_IM.**

The catalyst stability test was carried out at 120 °C for Au/S-1\_PAIR and Au/S-1\_IM samples, in order to develop on the sintering stability of gold nanoparticles during extended reaction times. The plots of STY numbers vs. time are shown in Figure 6.8. As visible, the test revealed no deactivation of the Au/S-1\_PAIR catalyst and Au/S-1\_IM catalyst over the course of 28 h. This might indicate that at the given temperature the particles in both catalysts are immobile and thus, unable to aggregate into larger clusters what would lower the active surface area of the catalyst and its activity.



**Figure 6.8.** STY at 120 °C over 28 h of reaction of formic acid decomposition performed over Au/S-1\_PAIR and Au/S-1\_IM catalysts.

It was shown that the gold in silicalite-1 catalysts prepared using the PAIR method exhibit high activity and sintering stability for dehydrogenation of formic acid in vapor-phase. Catalysts synthesized using the PAIR method showed higher activity for the reaction even after additional calcination than catalyst prepared using impregnation method. These results show the superiority of the PAIR method for synthesis of highly efficient catalysts with gold nanoparticles encapsulated inside silicalite-1 for selective dehydrogenation of formic acid.

### 6.3.2.2 $\text{HAuCl}_4 \cdot 3\text{H}_2\text{O} + 0.3 \text{ ml of different solvents}$

Decomposition of formic acid was performed over gold in silicalite-1 catalysts prepared by the PAIR method using  $\text{HAuCl}_4 \cdot 3\text{H}_2\text{O}$  as gold precursor dissolved in 0.3 ml of different solvents: water, methanol, acetonitrile, all described already in Chapter 4 (section 4.1.2 *Synthesis conditions:  $\text{HAuCl}_4 \cdot 3\text{H}_2\text{O} + 0.3 \text{ ml of different solvents}$* ). All fresh catalysts were additionally calcined in air at 400 °C for 2 h and tested in the same reaction conditions in order to evaluate on the sintering stability of gold nanoparticles. Figure 6.9 and Table 6.2 gather data from the performed experiments.

Figure 6.9 depicts the yield of hydrogen formation versus temperature of the reaction for all tested catalysts. The highest activity was recorded for the Au/S-1\_MeOH and Au/S-1\_ACN catalysts prepared with methanol and acetonitrile, respectively. They both reached 50% conversion at 130 °C, as shown in table 6.2. The activity of the Au/S-1\_ACN catalyst remained unchanged even after additional calcination in air at 400 °C for 2 h. The calcined sample prepared with methanol, Au/S-1\_MeOH\_C, reached 50% conversion at 140 °C. Catalysts prepared with water showed the lowest activity, reaching 50% conversion at 140 °C and 150 °C for the fresh and calcined sample, respectively. Selectivity towards  $\text{H}_2$  and  $\text{CO}_2$  ranged between 84 – 88% above 120 °C. The yield of CO remained within the constant range for all catalysts, being between 10% and

15% at the end of the reaction. The activity observed for Au/S-1\_3\_H<sub>2</sub>O is lower than for Au/S-1\_PAIR, presented in the previous section. The increased volume of water used during the synthesis of Au/S-1\_3\_H<sub>2</sub>O resulted in larger nanoparticles of gold having lower activity in decomposition of formic acid.

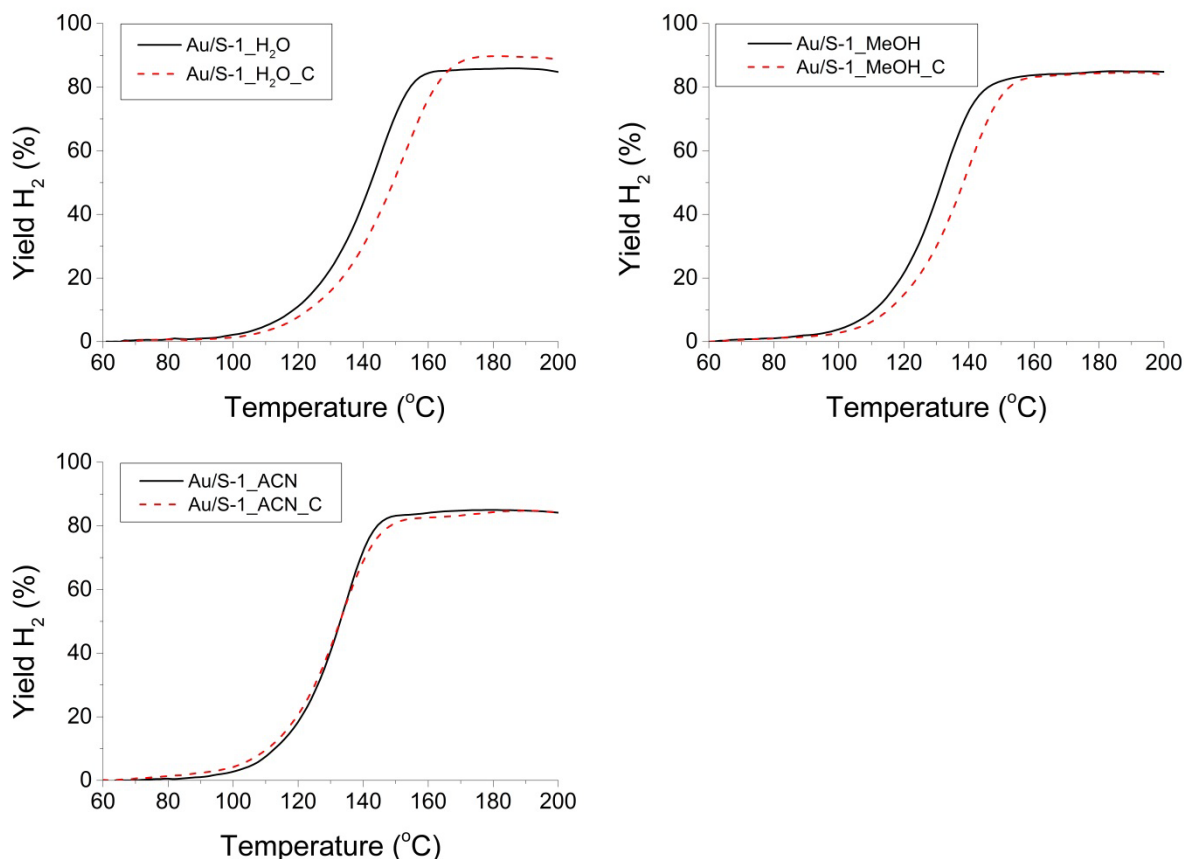


Figure 6.9. Yield of hydrogen formation in formic acid decomposition over fresh and calcined (in air at 400 °C for 2 h) catalysts prepared with the PAIR method using 0.3 ml of different solvents: water (top left), methanol (top right) and acetonitrile (bottom left), and chloroauric acid as gold precursor.

Table 6.2. Data obtained from formic acid decomposition over gold catalysts (fresh and calcined in air at 400 °C for 2 h) prepared by the PAIR method using 0.3 ml of different solvents: water, methanol and acetonitrile, and chloroauric acid as gold precursor.

Catalyst name	Selectivity H <sub>2</sub> (%)	Temperature of 50% conversion (°C)	Mean <sup>1</sup> particle size (nm)	Average <sup>1</sup> particle size (nm)	Total pore volume (cm <sup>3</sup> /g)
Au/S-1_3_H <sub>2</sub> O	85	142	3.5 ± 1.5	4.0 ± 1.6	0.175
Au/S-1_3_H <sub>2</sub> O_C	88	150	4.1 ± 1.9	5.3 ± 2.9	0.173
Au/S-1_3_MeOH	85	130	3.1 ± 2.1	4.5 ± 3.3	0.178
Au/S-1_3_MeOH_C	84	140	3.3 ± 1.3	4.5 ± 2.7	0.169
Au/S-1_3_ACN	84	130	3.4 ± 1.4	3.9 ± 1.9	0.176
Au/S-1_3_ACN_C	84	130	3.6 ± 1.6	4.5 ± 3.1	0.176

<sup>1</sup> Value determined from the measurement of 200 particles from TEM images.

For all catalysts, additional calcination resulted in the increase in the mean and average particle size of gold, probably due to sintering. The increase in particle size observed for the catalysts prepared with water and methanol was followed by a drop in activity of these catalysts. For samples prepared with acetonitrile additional calcination did not influence the activity. This could be associated with the porosity of this catalyst before and after calcination. The total pore volume, shown in Table 6.2, did not change after calcination for the catalyst prepared with acetonitrile, while it decreased for the catalyst prepared with methanol. Lower porosity of the catalyst might limit the accessibility to small particles located inside the silicalite-1 crystals and what could result in lower activity of the catalyst. A porosity related activity of the catalyst was observed by Wang et al. (1998) who showed that a low porosity of the support decreased the contact between the gas and the catalyst particles what resulted in lower conversion in CO<sub>2</sub> reforming of methane over nickel catalyst.

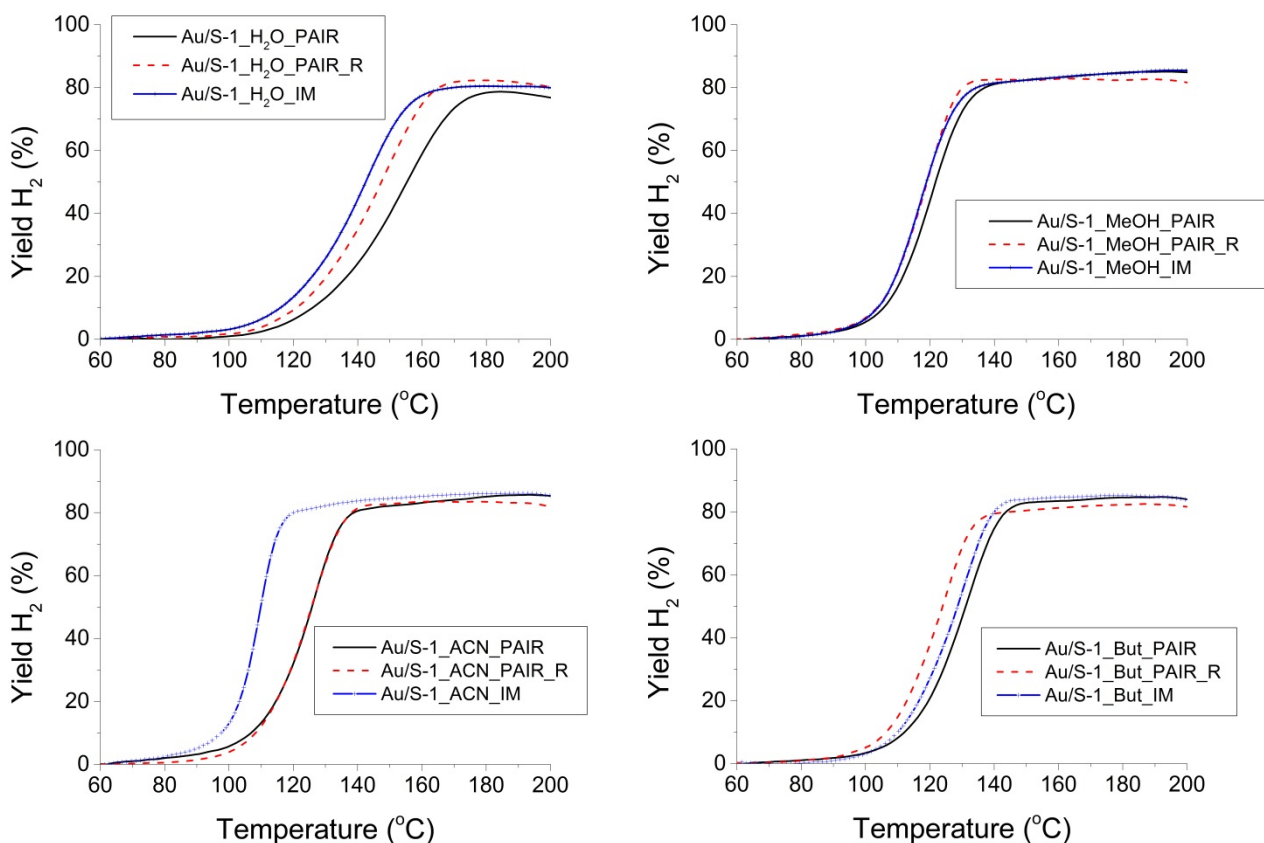
In general, the mean size of gold nanoparticles in all investigated catalysts is very similar. However, the activity of the respective catalysts in decomposition of formic acid is quite different. It was reported by Haruta (2004) that the difference in activity of gold nanoparticles might be associated with the shape of the particles and the number of active sites. Speculating, in case of presented results, various solvents might give rise to differently shaped particles with different kind or number of active sites which exhibit different activity in the formic acid decomposition. In the review published by Andreeva (2002), it is presented that for the CO oxidation in WGS reaction over Au/TiO<sub>2</sub> catalysts there was an optimal size of gold nanoparticles which exhibit the highest activity in WGS reaction. It could be that there is an optimal size of gold nanoparticles which gives the highest activity in dehydrogenation of formic acid. However, more experiments are necessary to confirm this hypothesis.

It was shown that gold in silicalite-1 materials synthesized using different solvents by the PAIR method exhibit high activity in dehydrogenation of formic acid in vapor-phase. The catalysts prepared using organic solvents presented higher activity and sintering stability than when water was used. The highest activity was observed for the catalyst prepared with acetonitrile. The increased volume of solvent used during the synthesis was shown to give larger gold nanoparticles which were less active in the reaction. The origin of the activity of the synthesized catalysts was speculated to depend on the selection of parameters including size and shape of nanoparticles, porosity of the support or kind and number of active sites.

### 6.3.2.3 AuCl<sub>3</sub> + 0.3 ml of different solvents

Decomposition of formic acid was performed over catalysts prepared with different methods: impregnation, PAIR and PAIR followed by reduction at 350 °C in 10% H<sub>2</sub> in N<sub>2</sub>, described already in Chapter 4 (section 4.1.3 *Synthesis conditions: AuCl<sub>3</sub> + 0.3 ml of different solvents*). All catalysts were prepared with AuCl<sub>3</sub> as gold precursor dissolved in different solvents: water, methanol, acetonitrile and 1-butanol. Results from the performed experiments are shown in Figure 6.10 and Table 6.3.

The catalyst prepared by the PAIR method with 1-butanol was tested for the residual solvent remaining in the sample after the synthesis, as was detected from ATR analysis (Chapter 4), and its possible contribution to the overall CO<sub>2</sub> evolution during the reaction. For the experiment, the reservoir with formic acid was removed from the set up and only argon gas was passed over the packed bed reactor containing the catalyst. No signals of CO or CO<sub>2</sub> were detected. This indicates no contribution of residual 1-butanol to the hydrogen yield calculated for the reaction carried out over materials prepared with 1-butanol.



**Figure 6.10.** Yield of hydrogen formation from formic acid decomposition as a function of temperature for gold catalysts prepared using different methods: PAIR, impregnation and PAIR followed by additional reduction (350 °C in 10% H<sub>2</sub> in N<sub>2</sub>), AuCl<sub>3</sub> as gold precursor and 0.3 ml of different solvents: water (top left), methanol (top right), acetonitrile (bottom left) and 1-butanol (bottom right).

The yield of hydrogen formation versus temperature of the reaction for all investigated catalysts is shown in Figure 6.10. Au/S-1\_ACN\_IM was the most active catalyst reaching 50% conversion at 110 °C, as shown in Table 6.3. The Au/S-1\_ACN\_PAIR and Au/S-1\_ACN\_PAIR\_R showed lower activity, reaching 50% conversion at 125 °C. Catalysts prepared with methanol exhibited second best results among all tested samples. They all showed very similar activity, achieving 50% conversion at temperatures between 118 °C – 122 °C. Catalysts prepared with 1-butanol reached 50% conversion at temperatures between 124 °C and 131 °C. The highest activity was observed for the catalyst prepared using the PAIR method followed by additional reduction – Au/S-1\_Butanol\_PAIR\_R, while the lowest for the one prepared with PAIR – Au/S-1\_Butanol\_PAIR. Catalysts prepared with water showed the lowest activity among all catalysts investigated in this section. The catalyst Au/S-1\_H<sub>2</sub>O\_IM prepared using impregnation method reached 50% conversion at 142 °C, while the PAIR catalyst at 155 °C. The additionally reduced PAIR catalyst, Au/S-1\_H<sub>2</sub>O\_PAIR\_R, reached 50% conversion at 147 °C. The selectivity towards hydrogen was between 77-85% for all catalysts. The yield of CO remained in the constant range between 15-19%, except for the water-prepared samples. The CO levels reached up to 23% for Au/S-1\_H<sub>2</sub>O\_PAIR catalyst.

The catalysts prepared with AuCl<sub>3</sub> dissolved in different solvents show higher activity in the formic acid decomposition than catalysts prepared with HAuCl<sub>4</sub>·3H<sub>2</sub>O dissolved in the same solvents, described in the previous section. The possible reason might be the size of gold nanoparticles in the respective catalysts.

Generally, materials prepared with AuCl<sub>3</sub> had smaller nanoparticles than when prepared with HAuCl<sub>4</sub>·3H<sub>2</sub>O, giving higher active surface area available for the reaction. The discussion on the possible influence of the choice of gold precursor on the size of nanoparticles was already provided in Chapter 4 (*section 4.6.5 Influence of the choice of precursor used during the PAIR procedure*).

**Table 6.3.** Data from formic acid decomposition over gold catalysts prepared using AuCl<sub>3</sub> as gold precursor and 0.3 ml of different solvents (water, methanol, acetonitrile, 1-butanol) by impregnation method, the PAIR method and the PAIR method followed by reduction at 350 °C in 10% H<sub>2</sub> in N<sub>2</sub> for 2 h.

Catalyst name	Selectivity H <sub>2</sub> (%)	Temperature of 50% conversion (°C)	Mean <sup>1</sup> particle size (nm)	Average <sup>1</sup> particle size (nm)
Au/S-1_H <sub>2</sub> O_IM_AuCl <sub>3</sub>	80	142	3.1 ± 1.2	4.4 ± 2.7
Au/S-1_H <sub>2</sub> O_PAIR_AuCl <sub>3</sub>	77	155	2.4 ± 1.4	3.7 ± 3.0
Au/S-1_H <sub>2</sub> O_PAIR_R_AuCl <sub>3</sub>	80	147	3.3 ± 1.7	4.5 ± 2.8
Au/S-1_MeOH_IM_AuCl <sub>3</sub>	85	119	3.4 ± 2.2	3.9 ± 2.1
Au/S-1_MeOH_PAIR_AuCl <sub>3</sub>	85	122	2.2 ± 1.0	2.6 ± 1.5
Au/S-1_MeOH_PAIR_R_AuCl <sub>3</sub>	81	118	2.7 ± 1.0	2.9 ± 0.9
Au/S-1_ACN_IM_AuCl <sub>3</sub>	85	110	2.2 ± 1.0	2.5 ± 1.3
Au/S-1_ACN_PAIR_AuCl <sub>3</sub>	85	125	2.0 ± 0.9	2.2 ± 0.9
Au/S-1_ACN_PAIR_R_AuCl <sub>3</sub>	82	125	1.6 ± 0.7	1.9 ± 1.1
Au/S-1_But_IM_AuCl <sub>3</sub>	84	129	2.0 ± 1.0	3.3 ± 2.7
Au/S-1_But_PAIR_AuCl <sub>3</sub>	84	131	1.6 ± 0.5	1.7 ± 0.7
Au/S-1_But_PAIR_R_AuCl <sub>3</sub>	81	124	1.6 ± 1.8	1.9 ± 1.1

<sup>1</sup> Value determined from the measurement of 200 particles from TEM images.

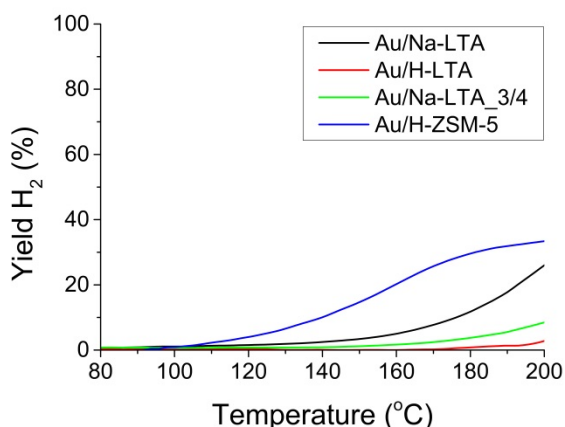
Generally, the impregnation method produced catalysts which were the most active when water, methanol and acetonitrile were used as solvents, or second best for 1-butanol. It is surprising since the impregnation method is well-known for producing very poor gold/silica catalysts with large nanoparticles of low activity (Ma et al. 2011). The catalysts prepared with the PAIR method showed the lowest activity in test reaction irrespectively of the solvent used during the synthesis, as presented in Table 6.3. The additional reduction of these catalysts resulted in the increase in activity, except for acetonitrile sample for which no change was observed. The differences in activity among catalysts prepared with different methods might be connected with the presence of Cl<sup>-</sup> ions remaining after the synthesis. Chloride ions coming from the gold precursor are well-known for lowering the activity of gold catalysts due to blockage of active sites and promoting agglomeration (Haruta et al. 1993, Corma et al. 2008). For the catalysts prepared with impregnation method or the PAIR method followed by reduction, Cl<sup>-</sup> ions could be removed from the catalyst with the gas flow, possibly in the form of HCl. During the PAIR procedure the possibility of removal of Cl<sup>-</sup> ions was limited since the synthesis was carried out under elevated pressure in a sealed autoclave. The XPS analysis was performed for all these catalysts in order to determine the presence and concentration of chlorine. However, no signal in the Cl2p region was observed, possibly due to too low concentration of chlorine in the samples.

The activities of the investigated catalysts do not correlate with the size of gold nanoparticles present in these samples. The observed differences in activity might be connected with the particle shape, number and kind of active sites taking part in the reaction, or interaction between the particles and the support, as was already mentioned in the previous section.

It was presented that gold nanoparticles synthesized using different gold precursor dissolved in organic solvents prepared using the PAIR method or impregnation method show high activity in decomposition of formic acid in vapor-phase. The additional reduction of the catalysts prepared with the PAIR method resulted in increased activity of the materials. The highest activity in the reaction was observed for the catalyst prepared with AuCl<sub>3</sub> and acetonitrile by the impregnation method. This could indicate that with the selected specific synthesis parameters it could be possible to synthesize highly active catalyst with gold nanoparticles encapsulated inside silicalite-1 for decomposition of formic acid.

### 6.3.3 Performance of gold in LTA and ZSM-5 zeolites

Decomposition of formic acid was carried out over various gold in LTA catalysts and gold in ZSM-5 catalyst prepared using the PAIR method and described already in Chapter 4 (section 4.2). Results from the performed experiments are gathered in Figure 6.11 and Table 6.4.



**Figure 6.11. Yield of hydrogen formation from formic acid decomposition as a function of temperature over various gold in LTA and gold in ZSM-5 catalysts.**

The yield of hydrogen as a function of temperature of the reaction is presented in Figure 6.11. None of the tested materials reached 50% conversion below 200 °C, as shown in Table 6.4. Au/H-ZSM-5 reached 33% yield towards hydrogen which is the highest among investigated catalysts. The CO yield for this catalyst was 30%. Among gold in LTA catalysts, Au/Na-LTA achieved the highest yield of hydrogen being 27%, while the two remaining catalysts showed almost no conversion of formic acid. The yield of CO was below 5% for all gold in LTA catalysts.

**Table 6.4. Selectivity towards hydrogen from formic acid decomposition over various gold in LTA and gold in ZSM-5 catalysts.**

Catalyst name	Selectivity H <sub>2</sub> (%)
Au/Na-LTA	27
Au/H-LTA	3
Au/LTA_3/4	9
Au/H-ZSM-5	33

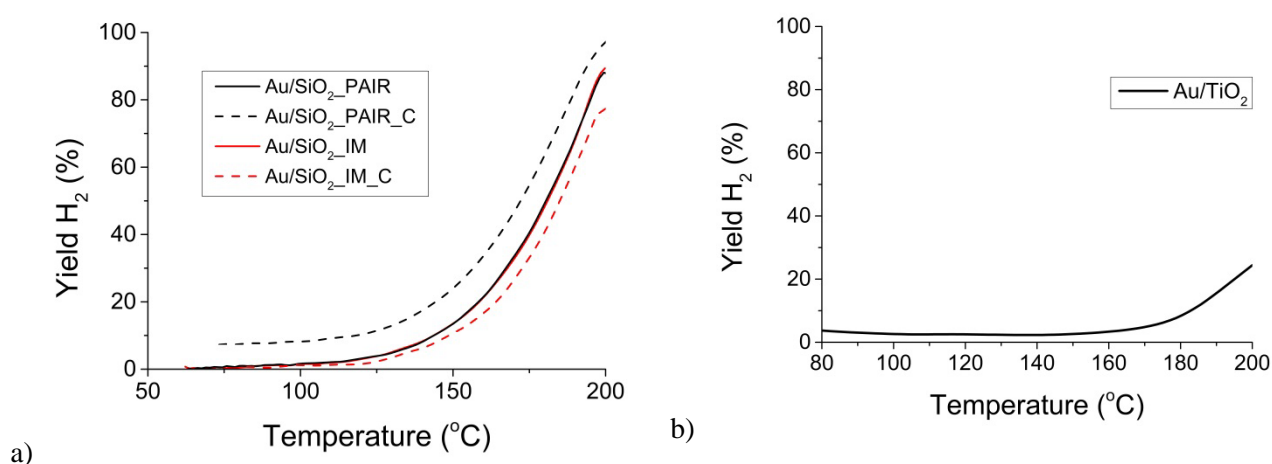
<sup>1</sup> Value determined from the measurement of 200 particles from TEM images.

The very poor activity of Au/H-ZSM-5 catalyst compared to gold in silicalite-1 catalysts, described in previous sections, could be explained by the acidic character of ZSM-5 zeolite. Acidic sites in zeolites are known to promote the formation of CO over CO<sub>2</sub>; hence these zeolites are usually employed when it is CO which is a desirable product from the WGS reaction (Supronowicz et al. 2015). The low activity of gold in LTA catalysts could be associated with a very small pore size in LTA which could act as a diffusion barrier for formic acid and disabling the reaction.

It was shown that gold nanoparticles encapsulated in ZSM-5 or LTA zeolites using the PAIR method exhibit low selectivity for dehydrogenation of formic acid due to acidic character of those zeolites and small pore size of LTA zeolite. Hence, ZSM-5 and LTA zeolites are not suggested as support materials for gold nanoparticles for selective dehydrogenation of formic acid.

### 6.3.4 Performance of gold on amorphous mesoporous silica and titanium oxide

Decomposition of formic acid was carried out over gold nanoparticles supported on amorphous mesoporous silica prepared by the PAIR and impregnation methods, already described in Chapter 4 (section 4.4) and gold supported on titanium oxide (supplied from Mintek). Gold on silica catalysts were subjected to additional calcination in air at 400 °C for 2 h in order to evaluate on sintering stability of nanoparticles. Results from the performed experiments are presented in Figure 6.12 and Table 6.5.



**Figure 6.12. Yield of formic acid decomposition versus temperature performed using: a) gold supported on silica prepared using the PAIR method and impregnation method, b) Au/TiO<sub>2</sub>.**



The yield of hydrogen formation versus temperature of formic acid decomposition over investigated catalysts is shown in Figure 6.12. All four gold on silica catalysts reach 50% conversion above 170 °C, as shown in Figure 6.12a. The selectivities towards hydrogen were between 78 – 90% for these catalysts, as shown in Table 6.5. The yield of CO was in the range of 10 – 15%. The yield of H<sub>2</sub> for Au/TiO<sub>2</sub> is shown in Figure 6.12b. Au/TiO<sub>2</sub> catalyst did not reach 50% conversion below 200 °C. The selectivity towards hydrogen was only 34% for this catalyst and the CO yield was at the level of 48% at the end of the test.

The low activity obtained for gold on silica catalysts, in comparison with gold in silicalite-1 described in previous sections, could be explained by the presence of large aggregates in the samples, as was shown in Chapter 4, Figure 4.14. The presence of large nanoparticles lowers down the activity of the catalyst due to lower active surface area available for the reaction. Aggregation and formation of large gold nanoparticles was more facilitated on the outer surface of silica where nanoparticles could easily migrate, than inside the matrix of a zeolite.

For Au/TiO<sub>2</sub> catalyst the low activity below 200 °C and high selectivity towards CO formation could be associated with the participation of titanium oxide in the reaction. Solymosi et al. (1985) and Henderson (1997) reported formic acid decomposition performed over pure titania in which the selectivity of the reaction was solely towards CO and H<sub>2</sub>O formation. Similarly, Blushev et al. (2010) reported formic acid decomposition in the gas phase over commercial Au/TiO<sub>2</sub> showing selectivity towards H<sub>2</sub> of about 50% at 200 °C and 50% conversion at 170 °C.

**Table 6.5. Data from formic acid decomposition over gold supported on silica prepared by the PAIR and impregnation methods both subjected to additional calcination in air at 400 °C for 2 h, and over gold supported on titanium oxide.**

Catalyst name	Selectivity H <sub>2</sub> (%)	Temperature of 50% conversion (°C)	Mean <sup>1</sup> particle size (nm)	Average <sup>1</sup> particle size (nm)
Au/SiO <sub>2</sub> _PAIR	88	180	4.9 ± 1.4	7.1 ± 5.3
Au/SiO <sub>2</sub> _PAIR_C	90	176	15.0 ± 1.6	16.7 ± 18.6
Au/SiO <sub>2</sub> _IM	90	181	2.9 ± 1.7	3.1 ± 1.0
Au/SiO <sub>2</sub> _IM_C	78	185	3.9 ± 0.5	4.6 ± 1.9
Au/TiO <sub>2</sub>	34	-	2.2 ± 0.5	2.5 ± 0.8

<sup>1</sup> Value determined from the measurement of 200 particles from TEM images.

So far it was shown that encapsulated gold nanoparticles exhibit high activity for decomposition of formic acid. Gold nanoparticles encapsulated inside the pores of silicalite-1 showed much higher activity than when prepared in ZSM-5 or LTA zeolites, or on amorphous mesoporous silica or titanium oxide.

It was presented that by using the PAIR method or impregnation method with the specific synthesis parameters, e.g. choice of gold precursor, solvent or solvent volume, materials with high activity towards dehydrogenation of formic acid and high sintering stability could be synthesized. The highest activity among all gold in silicalite-1 catalysts was observed for Au/S-1\_ACN\_IM\_AuCl<sub>3</sub> material synthesized using AuCl<sub>3</sub> precursor dissolved in acetonitrile and prepared by the impregnation method. Among the PAIR catalysts, the highest activity was shown by Au/S-1\_PAIR material prepared with H<sub>2</sub>AuCl<sub>4</sub>·3H<sub>2</sub>O dissolved in 0.15 ml of water. The origin of the activity of the investigated catalyst was difficult to assess. It was shown that the size of gold nanoparticles can be related to the activity of the catalyst; however, only to certain extent. It was

speculated that there is number of other parameters, like number and kind of active sites, shape of nanoparticles, their interaction with the support or concentration of chlorine ions that can significantly influence the activity of the catalysts for dehydrogenation of formic acid.

### 6.3.5 Performance of palladium in silicalite-1

Formic acid decomposition was carried out over palladium catalysts prepared using the PAIR method: Pd/S-1\_ACN, Pd/S-1\_H<sub>2</sub>O, Pd/S-1\_MeOH, each prepared with different solvent: acetonitrile, water, methanol, and *in situ* incorporation method: Pd/S-1. For the materials prepared using the PAIR method palladium nanoparticles were uniformly deposited on the outer surface of the silicalite-1 crystals, while for the materials synthesized using *in situ* incorporation method they were solely incorporated inside the zeolite matrix. Characterization of these catalysts was given in Chapter 4 (section 4.3.1 *Synthesis of palladium nanoparticles in silicalite-1*) and Chapter 5 (section 5.1 *Synthesis of palladium in silicalite-1*). Results from catalytic tests performed over the investigated catalysts are gathered in Figure 6.13 and Table 6.6.

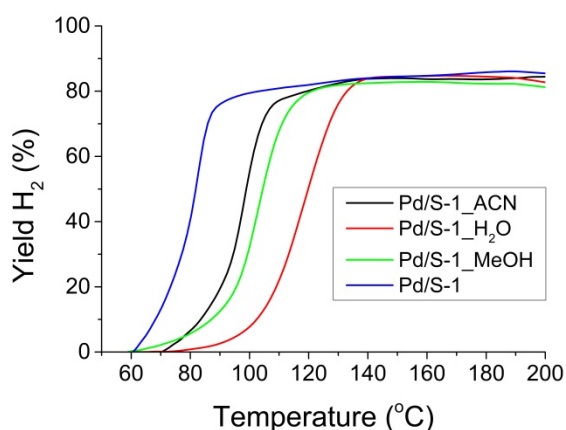


Figure 6.13. Yield of hydrogen formation versus temperature of formic acid decomposition over palladium catalysts prepared using different solvents (acetonitrile, water, methanol) by the PAIR method and *in situ* incorporation method.

Table 6.6. Data from formic acid decomposition over palladium catalysts prepared with different solvents (acetonitrile, water, methanol) using the PAIR method, and *in situ* incorporation method.

Catalyst name	Particles in/out	Selectivity H <sub>2</sub> (%)	Temperature of 50% conversion (°C)	Mean particle size <sup>1</sup> (nm)	Average particle size <sup>1</sup> (nm)	Metal loading (wt%)
Pd/S-1_ACN	out	84	99	2.2 ± 0.8	3.6 ± 2.3	1.0
Pd/S-1_H <sub>2</sub> O	out	82	120	4.3 ± 2.6	5.8 ± 3.7	1.0
Pd/S-1_MeOH	out	81	104	3.0 ± 1.7	4.9 ± 3.7	1.0
Pd/S-1	in	85	80	2.9 ± 1.7	3.3 ± 1.7	1.6

<sup>1</sup> Value determined from the measurement of 200 particles from TEM images.

The yield of hydrogen formation versus temperature of the reaction for all investigated catalysts is shown in Figure 6.13. The highest activity was obtained for palladium catalyst prepared with *in situ* incorporation method - Pd/S-1. It reached 50% conversion at 80 °C, as shown in Table 6.6. It had also the

highest loading of palladium among all investigated catalysts. The high activity obtained for this catalyst could indicate that encapsulation of nanoparticles inside a zeolite matrix did not create a limitation for diffusion of reactants or products during the reaction.

Among the PAIR catalysts, the material prepared with acetonitrile, Pd/S-1\_ACN, showed the highest activity. It reached 50% conversion at 99 °C. Pd/S-1\_MeOH reached 50% conversion at 104 °C and Pd/S-1\_H<sub>2</sub>O at 120 °C. Bulushev et al. (2010) reported 1wt% Pd supported on carbon which reached 50% conversion of formic acid at similar temperature around 100 °C. The selectivity towards hydrogen was at a constant level of 81-85% for all investigated catalysts. In comparison the most active catalyst of gold in silicalite-1 prepared in this study - Au/S-1\_ACN\_IM\_AuCl<sub>3</sub> reached 50% conversion at 110 °C. This is in good agreement with the results published by Yoo et al. (2014) who showed, from DFT calculations, that palladium or platinum were potentially more active than gold for dehydrogenation of formic acid.

The activity of the PAIR catalysts correlates with the size of palladium nanoparticles present in these materials. The smallest nanoparticles were found for Pd/S-1\_ACN, as shown in Table 6.6, giving the largest surface area of active palladium available for the reaction.

It was presented that palladium/silicalite-1 catalysts synthesized using the PAIR method and *in situ* incorporation method exhibit high activity in decomposition of formic acid towards hydrogen formation. Catalyst prepared with the highest Pd loading by the *in situ* incorporation method showed the highest activity among investigated catalysts. Catalyst prepared using acetonitrile as solvent achieved the highest activity among the PAIR catalysts. These results could indicate that the PAIR method and *in situ* incorporation method are feasible protocols for synthesis of highly active catalysts with small palladium nanoparticles selective for dehydrogenation of formic acid in vapor-phase.

### 6.3.6 Performance of platinum in silicalite-1

Vapor-phase decomposition of formic acid was carried out over platinum in silicalite-1 catalysts prepared by *in situ* incorporation method using different platinum precursors, already described in Chapter 5 (section 5.2 *Synthesis of platinum in silicalite-1*). The results from the performed tests are presented in Figure 6.14 and Table 6.7.

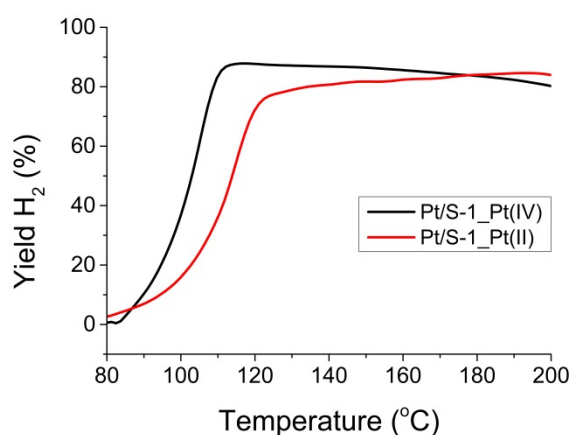


Figure 6.14. Yield of hydrogen formation versus temperature of the reaction for decomposition of formic acid over platinum in silicalite-1 catalysts prepared using different precursors by the *in situ* incorporation method.

**Table 6.7. Data from formic acid decomposition over platinum in silicalite-1 catalysts prepared using different platinum precursors by the *in situ* incorporation method.**

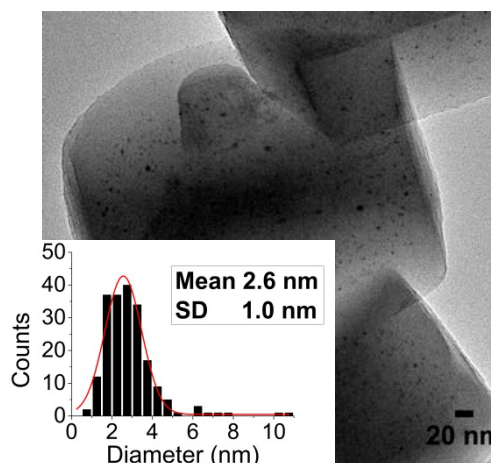
Catalyst name	Selectivity H <sub>2</sub> (%)	Temperature of 50% conversion (°C)	Mean <sup>1</sup> particle size (nm)	Average <sup>1</sup> particle size (nm)	Metal loading <sup>2</sup> (wt%)
Pt/S-1_Pt(IV)	80	103	2.2 ± 1.0	2.5 ± 1.1	1.1
Pt/S-1_Pt(II)	84	114	2.7 ± 1.0	3.2 ± 1.4	1.4

<sup>1</sup> Value based on 200 nanoparticles measured from TEM images; <sup>2</sup> determined from XRF.

The yield of hydrogen formation versus temperature of the reaction is shown in Figure 6.14. Pt/S-1\_Pt(IV) catalyst showed higher activity achieving 50% conversion of formic acid at 103 °C. It is roughly the same 50% conversion temperature as for Pd/S-1\_ACN catalyst prepared by the PAIR method and described in the previous section. Pt/S-1\_Pt(II) reached 50% conversion at 114 °C. The selectivity towards H<sub>2</sub> was similar for both investigated catalysts being 80% and 84% for Pt/S-1\_Pt(IV) and Pt/S-1\_Pt(II), respectively.

Pt/S-1\_Pt(IV) catalyst had smaller platinum nanoparticles than Au/S-1\_Pt(II) what could explain the higher activity in the reaction, even though the metal loading on this catalyst was lower, as shown in Table 6.7. Similarly, Murdoch et al. (2011) presented that too high gold loading on titania resulted in lowering the activity of the catalyst in photocatalytic decomposition of ethanol due to increased size of gold nanoparticles having insufficient number of active sites available for the reaction.

The spent Pt/S-1\_Pt(IV) catalyst was analyzed using TEM. The representative TEM image of the spent Pt/S-1\_Pt(IV) catalyst is shown in Figure 6.15. The mean size of platinum nanoparticles slightly increased from 2.2 ± 1.0 nm for the fresh catalyst to 2.6 ± 1.0 nm for the spent catalyst. The observed increase in size of platinum nanoparticles is very small. It could indicate a limited sintering occurring for this catalyst during the reaction as a result of encapsulation of nanoparticles inside zeolite framework.



**Figure 6.15. Representative TEM image and particle size distribution of spent Pt/S-1\_Pt(IV) catalyst.**

It was shown that platinum in silicalite-1 catalysts synthesized using the *in situ* incorporation method exhibited high activity towards dehydrogenation of formic acid in vapor-phase. Small platinum nanoparticles showed also increased stability towards sintering during the reaction. Based on presented results, the *in situ* incorporation method could be considered a feasible protocol for the synthesis of highly active sintering stable catalyst for decomposition of formic acid.

### 6.3.7 Performance of platinum and palladium in silicalite-1

Vapor-phase decomposition of formic acid was carried out over silicalite-1 with encapsulated palladium and platinum nanoparticles prepared with the *in situ* incorporation method. The investigated catalysts were already described in Chapter 5 (section 5.3 *Synthesis of palladium and platinum in silicalite-1 in random incorporation* and 5.4 *Synthesis of platinum and palladium in silicalite-1 in layered incorporation*). Results from the performed tests are shown in Figure 6.16 and Table 6.8.

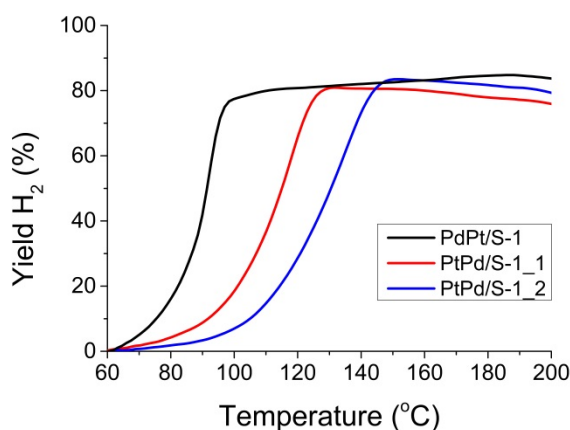


Figure 6.16. Yield of hydrogen formation as a function of temperature of formic acid decomposition over bi-metallic palladium/platinum in silicalite-1 catalysts prepared with the *in situ* incorporation method.

Table 6.8. Results from formic acid decomposition over bi-metallic palladium/platinum in silicalite-1 catalysts prepared with the *in situ* incorporation method.

Catalyst name	Selectivity H <sub>2</sub> (%)	Temperature of 50% conversion (°C)	Mean <sup>1</sup> particle size (nm)	Average <sup>1</sup> particle size (nm)	Pd/Pt metal loading <sup>2</sup> (wt%)
PdPt/S-1	84	91	2.4 ± 0.7	3.0 ± 1.3	0.8/0.9
PtPd/S-1_1	76	114	below 1 nm	-	0.3/0.6
PtPd/S-1_2	79	131	below 1 nm	-	0.2/0.3

<sup>1</sup> Value based on 200 nanoparticles measured from TEM images; <sup>2</sup> determined from XRF.

Figure 6.16 presents the yield of hydrogen evolution versus temperature of the reaction for all investigated catalysts. The highest activity was obtained for PdPt/S-1 catalyst which reached 50% conversion at 91 °C and 84% selectivity towards H<sub>2</sub>, as shown in Table 6.8. The catalysts PtPd/S-1\_1 and PtPd/S-1\_2 achieved a 50% conversion at 114 °C and 131 °C, respectively. The highest activity observed for PdPt/S-1 catalyst could be associated with the highest metal loading among investigated materials. Catalysts PtPd/S-1\_1 and PtPd/S-1\_2 having lower total metal loading and very small metal nanoparticles could provide insufficient number of active sites for the reaction (Murdoch et al. 2011) explaining the lower activity of these catalysts compared to PdPt/S-1.

Comparing the performance of palladium-platinum bi-metallic catalyst with the single metal palladium or platinum catalysts, the lowest 50% conversion temperature (80 °C) was achieved by the Pd/S-1 catalyst having 1.6 wt% metal loading (see Table 6.6). PdPt/S-1 catalyst having the total loading of 1.7 wt%

reached 50% conversion at higher temperature (91 °C). This might indicate that combination of palladium and platinum nanoparticles does not improve the performance of the single metal palladium catalyst.

It was shown that bi-metallic palladium-platinum nanoparticles encapsulated inside silicalite-1 framework exhibit high activity for selective dehydrogenation of formic acid in vapor-phase reaction. The highest activity was obtained for PdPt/S-1 having the highest total loading of palladium and platinum among investigated materials. These results show that the *in situ* incorporation method could be a feasible protocol for the synthesis of small mixed bi-metallic nanoparticles encapsulated inside silicalite-1 framework for decomposition of formic acid in vapor-phase.

## 6.4 Conclusion

All the results presented in this chapter show the activity of gold, palladium and platinum catalysts encapsulated inside silicalite-1 prepared using the PAIR method, impregnation method and *in situ* incorporation method for dehydrogenation of formic acid in vapor phase. The acidity of the zeolite used as a support was shown to be crucial for the selectivity of gold catalysts in the decomposition of formic acid. It was shown that the activity of gold in silicalite-1 catalysts is highly dependent on the size of gold nanoparticles; however only to a certain extent. It was speculated that there were other parameters, like number and kind of active sites, shape of nanoparticles or their interaction with the support, method of preparation and concentration of chlorine that had a large influence on the activity of gold in silicalite-1 catalysts. The catalysts of palladium and platinum in silicalite-1 were shown to be more active than gold in decomposition of formic acid reaching 50% conversion at lower temperature. Combination of palladium and platinum nanoparticles in silicalite-1 resulted in lower activity compared to single metal palladium in silicalite-1 with similar total metal loading.

The methods investigated in this study were shown to be feasible protocols for synthesis of sintering stable metal nanoparticles encapsulated inside the framework of silicalite-1 having high activity for selective dehydrogenation of formic acid. Considering the large scale applications, they could be potential candidates for the synthesis of catalysts for formic acid decomposition in vapor phase. Heterogeneous catalysts are well-known for being more stable and cheaper to synthesize or replace than homogeneous catalysts. These could be serious arguments in favor of such systems for large scale applications. However, the optimization of the procedures of the PAIR method and *in situ* incorporation method would have to be carried out in order to achieve higher activities and selectivities towards hydrogen.

On the other hand, the superb performance of homogeneous systems, shown in many reviews, might make these efforts unnecessary. As argued by Grasmann and Laurenczy (2012), the justification of use of heterogeneous catalyst connected with easier catalyst separation from product or harsh conditions during homogeneous reaction do not apply in case of formic acid decomposition. The product of this reaction is gaseous; hence the need of advanced separation techniques is ruled out. Most of homogeneous catalysts applied for this reaction operate at ambient conditions so the concern of thermal damage done to the catalyst is not an issue. Moreover, the multi-phase heterogeneous systems are known for their complex heat and mass transfer requirements, also true for the metal/zeolite catalysts synthesized in this study. Therefore, the application of heterogeneous catalysts for dehydrogenation of formic acid might require extensive and detailed analysis from financial, environmental and strategic point of view.



## Chapter 7

### Suzuki cross-coupling

The Suzuki cross-coupling reaction was chosen as a test reaction in order to assess the performance of the palladium catalysts synthesized in the course of this study. Three Pd catalysts obtained with the PAIR method – Pd/S-1\_ACN, Pd/S-1\_MeOH, Pd/S-1\_H<sub>2</sub>O described in Chapter 4, and Pd/S-1 catalyst synthesized with *in situ* method described in Chapter 5, were compared for the Suzuki cross-coupling of bromobenzene and 4-methoxyphenylboronic acid in methanol at 70 °C. Additionally, the size selectivity towards the reactant was investigated with bromonaphthalene as a starting reagent. The obtained results were compared with data already published in the literature in order to assess the performance of the investigated catalysts.

The content of this chapter includes the background about the Suzuki cross-coupling reaction based on recent literature, experimental section where the experimental procedures are explained, and results and discussion section presenting the results of performed experiments followed by discussion and comparison with the published data.

#### 7.1 Background

Suzuki cross-coupling reaction, also called Suzuki-Miyaura cross-coupling reaction, was discovered by Akira Suzuki, 2010-Noble Prize laureate, and Miyaura and first reported in 1979 (Miyaura et al. 1979). It belongs to the group of C-C bond formation reactions, together with, for instance, Heck, Kumada, Stille, Negishi and Sonogashira reactions (Franzén et al. 2005). Suzuki cross-coupling reaction is one of the most important transformations in organic chemistry (Miyaura et al. 1995, Suzuki 2011), being widely applied in the production of agrochemicals, natural products, pharmaceuticals and polymers (Chatterjee et al. 2016). The common protocol for the Suzuki reaction involves the palladium catalyzed cross-coupling of organoboronic acids with aryl halides to form biaryls. The general catalytic cycle for the cross-coupling reaction comprises oxidative addition, transmetalation and reductive elimination, as shown in Figure 7.1. The reaction is known for its versatility and applicability to a wide range of substrates with different functional groups under mild conditions. Besides, the availability and stability of diverse boronic acids, easy handling and removal of the boron by-products, compared to other organometallic reagents, makes the Suzuki cross-coupling reaction one of the most applied synthesis and preferred over other C-C bond formation protocols (Suzuki 2011).

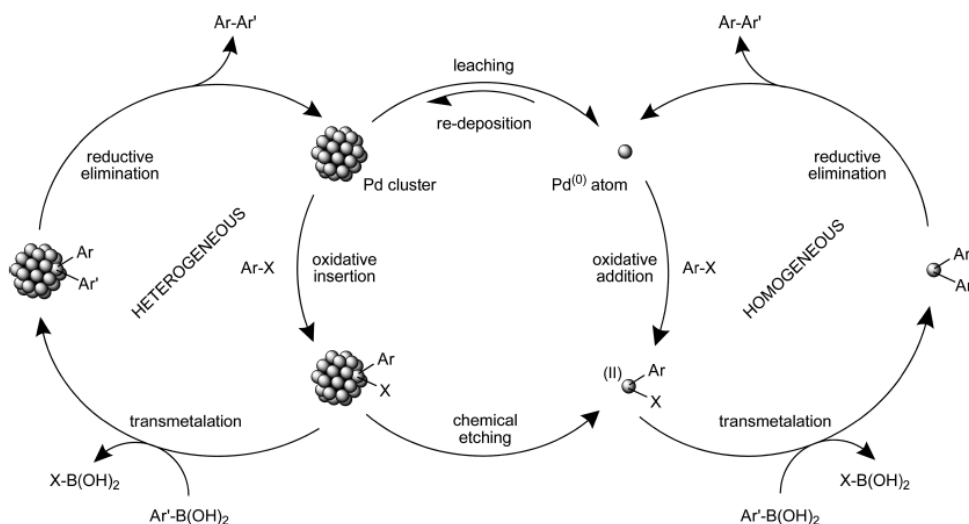
Traditionally, Suzuki cross-coupling is performed in the homogeneous reaction conditions catalyzed by Pd<sup>II</sup>/Pd<sup>0</sup> complexes with phosphine ligands, which except for being excellent stabilizing ligands are also



toxic, expensive and very sensitive for air and moisture (Durap et al. 2010). The catalyst recycling and separation is also an issue in such protocols. Hence, the heterogeneous catalysts or ligand-free systems have been widely desired and developed, even at the cost of lower activity and selectivity than homogeneous catalyst (Fihri et al. 2011). The heterogeneous systems imply catalysts with Pd nanoparticles supported on polymers, metal-organic frameworks, organic-inorganic composites, carbon-based materials, silica and zeolites (Dai et al 2015). However, even though the synthesis and development of the heterogeneous catalysts for Suzuki reaction has been well established over the past years, the mechanism of the heterogeneously catalyzed process and the parameters determining the activity and selectivity of the catalysts are still far from being well understood (Pérez-Lorenzo 2012). The effect of the nanoparticle size and shape, the role of stabilizer, reaction parameters, and the mechanism of the reaction have been discussed and reported extensively (Fihri et al. 2011, Chatterjee et al. 2016, Zhu et al. 2015), and will be reviewed shortly in this work.

### ***Mechanism of the heterogeneously catalyzed Suzuki cross-coupling***

The mechanism of the Suzuki cross-coupling reaction performed in the heterogeneous process has been a point of extensive investigation. There have been many reports supporting the purely homogeneous mechanism of the reaction where the catalytic activity of palladium is attributed to the soluble Pd species that leached out from the surface of solid nanoparticles into the solution (Gaikwad et al. 2007, Soomro et al. 2010) and undergo the reaction in the liquid phase. On the other hand, there is an extensive literature supporting the heterogeneous character of nanoparticle catalyzed Suzuki cross-coupling where both the reagents would come into contact by colliding on the surface of the nanoparticles rather than in the solution (Crudden et al. 2005, Broadwater et al. 2006, Ellis et al. 2010). A joined mechanism has been proposed where both homogeneous and heterogeneous pathways are involved in the catalytic process (Pérez-Lorenzo 2012). There, the reaction is believed to take place both on the surface of Pd nanoparticles which remained attached to the support, and in the solution where Pd atoms leached out or were “dragged” out by the adsorbed species. The soluble Pd would redeposit after the reaction cycle forming smaller nanoparticles or aggregating on the surface of the existing nanoparticles contributing to sintering (Pérez-Lorenzo 2012). Especially the latter is believed to be responsible for the dramatic loss of activity observed for all the catalysts after certain number of cycles (Fihri et al. 2011, Chen et al. 2009).



**Figure 7.1 Mechanism of the Suzuki cross-coupling reaction catalyzed by heterogeneous Pd catalyst. Both homogeneous and heterogeneous pathways are considered as occurring simultaneously during the course of reaction.**

### ***Key parameters in Suzuki cross-coupling***

It is believed that the parameters influencing the selectivity and yield of the Suzuki cross-coupling reaction, like Pd loading on/in the support, size of nanoparticles or choice of base, are directly related to the leaching phenomena occurring during the reaction. The temperature of the reaction was shown to govern the amount of soluble palladium in the reaction mixture (Soomro et al. 2010). An increased amount of leached Pd was observed in the reactions performed at lower temperatures, what correlated well with the increased conversion of the reagents and yield of the final product. On the other hand, too high temperature is believed to cause formation of Pd black and precipitation of active palladium. Therefore, a reasonable choice of temperature for the reaction must be achieved in order to balance the dissolution and precipitation of Pd species governing the performance of the catalyst.

Palladium loading in the supported catalyst was shown to have a tremendous influence on the Suzuki reaction. It was reported that catalysts prepared with lower loadings of Pd showed a superior activity in the reaction over the catalysts with higher loadings of Pd (Durap et al. 2010). This rather unexpected phenomenon is believed to be related, again, to the leaching process occurring during the reaction. Higher Pd loadings give rise to higher concentration of palladium in the reaction mixture; however, the redeposition of Pd species after catalytic cycle is less controlled and might lead to drop in activity due to agglomeration and sintering of Pd nanoparticles.

The size of nanoparticles of Pd was also reported to have a large influence on the activity of the catalyst. It was reported that decreasing the nanoparticle size caused an increase in the activity and selectivity of the catalyst (Narayanan et al. 2008). It was attributed to the increased number of edge and low-coordination-number Pd atoms which were believed to be the active species in the reaction. On the other hand, the same group showed that decreasing the size of Pd nanoparticles results in lower activity of the catalyst in terms of conversion and selectivity towards the Suzuki cross-coupling (Li et al. 2000). It was attributed to the stronger adsorption of the reaction intermediates on the catalytically active sites acting like a poison to the catalyst and lowering its performance. The shape of the palladium nanoparticles was observed to play an important role in the Suzuki reaction. Narayanan et al. (2005) reported that the change from spherical to tetrahedral shape leading to increase in the activity from none to moderate. Similar behavior was

reported by Collins et al. (2014) showing the increase in activity of Pd nanoparticles following the change in shape from octahedron to cubic. The reason for this enhancement is believed to be related to the number of active surface atoms on edges and corners of Pd nanoparticles that are playing a key role in catalyzing the cross-coupling reaction (Fihri et al. 2011).

In the cross-coupling reaction the presence of nucleophile is crucial in activating the organoboron compound (Soloduchko et al. 2013). The selection of base and solvent system for the reaction can provide markedly different yields of the coupled products (Suzuki, 2011). Recently, the water based systems for Suzuki cross-coupling reactions are of major interest since water is considered the greenest solvent contributing to the lowest environmental impact of the process (Chatterjee et al. 2016). The choice of the reagents is playing an important role in the reaction as well. Generally, the chlorides are known for their lowest reactivity in the Suzuki reaction what is attributed to the C-Cl bond strength. Based on the energies of bond dissociation for phenyl-halogen compounds, the C-Cl bond (96 kcal/mol) is the strongest compared to C-Br (81 kcal/mol) or C-I (65 kcal/mol); thus it is more difficult to break at the oxidative addition step in the Suzuki cross-coupling reaction (Littke et al. 2002) (Figure 7.1).

### ***Advances in the synthesis of heterogeneous catalysts for the Suzuki cross-coupling reaction***

As already mentioned before, the heterogeneous palladium based catalysts for the Suzuki cross-coupling reaction have been synthesized extensively utilizing a fair number of different supports (Fihri et al. 2011). Recently, Zhang et al. (2016) reported the synthesis of palladium nanoparticles supported on N-doped porous carbon affording almost quantitative yields of the cross-coupling product after 1 h of reaction. The use of carbon nanotubes as support for well dispersed and small Pd nanoparticles have been extensively reported by Siamaki et al. (2013), Sullivan et al. (2009) and Yoon et al. (2005) as highly active and selective catalyst for the Suzuki cross-coupling reaction.

The synthesis of highly stable and selective catalysts has been achieved using zeolites as supports for palladium or bimetallic-palladium nanoparticles. Dai et al. (2015) reported the synthesis of Pd and Pd-CuO nanoparticles trapped inside the hollow silicalite-1 spheres as highly reagent selective and active catalyst for the Suzuki cross-coupling protocol. Similarly, Guan et al. (2012) reported the synthesis of encaged PdCl<sub>2</sub>(pyridine)<sub>2</sub> complex inside the silicalite-1 hollow spheres as highly efficient catalyst joining the properties of very high activity achieved by homogeneous catalysts and size selectivity and easy separation provided by the heterogeneous catalysts. Kumbhar et al. (2013) reported the synthesis of ZSM-5 supported palladium catalyst. A large number of acidic sites in ZSM-5 facilitated the formation of well distributed small Pd nanoparticles, which together with the porous structure of the support showed high size selectivity towards the substituted aryl halides. Due to the presence of highly ordered large cavities with a diameter of 1.3 nm, the use of zeolite Y has been reported by Durap et al. (2010), Okumura et al. (2010), Bulut et al. (2003) as an excellent candidate as the host material for Pd NP for the Suzuki cross-coupling reaction, yielding catalysts which afford high yields of cross-coupling products in mild conditions and with excellent recyclability. Chang et al. (2012) reported the synthesis of Pd/SBA-15 and Pd/MCM-41 catalysts for the Suzuki cross-coupling using the microwave assisted protocol, resulting in catalysts very active for the conversion of iodobenzene and bromobenzene derivatives. Chen et al. (2009) reported a synthesis of mesoporous silica-based nanoreactor with entrapped Pd nanoparticles which showed superior size selectivity towards reagents.

The use of other metals than palladium for the Suzuki cross-coupling reaction has been increasingly studied due to the environmental and cost related issues. Especially, catalysts containing non-noble metals

are of great interest. Bimetallic or multimetallic systems with palladium and other metals like copper, nickel, silver or gold etc. have been developed and applied successfully in the Suzuki cross-coupling reaction. Thathagar et al. (2002) investigated the bi- and multi-metallic systems for Suzuki reaction showing the superior performance of the palladium/copper catalyst over other bimetallic systems, which was comparable to the activity of the purely Pd catalyst. Similar results were reported by Kim et al. (2008) who demonstrated increased catalytic activity of the Pd/Cu system compared to Pd/Ag or Pd/Ni catalyst. Other works report the use of Fe (Jana et al. 2011), Rh (Gniewek et al. 2013), and Au (Garcia et al. 2010, Corma et al. 2007) in mono-metallic systems for the Suzuki cross-coupling reaction.

Therefore, in the present study, Suzuki cross-coupling of bromobenzene and 4-methoxyphenylboronic acid was investigated using palladium in silicalite-1 catalysts synthesized using the PAIR method and *in situ* incorporation method. The size selectivity towards substrate was tested for 1-bromonaphthalene as a starting reagent in reaction catalyzed by palladium catalyst for which Pd nanoparticles were solely encapsulated inside silicalite-1 crystals synthesized using the *in situ* incorporation method.

## 7.2 Experimental

### 7.2.1 Materials

All the chemicals used in the study were obtained from commercial suppliers and used as received without further purification: bromobenzene ( $\geq 99.5\%$ , Supelco), bromonaphthalene (97%, Aldrich), 4-methoxyphenylboronic acid ( $\geq 95\%$ , Aldrich), potassium carbonate ( $\geq 99\%$ , Fluka), methanol (99.5%, Aldrich), dodecane ( $\geq 99.8\%$ , Sigma-Aldrich), dibenzyl ether ( $\geq 98\%$ , Sigma-Aldrich), 4-methoxybiphenyl (97%, Aldrich).

### 7.2.2 Catalyst characterization

All investigated catalysts were characterized using TEM, XRD, BET and XPS methods. Details about the catalysts in question are given in Chapter 4 and Chapter 5.

### 7.2.3 General procedure for the Suzuki cross-coupling reaction

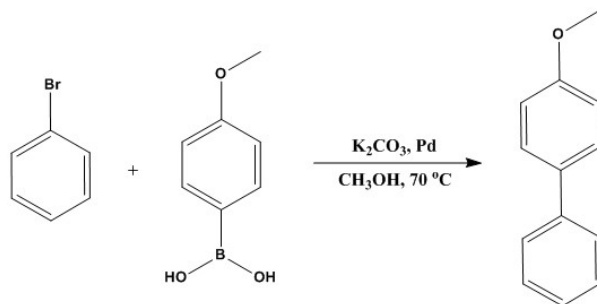
First, potassium carbonate was dissolved in 0.125 mol of bromobenzene or bromonaphthalene in a 5 ml capped vessel under continuous stirring. Then, 4-methoxyphenylboronic acid dissolved in 0.5 ml of methanol was added, and the mixture was stirred until homogeneity at 70 °C. Finally, the catalyst was added to the mixture according to data in Table 7.1. Samples were extracted at times: 0 min, 10 min, 15 min, 45 min, and analyzed by GC (bromobenzene,) or NMR (1-bromonaphthalene). Dodecane was used as internal standard for the reaction with bromobenzene, while dibenzyl ether was used for bromonaphthalene. Table 7.1 gathers details about the masses of all the reagents used in the study.

Table 7.1 Reagents and their masses used for the Suzuki cross-coupling reaction.

Reagent	Amount used in the reaction (mg)
Bromobenzene	19.6
1-Bromonaphthalene	25.8
Pd PAIR catalyst	20 (1.5 mol% Pd)
Pd in-situ catalyst	12.4 (3.2 mol% Pd)
Potassium carbonate	86.3
4-Methoxyphenylboronic acid	57

### 7.3 Results and Discussion

The Suzuki cross-coupling reaction between bromobenzene and 4-methoxyphenyl boronic acid to the corresponding cross-coupling product 4-methoxybiphenyl was performed according to the scheme depicted in Figure 7.2. Yields of the final product obtained for different catalysts are shown in Table 7.2 and Figure 7.3. Except for the main product, by-products such as anisole and homo-coupling products: biphenyl and 4,4'-dimethoxybiphenyl, were also detected at cumulative yield of 5% (not included in the results).



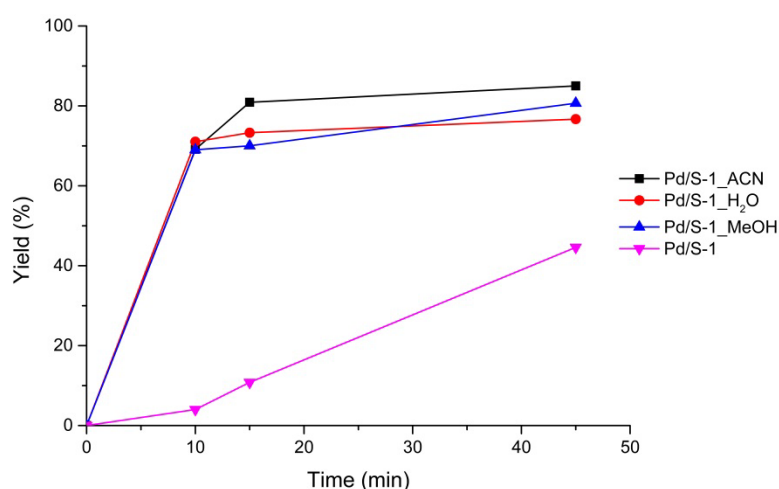
**Figure 7.2 showing the Suzuki cross-coupling reaction of bromobenzene with 4-methoxyphenylboronic acid yielding 4-methoxybiphenyl as final product investigated in the study.**

Table 7.2 and Figure 7.3 show the yields towards the final product for all investigated catalysts. An increase in the yield was observed for all tested catalysts in the course of the reaction. The yields of 4-methoxybiphenyl after 45 min of reaction were decreasing for the respective catalysts following the order: Pd/S-1\_ACN  $\approx$  Pd/S-1\_MeOH  $\approx$  Pd/S-1\_H<sub>2</sub>O > Pd/S-1. For the catalysts prepared with the PAIR method, for which Pd nanoparticles were located solely on the surface of the zeolite crystals, the difference in yield might be attributed to the available surface area of Pd nanoparticles, as determined in XPS study shown in Chapter 6. The size of Pd nanoparticles in Pd/S-1\_ACN catalyst was the smallest, giving the highest surface area of palladium available for the reaction to occur on. The Pd/S-1\_H<sub>2</sub>O resulted in the largest particles of Pd, lowest XPS signal for surface Pd; hence the lowest activity of this catalyst among the PAIR prepared samples. The Pd/S-1 catalyst, which was prepared in the *in situ* method, gave the lowest yield of all the investigated catalysts, even though it contained Pd nanoparticles which were the smallest in size (Table 7.2). The difference between this catalyst and the PAIR catalysts is that the particles of palladium in Pd/S-1 were exclusively located inside the channels of silicalite-1 making them more difficult to access for the reagents. More, the transport of the reagents in and out of the zeolite could be limited by the steric hindrance of the zeolite channels, resulting in trapping of reagents inside the matrix of the support, making them inaccessible for the analysis.

**Table 7.2** Data of yields obtained for the investigated catalysts in the Suzuki cross-coupling reaction of bromobenzene with 4-methoxyphenylboronic acid giving 4-methoxyphenyl at 70°C in methanol.

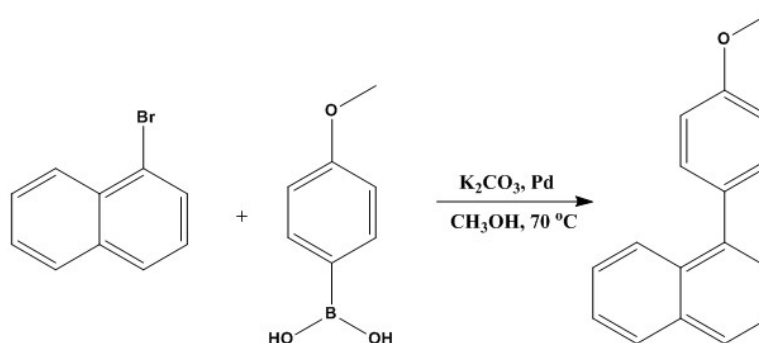
Catalyst	Particles in/out	Metal loading (wt%)	Mean particle size (nm)	Yield (%) <sup>1</sup>		
				10 min	15 min	45 min
Pd/S-1_ACN	out	1.0	2.2 ± 0.8	69	81	85
Pd/S-1_H <sub>2</sub> O	out	1.0	4.3 ± 2.6	71	73	77
Pd/S-1_MeOH	out	1.0	3.0 ± 1.7	69	70	81
Pd/S-1	in	1.6	2.9 ± 1.7	4	11	45

<sup>1</sup> Calculated based on GC analysis.



**Figure 7.3** Plots depicting the yields of 4-methoxyphenyl obtained for all investigated palladium catalysts at 70°C in methanol.

The size selectivity towards the reagent was investigated for Pd/S-1\_ACN and Pd/S-1 catalysts in the reaction of 1-bromonaphthalene with 4-methoxyboronic acid according to the scheme depicted in Figure 7.4. 1-bromonaphthalene was chosen as a much bulkier molecule than bromobenzene, aiming on depicting the differences caused by diffusion limitations governing the reaction using zeolite based catalysts for which the active particles are more or less accessible for the reagents. As mentioned before, Pd/S-1\_ACN catalyst has particles on the surface while Pd/S-1 has them inside the channels of the zeolite. The results from the performed study are shown in Table 7.3.



**Figure 7.4** showing the reaction of 1-bromonaphthalene coupled 4-methoxyphenylboronic acid yielding 1-(4-methoxyphenyl)naphthalene used for the study of size selectivity of Pd/S-1\_ACN and Ps/S-1 catalysts.

**Table 7.3 Yields of the respective products obtained in the Suzuki cross-coupling reaction for bromobenzene and 1-bromonaphthalene with 4-methoxyboronic acid after 3 h of reaction at 70°C in methanol using Pd/S-1\_ACN and Pd/S-1 catalysts.**

Catalyst	Yield (%) after 3 h of reaction	
	4-methoxybiphenyl <sup>1</sup>	1-(4-methoxyphenyl)naphthalene <sup>2</sup>
Pd/S-1_ACN	90	86
Pd/S-1	70	0

<sup>1</sup> Yield calculated from GC analysis; <sup>2</sup> Yield calculated from H<sup>1</sup>-NMR analysis.

Table 7.3 shows the yields of final products: 4-methoxybiphenyl and 1-(4-methoxyphenyl)naphthalene after 3 h of reaction at 70°C using Pd/S-1\_ACN and Pd/S-1 catalysts. Pd/S-1\_ACN afforded yields of 90% and 86% of 4-methoxybiphenyl and 1-(4-methoxyphenyl)naphthalene, respectively, after 3 h of reaction. In comparison, reaction catalyzed by Pd/S-1 resulted in 70% of 4-methoxybiphenyl and none of 1-(4-methoxyphenyl)naphthalene. These results indicate the size selectivity of the Pd/S-1 catalyst which could not convert the bulky 1-bromonaphthalene due to the diffusion limitation imposed by the channels of the zeolite. In case of Pd/S-1\_ACN, no such limitation was present since palladium nanoparticles were located solely on the surface of the crystals making them fully accessible for the reagents. The size selectivity achieved by using zeolites in the catalyst design for Suzuki cross-coupling reaction was showed in the works of Guan et al. (2012), Dai et al (2015) and Chen et al. (2009). Guan et al. (2012) presented the Pd-encaged silicalite-1 hollow spheres which were able to convert the non-substituted aryl halides but not the meta- and ortho- derivatives. Similarly, Dai et al (2015) showed excellent substrate selectivity towards meta- and para- substituted aryl bromides displayed by their Pd and Pd/CuO trapped in the hollow silicalite-1 catalysts. The sharp reactant shape selectivity in Suzuki cross-coupling reactions was observed by Chen et al. (2009) for the Pd@meso-SiO<sub>2</sub> catalyst, where the preferential adsorption of bulky molecules inside the mesopores of the support inhibited the diffusion of smaller reactants and consequently stopped the reaction.

It was shown in the presented study the palladium/silicalite-1 catalysts synthesized using the PAIR method and *in situ* incorporation method show good performance in the Suzuki cross-coupling of bromobenzene and 4-methoxyboronic acid. The size selectivity towards reactant was achieved by using the palladium encapsulated silicalite-1 synthesized using *in situ* incorporation method. The activities of these catalysts in terms of yields and selectivities achieved in the Suzuki cross coupling reaction were showed to be in the range reported in the literature. Therefore, the PAIR method and *in situ* incorporation method could be considered feasible protocols for synthesis of highly active catalyst for Suzuki cross-coupling reaction. However, more experiments involving different Pd loading, amount of catalyst used, activated or non-activated reagents, and recyclability tests are required for the full assessment of the catalysts prepared using these methods.

## Chapter 8

### Oxidation of allyl alcohol

The oxidation of allyl alcohol to its corresponding methyl esters: methyl acrylate (MA) and methyl methoxypropionate (MMP) was investigated using commercial catalyst of gold supported on titanium oxide at ambient conditions and with oxygen as the oxidant, according to scheme presented in Figure 8.1. The analysis included the variation in the kind of base and its loading in the reaction mixture. The influence of the substrate/solvent ratio and the reusability of the catalyst were investigated. The optimized conditions were applied to the selection of other allylic and aromatic alcohols in order to widen the scope of the reaction. Furthermore, the oxidation of allyl alcohol at ambient conditions was performed using gold incorporated silicalite-1 catalyst – Au/S-1\_PAIR, which was synthesized using the PAIR method (4.2.1  $H AuCl_4 + 0.15\text{ ml water}$ ), as described in Chapter 4.

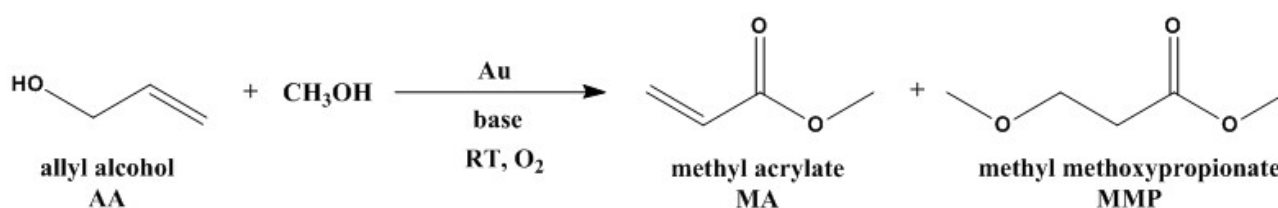


Figure 8.1. Scheme of the oxidation of allyl alcohol (AA) to its corresponding esters: methyl acrylate (MA) and methyl methoxypropionate (MMP) performed in this study.

This chapter is based on the scientific article submitted for publication by authors: Agata Gallas-Hulin, Rama Krishna Kotni, Martin Nielsen, Søren Kegnæs, see Appendix A. The chapter includes the background about the oxidation of alcohols based on the recent publications, experimental section where the performed procedures are explained and the results and discussion section providing the insight into the results.

### 8.1 Background

Over the past decade there has been a strong interest in alcohol oxidation using gold catalysts. Conventional alcohol oxidation requires toxic metal oxidants and is usually performed in harsh conditions (Della Pina et al. 2012). Although a number of methods have been developed, the search for new facile, cost effective and environmentally benign procedures that can avoid the use of large excess of toxic and expensive stoichiometric metal oxidants has attracted significant interest. Development of environmentally-friendly catalytic reaction is crucial, in particular with respect to the production of bulk chemicals. The



selective oxidative esterification of alcohol is a key reaction used to produce numerous important chemical intermediates and commodity chemicals (Oliviera et al. 2009). Over the past decade, gold has been identified as an active catalyst in a variety of reactions, in particular in the selective oxidations of alcohols to its corresponding carbonyl compounds such as aldehydes, carboxylic acids and esters (Parmeggiani et al. 2012). Therefore, the gold-based catalysis of selective oxidation of alcohols has received particular attention, particularly due to the possibility of biomass conversion to fuels, commodity and fine chemicals (Gallezot, 2012), especially, utilizing molecular oxygen as a green oxidant and water as reaction medium (Sheldon, 2015).

### ***Mechanism of alcohol oxidation***

The oxidation of primary alcohols proceeds first to an aldehyde and then further to carboxylic acid. The oxidation of alcohol to an aldehyde performed with heterogeneous catalyst occurs in three steps (Davis et al. 2013):

- adsorption of the alcohol molecule on the metal surface, producing a metal alkoxide;
- $\beta$ -hydride elimination to produce metal hydride and carbonyl species;
- oxidation of metal hydride by dioxygen to regenerate the metal surface.

The initial alcohol deprotonation plays an important role in the kinetics of the first step of alcohol oxidation. It can occur either in the solution, where it is controlled by the pH and  $pK_a$  of the alcohol, or on the surface of the metal. Next, the  $\beta$ -hydride elimination, yielding the carbonyl group – aldehyde in case of primary alcohol oxidation, happens on the surface of the metal. The formed aldehyde is hydrated to geminal diol, which after second  $\beta$ -hydride elimination is transformed to carboxylic acid or its methyl ester. All the above steps are facilitated by hydroxide ions which are either adsorbed on the surface of the metal or present in the solution. It depicts the crucial role of base in the alcohol oxidation reaction (Davis et al. 2013).

The role of oxygen in the reaction mechanism was investigated by Zope et al. (2010) who proposed the dissociative adsorption of oxygen on the metal surface. They report that the role of oxygen in alcohol oxidation is to remove surplus electrons from the metal surface, oxidize the metal-hydride bonds, and regenerate hydroxide ions. It was based on the use of  $^{18}O_2$  in the experiments which confirmed no insertion of  $^{18}O$  into the final product; however revealed the formation of labeled peroxide.

### ***Key parameters affecting the alcohol oxidation reaction***

The deactivation of the catalyst is known as one of the major drawbacks affecting the performance of heterogeneous systems. Leaching, sintering and over-oxidation of metal species together with adsorption of by-products on the surface of metal are common problems encountered in the oxidation of alcohols using heterogeneous catalyst. Zope et al. (2011) showed the adsorption of ketones on the surface of Pt and Au catalysts inhibiting the reaction, while Ferri et al. (2009) reported the adsorption of CO on the surface of Pt catalyst during benzaldehyde oxidation.

As outlined earlier, the liquid phase oxidation of alcohols is strongly facilitated by the presence of homogeneous base in the reaction medium. However, the use of base raises environmental concerns and creates additional costs connected with neutralization and disposal of waste after the reaction. There have been plenty of reports documenting the use of solid bases, such as hydrotalcite, as supports for the heterogeneous catalysts (Ebitani et al. 2005). Hydrotalcite was shown to be an effective support for alcohol oxidation yielding aldehyde as a final product performed in organic solvent. However, hydrotalcite was

observed to leach out into the solution when reaction was carried out in the aqueous media and when acids were formed as final products (Jobbagy et al. 2011).

The mass transfer limitation coming from the limited solubility of oxygen in the reaction mixture is an important factor that must be carefully addressed while designing the experiment. The flux of oxygen provided to the system must be adjusted in a way that the consumption of oxygen in the oxidation reaction is not faster than its diffusion into the liquid phase, what is directly related to the amount of catalyst used in the reaction. Additionally, the porosity of the catalyst which creates additional constrains for diffusion of reactants and products must be considered.

The contact area between the catalytic active sites on the surface of metal nanoparticles and the reactant molecules in the solution is increased by lowering the size of nanoparticles of the catalytically active metal. Among other metals, gold is particularly known for its size-dependent properties and catalytic activity (Ishida et al. 2007). The effect of size of nanoparticles of active metal on the support used as heterogeneous catalyst for the oxidation of alcohols has been studied by Fang et al. (2011) who correlated the increase in conversion of benzyl alcohol with the size of gold nanoparticles catalyzing the reaction. Similarly, Abad et al. (2008) reported the decreased performance of Au nanoparticle-based catalyst for the oxidation of cinnamyl alcohol with respect to increase of the nanoparticle size of gold.

### ***Advances in oxidation of selected industrially important alcohols***

Recent literature shows a growing amount of fundamental research performed with selective alcohol oxidation (Sharma et al. 2016). Industrially important alcohols such as ethanol, benzyl alcohol, HMF, glycerol, together with sugars are primary targets for selective oxidations to form carboxylic acids or their methyl esters. Among them, allyl alcohol has a particular importance as a potential starting material for the production of acrylic acid or its methyl ester which are widely used for the production of superabsorbent polymers. Marsden et al. (2008) oxidized acrolein – aldehyde of allyl alcohol, in methanol under oxygen atmosphere using commercial gold supported on zinc oxide, producing methyl acrylate with 87% selectivity at 97% conversion. Della Pina et al. (2009) oxidized allyl alcohol in water at room temperature using commercial Au/TiO<sub>2</sub> giving 3-hydroxypropionic acid and acrylic acid with yields 8% and 23.5%, respectively. Yamakawa et al. (2001) used various metal oxides and zeolites in hydrogenation of allyl alcohol in methanol with the main product being 3-methoxy-1-propanol at yields of approximately 80%.

Therefore, in this study, oxidation of allyl alcohol to its corresponding methyl esters is investigated over gold supported on titanium oxide. The optimization of reaction conditions in terms of kind and amount of base, substrate to solvent ratio and reusability of the catalyst was performed. Gold in silicalite-1 catalyst prepared using the PAIR method was tested in the reaction as well.

## **8.2 Experimental**

### **8.2.1 Materials**

All the chemicals used for the study were purchased from commercial sources and were used without further purification: allyl alcohol (99%, Aldrich), benzyl alcohol (99%, Aldrich), cinnamyl alcohol (98%, Aldrich), 2-methyl-2-propen-1-ol (99%, Aldrich), trans-2-penten-1-ol (95%, Aldrich), methanol (99.5%, Aldrich), mesitylene (98%, Aldrich), potassium methoxide (25% in methanol, Aldrich), sodium hydroxide (98%, Aldrich), sodium methoxide (30% in methanol, Fluka), methyl acrylate (99%, Aldrich), methyl methoxypropionate (99%, Aldrich). Commercial Au/TiO<sub>2</sub> was provided by Mintek.

### 8.2.2 Catalyst characterization

The analysis of Au/TiO<sub>2</sub> catalyst was performed using TEM and XRD methods. The gold incorporated silicalite-1 catalyst – Au/S-1\_PAIR, was characterized by TEM, XRD, and BET methods, as described already in Chapter 4 (4.2.1  $H AuCl_4 + 0.15\text{ ml water}$ ). Both catalysts were characterized after 24 h of reaction using TEM in order to investigate for the possible morphological changes due to the reaction. Additionally, the reaction mixture after 24 h of reaction was analyzed, without the catalyst, by XRF in order to determine whether any gold species leached out of the support into the solution.

### 8.2.3 Procedure of catalytic oxidation of allyl alcohol

All reactions were performed on a Radleys carousel in ambient conditions under stirring and oxygen flow. In a typical experiment, a 20 mL glass vessel was loaded with 50 mg of catalyst, 2 mmol of allyl alcohol (130  $\mu\text{L}$ ), 148 mmol of methanol (6.0 mL), 0.2 mmol of mesitylene (28  $\mu\text{L}$ ) used as an internal standard, and 60  $\mu\text{L}$  of potassium methoxide. Samples from the reaction were taken at intervals 0 h, 2 h, 5 h, 24 h, and analyzed directly using GC-MS (Agilent 7890A).

## 8.3 Results and Discussion

### 8.3.1 Catalyst characterization

Figure 8.2a shows the XRD diffractogram of the investigated catalyst. The characteristic reflexes corresponding to titania phase are visible; however, no characteristic reflexes of gold were observed. TEM analysis of Au/TiO<sub>2</sub> catalyst showed gold particles of size 2-3 nm, evenly distributed on the support without any tendency to form large clusters, as shown in Figure 8.2b. Lack of visible gold peaks in XRD diffractograms and TEM images recorded for this catalyst indicates a uniform distribution and a small size of gold nanoparticles on the surface of titanium oxide. The detailed characterization of Au/S-1\_PAIR catalyst can be found in Chapter 4.

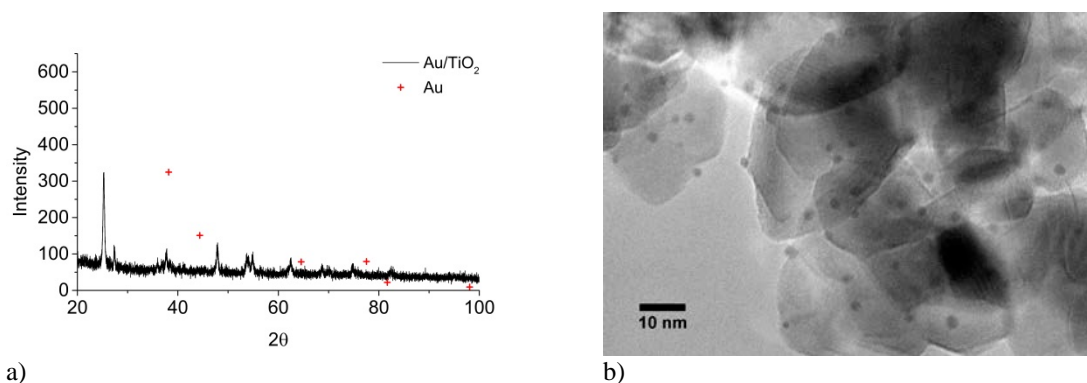


Figure 8.2 (a) XRD pattern of the Au/TiO<sub>2</sub> catalyst; red crosses indicate the positions where the characteristic reflexes of gold occur; (b) TEM image of Au/TiO<sub>2</sub> catalyst used in the study.

### 8.3.2 Catalytic activity

The results from allyl alcohol oxidation to its corresponding esters: methyl acrylate and methyl methoxypropionate are shown in Table 8.1. The oxidation of allyl alcohol performed at 25 °C and 1 bar O<sub>2</sub> with 10% of the base CH<sub>3</sub>OK obtained with Au/TiO<sub>2</sub> reached 99% conversion after 24 h with the yield towards MMP of 85% and 15% towards MA. The performance of Au/S-1\_PAIR catalyst was much lower than Au/TiO<sub>2</sub>. The conversion after 24 h reached only 17%. MA and MMP were detected in trace amounts

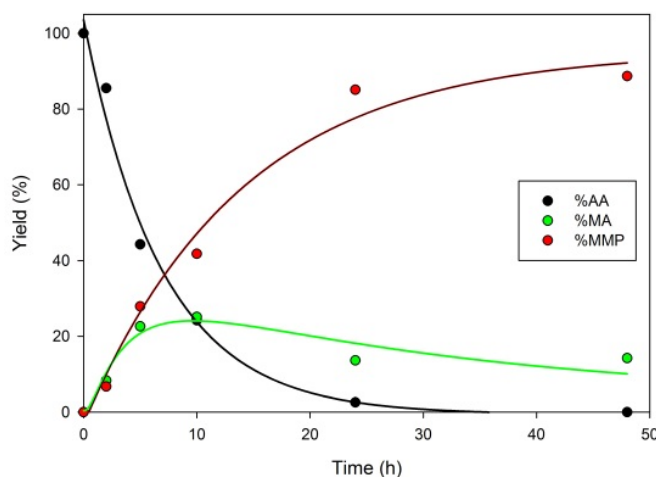
only after 24h of reaction with yields of 0.3% and 0.2% towards MA and MMP. On the other hand, in samples taken at 2 h and 5 h of reaction, the presence of 1,3-propanediol was confirmed qualitatively by GC-MS. The low conversion of allyl alcohol in the reaction catalyzed by Au/S-1\_PAIR might be associated with the diffusion limitations met by molecules of allyl alcohol which have to migrate inside the zeolite channels to reach the nanoparticles of gold and undergo the reaction (Højholt et al. 2011). In order to confirm the role of gold in oxidation of allyl alcohol, a control experiment was performed in which pure TiO<sub>2</sub> is used as a catalyst. After 24 h no conversion of allyl alcohol was detected (Table 8.1).

The conversion of allyl alcohol to MA and then to MMP is shown in Figure 8.3. The suggested sequential product formation with MA as an intermediate towards MMP is based on the classic Michael addition, which is favored under, for example, alkaline activation of the nucleophile. However, too high base concentration might shift the equilibrium towards MA and polymerization through an E1cb intermediate, as shown in Figure 8.4. As such, MA and MMP are interconvertible.

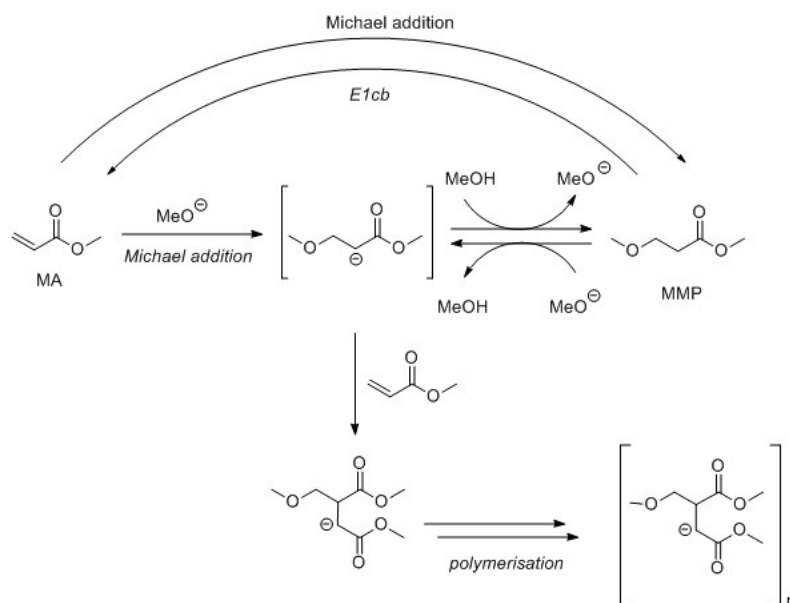
**Table 8.1 Results from oxidation of allyl alcohol using different catalysts with 1 bar of O<sub>2</sub> and room temperature.**

Catalyst <sup>1</sup>	Particle size (nm) <sup>2</sup>	Conversion (%) <sup>3</sup>		
		2 h	5 h	24 h
Au/TiO <sub>2</sub>	2-3	18	33	99
TiO <sub>2</sub>	-	0	0	0
Au/S-1_PAIR	2.7 ± 2.2	ND	14	17

<sup>1</sup> 50 mg of 1wt% catalyst and 10% of base (with respect to allyl alcohol) is used; <sup>2</sup>obtained from TEM analysis; <sup>3</sup>obtained from GC analysis.



**Figure 8.3 Conversion of allyl alcohol (AA) to methyl acrylate (MA) and methyl 3-methoxypropionate (MMP) as a function of time catalyzed by Au/TiO<sub>2</sub>, 10% CH<sub>3</sub>OK, 1 bar O<sub>2</sub> at room temperature.**



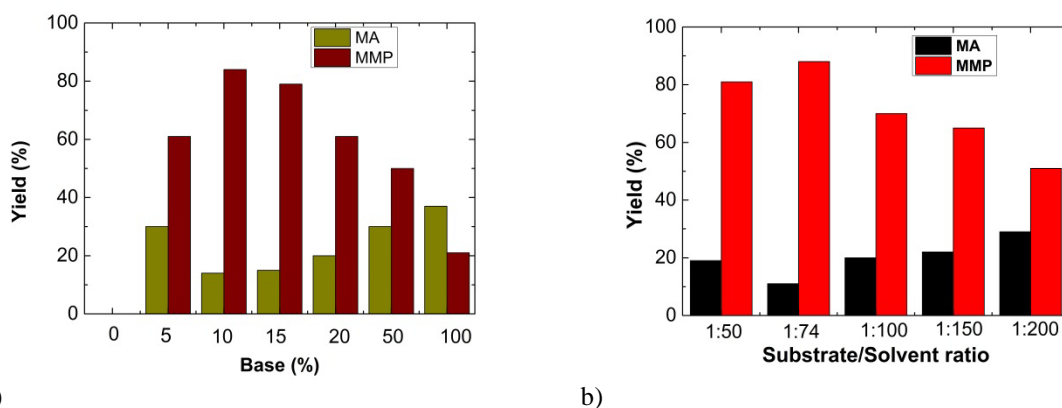
**Figure 8.4 Detailed mechanism of sequential product formation from MA to MMP based on the classic Michael addition reaction.**

To get more insight in to the role of base, a set of reactions with different types of bases (potassium methoxide, sodium methoxide and sodium ethoxide) was performed with Au/TiO<sub>2</sub>. All three examined bases were able to drive the reaction successfully; however, potassium methoxide showed slight superiority (Table 8.2). The effect of the amount of base on the oxidation of allyl alcohol was studied by conducting a series of experiments using different loadings of CH<sub>3</sub>OK i.e. 0, 5, 10, 15, 20, 50 and 100% under the same reaction conditions. Figure 8.5a depicts the results obtained with different base loadings. The highest yield of MMP is observed for the reaction with 10% of base. When the reaction was performed with increasing amount of base, the yield of MMP is observed to be decreasing gradually. On the other hand, the yield of MA is increased up to approximately 30%. Moreover, the total combined yield of MMP and MA is observed to decrease from quantitative to approximately 50%. Large amounts of base could facilitate polymerization of MA leading to compounds with high molecular weights which are not detected by GC-MS, see Figure 8.4.

**Table 8.2 Results from oxidation of allyl alcohol using 50 mg of 1wt% Au/TiO<sub>2</sub> as catalyst with 1 bar of O<sub>2</sub> and room temperature.**

Base <sup>1</sup>	Yield <sup>2</sup> of MMP (%)		
	2 h	5 h	24 h
CH <sub>3</sub> OK	7	28	85
CH <sub>3</sub> ONa	7	17	72
CH <sub>3</sub> CH <sub>2</sub> ONa	7	17	82

<sup>1</sup>10% of base (with respect to allyl alcohol); <sup>2</sup>results obtained from GC analysis.



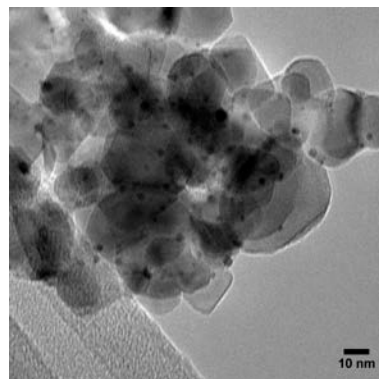
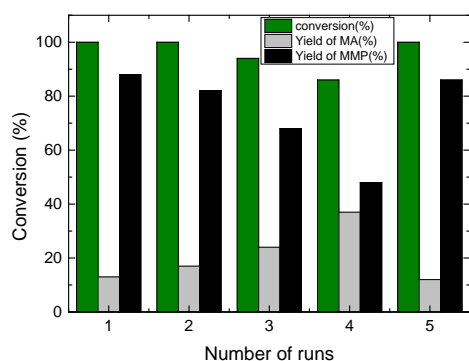
**Figure 8.5** (a) Yields of MA and MMP obtained in the oxidation of allyl alcohol with different base ( $\text{CH}_3\text{OK}$ ) loadings at ambient conditions with 1 bar  $\text{O}_2$ ; (b) The yields of MA and MMP after 24 hours of the oxidation of allyl alcohol at different allyl alcohol to methanol ratios using standard reaction conditions.

The effect of substrate to solvent ratio was studied as well. The reaction was performed using different ratios of allyl alcohol to methanol. Data obtained for these experiments is shown in Figure 8.5b. The highest yield of MMP was obtained for substrate to solvent ratio of 1:74 giving 88% yield after 24 h. It was shown that increasing excess of methanol in the reaction leads to a gradual decrease in the yield of MMP down to 57% with a slight increase in the yield of MA up to 29%. The total cumulative yield of MA and MMP decreased as well. The possible explanation of this behavior might be the lowered total concentration of base in the reaction mixture for the systems with increased amount of methanol, see Figure 8.5. The mechanism for the formation of allyl alcohol coupling with methanol on an O-activated Au surface has previously been studied by C. M. Friend et al. (Zugic et al, 2016). The results showed that the product selectivity could be tuned with the concentration of unsaturated alcohol and methanol.

The reusability of the catalyst was examined by performing several reaction cycles with the same catalyst. After each catalytic cycle, the catalyst was filtered, washed with methanol, dried in air for 24 h, and used in the new reaction cycle. After the fourth cycle, the catalyst was additionally reduced in 10% formier gas (10%  $\text{H}_2$  in  $\text{N}_2$ ) at 350 °C for 2 h. Data from these experiments is shown in Figure 8.6a. It is visible, that the conversion of allyl alcohol decreased with the number of runs from 99% in the first run to 91% in the fourth run. A similar but more significant pattern is observed for the yield of MMP which decreased from 87% to 48%. On the contrary, the yield of MA increased from 13% to 38%. The total combined yield of MMP and MA is observed to decrease from quantitative to approximately 86% after the fourth run. In the fifth run, when the regenerated catalyst was used, the activity of the catalyst is recovered giving the yields of the products identical those in the first run. The reason for the drop of activity of the catalyst might be due to the formation of carboxylic acid (Klitgaard et al, 2008), since no morphological changes in the catalyst or size of gold nanoparticles are observed from TEM analysis, as shown in Figure 8.6b. The size of gold nanoparticles remained in the range of 2-3 and no visible agglomeration of nanoparticles was detected during the analysis.

In order to study the heterogeneity of the reaction, the catalyst was removed from the reaction mixture after 5 h, while all the other parameters remained unchanged. Filtering off the catalyst resulted in the inhibition of the reaction with no increase in yield of any of the products after 24 h, which is shown in Figure 8.7a. This means that even in case of leaching of gold particles from the support material, the activity of the catalyst for the oxidation of allyl alcohol comes from the interaction of gold particles with titanium oxide,

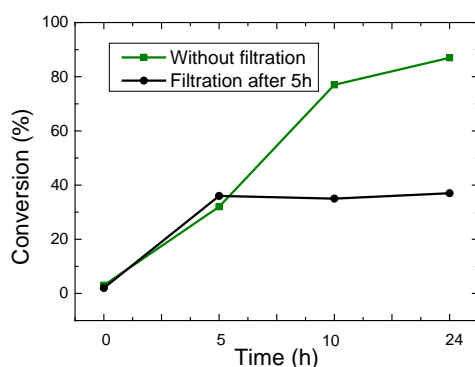
and not gold species alone that could leach out of the support into the solution. Furthermore, no gold was observed in the solution by XRF analysis as shown in Figure 8.7b.



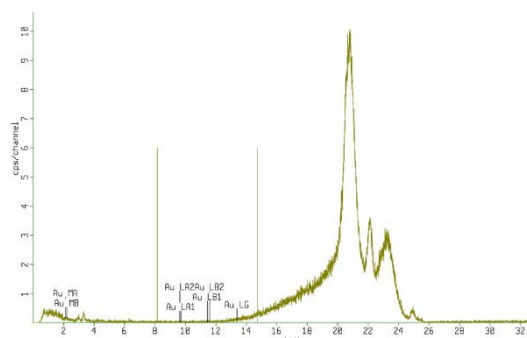
(a)

(b)

**Figure 8.6 (a)** Conversion of allyl alcohol into methyl acrylate and methyl methoxypropionate in four cycles using recycled catalyst; in the fifth cycle, the catalyst is regenerated by reduction in 350 °C with 10% formier gas (10% H<sub>2</sub> in N<sub>2</sub>); **(b)** TEM image of the catalyst Au/TiO<sub>2</sub> after the reaction.



a)




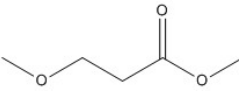
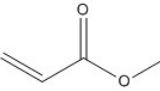
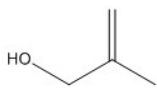
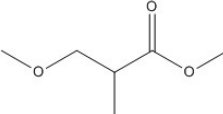
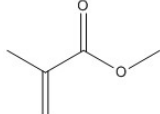
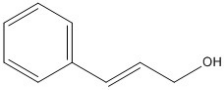
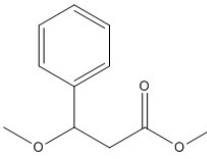
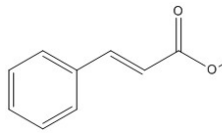
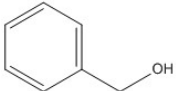
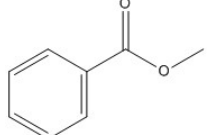
b)

**Figure 8.7 (a)** Change of conversion of allyl alcohol catalyzed by Au/TiO<sub>2</sub> to its corresponding esters at ambient conditions with 1 bar O<sub>2</sub> and 10% CH<sub>3</sub>OK as a function of time for the system with catalyst and after removal of catalyst after 5 h. **(b)** XRF spectrum of reaction mixture at the end of reaction after removal of the catalyst. No gold peaks are observed in the spectrum, indicating no gold species leached out into the solution.

Having established the optimal reactions conditions, a scope of the reaction was examined (Table 8.3). In addition to allyl alcohol, both alkyl and aryl alkene substituted substrates undergo conversion to the desired products in high yields. As such, conducting the reaction with 2-isobutenol afforded the corresponding ester product in a quantitative combined yield (entry 2), and a combined yield of 86% is obtained with cinnamyl alcohol (entry 3). In addition, employing simply benzyl alcohol also resulted in a quantitative yield of methyl benzoate (entry 4).

Comparing entry 1 with entries 2 and 3, selectivity changes from predominantly favoring the Michael addition product in entry 1 to favoring the unsaturated products in the other product mixtures. This is not surprising considering the alkene stabilization effects of both  $\sigma$ -donation and hyperconjugation of the methyl substituent (entry 2) and of  $\pi$ -system conjugation (entry 3) towards nucleophilic attack of the methoxide anion.

**Table 8.3 Results from oxidations of different allylic alcohols using 1wt% Au/TiO<sub>2</sub> at ambient conditions with 1 bar O<sub>2</sub> and 10% CH<sub>3</sub>OK after 24 h.**

Entry	Substrate	Product A	Product B	Conversion (%)	Yield A-B (%)
1				99	85 - 15
2				100	24 - 76
3				100	7 - 79
4		none		100	n/a - >99

In summary, the study showed superior activity of Au/TiO<sub>2</sub> over the gold encapsulated silicalite-1 catalyst synthesized using the PAIR method. The study of different parameters of the reaction revealed a high dependence of the substrate/solvent ratio and base loading on the selectivity of allyl alcohol oxidation in methanol. Due to high conversions and high selectivities achieved in the study, gold supported on titanium oxide operating at ambient conditions represents a promising and environmentally-friendly approach for oxidation of allylic alcohols to its methyl esters.





## Conclusion

The work presented in this thesis contributed to the development of heterogeneous sintering stable catalysts based on metal nanoparticles encapsulated inside zeolite matrix. Two methods were developed – pressure assisted impregnation and reduction (PAIR) and *in situ* incorporation. They were applied to synthesize gold, palladium and platinum nanoparticles encapsulated inside silicalite-1.

The PAIR method was successfully applied in a range of experiments to yield catalysts of gold-incorporated silicalite-1. The synthesized samples showed small nanoparticles 2-3 nm in size with increased stability towards sintering. From the study of different synthesis parameters it was shown that the use of  $\text{HAuCl}_4 \cdot 3\text{H}_2\text{O}$  as precursor in water and  $\text{AuCl}_3$  as precursor in organic solvents gave superior results, the latter even without the use of PAIR. The application of PAIR was successfully shown for the synthesis of palladium/silicalite-1 and gold/ZSM-5 materials.

The *in situ* incorporation method was successfully applied to yield materials with Pd, Pt and PdPt nanoparticles incorporated in silicalite-1. The synthesized materials had small metal nanoparticles that are 2 – 3 nm in size, and were incorporated inside the crystals of silicalite-1.

Dehydrogenation of formic acid showed a high activity of gold, palladium and platinum catalysts prepared inside silicalite-1 using the PAIR method and *in situ* incorporation method. High selectivities towards hydrogen were obtained at temperature around 100 °C. It was shown that the activity of the synthesized catalysts highly depends on the size of nanoparticles and metal loading. It was speculated that there might be other parameters, e.g. number and kind of active sites, shape of nanoparticles or their interaction with the support or presence of chloride ions influencing the catalytic activity of these materials. The catalysts showed stable activity over extended reaction times.

The palladium/silicalite-1 catalysts synthesized using the PAIR method and *in situ* incorporation method showed good performance in the Suzuki cross-coupling of bromobenzene and 4-methoxyboronic acid. The size selectivity was confirmed in the reaction with 1-bromonaphthalene which resulted in no conversion of reactant.

The oxidation of allyl alcohol to its corresponding methyl esters revealed superior activity of  $\text{Au/TiO}_2$  catalyst over gold/silicalite-1 catalyst synthesized using PAIR. It was suspected that the porous nature of silicalite-1 and encapsulation of nanoparticles could be a limiting factor for diffusion of reactants and products into and out of the catalyst matrix.

Based on the presented results the PAIR method and *in situ* incorporation method can be considered as facile and easy protocols to obtain metal nanoparticle-encapsulated silicalite-1. The increased stability towards sintering and high activity in catalytic reactions could justify further development and optimization of these methods for other metals and different zeolite structures.



## Appendix A

### List of publications and disseminations

#### International journals

A. Gallas-Hulin, J. Mielby, S. Kegnæs, "Efficient production of hydrogen from decomposition of formic acid over zeolite incorporated gold nanoparticles", *ChemistrySelect.*, 2016, 1, p. 3942-3945 (attached)

A. Gallas-Hulin, R. K. Kotni, M. Nielsen, S. Kegnæs, "Catalytic oxidation of allylic alcohols to methyl esters". Submitted and accepted in *Topics in Catalysis*.

#### Oral presentations at national/international conferences

A. Gallas-Hulin, S. Kegnæs, "Incorporation of gold into zeolite silicalite-1 using pressure assisted impregnation and reduction method", Proceedings of the Annual Meeting of Danish Chemical Society, Odense, Denmark, 09.06.2016

A. Gallas-Hulin, T. Willum Hansen, J. Mielby, S. Kegnæs, "eTEM investigation of gold nanoparticle formation in recrystallized zeolite silicalite-1", Proceedings of the 12<sup>th</sup> European Congress on Catalysis – EuropaCat-XI, Kazan, Russia, 30-08.2015 – 04.09.2015

A. Gallas-Hulin, S. Kegnæs, "Gold encapsulation in zeolites", Proceedings of PhD Symposium at Department of Chemistry, Technical University of Denmark, Kgs. Lyngby, Denmark, 05.11.2015 – 06.11.2015

A. Gallas-Hulin, R. Kotni, M. Nielsen, S. Kegnæs, "Aerobic oxidation of allyl alcohol in ambient conditions using supported nanoparticle gold catalyst", Proceedings of the 7<sup>th</sup> Tokyo Conference on advanced Catalysis Science and technology (TOCAT7), Kyoto, Japan, 01.06.2014 – 06.06.2014

#### Poster presentations at national/international conferences

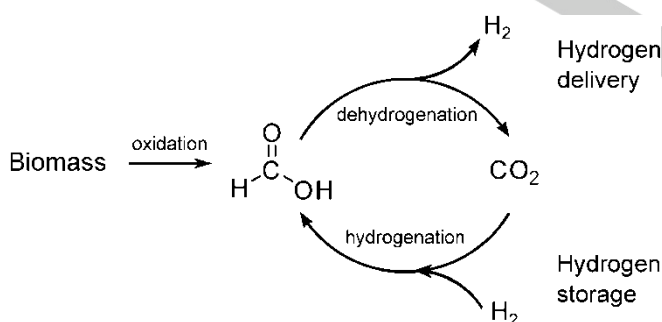
A. Gallas-Hulin, R. Kotni, M. Nielsen, S. Kegnæs, "Mechanistic study of TiO<sub>2</sub> – Au – base interaction in aerobic oxidation of allyl alcohol in ambient conditions", Proceedings of 16<sup>th</sup> Nordic symposium on Catalysis, Oslo, Norway, 15.06.2014 – 17.06.2014

# Efficient production of hydrogen from decomposition of formic acid over zeolite incorporated gold nanoparticles

Agata Gallas-Hulin,<sup>[a]</sup> Jerrik Mielby,<sup>[a]</sup> Søren Kegnæs<sup>\*[a]</sup>

**Abstract:** Formic acid has a great potential as a safe and convenient source of hydrogen for the sustainable chemical synthesis and renewable energy storage. Here, we report a heterogeneous gold nanoparticles catalyst for efficient production of hydrogen from vapor phase decomposition of formic acid using zeolite incorporated gold nanoparticles. The catalyst is prepared by pressure assisted impregnation and reduction (PAIR), which results in a uniform distribution of small gold nanoparticles that are incorporated into zeolite silicalite-1 crystals. Consequently, the incorporated nanoparticles exhibit increased sintering stability. Based on these results, we believe that incorporation of metal nanoparticles in zeolites may find use as highly active and selective heterogeneous catalysts for the production of hydrogen in future renewable energy applications.

Hydrogen produced from renewable resources holds great promise for the sustainable production of chemicals and clean energy. Unfortunately, the physical properties of hydrogen gas make transportation, handling and refueling difficult. Formic acid (HCOOH) has recently attracted considerable attention due to its potential as a hydrogen storage material and as a way to utilize CO<sub>2</sub> [1]. Since formic acid can be synthesized by hydrogenation of CO<sub>2</sub>, a possible carbon-neutral storage-and-release cycle can be envisioned, although this requires that a large amount of renewable hydrogen is readily available. Alternatively, formic acid may be produced from biomass, for instance by the catalytic oxidation of cellulose [2], see Figure 1.

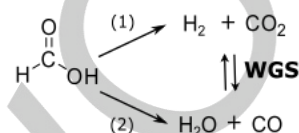


**Figure 1. A possible carbon-neutral cycle for the production, storage and delivery of renewable hydrogen.**

The history of formic acid activation dates back to the pioneering work of Sabatier [3], who showed that its decomposition might occur via dehydrogenation (1) or

dehydration (2). The two reactions pathways are linked by the well-known water-gas shift reaction (WGS), see Figure 2.

**Figure 2. Possible pathways for formic acid decomposition: dehydrogenation (1) and dehydration (2).**



The first reaction is slightly exothermic, while the second is slightly endothermic. In general, the selective formation of H<sub>2</sub> is favored at low reaction temperatures [4].

Supported Au nanoparticles have been studied as catalysts for formic acid decomposition in both liquid [5] and vapor phase [6]. In particular, Ojeda and Iglesia [7] showed that well-dispersed Au catalysts decomposed formic acid with metal-time yields higher than similar Pt catalysts under mild conditions in liquid phase. In another study, Gazsi et al. performed vapor-phase experiments to study the effect of the support and showed Au/SiO<sub>2</sub> to be the most active and selective catalyst with respect to the decomposition of formic acid and H<sub>2</sub> formation [8]. More recently, the decomposition of formic acid has also been investigated by means of periodic density functional theory calculations. In particular, Studt et al. [9] investigated the reaction over Ag, Cu, Pd and Pt. According to their calculations, small Au gold clusters of 0.8 nm in diameter are able to bind CO and OH more strongly than bulk Au, and even be more active and selective than Pt.

The encapsulation of metal nanoparticles in zeolites has recently attracted much attention [10]. In particular, the zeolite framework may introduce selectivity in terms of size- and shape selectivity [11][12] or prevent the encapsulated nanoparticles from sintering [13][14]. However, incorporating metal nanoparticles in zeolites often rely on complex synthetic procedures and expensive additives, which may prevent large-scale production and general implementation [15].

Here, we report a simple and effective method for the incorporation of gold nanoparticles in zeolite silicalite-1. The method is based on pressure assisted impregnation and reduction. In this method, the sample is first impregnated with the gold precursor solution and then reduced in an autoclave under pressure. The pressure assisted impregnation and reduction facilitates the formation of small and well-dispersed gold nanoparticles, while conventional impregnation typically results in relatively large (> 5 nm) and unreactive nanoparticles on silica [16]. Although, absence of strong metal-support interactions may result in severe redistribution of the impregnated metal during drying and reduction [17], simple impregnation is often preferred over more complicated preparative methods such as deposition-precipitation or co-precipitation [17]. The following results demonstrate that pressure assisted impregnation and reduction is a simple and

[a] A. Gallas-Hulin, J. Mielby, S. Kegnæs  
Department of Chemistry  
Technical University of Denmark  
2800 Kgs. Lyngby  
E-mail: [skk@kemi.dtu.dk](mailto:skk@kemi.dtu.dk)

effective method to prepare highly active catalysts comprised of zeolite incorporated gold nanoparticles

In order to investigate the effect of the impregnation method on the size distribution and activity of the supported gold nanoparticles, four catalysts were prepared. The first catalyst, Au/S1\_PAIR, comprised 1 wt% Au on MFI zeolite silicalite-1 (S-1) was prepared by pressure assisted impregnation and reduction (PAIR) using an aqueous solution of  $\text{HAuCl}_4$  as metal precursor. After impregnation the catalyst was placed in the autoclave and subjected to 8 bar of  $\text{H}_2/\text{N}_2$  and  $150^\circ\text{C}$  to reduce the gold precursor to nanoparticles. The second catalyst, Au/S-1\_IM was obtained by simple impregnation (IM) followed by drying and reduction in  $\text{H}_2$  flow at  $350^\circ\text{C}$  and atmospheric pressure. In order to investigate the sintering stability of gold nanoparticles, the two samples were additionally calcined (C) after the synthesis at  $400^\circ\text{C}$  for 3h in air. These samples are named Au/S-1\_PAIR\_C and Au/S-1\_IM\_C, respectively. The detailed synthetic procedures and characterization by HRTEM, XRPD and nitrogen physisorption can be found in the Supporting Information. Table 1 shows an overview of the investigated catalysts. Additionally, the two above mentioned methods were applied to produce gold nanoparticles supported on mesoporous silica. These catalysts were used as reference samples and the information about their synthesis and characterization can be found in the Supporting Information.

**Table 1. Overview of the investigated catalysts.**

Catalyst <sup>a</sup>	Average diameter <sup>b</sup> [nm]	Temperature of 50% conversion [°C]	STY at $120^\circ\text{C}$
Au/S-1_PAIR	$2,7 \pm 2,2$	113	113
Au/S-1_IM	$4,5 \pm 3,0$	122	62
Au/S-1_PAIR_C	$4,0 \pm 2,5$	118	98
Au/S-1_IM_C	$8,6 \pm 3,6$	131	45

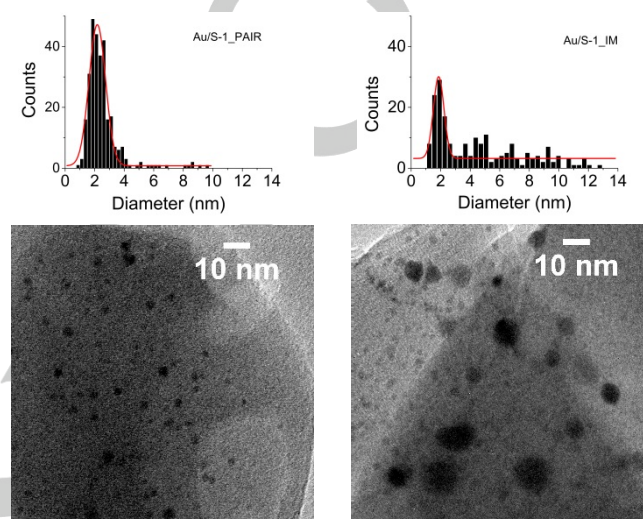
[a] All catalysts were impregnated with an amount of  $\text{HAuCl}_4(\text{aq})$  corresponding to 1wt% Au. [b] As measured from approximately 200 nanoparticles by TEM. PAIR-pressure assisted impregnation and reduction, IM-impregnation, C-additional calcination at  $300^\circ\text{C}$  for 3h in air.

All catalysts were characterized by TEM. For the Au/S-1\_PAIR catalyst the gold nanoparticles were almost exclusively located inside the zeolite crystals. The average diameter of the Au nanoparticles were  $2,7 \pm 2,2$  nm. For comparison, the average diameter of the nanoparticles in Au/S-1\_IM were  $4,5 \pm 3,0$  nm. The TEM image of Au/S-1\_IM in Figure 3 shows that two kinds of nanoparticles are present in the sample. Small nanoparticles, which are around 2 nm located inside the crystal, and large nanoparticles, which are  $>5$  nm in diameter and located on the external surface of the zeolite crystal. Based on the histogram of the particle size distribution presented in Figure 3, particles which are the most abundant in samples Au/S-1\_PAIR and Au/S-1\_IM are around  $2,2 \pm 0,6$  nm and  $1,9 \pm 0,4$  nm, respectively.

The TEM analysis of the calcined catalysts revealed that the Au/S-1\_PAIR\_C had an average particle size of  $4,0 \pm 2,5$  nm, while Au/S-1\_IM\_C had an average particles of  $8,6 \pm 3,6$  nm, see Table 1. These results clearly show that the catalyst prepared by pressure assisted impregnated and reduction were

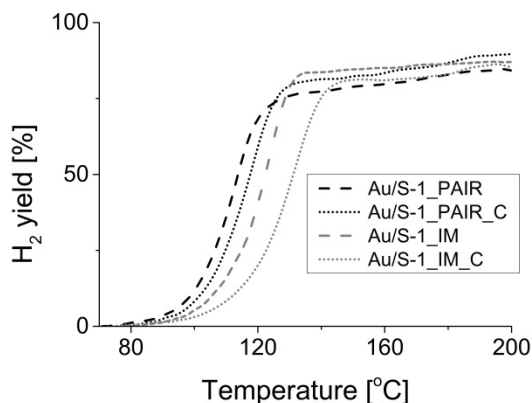
significantly more stable towards sintering than the catalyst prepared by conventional impregnation.

All catalysts were tested in vapor phase decomposition of formic acid into  $\text{CO}_2$  and  $\text{H}_2$ . In a typical experiment, formic acid vapour was passed through a fixed-bed quartz reactor by bubbling 40 ml/min of Ar through pure formic acid at  $20^\circ\text{C}$ . The products were analyzed by an online non-dispersive infrared detector to quantify the amounts of formed CO and  $\text{CO}_2$ . The formation of  $\text{H}_2$  was followed by MS.



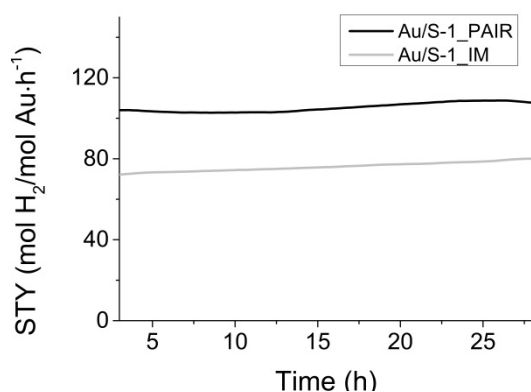
**Figure 3. TEM images and nanoparticle size distribution for Au/S-1\_PAIR and Au/S-1\_IM catalysts.**

Figure 4 shows the yield of  $\text{H}_2$  against the temperature of the reaction. The Au/S-1\_PAIR catalyst exhibited the highest catalytic activity for formic acid decomposition and reached 50% conversion at  $113^\circ\text{C}$ . Even after calcination at  $400^\circ\text{C}$  in air, the catalyst remained very active and reached 50% conversion at  $118^\circ\text{C}$ . The Au/S-1\_IM catalyst, prepared by conventional impregnation, reached 50% conversion at  $122^\circ\text{C}$ , while the calcined sample only reached 50% conversion at  $131^\circ\text{C}$ , see Figure 4. The low activity is a direct consequence of the thermal deactivation caused by sintering. Selectivity towards  $\text{H}_2$  and  $\text{CO}_2$  ranged between 85-90% above  $100^\circ\text{C}$ . In general, this selectivity is lower than in liquid phase (up to 100%) [18,19], but significantly higher than previously reported for e.g. Au/ $\text{TiO}_2$  in vapor phase (70%) [20].



**Figure 4.** Yield of hydrogen as a function of temperature of the reaction temperature.

The catalyst stability tests were carried out at 120°C (around 50% conversion) of the Au/S-1\_PAIR catalyst and Au/S-1\_IM catalyst over the course of 28h, see Figure 5. The catalytic tests revealed that the catalysts were stable and showed no sign of



deactivation.

**Figure 5.** Catalyst stability test performed at 120°C for Au/S-1\_PAIR and Au/S-1\_IM for 28 h. STY is defined as mol H<sub>2</sub>/mol Au hour<sup>-1</sup>.

In conclusion, we have developed a simple and effective method to incorporate gold nanoparticles into silicalite-1 zeolite crystals using pressure assisted impregnation and reduction. The prepared catalysts contain small nanoparticles with a narrow size distribution of around 2 nm, which are readily accessible to formic acid through the inherent microporous framework. The incorporated nanoparticles were highly active for the formation of H<sub>2</sub> by vapor phase decomposition of formic acid, even after exposure to high temperatures. We therefore expect that pressure assisted impregnation and reduction of zeolites and zeolite like materials may become a helpful tool in the development of new materials with improved catalytic properties.

## Experimental Section

The detailed synthesis and characterization of all investigated catalysts by TEM, XRPD and nitrogen physisorption are given in the Supporting Information.

**Synthesis of Silicalite-1:** Tetraethyl orthosilicate (8.3 mL) was added dropwise to a tetrapropylammonium hydroxide solution (1.0M, 13.3 mL) under stirring in a Teflon beaker. The mixture was stirred for 1 hour and then heated in a Teflon-lined stainless steel autoclave at 180°C for 24 h under autogenous pressure. The product was collected by filtration, thoroughly washed with water, dried at room temperature and then calcined for 10 h at 550°C.

**Synthesis of pressure impregnated 1 wt% Au/S-1\_PAIR:** The as-prepared silicalite-1 (0.9900 g) was impregnated with 0.15 mL of an aqueous solution of HAuCl<sub>4</sub>·3H<sub>2</sub>O (0.0199 g). The material was immediately placed in the Teflon-lined stainless steel autoclave under 3 bar N<sub>2</sub> for 2h for pressure assisted impregnation. Then, 5 bar of H<sub>2</sub> was added and the material was reduced under cumulative 8 bar pressure at 150°C for 3h.

**Synthesis of 1 wt% Au/S-1\_IM:** The as-prepared silicalite-1 (0.9900 g) was impregnated with 0.15 mL of an aqueous solution of HAuCl<sub>4</sub>·3H<sub>2</sub>O (0.0199 g). The material was dried at room temperature overnight and then reduced in a flow of 10% H<sub>2</sub> in N<sub>2</sub> for 2 h at 350°C.

**Catalytic activity:** The vapor-phase decomposition of HCOOH was performed at atmospheric pressure in a 3 mm quartz fixed-bed reactor. The formic acid was introduced to the reactor by bubbling 40 ml/min of Ar through pure formic acid at 20°C, which resulted in gas composition of around 7% formic acid in Ar. The reaction gas was passed through the reactor, which contained 50 mg fractionated catalyst (180–355 μm) held in place by two pieces of quartz wool. The product gas was analyzed by an online non-dispersive infrared detector to quantify CO and CO<sub>2</sub> as well as by an online mass spectrometer to follow the formation of other products, in particular H<sub>2</sub>. All catalysts were tested under the same reaction conditions by heating the reactor from 20–200°C by 2°C/min.

## Acknowledgements

The authors gratefully acknowledge the support of the Danish Council for Independent Research, Grant No. 12-127580, the support of the Lundbeck Foundation (Lundbeckfonden), Grant No. R141-2013-13244 and the support from VILLUM FONDEN research grant (13158).

**Keywords:** encapsulation • formic acid • gold nanoparticles • heterogeneous catalysis • zeolites

- [1] S. Moret, P. J. Dyson, G. Laurenczy, *Nat. Commun.*, **2014**, 5, 4017
- [2] R. Wölfel, N. Taccardi, A. Bösmann, P. Wasserscheid, *Green Chem.*, **2011**, 13, 2759.
- [3] P. Sabatier, A. Maille, *Compt. Rendus* **1911**, 152, 1212.
- [4] D. A. Bulushev, S. Beloshapkin, J. R.H. Ross, *Catal. Today*, **2010**, 154, 7.
- [5] M. Yadav, T. Akita, N. Tsumori, Q. Xu, *J. Mater. Chem.*, **2012**, 22, 12582.
- [6] D. A. Bulushev, J.H.R. Ross, *Catal. Today*, **2011**, 163, 42.
- [7] M. Ojeda, E. Iglesia, *Angew. Chem.* **2009**, 121, 4894.
- [8] Gazsi, T. Bansagi, F. Solymosi, *J. Phys. Chem.*, **2011**, 60.
- [9] J. Suk Yoo, F. Abild-Pedersen, J. K. Nørskov, F. Studt, *ACS Catal.* **2014**, 4, 1226.
- [10] W. Grunert et al, *Phys. Status Solidi B*, **2013**, 250, 1081.

- [11] A. B. Laursen, K. T. Højholt, S. B. Simonsen, L. F. Lundegaard, S. Helveg, F. Schüth, M. Paul, J. D. Grunwaldt, S. Kegsnæs, C. H. Christensen, K. Egeblad, *Angew. Chem.*, **2010**, 49, 3505.
- [12] J. Mielby, J. O. Abildstrøm, F. Wang, T. Kasama, C. Weidenthaler, S. Kegsnæs, *Angew. Chem.*, **2014**, 53, 12513.
- [13] K. Højholt, A. B. Laursen, S. Kegsnæs, C. H. Christensen, *Top. Catal.*, **2011**, 54 (16) 1026.
- [14] T. W. Hansen, A. T. DeLaRiva, S. R. Challa, A. K. Datya, *Acc. Chem. Res.*, **2013**, 46, 1720.
- [15] S. Goel, S. I. Zones, E. Iglesia, *J. Am. Chem. Soc.* **2014**, 136, 15280.
- [16] M. Haruta, *Gold Bull.*, **2004**, 37, 1.
- [17] J. A. Schwarz, *Chem. Rev.*, **1995**, 95, 477.
- [18] Q. Bi, X. Du, L. He, Y. Liu, Y. Cao, H. He, et al., *J. Am. Chem. Soc.*, **2012**, 134, 8926.
- [19] M. Yadav, T. Akita, N. Tsumori, Q. Xu, *J. Mater. Sci.*, **2012**, 22, 12582.
- [20] D.A. Bulushev, S. Beloshapkin, J.R.H. Ross, *Catal. Today.*, **2010**, 154, 7.

WILEY-VCH





## Bibliography

- Abad A., Corma A., Garcia H., *Chem. – Eur. J.*, 2008, 14, 212
- Andreeva D., *Gold Bull.*, 2002, 35, 82-88
- Armor J.N., *Catal. Today*, 2011, 163, 3-9
- Baatz C., Decker N., Prüße, *J. Catal.*, 2008, 258, 165-169
- Bell A.T., *Science*, 2003, 299, 1688-1691
- Boddien A., Loges B., Junge H., Beller M., *ChemSusChem*, 2008, 1, 751-758
- Boddien A., Mellmann D., Gärtner F., Jackstell R., Junge H., Dyson P.J., Laurenczy G., Ludwig R., Beller M., *Science*, 2011, 333, 1733-1736
- Bore M.T., Pham H.N., Switzer E.E., Ward T.L., Fukuoka A., Datye A.K., *J. Phys. Chem. B*, 2005, 109, 2873-2880
- Broadwater S. J., McQuade D. T., *J. Org. Chem.*, 2006, 71, 2131-2134
- Bulushev D.A., Beloshapkin S., Ross J.R.H., *Catal. Today*, 2010, 154, 7-12
- Bulut H., Artok L., Yilmaz S., *Tetrahedron Lett.*, 2003, 44, 289-291
- Beckhoff B., Kanngießer B., Langhoff N., Wedell R., Wolff H., *Handbook of Practical X-Ray Fluorescence Analysis*, Springer-Verlag Berlin Heidelberg, 2006
- Cai J., Ma H., Zhang J., Song Q., Du Z., Huang Y., Xu J., *Chem. Eur. J.*, 2013, 19, 14215-14223
- Cao G., *Nanostructures and Nanomaterials. Synthesis, Properties and Applications. Chapter 8*, Imperial College Press, London, 2004
- Čejka J., Mintova S., *Catal. Rev. Sci. Eng.*, 2007, 49, 457
- Chang W., Chae G., Jang S.R., Shin J., Ahn B.J., *J. Ind. Eng. Chem.*, 2012, 18, 581-585
- Chatterjee A., Ward T.R., *Catal. Lett.*, 2016, 146, 820-840
- Chen Y.-H., Hung H.-H., Huang M. H., *J. Am. Chem. Soc.*, 2009, 131, 9114-9121
- Clayden J., Greeves N., Warren S., Wothers P., *Organic Chemistry 1<sup>st</sup> Edition*, Oxford University Press, New York, 2001
- Collins G., Schmidt M., O'Dwyer C., Holmes J. D., McGlacken G. P., *Angew. Chem. Int. Ed.*, 2014, 53, 4142-4145
- Corma A., Garcia H., *Chem. Soc. Rev.*, 2008, 37, 2096-2126

Corma A., González-Arellano C., Iglesias M., Pérez-Ferreras S., Sánchez F., *Synlett*, 2007, 11, 1771-1774

Crudden C. M., Sateesh M., Lewis R., *J. Am. Chem. Soc.*, 2005, 127, 10045-10050

Cui T.-L., Ke W.-Y., Zhang W.-B., Wang H.-H., Li X.-H., Chen J.-S., *Angew. Chem. Int. Ed.*, 2016, 55, 9178-9182

Dai C., Li X., Zhang A., Liu C., Song C., Guo X., *RSC Adv.*, 2015, 5, 40297-40302

Dai C., Zhang A., Liu M., Guo X., Song C., *Adv. Funct. Mater.*, 2015, 25, 7479-7487

Davis S.E., Ide M.S., Davis R.J., *Green Chem.*, 2013, 15, 17-45

Delannoy L., El Hassan N., Musi A., Le To N.N., Krafft J.-M., Louis C., *J. Phys. Chem. B*, 2006, 110, 22471-22478

Della Pina C., Falletta E., Rossi M., *ChemSusChem*, 2009, 2, 57-58

Della Pina C., Falletta E., Rossi M., *Chem. Soc. Rev.*, 2012, 41, 350-369

Ding S., Yan Q., Jiang H., Zhong Z., Chen R., Xing W., *Chem. Eng. J.*, 2016, 296, 146-153

Durap F., Rakap M., Aydemir M., Özkar S., *Appl. Catal. A*, 2010, 382, 339-344

Ebitani K., Motokura K., Mizugaki T., Kaneda K., *Angew. Chem. Int. Ed.*, 2005, 44, 3423-3426

Ellis P. J., Fairlamb I. J. S., Hackett S. F. J., Wilson K., Lee A. F., *Angew. Chem. Int. Ed.*, 2010, 49, 1820-1824

Engelbrekt C., Jensen P. S., Sørensen K., Ulstrup J., Zhang J., *J. Phys. Chem. C*, 2013, 117, 11818-11828

Enthaler S., von Langermann J., Schmidt T., *Energy Environ. Sci.*, 2010, 3, 1207-1217

Eroshenko V., Regis R.-C., Soulard M., Patarin J., *J. Am. Chem. Soc.*, 2001, 123, 8129

Fang W., Chen J., Zhang Q., Deng W., Wang Y., *Chem. – Eur. J.*, 2011, 17, 1247

Ferey G., *Introduction to Zeolite Science and Practice*, Chapter 15, Elsevier, Amsterdam, 2007

Ferri D., Baiker A., *Top. Catal.*, 2009, 52, 1323-1333

Fihri A., Bouhrara M., Nekoueishahraki B., Basset J.-M., Polshettiwar V., *Chem. Soc. Rev.*, 2011, 40, 5181-5203

Franzén R., Xu Y., *Can. J. Chem.*, 2005, 83, 266-272

Gaikwad A. V., Holuigue A., Thathagar M. B., ten Elshof J. E., Rothenberg G., *Chem. – Eur. J.*, 2007, 13, 6908-6913

Gallezot P., *Chem. Soc. Rev.*, 2012, 41, 1538-1558

Garcia P., Malacria M., Aubert C., Gandon V., Fensterbank L., *ChemCatChem*, 2010, 2, 493-497

Giovambattista N., Debenedetti P.G., Rossky P.J., *J. Phys. Chem. B*, 2007, 111, 9581-9587

Gniewek A., Trzeciak A.M., *Top Catal.*, 2013, 56, 1239-1245

Goodhew P.J., Humphreys J., Beanland R., *Electron Microscopy and Analysis*, 3<sup>rd</sup> Edition, Taylor & Francis, London, 2001

Grasemann M., Laurency G., *Energy Environ. Sci.*, 2012, 5, 8171-8181

Greenwood N.N., Earshaw A., *Chemistry of Elements* 2<sup>nd</sup> Edition (p.1184), Butterworth-Heinemann, Oxford, 2001,

Gu J., Zhang Z., Hu P., Ding L., Xue N., Peng L., Guo X., Lin M., Ding W., *ACS Catal.*, 2016, 5, 6893-6901

Guan Z., Hu J., Gu Y., Zhang H., Li G., Li T., *Green Chem.*, 2012, 14, 1964-1970

Hansen T.W., Delariva A.T., Challa S.R., Datye A.K., *Accounts Chem. Res.*, 2013, 46, 1720-1730

Haruta M., *Chem. Rec.*, 2003, 3, 75-87

Haruta M., *J. New Mat. Electr. Sys.*, 2004, 7, 163-172

Haruta M., Kobayashi T., Sano H., Yamada N., *Chem. Lett.*, 1987, 405

Haruta M., Tsubota S., Kobayashi T., Kageyama H., Genet M.J., Delmon B., *J. Catal.*, 1993, 144, 175-192

Hashimoto S., Uwada T., Masuhara H., Asahi T., *J. Phys. Chem. C.*, 2008, 112, 15089-15093

Henderson M.A., *J. Phys. Chem. B*, 1997, 101, 221

Horng P., Brindza M.R., Walker R.A., Fourkas J.T., *J. Phys. Chem. C.*, 2010, 114, 394-402

Hoshi N., Nakamura M., Kida K., *Electrochem. Commun.*, 2007, 9, 279-282

Højholt K.T., Laursen A.B., Kegnæs S., Christensen C.H., *Top Catal.*, 2011, 54, 1026-1033

Huang Y., Zhou X., Yin M., Liu C., Xing W., *Chem. Mater.*, 2010, 22, 5122-5128

Huang Z., Guan H., Tan W., Qiao X., Kulprathipanja S., *J. Membr. Sci.*, 2006, 276, 260-271

Ishida T., Haruta M., *Angew. Chem. Int. Ed.*, 2007, 46, 7154

Ivanova S., Petit C., Pitchon V., *Appl. Catal. A*, 2004, 267, 191-201

Jana R., Pathak T.P., Sigman M.S., *Chem. Rev.*, 2011, 11, 1417-1492

Jayaraman K., Okamoto K., Son S.J., Lockett C., Gopalani A.H., Lee S.B., English D.S., *J. Am. Chem. Soc.*, 2005, 127, 17385-17392

- Jesionowski T., Urawska J., Krysztafkiewicz A., Pokore M., Waszak D., Tylus W., *Appl. Surf. Sci.*, 2003, 205, 212-224
- Jiang H., Yan Q., Chen R., Xing W., *Microp. Mesop. Mater.*, 2016, 225, 33-40
- Jiang H.-L., Liu B., Akita T., Haruta M., Sakurai H., Xu Q., *J. Am. Chem. Soc.*, 2009, 131, 11302-11303
- Jobby M., Regazzoni A., *Appl. Clay Sci.*, 2011, 51, 366-369
- Kim K.S., Barteau M.A., *Langmuir*, 1990, 6, 1485-1488
- Kim S.-J., Oh S.-D., Lee S., Choi S.-H., *J. Ind. Eng. Chem.*, 2008, 14, 449-456
- Klitgaard S. K., DeLaRiva A. T., Helveg S., Werchmeister R. M., Christensen C. H., *Catal. Lett.*, 2008, 126, 213-217
- Kumbhar A., Kamble S., Mane A., Jha R., Salunkhe R., *J. Organomet. Chem.*, 2013, 738, 29-34
- Laursen A.B., Højholt K.T., Lundegaard L.F., Simonsen S.B., Helveg S., Schüth F., Paul M., Grunwaldt J.-D., Kegnæs S., Christensen C.H., *Angew. Chem.*, 2010, 122, 3582-3585
- Li C.C., Zhang W., Ang H., Yu H., Xia B.Y., Wang X., Yang Y.H., Zhao Y., Hng H.H., Yan Q., *J. Mater. Chem. A*, 2014, 2, 10676-10681
- Li H., Li K., Zhang L., Fu A., Zhu Y., Wan Y., Zhao X., *Materials Science Forum*, 2010, 663-665, 721-724
- Li S., Boucheron T., Tuel A., Farruseng D., Meunier F., *Chem. Commun.*, 2014, 50, 1824-1826
- Li S., Burel L., Aquino C., Tuel A., Morfin F., rousset J.-L., Farrusseng D., *Chem. Commun.*, 2013, 49, 8507-8509
- Li<sup>2</sup> X., Fan X., Brandani S., *Chem. Eng. Sci.*, 2014, 117, 137-145
- Li Y., Hong X.M., Collard D.M., El-Sayed M.A., *Org. Lett.*, 2000, 2, 2385
- Liao F., Lo T.W.B., Tsang S.C.E., *ChemCatChem*, 2015, 7, 1998-2014
- Littke A. F., fu G. C., *Angew. Chem. Int. Ed.*, 2002, 41, 4176-4211
- Liu L., Díaz U., Arenal R., Agostini G., Concepción P., Corma A., *Nature Mater.*, Published on line September 2016, DOI:10.1038/NMAT4757
- Loges B., Boddien A., Junge H., Beller M., *Angew. Chem.*, 2008, 120, 4026-4029; *Angew. Chem. Int. Ed.*, 2008, 47, 3962-3965
- Ma Z., Dai S., *Nano. Res.*, 2011, 4, 3-32
- Marcon G., Messori L., Orioli P., Cinellu M.A., Minghetti G., *Eur. J. Biochem.*, 2003, 270, 4655-4661

Marsden C., Taarning E., Hansen D., Johansen L., Klitgaard S.K., Egeblad K., Christensen C.H., *Green Chem.*, 2008, 10, 168

McCusker L.B., Liebau F., D, Engelhardt G., *Pure Appl. Chem.*, 2001, 73, 381–394

Merga G., Saucedo N., Cass L.C., Puthussery J., Meisel D., *J. Phys. Chem. C*, 2010, 114, 14811

Mielby J., Abildstrøm J.O., Wang F., Kasama T., Weidenthaler C., Kegnæs S., *Angew. Chem.*, 2014, 126, 12721-12724

Mijri S.A., Halligudi S.B., Mathew N., Ravi V., Jacob N.E., Patil K.R., *Colloids Surf. A Physicochem. Eng. Asp.*, 2006, 287, 51-58

Miyaura N., Suzuki A., *J. Chem. Soc. Chem. Commun.*, 1979, 866

Miyaura N., Suzuki A., *Chem. Rev.*, 1995, 95, 2457-2483

Morris D.J., Clarkson G.J., Wills M., *Organometallics*, 2009, 28, 4133-4140

Murdoch M., Waterhouse G.I.N., Nadeem M.A., Metson J.B., Keane M.A., Howe R.F., Liorca J., Idriss H., *Nature Chem.*, 2011, 3, 489-492

Nakamoto H., Takahashi H., *Zeolites*, 1982, 2, 67

Naknam P., Luengnaruemitachai A., Wongkasemjit S., Osuwan S., *J. Power Sources*, 2007, 165, 353-358

Narayanan R., El-Sayed M.A., *Langmuir*, 2005, 21, 2027

Narayanan R., Tabor C., El-Sayed M. A., *Top Catal.*, 2008, 48, 60-74

Navlani-García M., Miguel-García I., Berenguer-Murcia Á., Lozano-Castelló D., Cazorla-Ámoros D., Yamashita H., *Catal. Sci. Technol.*, 2016, 6, 2623-2632

Niaz S., Manzoor T., Hussain Pandith A., *Renew. Sust. Energ. Rev.*, 2015, 50, 457-469

Okumura K., Murakami C., Oyama T., Sanada T., Isoda A., Katada N., *Gold Bull.*, 2012, 45, 83-90

Okumura K., Tomiyama T., Okuda S., Yoshida H., Niwa M., *J. Catal.*, 2010, 273, 156-166

Oliviera R.L., Kiyohara P.K., Rossi L.M., *Green Chem.*, 2009, 11, 1366-1370

Osman A.I., Abu-Dahrieh J.K., Laffir F., Curtin T., Thompson J.M., Rooney D.W., *Appl. Catal. B Environ.*, 2016, 187, 408-418

Otto T., Zones S. I., Iglesia E., *J. Catal.*, 2016, 339, 195-208

Parmeggiani C., Cardona F., *Green Chem.*, 2012, 14, 547-564

Pérez-Lorenzo M., *J. Phys. Lett.*, 2012, 3, 167-174

Philippaerts A., Poulussen S., Breesch A., Turner S., Lebedev O.I., Van Tendeloo G., Sels B., Jacobs P., *Angew. Chem. Int. Ed.*, 2011, 50, 3947-3949

Prieto A., Palomino M., Díaz U., Corma A., *Appl. Catal. A*, 2016, 523, 73-84

Puddephat R.J., *The Chemistry of Gold* (p. 18), Elsevier Scientific, Amsterdam, 1978

Qian X., Xiong D., Asiri A., Khan S.B., Rahman M.M., Xu H., Zhao D., *J. Mater. Chem. A*, 2013, 1, 7525-7532

Ramôa Ribeiro F., Alvarez F., Henriques C., Lemos F., Lopes J.M., Ribeiro M.F., *J. Mol. Catal. A Chem.*, 1995, 96, 245-270

Sadjadi S., heravi M.M., *RSC Adv.*, 2016, 6, 88588-88624

Sakurai H., Koga K., Iizuka Y., Kiuchi M., *Appl. Catal. A General.*, 2013, 462-463, 236-246

Sánchez F., Motta D., Dimitratos N., *Appl. Petrochem. Res.*, 2016, 6, 269-277

Schauer mann S., Nilus N., Shaikhutdinov S., Freund H.-J., *Acc. Chem. Res.*, 2013, 46, 1673-1681

Selvakannan P.R., Mantri K., Tardio J., Bhargava S.K., *J. Coll. Inter. Sci.*, 2013, 394, 475-484

Sharma A.S., Kaur H., Shah D., *RCS Adv.*, 2016, 6, 28688-28727

Sheldon R.A., *Catal. Today*, 2015, 247, 4-13

Siamaki A.R., Lin Y., Woodberry K., Connell J.W., Gupton B.F., *J. Mater. Chem. A*, 2013, 1, 12909-12918

Siddiqi G., Mougel V., Copéret C., *Dalton Trans.*, 2015, 44, 14349-14353

Silva B., Figueiredo H., Soares O.S.G.P., Rereira M.F.R., Figueiredo J.L., Lewandowska A.E., Bañares M.A., Neves I.C., Taveres T., *Appl. Catal. B*, 2012, 117-118, 406-413

Soloduch J., Olech K., Swist A., Zajac D., Cabaj J., *Adv. Chem. Eng. Sci.*, 2013, 3, 19-32

Soly mosi F., Erdohelyi A., *J. Catal.*, 1985, 91, 327

Soomro S. S., Ansari F. L., Chatziapostolou K., Köhler K., *J. Catal.*, 2010, 273, 138-146

Stuart B., *Infrared Spectroscopy: Fundamentals and Applications*, Wiley, 2005

Sullivan J.A., Flanagan K.A., Hain H., *Catal. Today*, 2009, 145, 108-113

Supronowicz W., Ignatyev I.A., Lolli G., Wolf A., Zhao L., Mleczko L., *Green Chem.*, 2015, 17, 2904-2911

Suzuki A., *Angew. Chem. Int. Ed.*, 2011, 50, 6723-6737

Tedsree K., Li T., Jones S., Chan C.W.A., Bagot P.A.J., Marquis e.A., Smith G.D.W., Yu K.M.K., Tsang S.C.E., *Nat. Nanotechnol.*, 2011, 6, 302-307

Thathagar M. B., Beckers J., Rothenberg G., *J. Am. Chem. Soc.*, 2002, 124, 11858-11859

Thommes M., *Chemie Ingenieur Technik*, 2010, 82, 1059-1073

Trzpit M., Soulard M., Patarin J., Desbiens N., Cailiez F., Boutin A., Demachy I., Fuchs A.H., Proceedings of the 4<sup>th</sup> International FEZA Conference, Elsevier, 2008

Usher Al, McPhail D.C., Brugger J., *Geochim. Cosmochim. Acta*, 2009, 73, 3359-3380

Uznanski P., Bryszewska E., *J. Mater. Sci.*, 2010, 45, 1547-1552

Valden M., Lai X., Goodman D.W., *Science*, 1998, 281, 1647

Valtchev V., *J. Mater. Chem.*, 2002, 12, 1914-1918

Wagner C.D., Davis E., Moulder J.F., Muilenberg G.E., Handbook of X-ray photoelectron Spectroscopy, Perkin-Elmer Corp., Minnesota, 1979

Wang C., Chen L., Qi Z., *Catal. Sci. Technol.*, 2013, 3, 1123-1128

Wang<sup>2</sup> C., Wang L., Zhang J., Wang H., Lewis J.P., Xiao F.-S., *J. Am. Chem. Soc.*, 2016, 138, 7880-7883

Wang N., Sun Q., Bai R., Li X., Guo G., Yu J., *J. Am. Chem. Soc.*, 2016, 138, 7484-7487

Wang S., Lu G.Q.M., *Appl. Catal. B Environ.*, 1998, 16, 269-277

Wang<sup>3</sup> Z.L., Yan J.M., Ping Y., Wang H.L., Zheng W.T., Jiang Q., *Angew. Chem. Int. Ed.*, 2013, 52, 4406-4409

Wang<sup>3</sup> Z.L., Ping Y., Yan J.M., Wang H.L., Jiang Q., *Int. J. Hydrog. Energy*, 2014, 39, 4850-4856

Webb P.A., Introduction to Chemical Adsorption Analytical Techniques and their Applications to Catalysis, Micromeritics Instrument Corp., Norcross, Georgia, 2003

Weitkamp J., *Solid State Ionics*, 2000, 131, 175-188

Wiberg E., Wiberg N., Holleman A.F., Inorganic Chemistry, Academic Press, New York, 2001

Yamakawa Y., Takizawa M., Ohnishi T., Koyama H., Shinoda S., *Catal. Comm.*, 2001, 2, 191-194

Yaw C.L., Andrew W., Thermophysical Properties of Chemicals and Hydrocarbons, Norwich, New York, 2008

Yoo J.S., Abild-Pedersen F., Nørskov J.K., Studt F., *ACS Catal.*, 2014, 4, 1226-1233

Yoon B., Wai C.M., *J. Am. Chem. Soc.*, 2005, 127, 17174-17175

Zhang S., Metin O., Su D., Sun S., *Angew. Chem. Int. Ed.*, 2013, 52, 1-5

Zhang X., Ke X., Zhu H., *Chem. Eur. J.*, 2012, 18, 8048-8056



Zhang L., Dong W.-H., Shang N.-Z., Feng C., Dao S.-T., Wang C., *Chin. Chem. Lett.*, 2016, 27, 149-154

Zhou H., Zhang J., Dong J., Yuan A., Shen X., *Microp. Mesop. Mater.*, 2016, 229, 68-75

Zhou X., Huang Y., Xing W., Liu C., Liao J., Lu T., *Chem. Commun.*, 2008, 30, 3540-3542

Zope B.N., Davis J.R., *Green Chem.*, 2011, 13, 3484-3491

Zope B.N., Hibbitts D.D., Neurock M., Davis J.R., *Science*, 2010, 330, 74-78

Zugic B., Karakalos S., Stowers K. J., Biener M. M., Biener J., Madix R. J., Friend C. M., *ACS Catal.*, 2016, 6, 1833–1839



**DTU Chemistry**  
**Department of Chemistry**  
Technical University of Denmark

Kemitorvet, Building 206  
2800 Kgs. Lyngby  
Tel. +45 45 25 24 19

[www.kemi.dtu.dk/english](http://www.kemi.dtu.dk/english)